Supporting information for the paper entitled,

An Organometallic Strategy for Assembling Atomically Precise Hybrid Nanomaterials

Julia M. Stauber[1], Elaine A. Qian[1,2,3], Yanxiao Han[4], Arnold L. Rheingold[5], Petr Král[4,6,7*], Daishi Fujita[8*], Alexander M. Spokoyny[1,3*]

[1]*Department of Chemistry and Biochemistry, University of California, Los Angeles, Los Angeles, California, 90095, United States.*

[2]*Department of Bioengineering, University of California, Los Angeles, Los Angeles, California, 90095, United States.*

[3]*California NanoSystems Institute, University of California, Los Angeles, Los Angeles, California, 90095, United States.*

[4]*Department of Chemistry, University of Illinois at Chicago, Chicago, Illinois, 60607, United States.*

[5]*Department of Chemistry and Biochemistry, University of California, San Diego, La Jolla, California, 92093, United States.*

[6]*Department of Physics, University of Illinois at Chicago, Chicago, Illinois, 60607, United States.*

[7]*Department of Biopharmaceutical Sciences, University of Illinois at Chicago, Chicago, Illinois, 60612, United States.*

[8]*Institute for Integrated Cell-Material Sciences, Kyoto University, Kyoto, 606-8302, Japan.*

*Correspondence to: spokoyny@chem.ucla.edu (A.M.S.), dfujita@icems.kyoto-u.ac.jp (D.F.), pkral@uic.edu (P.K.)

Contents

S1. General considerations

S1.1. Materials

All manipulations were performed under open atmosphere conditions in a fume hood unless otherwise indicated. All reagents were purchased from Sigma Aldrich, Strem Chemicals, ChemImpex, Oakwood Chemicals, TCI, Fisher Scientific, Carbosynth, Combi-Blocks, or Alfa Aesar, and used as received unless otherwise noted. Solvents (EtOH (ethanol), dichloromethane (DCM), methanol (MeOH), acetone, acetonitrile (MeCN), dimethoxyethane (DME), diethyl ether (Et_2O), *N*,*N*-dimethylformamide (DMF), ethyl acetate (EtOAc), hexanes, and dimethyl sulfoxide (DMSO)) were used as received without further purification unless otherwise specified. *Para*-iodo thiophenol,[1] Me-DalPhos (**Section S2.1)**,[2] $[((Me\text{-}DalPhos)AuCl)_2C_6H_4][SbF_6]_2$,[3] and $[TBA]_2[B_{12}(OH)_{12}]$[4] were prepared following previously reported procedures. The (Me-DalPhos)AuCl complex was either used as received (Sigma Aldrich) or prepared according to a procedure adapted from the literature (**Section S2.2**).[5] Glutathione (reduced), concanavalin A (ConA), and Shiga toxin 1, B subunit were purchased from Sigma Aldrich and stored at -20 °C prior to use. Na[1-thio-β-D-glucose] (Sigma Aldrich), Na[1-thio-β-D-galactose] (ChemImpex), and Na[1-thio-α-D-mannose] (Carbosynth) were purchased from commercial sources and used as received. $AgSbF_6$ and $[TBA]_2[B_{12}(OH)_{12}]$ were stored under an atmosphere of purified N_2 in a Vacuum Atmospheres NexGen glovebox prior to use. Deuterated solvents (CD_3CN, CD_3OD, acetone-d_6, CD_2Cl_2, $CDCl_3$, and D_2O) were obtained from Cambridge Isotope Laboratories and used as received. Aqueous solutions of TRIS (tris(hydroxymethyl)aminomethane) buffer were prepared by dissolution of TRIS•HCl (Sigma Aldrich) in Milli-Q water and adjustment to the appropriate pH with NaOH. TRIS buffer solutions in DMF were prepared by dissolution of the free Trizma base (Sigma Aldrich) in DMF.

S1.1.1. Expression and purification of DC-SIGN Extracellular Domain (ECD)

Soluble recombinant DC-SIGN ECD was produced in *E. coli* and purified *via* affinity chromatography and refolded as described previously,[6] and then further purified *via* size exclusion chromatography.

S1.2. Methods

All NMR spectra were obtained on Bruker Avance 400 or 300 MHz broad band FT NMR spectrometers. ^1H NMR and $^{13}C\{^1H\}$ NMR spectra were referenced to residual protio-solvent signals, $^{31}P\{^1H\}$ NMR chemical shifts are reported with respect to an external reference (85% H_3PO_4 in H_2O, δ 0.0 ppm), ^{19}F NMR spectra were referenced to freon-113 (1% in C_6D_6, δ -68.22 and -72.50 ppm relative to $CFCl_3$), and $^{11}B\{^1H\}$ chemical shifts were referenced to BF_3•Et_2O (15% in $CDCl_3$, δ 0.0 ppm). ESI-MS data were collected on a Thermo Instruments Q-Exactive Plus Hybrid Quadrupole-Orbitrap instrument operating in ESI-negative mode for all detections. Full mass scan (1000 to 5000 *m/z*) was used at 70,000 resolution, with automatic gain control (AGC) target of 1×10^6 ions, electrospray ionization operating at a 1.5 kV spray voltage, and a capillary temperature of 250 °C. LC-MS data were collected on an Agilent 1260 Infinity 6530 Q-TOF ESI instrument using an Agilent ZORBAX 300SB-C18 column (2.1 × 150 mm, 5 µm). Elemental analyses (C, H, N) were performed by Atlantic Microlab Inc. EPR measurements were carried out using an X-band ADANI SPINSCAN X instrument with a microwave frequency of 9.42 GHz and cavity temperature of 32 °C, and the data were processed using ADANI e-SPINOZA software. UV-vis measurements were conducted using an Ocean Optics Flame-S-UV-VIS-ES miniature spectrometer equipped with a DH-2000 UV-vis NIR light source. All measurements were carried out using quartz cuvettes (1 cm path length) and conducted at 25 °C with solution samples ranging

in concentration from 0.1–0.06 mM. Cyclic voltammetry measurements were performed with a CH Instruments CHI630D potentiostat using a glassy carbon working electrode, platinum wire counter electrode and Ag/Ag+ pseudo-reference electrode wire. Measurements were conducted at a scan rate of 100 mV/s with [TBA][PF_6] (0.1 M, DCM) supporting electrolyte under an inert atmosphere of N_2 and referenced *vs.* Fc/Fc^+. High performance liquid chromatography (HPLC) purification was performed on an Agilent Technologies 1260 Infinity II HPLC instrument equipped with a Variable Wavelength Detector (VWD, 254, 214 nm) and using an Agilent ZORBAX SB-C18 (9.4 × 250 mm, 5 µm) reversed-phase column.

Microwave reactions were performed using a CEM Discover SP microwave synthesis reactor. All reactions were performed in 10 mL glass microwave reactor vials purchased from CEM with silicone/PTFE caps. Teflon coated stir bars were used in the vials with magnetic stirring set to high with 15 s of premixing prior to the temperature ramping. All microwave reactions were carried out at 140 °C with the pressure release limit set to 250 psi and the maximum wattage set to 250 W. The power applied was dynamically controlled by the microwave instrument and did not exceed this limit for any reactions.

See **Section S7** for information pertaining to DC-SIGN cell microscopy studies, and **Section S9** for a detailed description of the X-ray crystallographic experimental parameters.

S2. Synthetic procedures and characterization data for all compounds

S2.1. Me-DalPhos

The Me-DalPhos ligand was prepared as previously reported by Stradiotto *et al.*[2] The ^{1}H (**Figure S1**) and $^{31}P\{^{1}H\}$ (**Figure S2**) NMR spectra are provided below and match the reported data.
^{1}H NMR (400 MHz, 25 °C, $CDCl_3$) δ: 7.71 (m, 1H, Ar-*H*), 7.32 (m, 1H, Ar-*H*), 7.20 (m, 1H, Ar-*H*), 7.05 (m, 1H, Ar-*H*), 2.71 (s, 6H, $N(CH_3)_2$), 2.01–1.89 (m, 18H, 1-Ad), 1.67 (s, 12H, 1-Ad) ppm.
$^{31}P\{^{1}H\}$ NMR (162 MHz, 25 °C, $CDCl_3$) δ: 20.1 ppm.

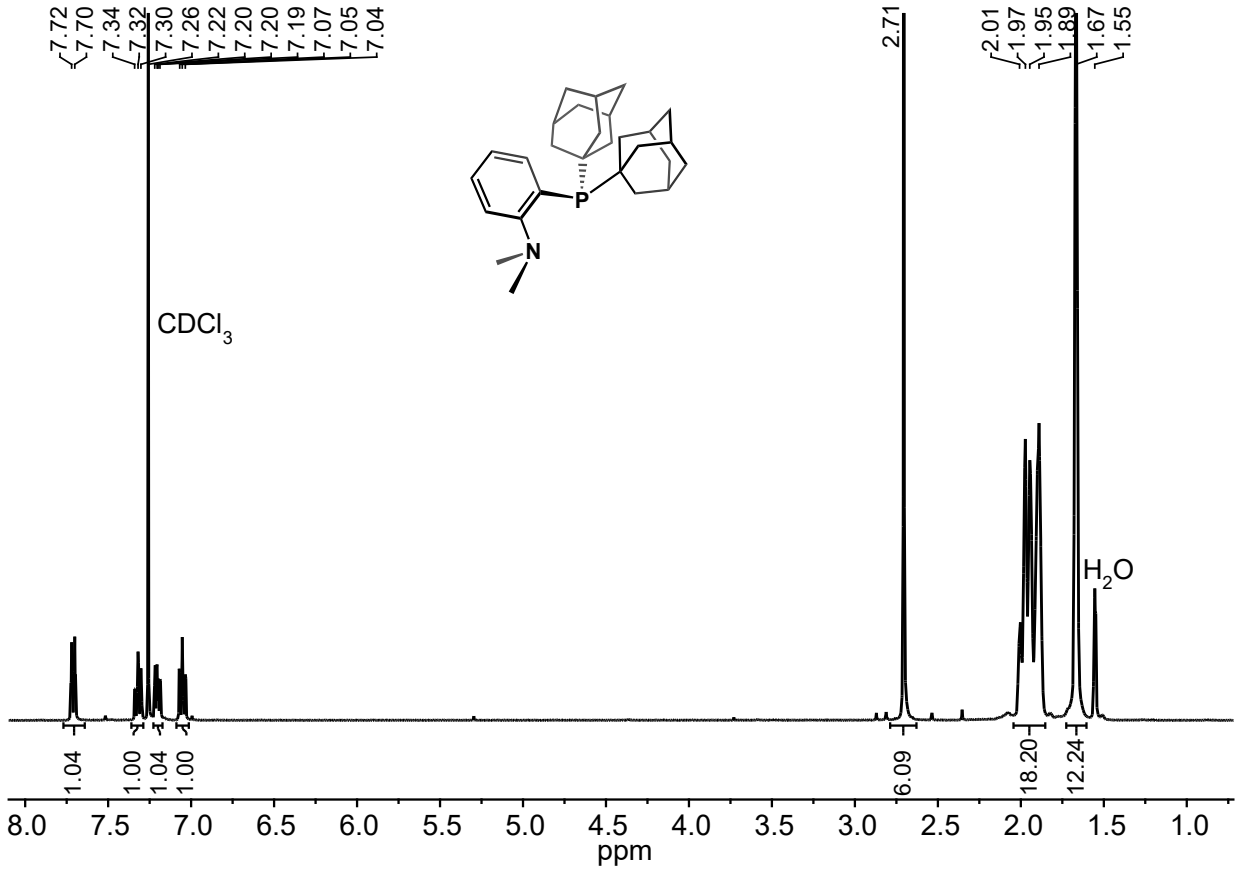

Figure S1. ^{1}H NMR spectrum of Me-DalPhos ($CDCl_3$, 400 MHz, 25 °C).

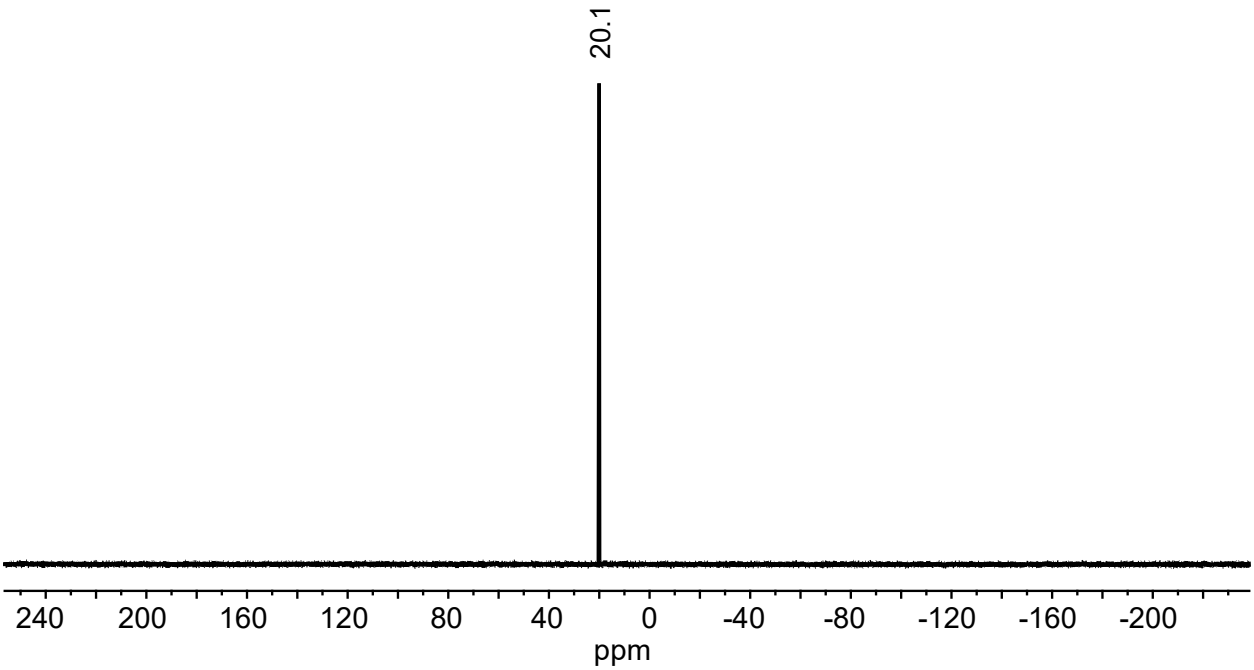

Figure S2. $^{31}P\{^{1}H\}$ NMR spectrum of Me-DalPhos ($CDCl_3$, 162 MHz, 25 °C).

S2.2. (Me-DalPhos)AuCl

The preparation of (Me-DalPhos)AuCl was adapted from a similar procedure reported by Stradiotto *et al*.[5]

To a stirring solution of $HAuCl_4 \bullet 3H_2O$ (165 mg, 0.419 mmol, 1.00 equiv) in H_2O (1 mL) was added 2,2'-thiodiethanol (126 µL, 1.22 mmol, 3.00 equiv) over the course of 30 min during which time the color of the reaction mixture changed from yellow to colorless. To this mixture was added solid Me-DalPhos (177 mg, 0.420 mmol, 1.00 equiv) all at once followed by EtOH (3 mL), and the resulting colorless suspension was allowed to stir at 25 °C for an additional 3 h. The suspension was then filtered, and the colorless solids were washed with MeOH (4 × 2 mL), and dried under reduced pressure to afford (Me-DalPhos)AuCl as a colorless powder (184 mg, 0.280 mmol, 67%). ^{1}H NMR (400 MHz, 25 °C, CD_2Cl_2) δ: 7.77 (m, 1H, Ar-*H*), 7.60–7.52 (m, 2H, Ar-*H*), 7.31 (m, 1H, Ar-*H*), 2.57 (s, 6H, N(C*H*$_3$)$_2$), 2.25–2.21 (m, 6H, 1-Ad), 2.11–2.07 (m, 6H, 1-Ad), 1.99 (m, 6H, 1-Ad), 1.69 (s, 12H, 1-Ad) ppm. ^{31}P{^{1}H} NMR (162 MHz, 25 °C, CD_2Cl_2) δ: 56.8 ppm.

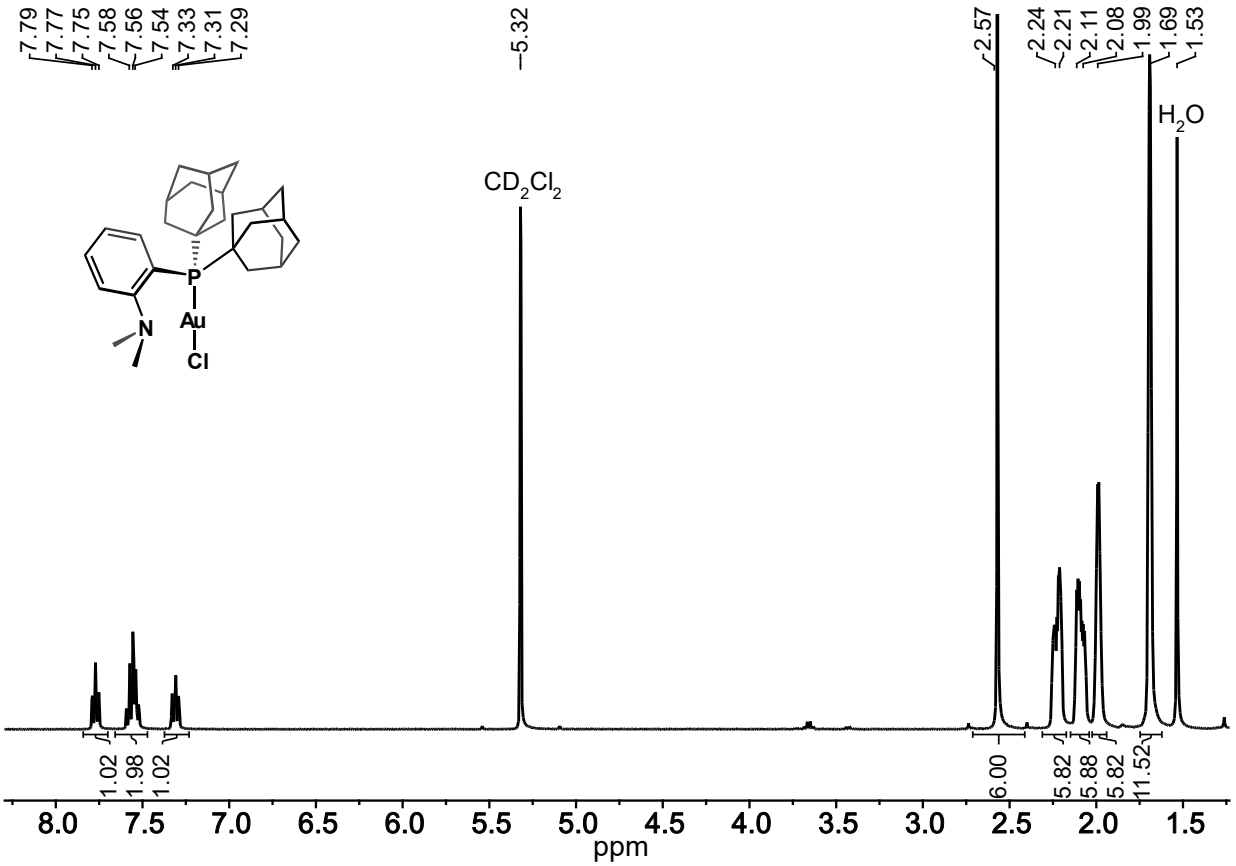

Figure S3. ^{1}H NMR spectrum of (Me-DalPhos)AuCl (CD_2Cl_2, 400 MHz, 25 °C).

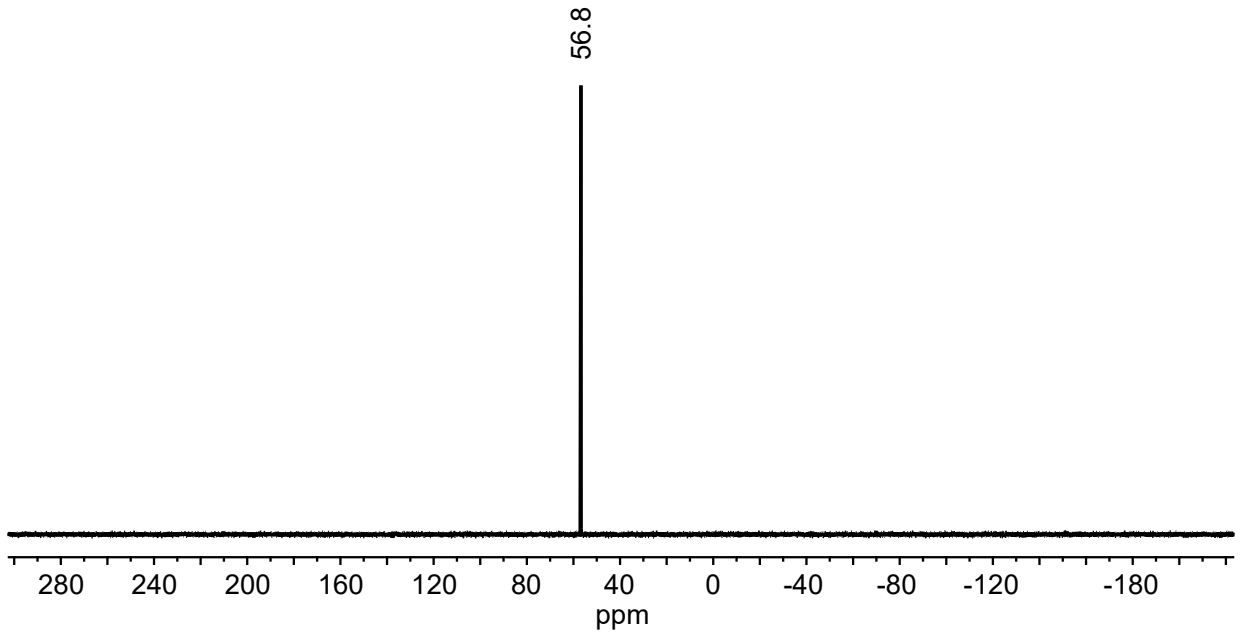

Figure S4. $^{31}P\{^{1}H\}$ NMR spectrum of (Me-DalPhos)AuCl (CD_2Cl_2, 162 MHz, 25 °C).

S2.3. $B_{12}(OCH_2C_6H_4I)_{12}$

$[TBA]_2[B_{12}(OH)_{12}]$ (100 mg, 0.122 mmol, 1.00 equiv) was removed from a nitrogen-filled glovebox and transferred to a 10 mL microwave reaction tube equipped with a Teflon-coated stir bar. To this tube was added 4-iodobenzylbromide (1.090 g, 3.671 mmol, 30.00 equiv) and *N*,*N*-diisopropylethylamine (400 µL, 2.30 mmol, 18.8 equiv), followed by MeCN (2 mL). The reaction tube was capped with a PTFE/silicone cap and the mixture was heated to 140 °C with stirring in the microwave for 1 h. The reaction mixture was then removed from the microwave, and the resulting bright magenta reaction mixture was evaporated to dryness, and the residue was suspended in a mixture of 35/65 EtOAc/hexanes (4 mL) and acetone (1 mL), and then loaded into a silica-packed column. The excess 4-iodobenzyl bromide was eluted first using a 35:65 EtOAc:hexanes mixture, followed by elution of the magenta band consisting of a mixture of the $[TBA][B_{12}(OCH_2C_6H_4I)_{12}]$/$[TBA]_2[B_{12}(OCH_2C_6H_4I)_{12}]$ species with acetone. The acetone solution was evaporated to dryness and then the resulting magenta residue was suspended in a 90:10 EtOH:MeCN mixture (5 mL). To this suspension was added $FeCl_3$•$6H_2O$ (300 mg, 1.11 mmol, 9.10 equiv) as a solid, resulting in an immediate darkening of the color of the reaction mixture. The suspension was allowed to stir at 25 °C for a total of 20 h, at which point all volatiles were removed *in vacuo*. The resulting dark red residue was dissolved in DCM (4 mL) and eluted through a silica plug with DCM. A dark red band was recovered, and all volatiles were removed from the solution under reduced pressure, resulting in isolation of the neutral $B_{12}(OCH_2C_6H_4I)_{12}$ product as a dark red, crystalline solid in 76% yield (273 mg, 0.0933 mmol). Single dark red crystals of suitable quality for an X-ray diffraction study were grown by vapor diffusion of Et_2O into a saturated DCM solution of $B_{12}(OCH_2C_6H_4I)_{12}$ at 25 °C over the course of 24 h, and the solid-state structure is shown in **Figure S131**. Elem. Anal. found for $C_{84}H_{72}O_{12}B_{12}I_{12}$ (calc'd): C: 34.70 (34.43); H: 2.46 (2.48). UV-vis (DCM, 25 °C, 0.1 mM) [Ɛ]: 451 nm [15,500 $M^{-1}cm^{-1}$]. ^{1}H NMR (400 MHz, 25 °C, $CDCl_3$) δ: 7.51 (d, 24H, Ar-*H*, ^3J = 8 Hz), 6.71 (d, 24H, Ar-*H*, ^3J = 8 Hz), 5.03 (s, 24H, –CH_2–) ppm. $^{13}C\{^1H\}$ NMR (101 MHz, 25 °C, $CDCl_3$) δ: 139.3 (C_{Ar}-O), 137.7 (C_{Ar}H), 128.8 (C_{Ar}H), 93.2 (C_{Ar}-I), 72.8 (–CH$_2$–) ppm. $^{11}B\{^1H\}$ NMR (128 MHz, 25 °C, $CDCl_3$) δ: 41.5 ppm. ESI-MS(–) (MeCN): 2926.4649 (calc'd, 2926.4778) *m/z.* The monoanionic species is observed under ESI-MS conditions in MeCN (**Figure S9**).

Due to the presence of oxygen during the microwave-assisted preparation of $B_{12}(OCH_2C_6H_4I)_{12}$, the fully reduced cluster core ($[B_{12}]^{2-}$) undergoes both one and two-electron oxidation reactions, which results in a mixture of the $[B_{12}(OR)_{12}]^{2-}$, $[B_{12}(OR)_{12}]^{-}$, and $[B_{12}(OR)_{12}]^{0}$ clusters. The two-electron chemical oxidation of that mixture to generate the neutral species is performed in order to work with the cluster in one charge state for the subsequent metalation reaction.

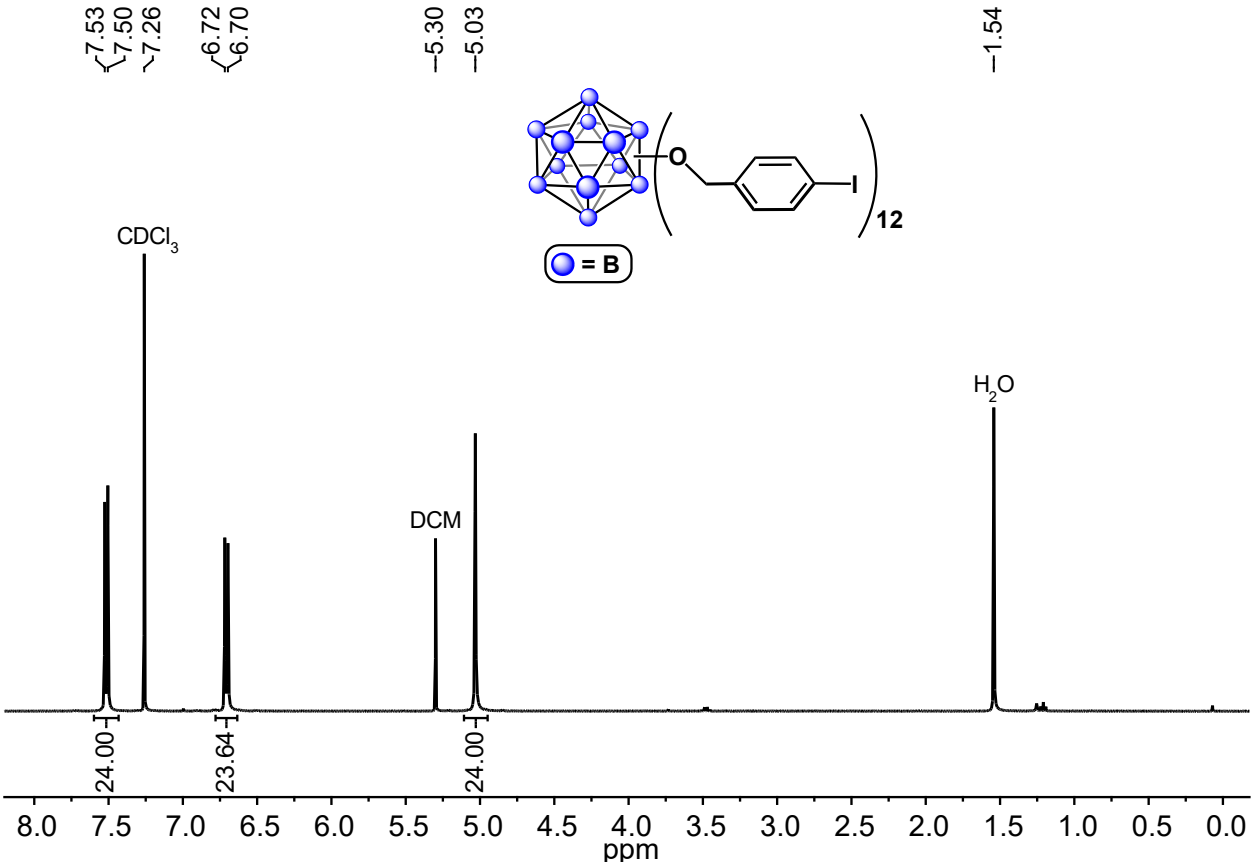

Figure S5. ^{1}H NMR spectrum of $B_{12}(OCH_2C_6H_4I)_{12}$ ($CDCl_3$, 400 MHz, 25 °C).

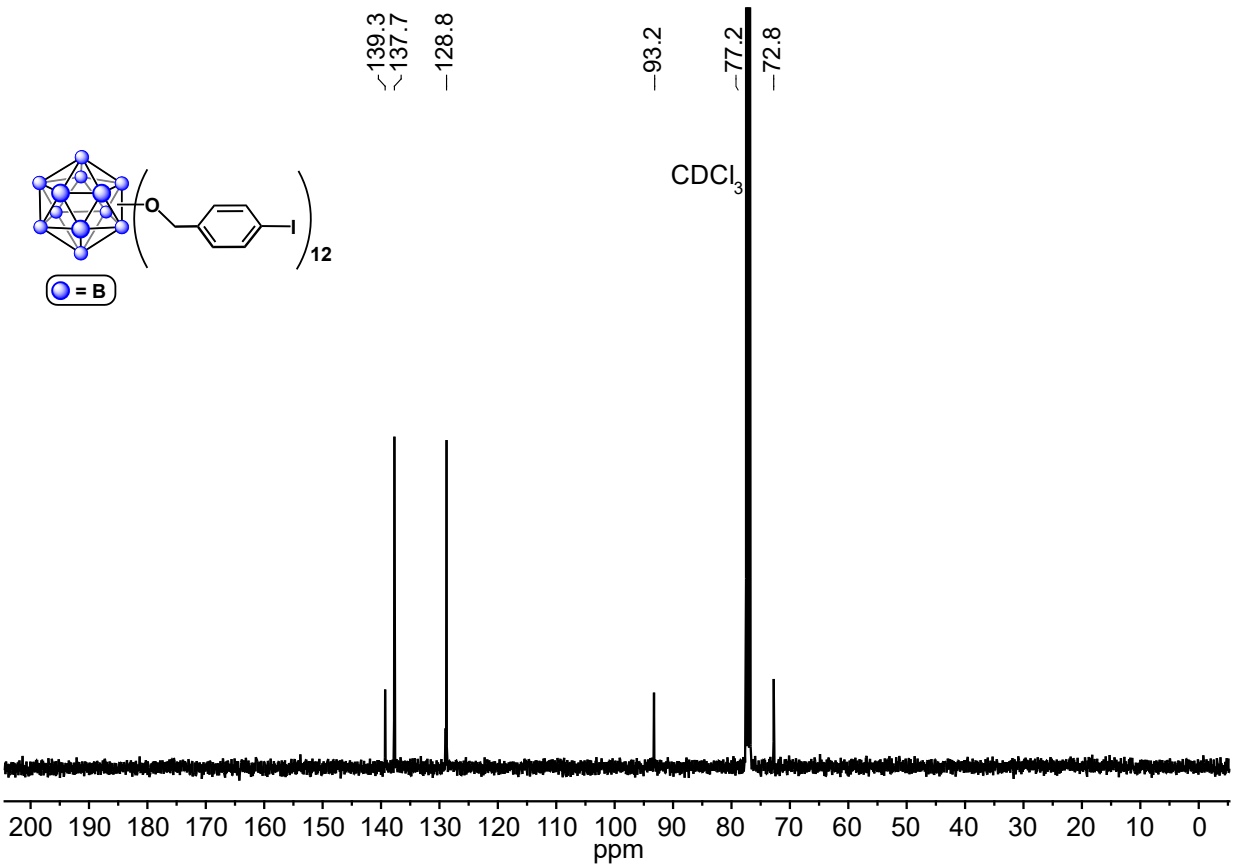

Figure S6. $^{13}C\{^{1}H\}$ NMR spectrum of $B_{12}(OCH_2C_6H_4I)_{12}$ ($CDCl_3$, 101 MHz, 25 °C).

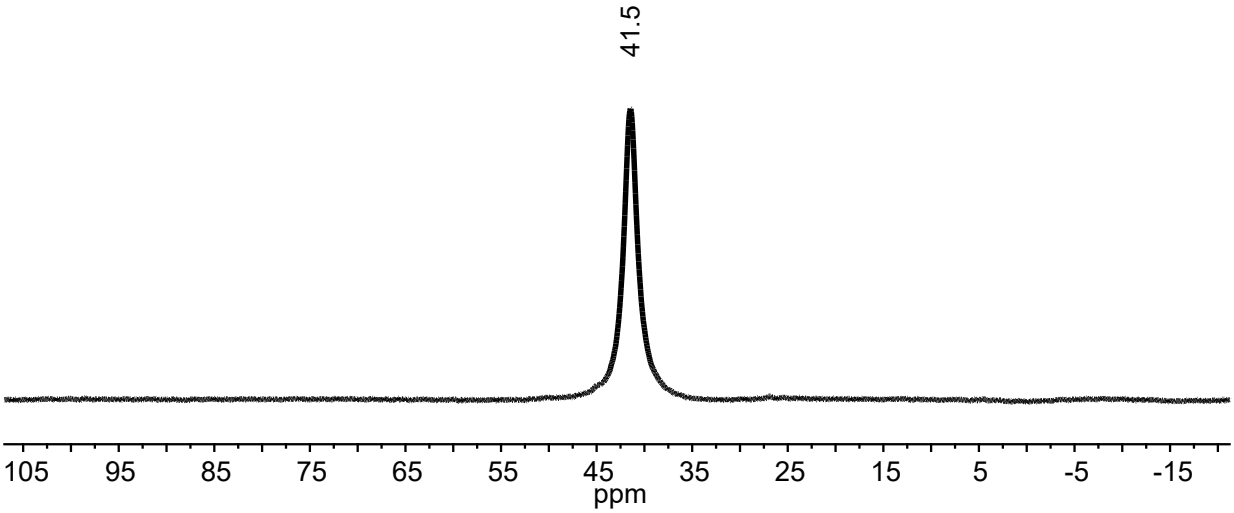

Figure S7. $^{11}B\{^{1}H\}$ NMR spectrum of $B_{12}(OCH_2C_6H_4I)_{12}$ ($CDCl_3$, 128 MHz, 25 °C).

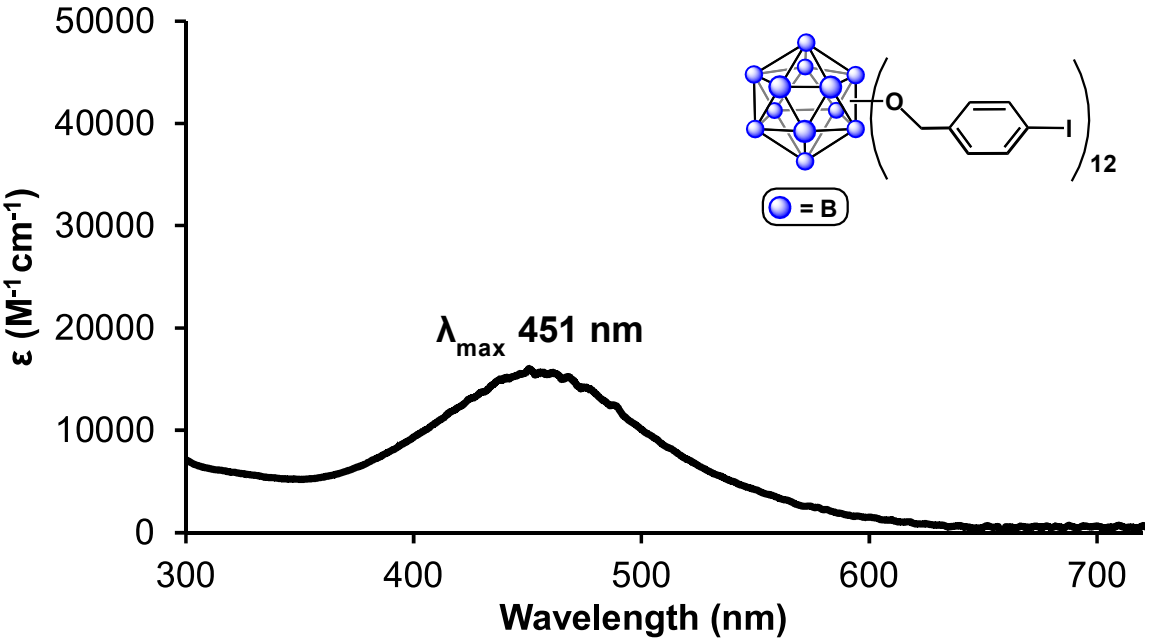

Figure S8. UV-vis spectrum of $B_{12}(OCH_2C_6H_4I)_{12}$ (DCM, 0.1 mM, 25 °C).

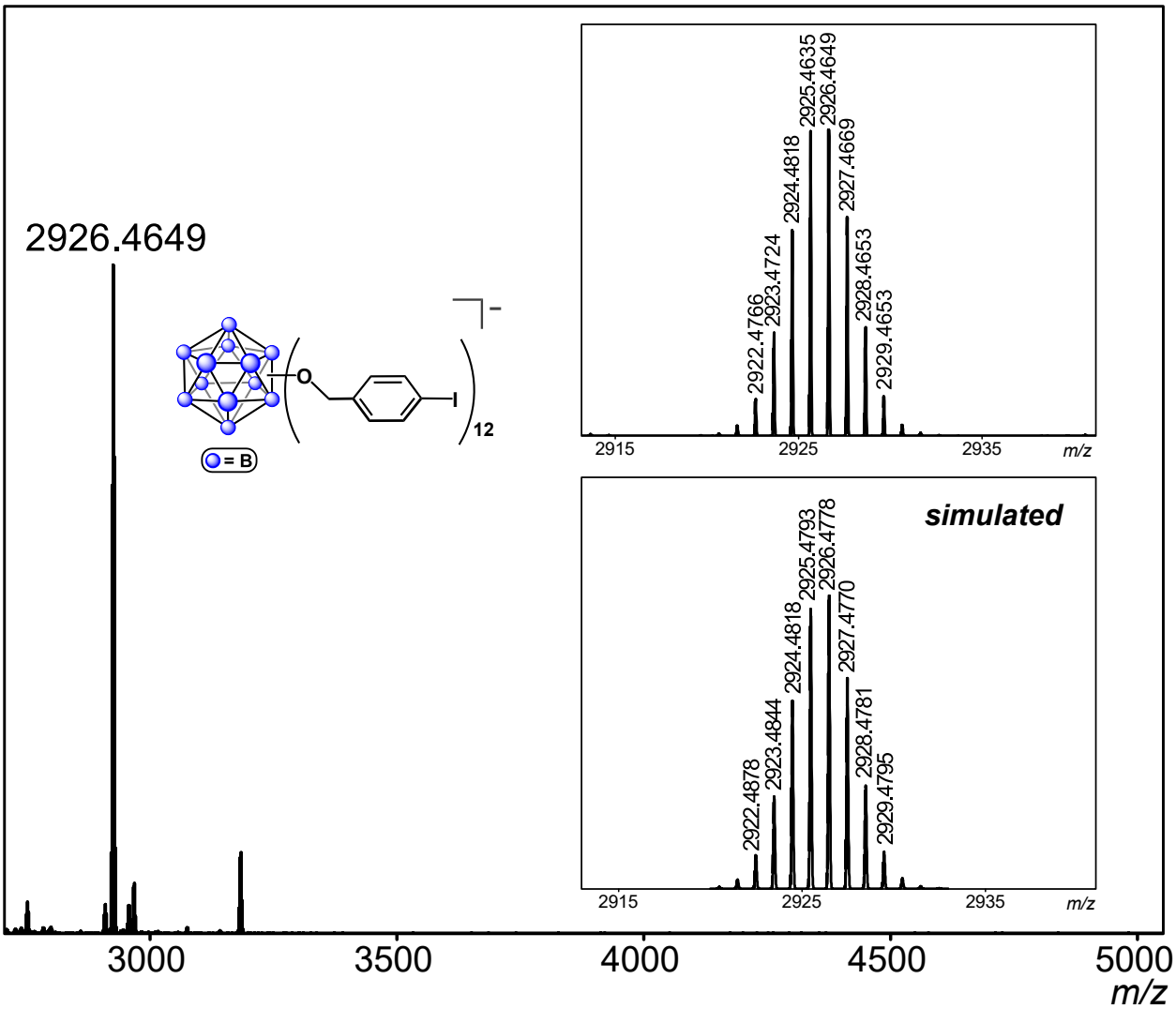

Figure S9. ESI-MS(–) of $B_{12}(OCH_2C_6H_4I)_{12}$ (MeCN, 1.5 kV). This species is observed as a monoanion under ESI-MS conditions in MeCN.

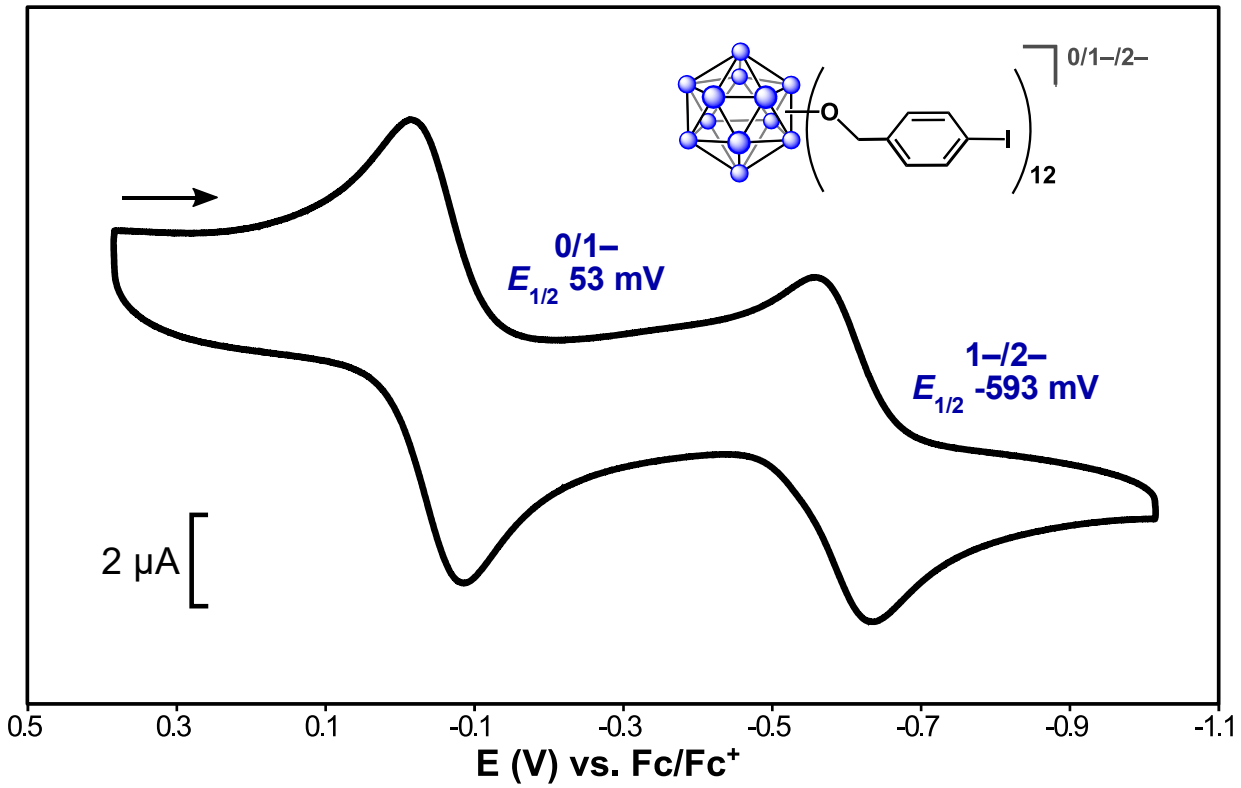

Figure S10. Cyclic voltammogram of $B_{12}(OCH_2C_6H_4I)_{12}$ measured at a scan rate of 100 mV/s with 0.1 M [TBA][PF_6] supporting electrolyte and referenced *vs*. Fc/Fc^+ (glassy carbon working electrode, platinum counter electrode and Ag/Ag+ pseudo-reference electrode wire; DCM, 0.3 mM, 25 °C).

S2.4. $[B_{12}(OCH_2C_6H_4((Me\text{-}DalPhos)AuCl)_{12}][SbF_6]_{11}$ ([1][SbF$_6$]$_{11}$)

To a cooled (-4 °C) solution of $AgSbF_6$ (10 mg, 0.029 mmol, 20 equiv) in DCM (1 mL) was added a cooled (-4 °C) solution of $B_{12}(OCH_2C_6H_4I)_{12}$ (4 mg, 0.001 mmol, 1 equiv) and (Me-DalPhos)AuCl (19 mg, 0.029 mmol, 20 equiv) in DCM (1 mL) under protection from light. The reaction mixture was sealed and placed in a preheated oil bath set to 45 °C and allowed to stir for a total of 16 h under protection from light. The maroon suspension was then filtered through a pad of Celite, resulting in a pale-yellow filtrate and dark red filter cake containing the product. The filter cake was washed with DCM (3 × 2 mL) to remove unreacted (Me-DalPhos)AuCl, and then the product was extracted with DMF (1.5 mL) and filtered through the pad of Celite to give a purple/red filtrate. To the filtrate was added Et_2O (20 mL) with stirring, resulting in the precipitation of $[B_{12}(OCH_2C_6H_4((Me\text{-}DalPhos)AuCl)_{12}][SbF_6]_{11}$ as a dark pink powder*. The precipitate was collected by filtration, washed with Et_2O (2 × 3 mL), and dried under reduced pressure to afford a pink solid (7 mg, 40%, 0.6 μmol). The resulting solids were dissolved in MeCN (0.5 mL) and then the solution was filtered through a piece of glass microfiber filter paper. DME (0.5 mL) was carefully layered on top of the resulting dark pink solution followed by careful layering of Et_2O (1 mL). This solution was allowed to stand at 25 °C for 18 h to afford a crop of dark pink crystals of suitable quality for an X-ray diffraction study (5 mg, 30%, 0.4 μmol). The crystalline material obtained following the described procedure was used for structural determination (See **Section S9.2** for crystallographic information) and all subsequent characterization of [**1**][SbF_6]$_{11}$. Elem. Anal. found for $[B_{12}(OCH_2C_6H_4((Me\text{-}DalPhos)AuCl)_{12}][SbF_6]_{11}$ ($C_{420}H_{552}N_{12}O_{12}Au_{12}B_{12}Cl_{12}Sb_{11}F_{66}$) (calc'd): C: 42.47 (42.56); H: 4.85 (4.70); N: 1.44 (1.42). UV-vis (MeCN, 25 °C, 0.06 mM) [Ɛ]: 350 [25,200 $M^{-1}cm^{-1}$], 543 [15,900 $M^{-1}cm^{-1}$] nm. ^{1}H NMR (400 MHz, 25 °C, CD_3CN) δ: 8.02 (m, 12H, Me-DalPhos Ar-*H*), 7.96 (m, 24h, Me-DalPhos Ar-*H*), 7.70 (t, 12H, Me-DalPhos Ar-*H*, ^3J = 6 Hz), 7.51 (br s, 48H, Ar-*H*), 3.42 (s, 72H, N(C*H*$_3$)$_2$), 2.23 (m, 72H, 1-Ad), 2.01 (m, 144H, 1-Ad, signals overlapping with CD_3CN residual solvent signal), 1.67 (m, 144H, 1-Ad) ppm. The signals attributed to the aryl and methylene protons of the –$OCH_2C_6H_4$– spacer are broadened due to their proximity to the paramagnetic $[B_{12}]^-$ core.* $^{31}P\{^1H\}$ NMR (162 MHz, 25 °C, CD_3CN) δ: 75.8 ppm. $^{11}B\{^1H\}$ NMR (128 MHz, 25 °C, CD_3CN) δ: A silent $^{11}B\{^1H\}$ NMR spectrum was observed for [**1**][SbF_6]$_{11}$ due to the paramagnetic dodecaborate $[B_{12}]^-$ core (See **Figure S13** for the $^{11}B\{^1H\}$ NMR spectrum and **Figure S15** for the EPR spectrum).*

*It is noted that during the course of this reaction/workup procedure, the $[B_{12}]$ cluster core undergoes a one-electron reduction from the neutral ($[B_{12}]^0$) to monoanionic charge state ($[B_{12}]^-$). This redox chemistry corresponds to an overall charge for the permetalated complex, **1**, of 11+ as opposed to the expected 12+ charge, which would be the case in the absence of any cluster-based reduction (each (Me-DalPhos)Au^{III}ClAr fragment carries a 1+ charge together with a charge compensating $[SbF_6]^-$ anion). It has been reported by our group and others that perfunctionalized dodecaborate clusters undergo redox chemistry,[4,7–9] and it is likely that the DMF used in the described workup procedure serves as the reducing agent[10] to result in the formation of the [**1**][SbF_6]$_{11}$ species.

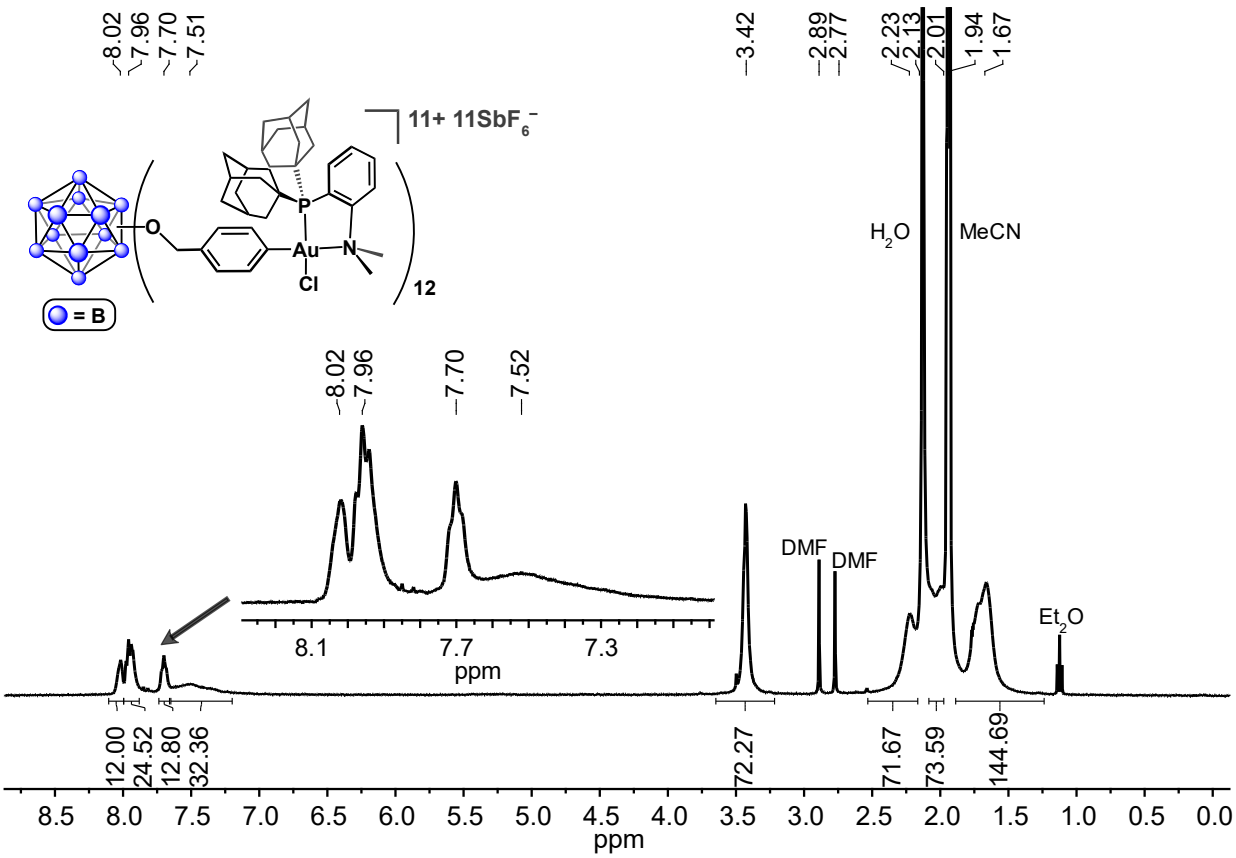

Figure S11. ^{1}H NMR spectrum of $[B_{12}(OCH_2C_6H_4(Me\text{-}DalPhos)AuCl)_{12}][SbF_6]_{11}$ (CD_3CN, 400 MHz, 25 °C).

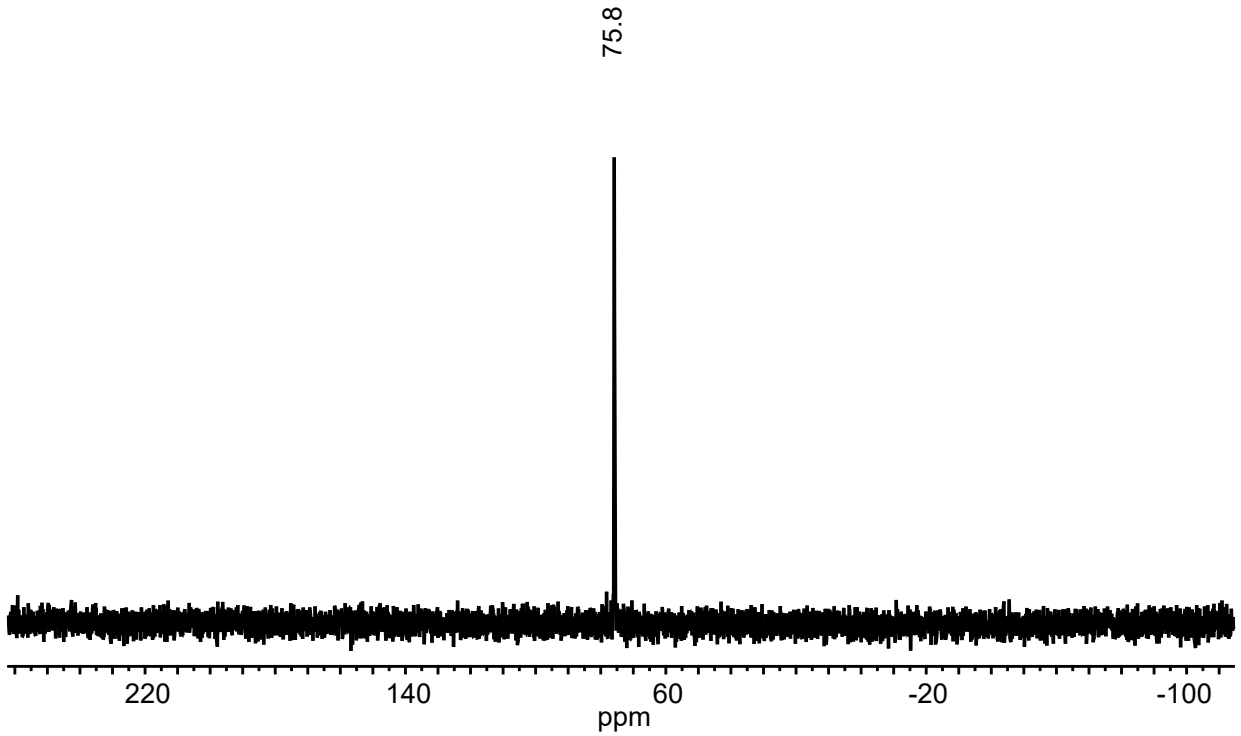

Figure S12. $^{31}P\{^{1}H\}$ NMR spectrum of $[B_{12}(OCH_2C_6H_4(Me\text{-}DalPhos)AuCl)_{12}][SbF_6]_{11}$ (CD_3CN, 162 MHz, 25 °C).

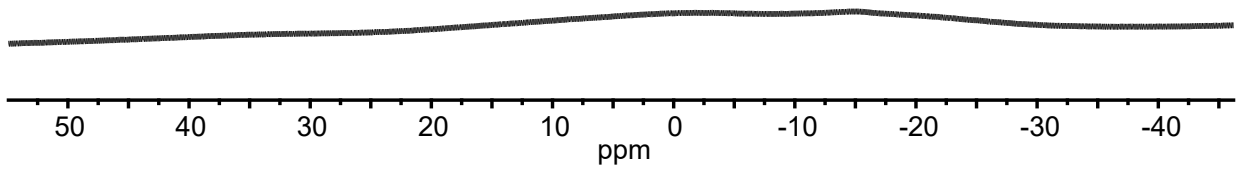

Figure S13. $^{11}B\{^{1}H\}$ NMR spectrum of $[B_{12}(OCH_2C_6H_4((Me\text{-}DalPhos)AuCl)_{12}][SbF_6]_{11}$ (CD_3CN, 128 MHz, 25 °C).

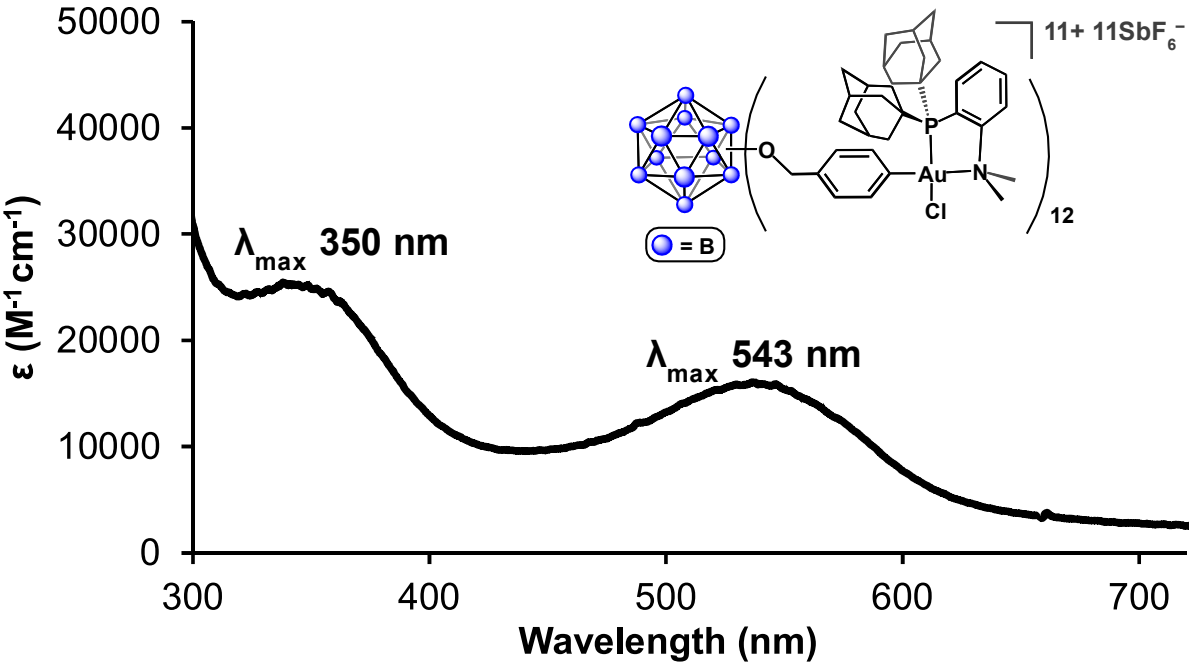

Figure S14. UV-vis spectrum of $[B_{12}(OCH_2C_6H_4((Me\text{-}DalPhos)AuCl)_{12}][SbF_6]_{11}$ (MeCN, 0.06 mM, 25 °C).

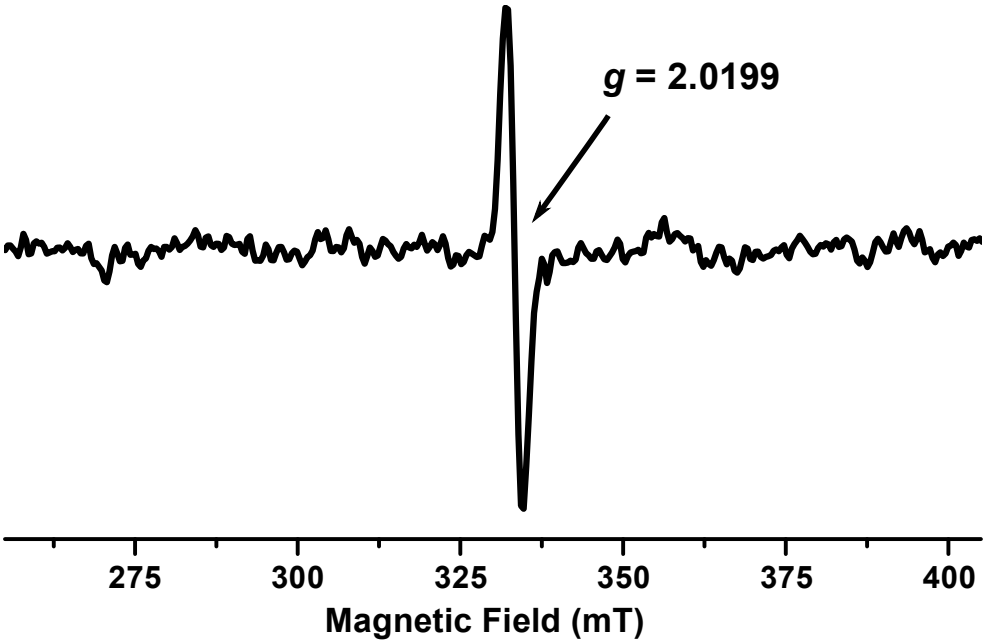

Figure S15. EPR spectrum of $[B_{12}(OCH_2C_6H_4((Me\text{-}DalPhos)AuCl)_{12}][SbF_6]_{11}$ (1:9 MeCN:toluene, 9.42 GHz MW frequency, 32 °C cavity temperature).

S2.5. General procedure for conjugation reactions with [1][SbF_6]$_{11}$

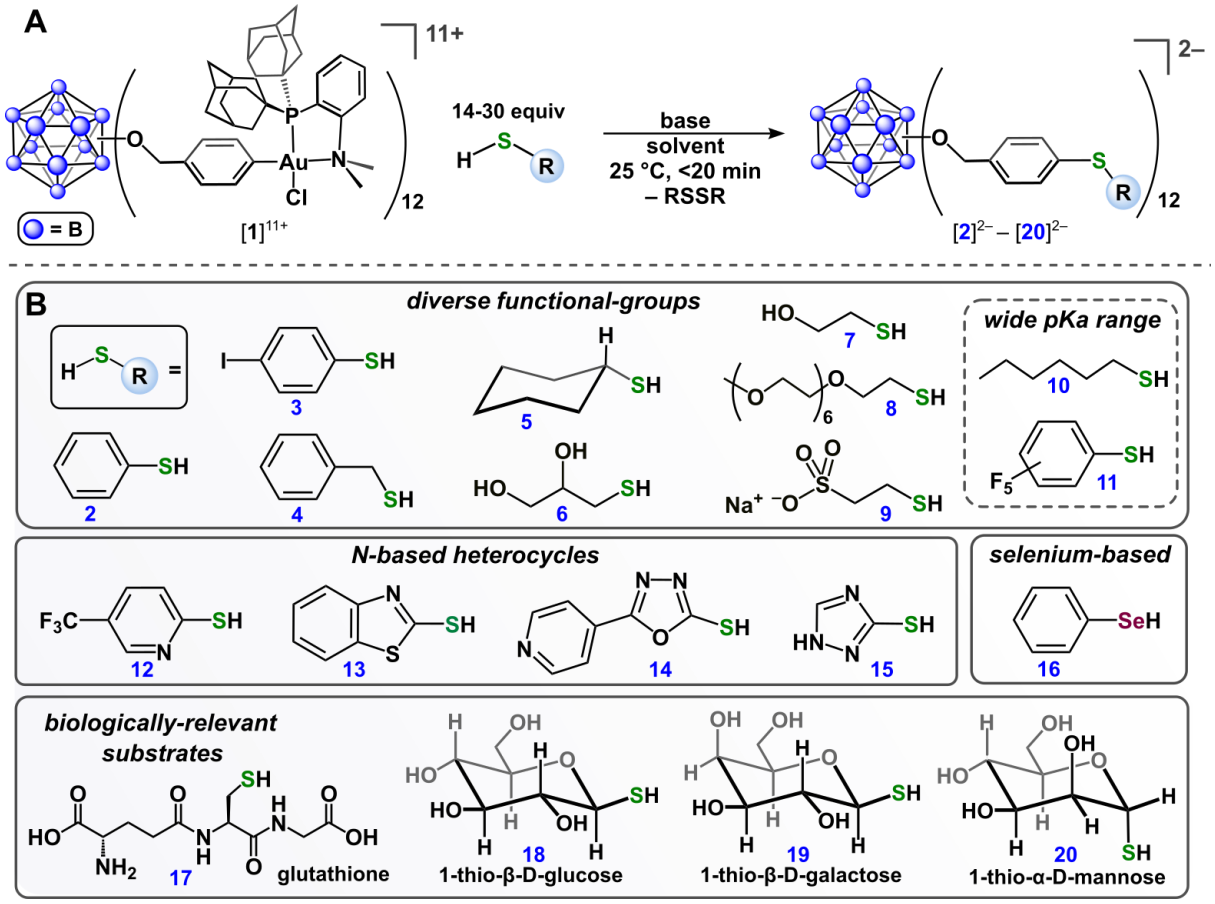

Figure S16. (A) General scheme for conjugation reactions of [**1**][SbF_6]$_{11}$ with thiol-containing substrates. (B) Scope of nanocluster thioether conjugates.

To a cooled (-4 °C) solution of $AgSbF_6$ (10 mg, 0.029 mmol, 20 equiv) in DCM (1 mL) was added a cooled (-4 °C) solution of $B_{12}(OCH_2C_6H_4I)_{12}$ (4 mg, 0.001 mmol, 1 equiv) and (Me-DalPhos)AuCl (19 mg, 0.029 mmol, 20 equiv) in DCM (1 mL) under protection from light. The reaction mixture was sealed and placed in a preheated oil bath set to 45 °C and allowed to stir for a total of 16 h under protection from light. The maroon suspension was then filtered through a pad of Celite, resulting in a pale-yellow filtrate and dark red filter cake containing the product. The filter cake was then washed with DCM (3 × 2 mL), at which point the product was extracted with DMF (1 mL) and filtered through the pad of Celite to give a purple/red filtrate. The [**1**][SbF_6]$_{11}$ complex was used in this DMF solution for all conjugation reactions and without further purification. This solution was treated with the corresponding thiol substrate and base as described in the following sections.

S2.6. $[K_2][B_{12}(OCH_2C_6H_4SPh)_{12}]$ ($[K_2][2]$)

The general reaction procedure to generate $[\mathbf{1}][SbF_6]_{11}$ (**Section S2.5**) was followed. The DMF solution containing $[\mathbf{1}][SbF_6]_{11}$ (0.0014 mmol, 1 mL) was transferred to a vial containing solid K_3PO_4 (9 mg, 0.04 mmol, 30 equiv), and a Teflon-coated stir bar. To this solution was added a solution of thiophenol (35 µL of a 0.97 M solution in MeCN, 0.034 mmol, 24 equiv) with stirring. The color of the reaction mixture gradually changed from dark purple to colorless over the course of 15 min, at which point all volatiles were removed under reduced pressure with gentle heating (35 °C). The resulting colorless residue was suspended in a 65:35 hexanes:EtOAc mixture and loaded into a silica-packed pipette column. Using a 65:35 hexanes:EtOAc solvent combination, unreacted thiophenol and the (Me-DalPhos)AuCl byproduct were eluted first, followed by elution of the $[K_2][B_{12}(OCH_2C_6H_4SPh)_{12}]$ product with DCM. The product fractions were combined, and all volatiles were removed under reduced pressure to afford $[K_2][B_{12}(OCH_2C_6H_4SPh)_{12}]$ in 70% yield (3 mg, 0.001 mmol) as a pale pink, oily solid. ^{1}H NMR (400 MHz, 25 °C, CD_2Cl_2) δ: 7.24-7.14 (m, 108H, Ar-*H*, all aromatic signals overlapping), 5.29 (s, 24H, –C*H*$_2$–) ppm. ^{11}B{^{1}H} NMR (128 MHz, 25 °C, CD_2Cl_2) δ: -15.6 ppm. ESI-MS(–): 1356.3758 (calc'd, 1356.3772) *m/z*.

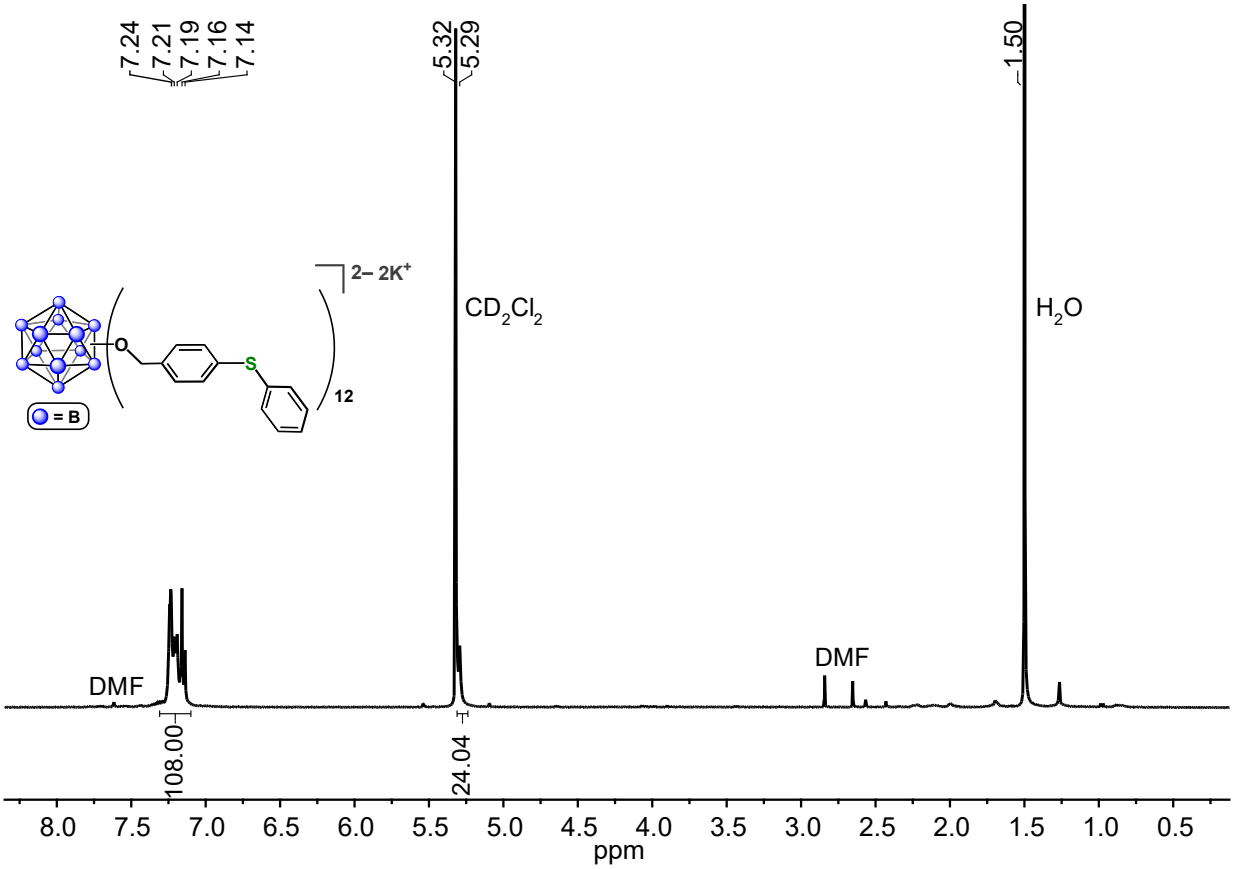

Figure S17. ^{1}H NMR spectrum of $[K_2][B_{12}(OCH_2C_6H_4SPh)_{12}]$ (400 MHz, CD_2Cl_2, 25 °C).

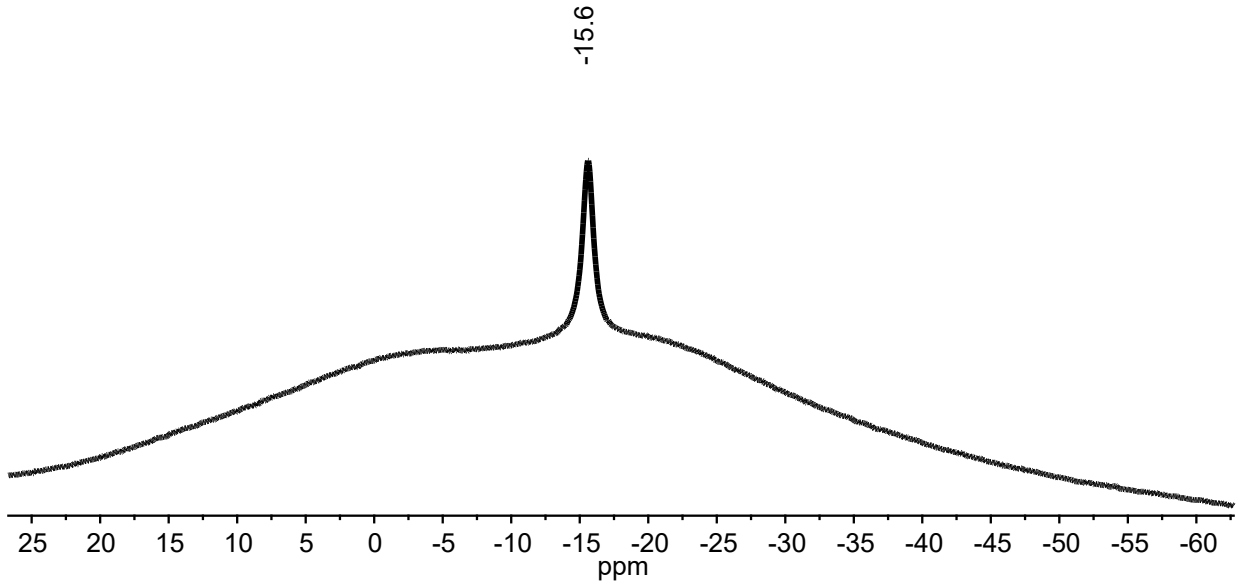

Figure S18. $^{11}B\{^{1}H\}$ NMR spectrum of $[K_2][B_{12}(OCH_2C_6H_4SPh)_{12}]$ (128 MHz, CD_2Cl_2, 25 °C).

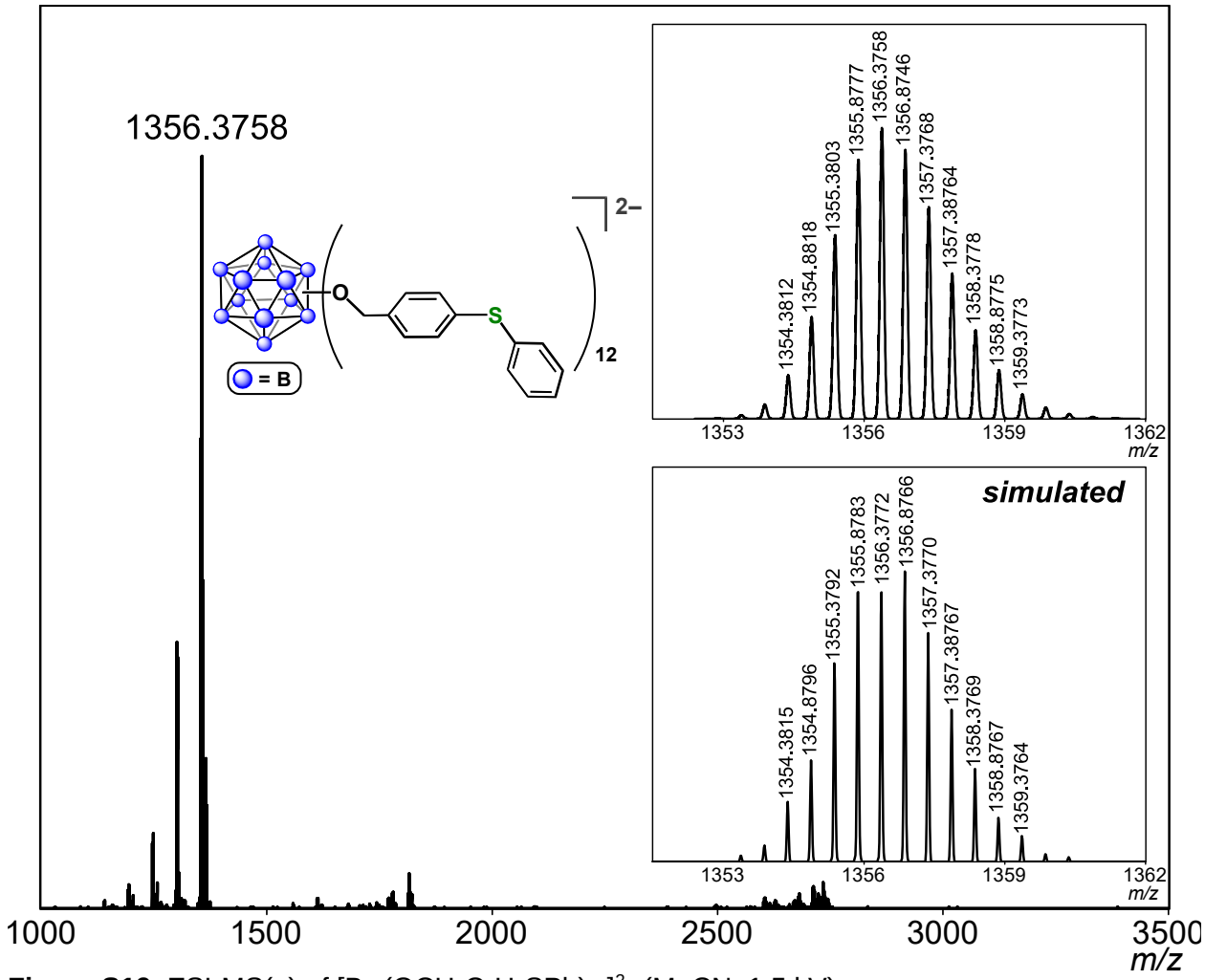

Figure S19. ESI-MS(–) of $[B_{12}(OCH_2C_6H_4SPh)_{12}]^{2-}$ (MeCN, 1.5 kV).

S2.7. $[K_2][B_{12}(OCH_2C_6H_4SC_6H_4I)_{12}]$ ($[K_2][3]$)

The general reaction procedure to generate $[\mathbf{1}][SbF_6]_{11}$ (**Section S2.5**) was followed. The DMF solution containing $[\mathbf{1}][SbF_6]_{11}$ (0.0014 mmol, 1 mL) was transferred to a vial containing solid K_3PO_4 (9 mg, 0.04 mmol, 30 equiv), *p*-iodothiophenol [1] (10 mg, 0.042 mmol, 30 equiv), and a Teflon-coated stir bar. The reaction mixture was allowed to stir at 25 °C for 15 min, during which time the color of the reaction mixture gradually changed from dark purple to colorless. All volatiles were then removed from the reaction mixture under reduced pressure with gentle heating (35 °C). The resulting colorless residue was suspended in a 65:35 hexanes:EtOAc mixture and loaded into a silica-packed pipette column. Using a 65:35 hexanes:EtOAc solvent combination, unreacted *p*-iodothiophenol and the (Me-DalPhos)AuCl byproduct were eluted first, followed by elution of the $[K_2][B_{12}(OCH_2C_6H_4SC_6H_4I)_{12}]$ product with DCM. The product fractions were combined, and all volatiles were removed *in vacuo* to afford $[K_2][B_{12}(OCH_2C_6H_4SC_6H_4I)_{12}]$ in 80% yield (5 mg, 0.001 mmol) as a colorless solid. ^{1}H NMR (400 MHz, 25 °C, acetone-d_6) δ: 7.55 (d, 24H, Ar-*H*, ^3J = 8 Hz), 7.41 (d, 24H, Ar-*H*, ^3J = 8 Hz), 7.16 (d, 24H, Ar-*H*, ^3J = 8 Hz), 6.92 (d, 24H, Ar-*H*, ^3J = 8 Hz), 5.52 (s, 24H, –C*H*$_2$–) ppm. ^{11}B{^{1}H} NMR (128 MHz, 25 °C, acetone-d_6) δ: -16.1 ppm. ESI-MS(–): 2111.7569 (calc'd, 2111.7606) *m/z*.

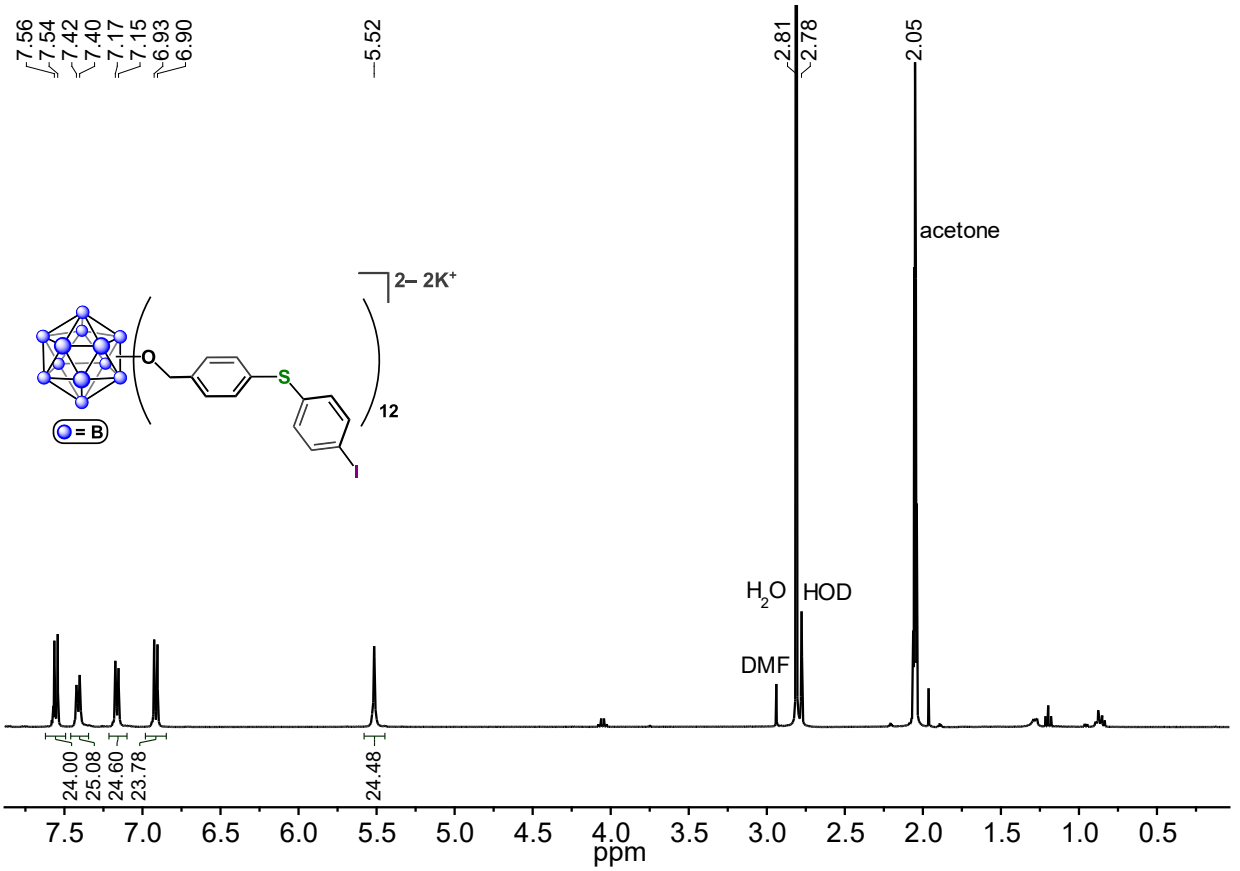

Figure S20. ^{1}H NMR spectrum of $[K_2][B_{12}(OCH_2C_6H_4SC_6H_4I)_{12}]$ (400 MHz, acetone-d_6, 25 °C).

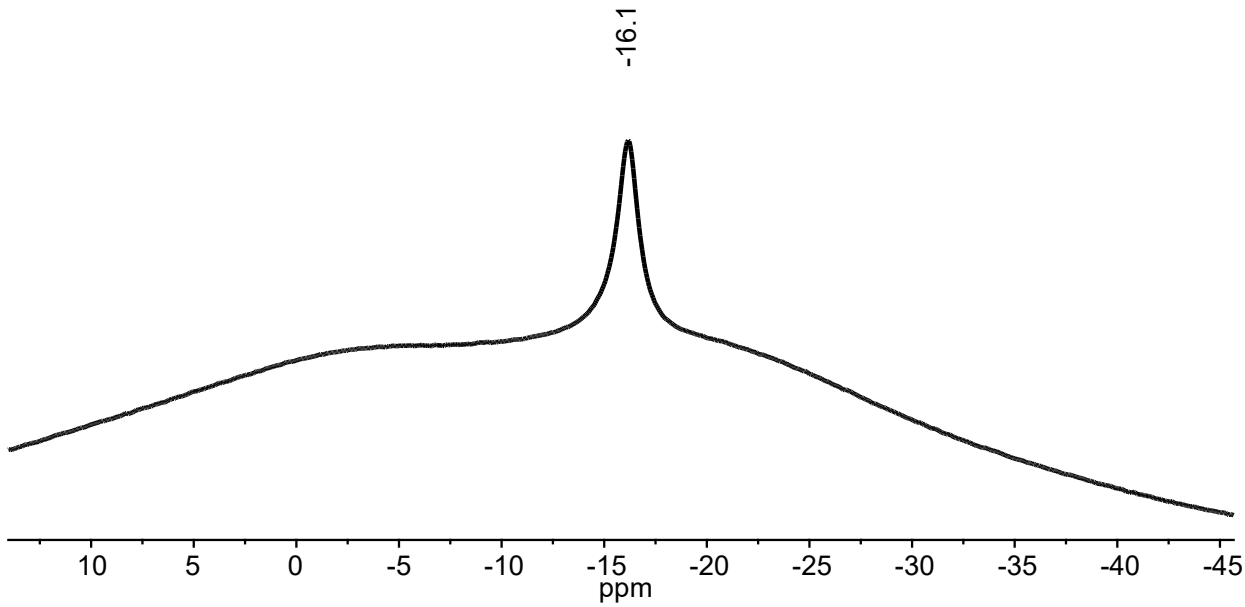

Figure S21. $^{11}B\{^{1}H\}$ NMR spectrum of $[K_2][B_{12}(OCH_2C_6H_4SC_6H_4I)_{12}]$ (128 MHz, acetone-d_6, 25 °C).

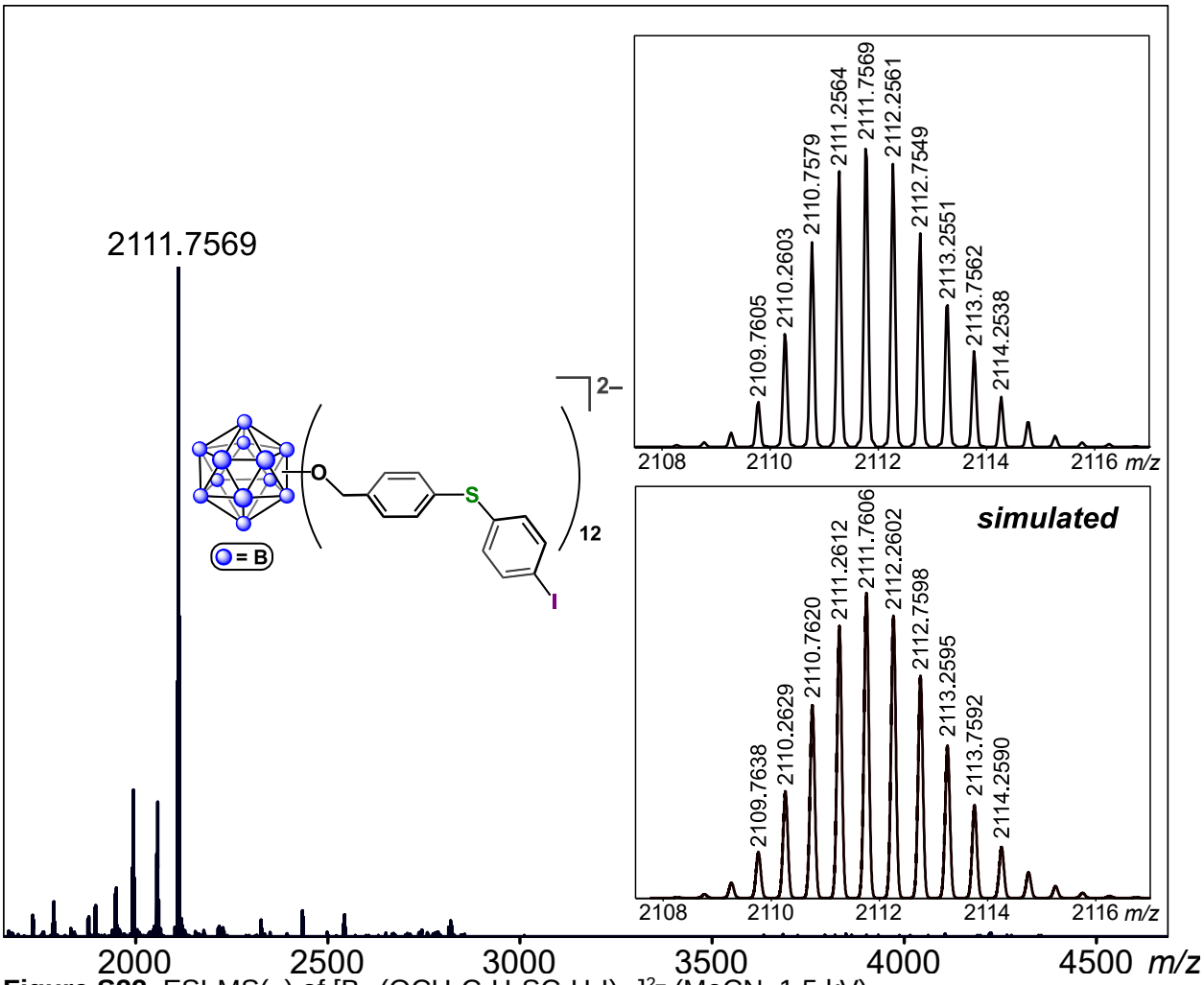

Figure S22. ESI-MS(–) of $[B_{12}(OCH_2C_6H_4SC_6H_4I)_{12}]^{2-}$ (MeCN, 1.5 kV).

S2.8. $[K_2][B_{12}(OCH_2C_6H_4SCH_2C_6H_5)_{12}]$ ($[K_2][4]$)

The general reaction procedure to generate $[\mathbf{1}][SbF_6]_{11}$ (**Section S2.5**) was followed. The DMF solution containing $[\mathbf{1}][SbF_6]_{11}$ (0.0014 mmol, 1 mL) was transferred to a vial containing solid K_3PO_4 (9 mg, 0.04 mmol, 30 equiv) and a Teflon-coated stir bar. To this solution was added a solution of benzylmercaptan (33 µL of a 0.85 M solution in MeCN, 0.028 mmol, 20 equiv) with stirring. The color of the reaction mixture gradually changed from dark purple to colorless over the course of 15 min, at which point all volatiles were removed under reduced pressure with gentle heating (35 °C). The resulting colorless residue was suspended in a 65:35 hexanes:EtOAc mixture and loaded into a silica-packed pipette column. Using a 65:35 hexanes:EtOAc solvent combination, unreacted benzylmercaptan and the (Me-DalPhos)AuCl byproduct were eluted first, followed by elution of the $[K_2][B_{12}(OCH_2C_6H_4SCH_2C_6H_5)_{12}]$ product with DCM. The product fractions were combined, and all volatiles were removed *in vacuo* to afford $[K_2][B_{12}(OCH_2C_6H_4SCH_2C_6H_5)_{12}]$ as a pale-pink residue in 70% yield (3 mg, 0.9 µmol). ^{1}H NMR (400 MHz, 25 °C, CD_2Cl_2) δ: 7.27–7.15 (m, 108H, Ar-*H*, all aromatic resonances overlapping), one C*H*$_2$ resonance overlapping with residual DCM solvent peak, 4.08 (s, 24H, –C*H*$_2$–) ppm. ^{11}B{^{1}H} NMR (128 MHz, 25 °C, CD_2Cl_2) δ: -15.7 ppm. ESI-MS(–): 1440.4703 (calc'd, 1440.4749) *m/z*.

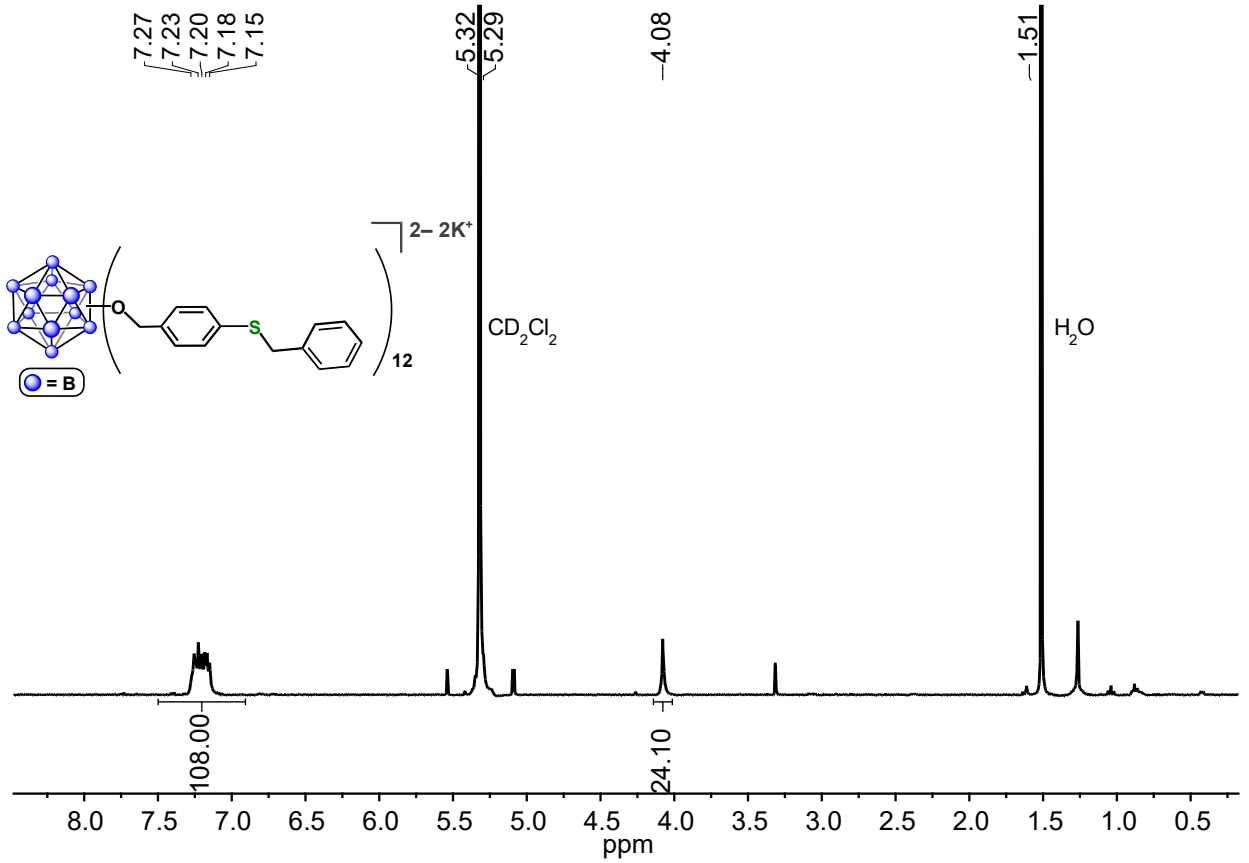

Figure S23. ^{1}H NMR spectrum of $[K_2][B_{12}(OCH_2C_6H_4SCH_2C_6H_5)_{12}]$ (400 MHz, CD_2Cl_2, 25 °C).

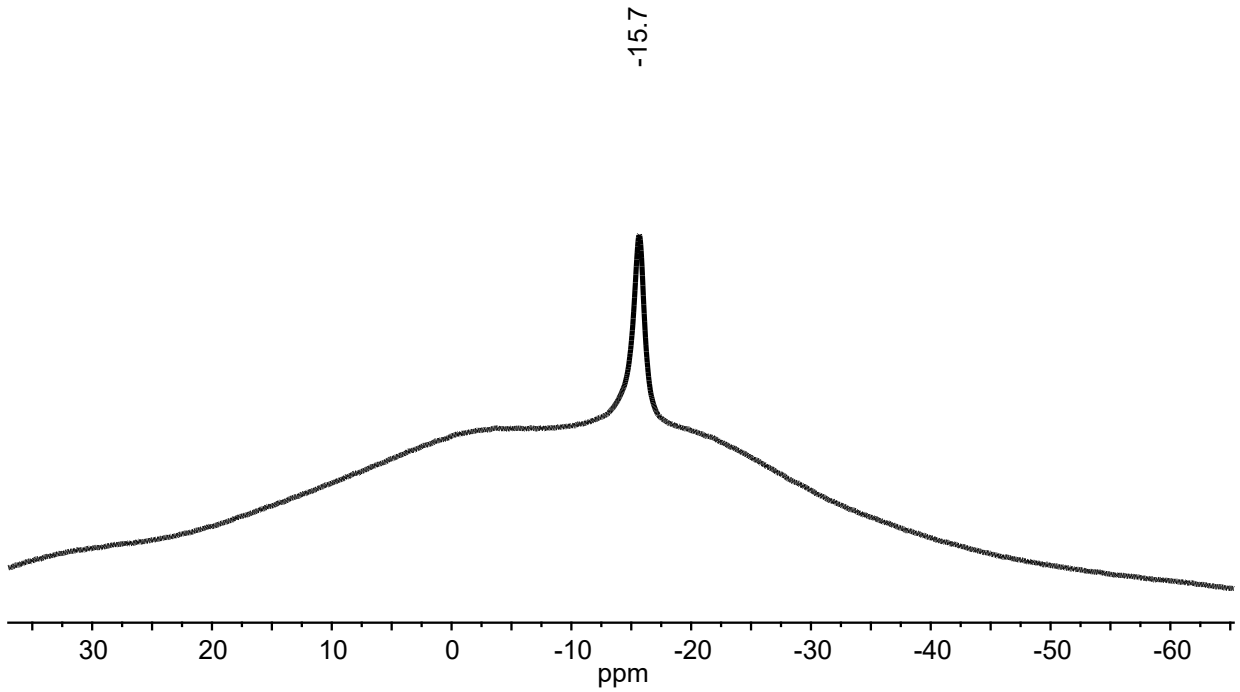

Figure S24. $^{11}B\{^{1}H\}$ NMR spectrum of $[K_2][B_{12}(OCH_2C_6H_4SCH_2C_6H_5)_{12}]$ (128 MHz, CD_2Cl_2, 25 °C).

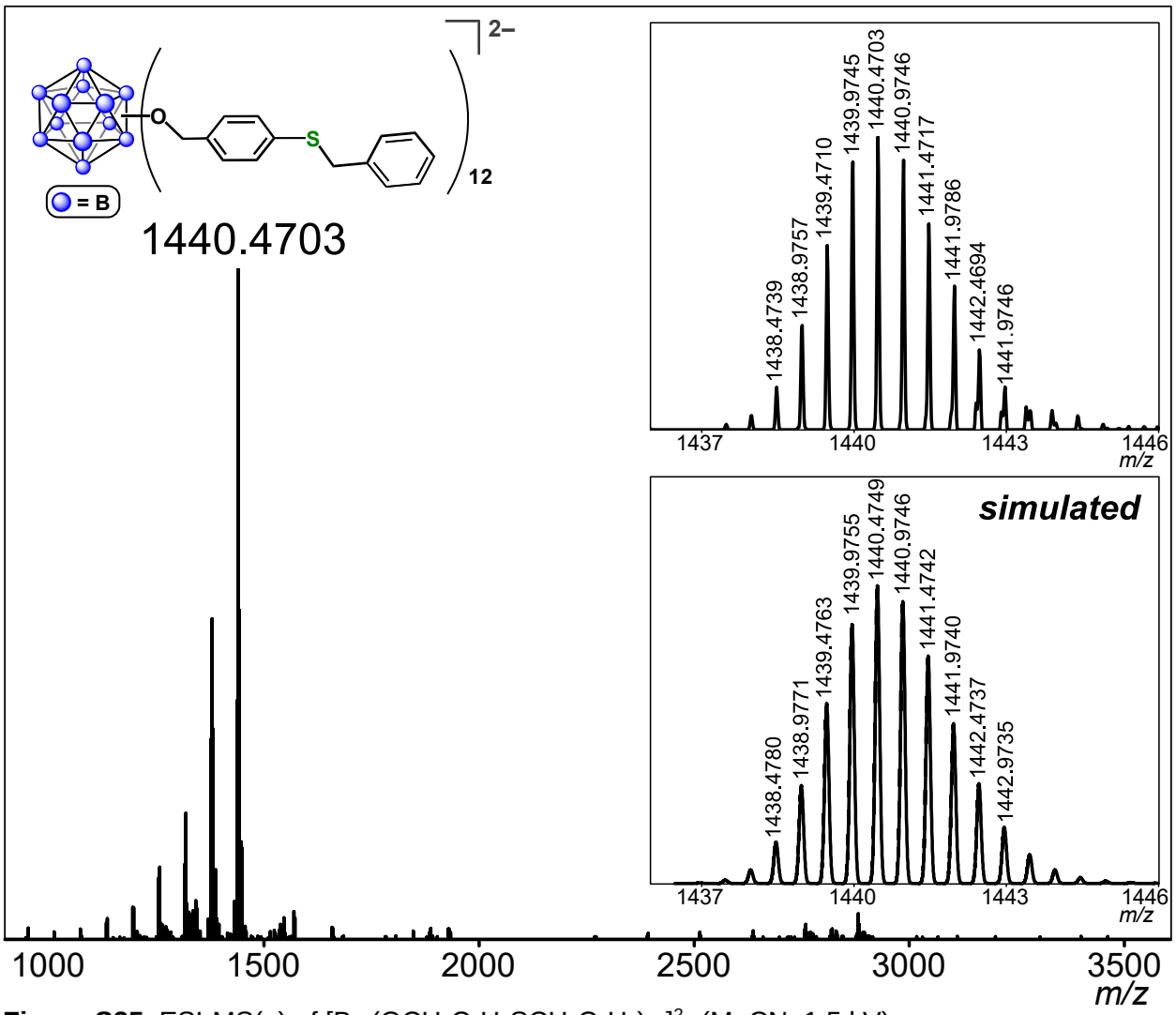

Figure S25. ESI-MS(–) of $[B_{12}(OCH_2C_6H_4SCH_2C_6H_5)_{12}]^{2-}$ (MeCN, 1.5 kV).

S2.9. $[K_2][B_{12}(OCH_2C_6H_4(\text{cyclohexanethiol}))_{12}]$ ($[K_2][5]$)

The general reaction procedure to generate $[\mathbf{1}][SbF_6]_{11}$ (**Section S2.5**) was followed. The DMF solution containing $[\mathbf{1}][SbF_6]_{11}$ (0.0014 mmol, 1 mL) was transferred to a vial containing solid K_3PO_4 (9 mg, 0.04 mmol, 30 equiv), and a Teflon-coated stir bar. To this solution was added a solution of cyclohexanethiol (50 µL of a 0.83 M solution in MeCN, 0.042 mmol, 30 equiv) with stirring. The color of the reaction mixture gradually changed from dark purple to colorless over the course of 15 min, at which point all volatiles were removed under reduced pressure with gentle heating (35 °C). The resulting colorless residue was suspended in an 80:20 hexanes:EtOAc mixture and loaded into a silica-packed pipette column. Using an 80:20 hexanes:EtOAc solvent combination, unreacted cyclohexanethiol and the (Me-DalPhos)AuCl byproduct were eluted first, followed by the $[K_2][B_{12}(OCH_2C_6H_4(\text{cyclohexanethiol}))_{12}]$ product. The product fractions were combined, and all volatiles were removed under reduced pressure to afford $[K_2][B_{12}(OCH_2C_6H_4(\text{cyclohexanethiol}))_{12}]$ as an oily pale-pink residue in 75% yield (3 mg, 0.001 mmol). ^{1}H NMR (400 MHz, 25 °C, acetone-d_6) δ: 7.29 (d, 24H, Ar-*H*, ^3J = 8 Hz), 7.18 (d, 24H, Ar-*H*, ^3J = 8 Hz), 5.45 (s, 24H, –C*H*$_2$–), 3.10–3.08 (m, 12H, S–C*H* cyclohexane),1.96–1.92 (m, 24H, cyclohexane), 1.77–1.74 (m, 24H, cyclohexane), 1.39–1.22 (m, 72H, cyclohexane) ppm. ^{11}B{^{1}H} NMR (128 MHz, 25 °C, acetone-d_6) δ: -15.1 ppm. ESI-MS(–): 1392.6616 (calc'd, 1392.6625) *m/z*.

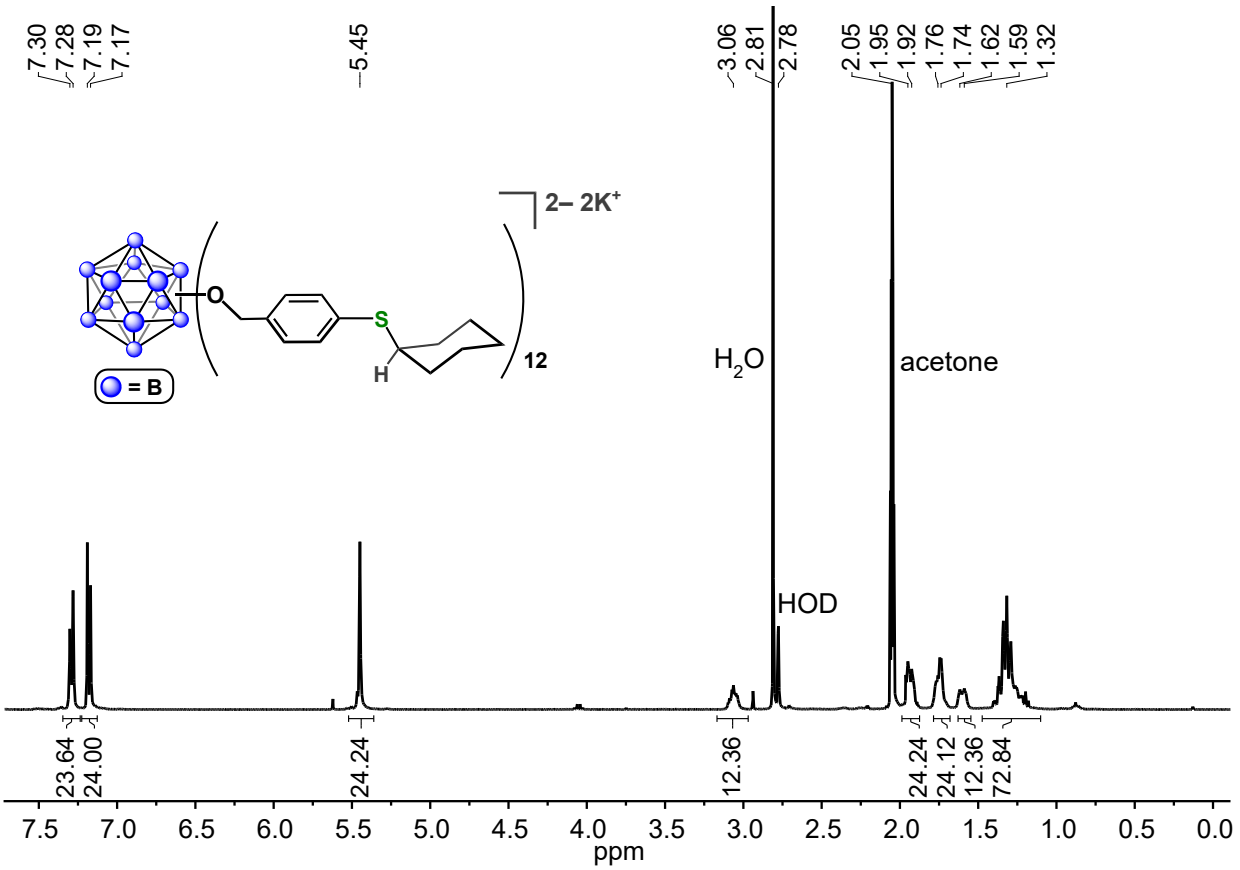

Figure S26. ^{1}H NMR spectrum of $[K_2][B_{12}(OCH_2C_6H_4(\text{cyclohexanethiol}))_{12}]$ (400 MHz, acetone-d_6, 25 °C).

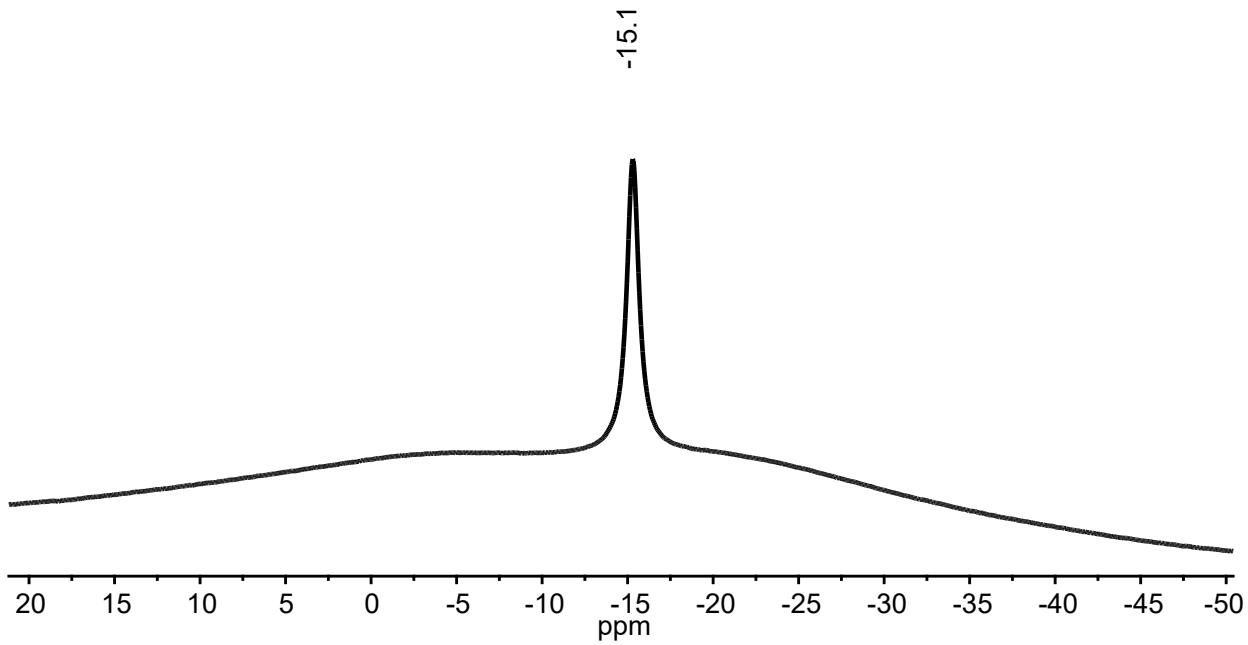

Figure S27. $^{11}B\{^{1}H\}$ NMR spectrum of $[K_2][B_{12}(OCH_2C_6H_4(cyclohexanethiol))_{12}]$ (128 MHz, acetone-d_6, 25 °C).

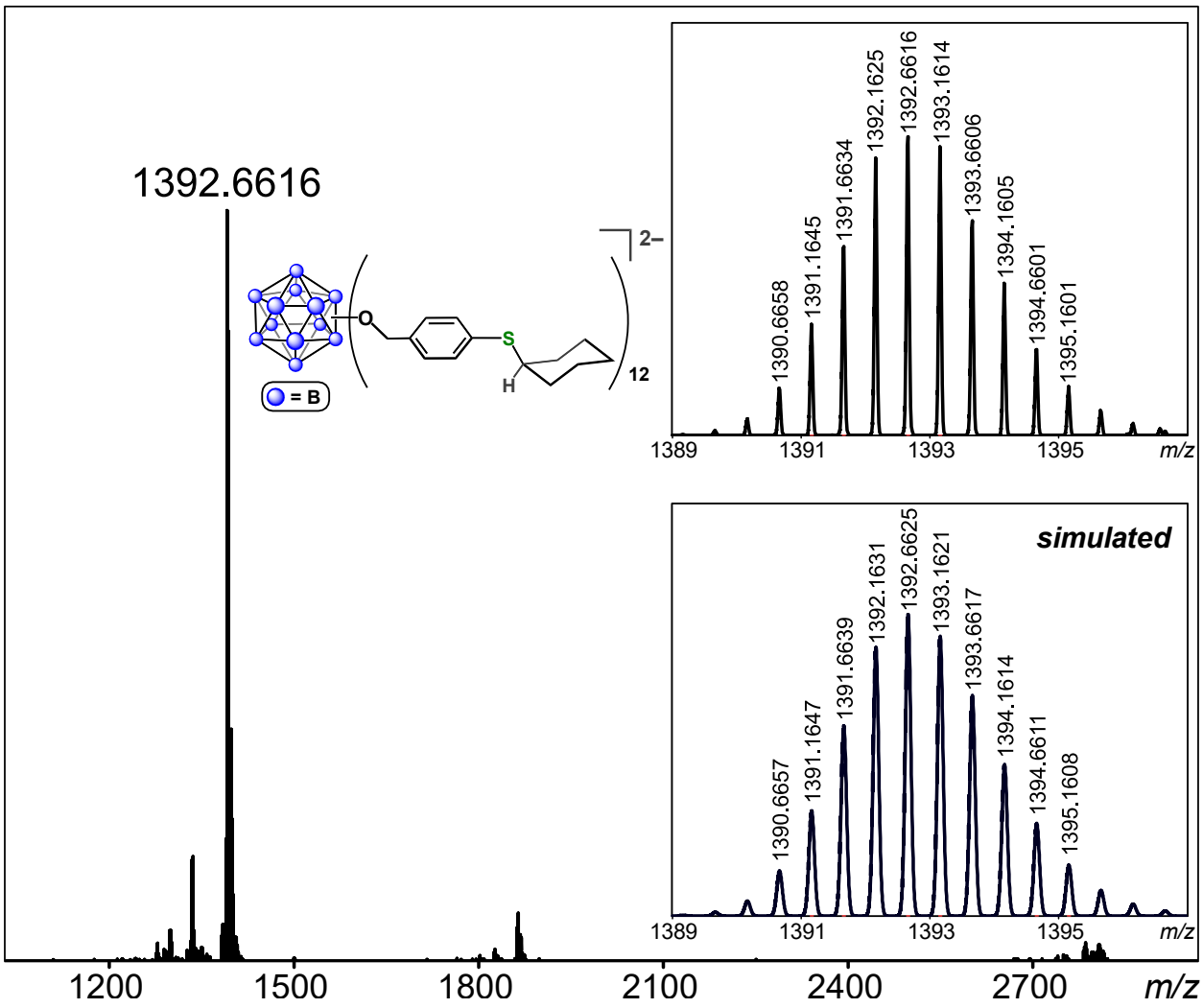

Figure S28. ESI-MS(–) of $[B_{12}(OCH_2C_6H_4(\text{cyclohexanethiol}))_{12}]^{2-}$ (MeCN, 1.5 kV).

S2.10. $[K_2][B_{12}(OCH_2C_6H_4(1\text{-thioglycerol}))_{12}]$ ($[K_2][6]$)

The general reaction procedure to generate $[\mathbf{1}][SbF_6]_{11}$ (**Section S2.5**) was followed. The DMF solution containing $[\mathbf{1}][SbF_6]_{11}$ (0.0014 mmol, 1 mL) was transferred to a vial containing solid K_3PO_4 (9 mg, 0.04 mmol, 30 equiv), and a Teflon-coated stir bar. To this solution was added a solution of 1-thioglycerol (36 µL of a 1.2 M solution in MeCN, 0.042 mmol, 30 equiv) with stirring. The color of the reaction mixture gradually changed from dark purple to colorless over the course of 15 min, at which point all volatiles were removed under reduced pressure with gentle heating (35 °C). The resulting colorless residue was suspended in an 65:35 hexanes:EtOAc mixture and loaded into a silica-packed pipette column. Using a 65:35 hexanes:EtOAc solvent combination, the (Me-DalPhos)AuCl byproduct was eluted first, followed by elution of unreacted 1-thioglycerol with acetone. The $[K_2][B_{12}(OCH_2C_6H_4(1\text{-thioglycerol}))_{12}]$ product was then eluted with MeOH. The fractions containing the product were combined and then all volatiles were removed under reduced pressure to afford $[K_2][B_{12}(OCH_2C_6H_4(1\text{-thioglycerol}))_{12}]$ in 50% yield (2 mg, 0.7 µmol) as a pale-pink oily solid. ^{1}H NMR (400 MHz, 25 °C, CD_3OD) δ: 7.24–7.18 (two sets of doublets overlapping, 48H, Ar-*H*), 5.35 (s, 24H, –C*H*$_2$–), 3.74–3.69 (m, 12H, –C*H*– glycerol), 3.62–3.53 (m, 24H, –C*H*$_2$– glycerol), 3.08–2.90 (m, 24H, –C*H*$_2$– glycerol) ppm. ^{11}B{^{1}H} NMR (128 MHz, 25 °C, CD_3OD) δ: -14.6 ppm. ESI-MS(–): 1344.4214 (calc'd, 1344.4129) *m/z*.

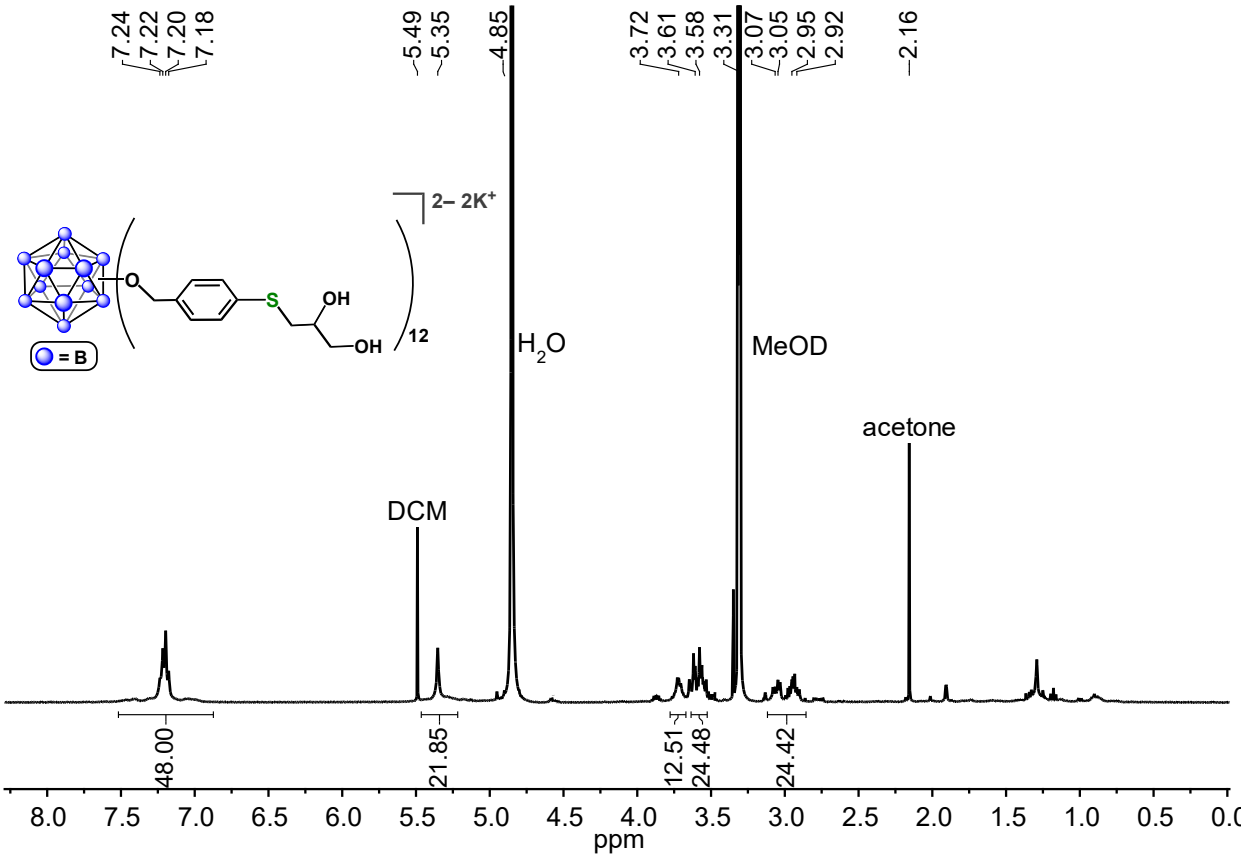

Figure S29. ^{1}H NMR spectrum of $[K_2][B_{12}(OCH_2C_6H_4(1\text{-thioglycerol}))_{12}]$ (400 MHz, CD_3OD, 25 °C).

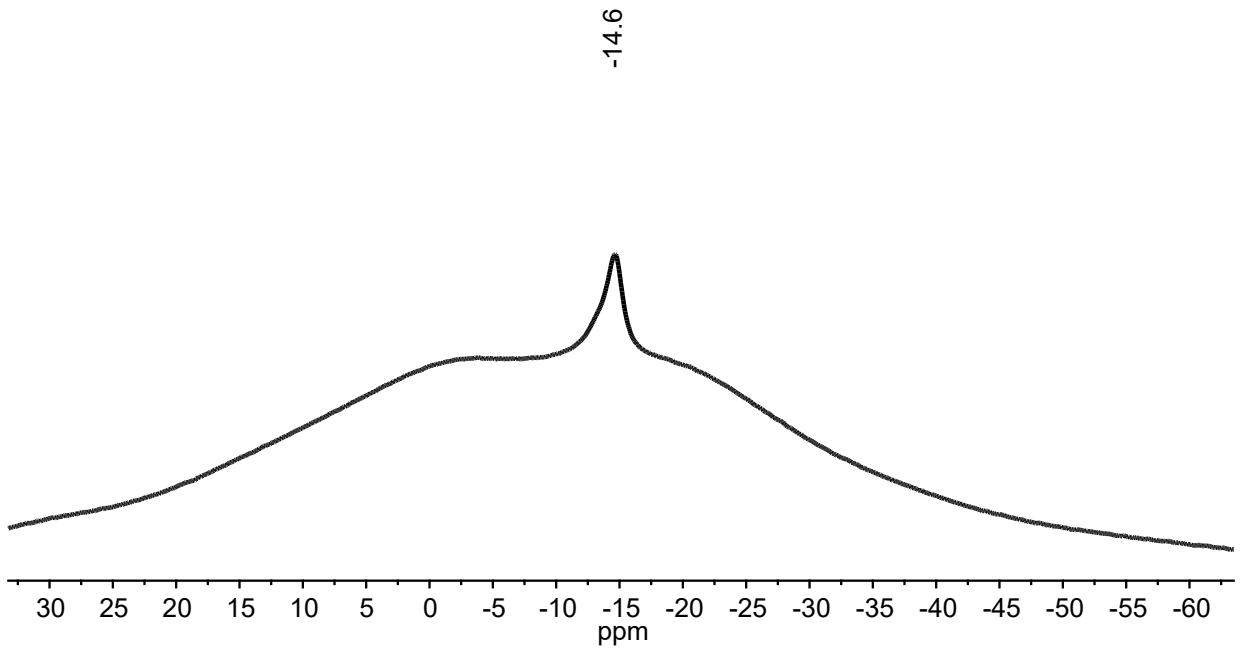

Figure S30. $^{11}B\{^{1}H\}$ NMR spectrum of $[K_2][B_{12}(OCH_2C_6H_4(1\text{-thioglycerol}))_{12}]$ (128 MHz, CD_3OD, 25 °C).

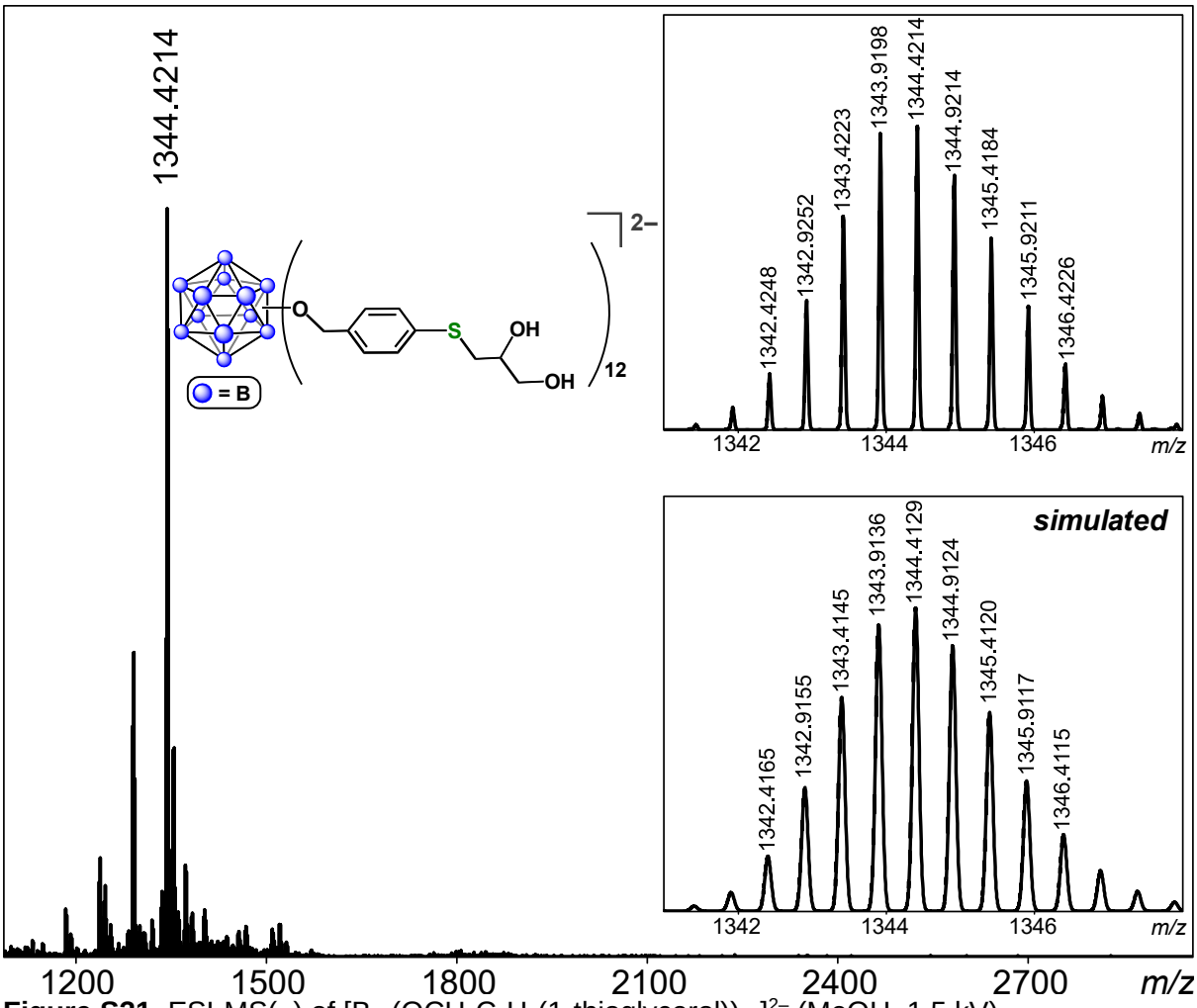

Figure S31. ESI-MS(–) of $[B_{12}(OCH_2C_6H_4(1\text{-thioglycerol}))_{12}]^{2-}$ (MeOH, 1.5 kV).

S2.11. $[K_2][B_{12}(OCH_2C_6H_4(2\text{-mercaptoethanol}))_{12}]$ ($[K_2][7]$)

The general reaction procedure to generate $[\mathbf{1}][SbF_6]_{11}$ (**Section S2.5**) was followed. The DMF solution containing $[\mathbf{1}][SbF_6]_{11}$ (0.0014 mmol, 1 mL) was transferred to a vial containing solid K_3PO_4 (9 mg, 0.04 mmol, 30 equiv), and a Teflon-coated stir bar. To this solution was added a solution of 2-mercaptoethanol (29 µL of a 1.4 M solution in MeCN, 0.042 mmol, 30 equiv) with stirring. The color of the reaction mixture gradually changed from dark purple to colorless over the course of 15 min, at which point all volatiles were removed under reduced pressure with gentle heating (35 °C). The resulting colorless residue was suspended in EtOAc and loaded into a silica-packed pipette column. The unreacted (Me-DalPhos)AuCl byproduct was eluted with EtOAc first, followed by elution of the $[K_2][B_{12}(OCH_2C_6H_4(2\text{-mercaptoethanol}))_{12}]$ product with acetone. The fractions containing the product were combined and then all volatiles were removed under reduced pressure to afford $[K_2][B_{12}(OCH_2C_6H_4(2\text{-mercaptoethanol}))_{12}]$ as a pale pink residue in 60% yield (2 mg, 0.8 µmol). ^{1}H NMR (400 MHz, 25 °C, acetone-d_6) δ: 7.29 (d, 24H, Ar-*H*, ^3J = 8 Hz), 7.18 (d, 24H, Ar-*H*, ^3J = 8 Hz), 5.45 (s, 24H, –C*H*$_2$–), 3.67 (t, 24H, C*H*$_2$-OH, ^3J = 6 Hz), 3.02 (t, 24H, C*H*$_2$-S, ^3J = 6 Hz) ppm. ^{11}B{^{1}H} NMR (128 MHz, 25 °C, acetone-d_6) δ: -15.1 ppm. ESI-MS(–): 1164.3479 (calc'd, 1164.3491) *m/z*.

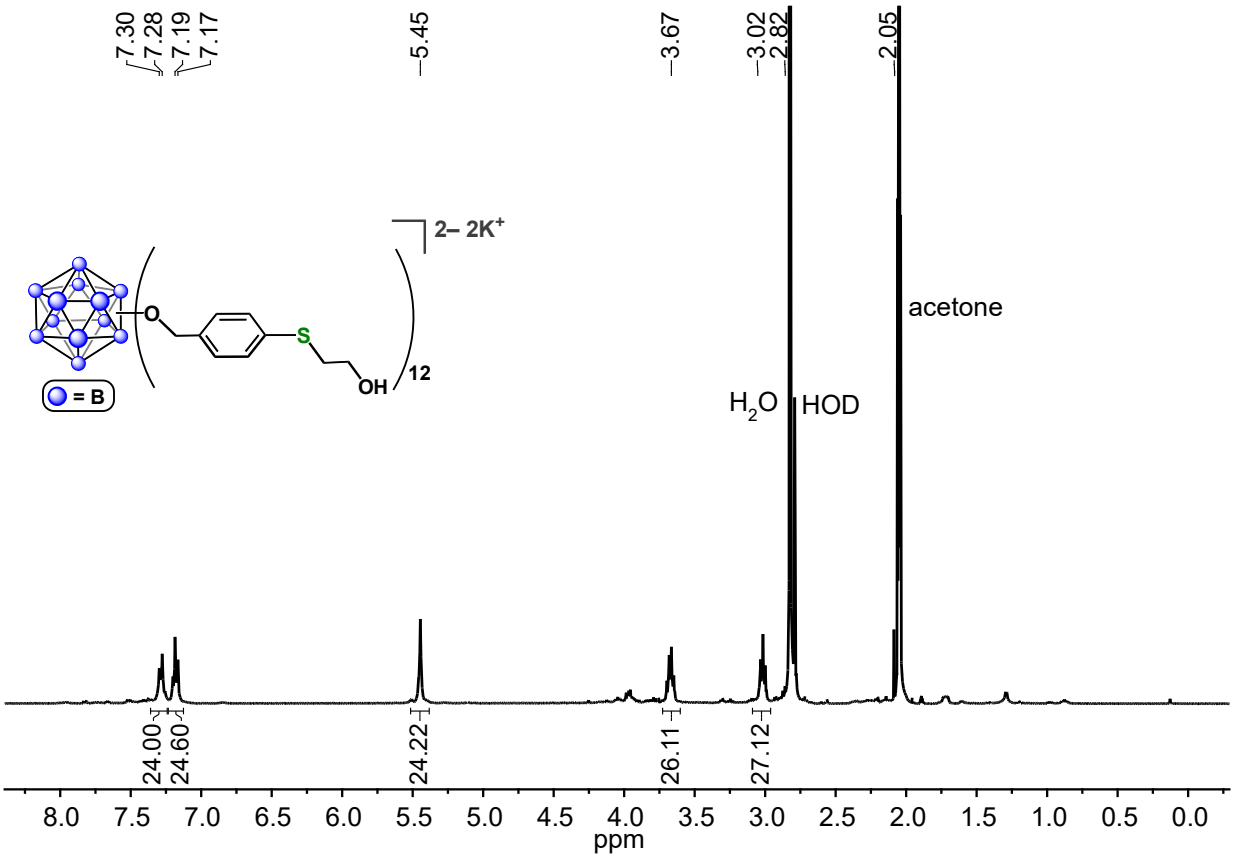

Figure S32. ^{1}H NMR spectrum of $[K_2][B_{12}(OCH_2C_6H_4(2\text{-mercaptoethanol}))_{12}]$ (400 MHz, acetone-d_6, 25 °C).

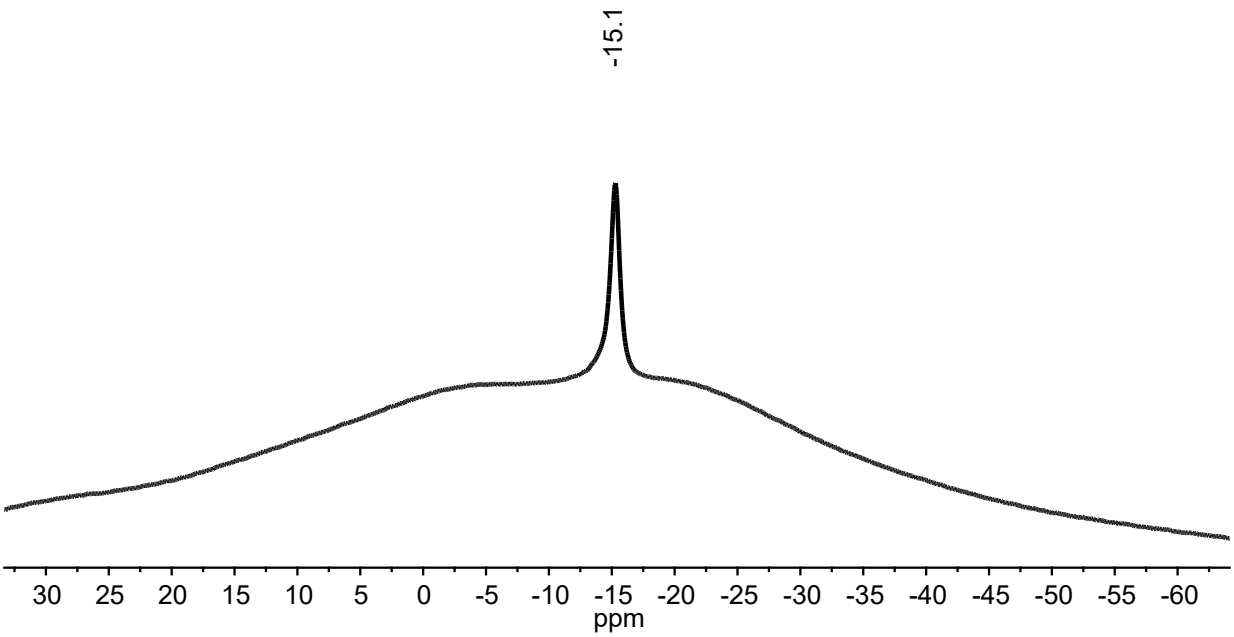

Figure S33. $^{11}B\{^{1}H\}$ NMR spectrum of $[K_2][B_{12}(OCH_2C_6H_4(2\text{-mercaptoethanol}))_{12}]$ (128 MHz, acetone-d_6, 25 °C).

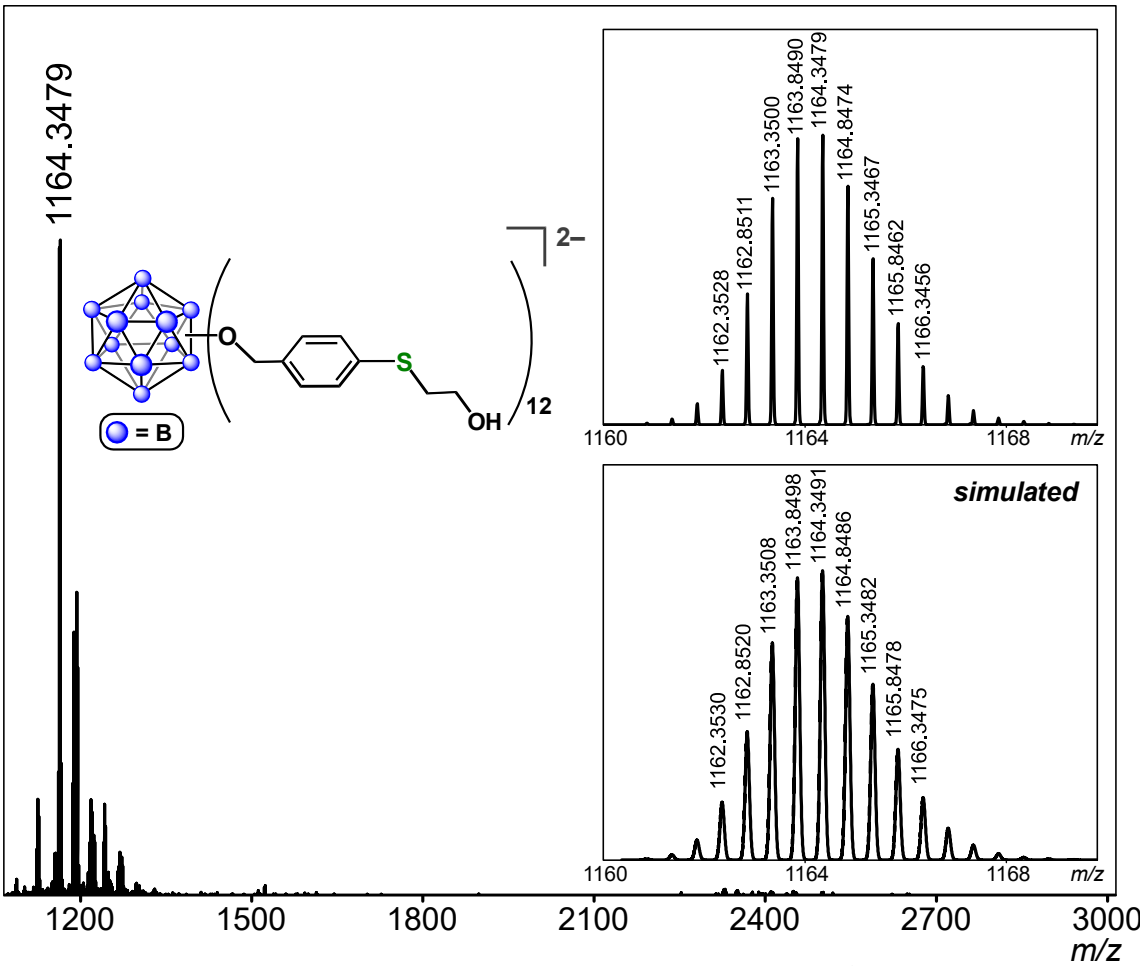

Figure S34. ESI-MS(–) of $[B_{12}(OCH_2C_6H_4(2\text{-mercaptoethanol}))_{12}]^{2-}$ (MeOH, 1.5 kV).

S2.12. $[K_2][B_{12}(OCH_2C_6H_4(mPEG_{350}\ thiol))_{12}]$ ($[K_2][8]$)

The general reaction procedure to generate [**1**][SbF_6]$_{11}$ (**Section S2.5**) was followed. The DMF solution containing [**1**][SbF_6]$_{11}$ (0.0014 mmol, 1 mL) was transferred to a vial containing solid K_3PO_4 (9 mg, 0.04 mmol, 30 equiv), and a Teflon-coated stir bar. To this solution was added a solution of *m*PEG$_{350}$ thiol (*O*-(2-Mercaptoethyl)-*O'*-methyl-hexa(ethylene glycol) purchased from Sigma Aldrich) (15 mg, 0.042 mmol, 30 equiv) in H_2O (0.5 mL) with stirring. The reaction mixture was allowed to stir at 25 °C for 20 min, during which time the color changed from purple to colorless. All volatiles were then removed under reduced pressure with gentle heating (35 °C). The resulting residue was dissolved in MeOH (0.5 mL) and loaded into a column packed with Sephadex LH20 medium in MeOH. The pure product was eluted as a pale pink band first, followed by elution of fractions containing (Me-DalPhos)AuCl and unreacted *m*PEG$_{350}$ thiol. The fractions containing the pure product were combined, and all volatiles were removed under reduced pressure to afford $[K_2][B_{12}(OCH_2C_6H_4(mPEG_{350}\ thiol))_{12}]$ as an oily pink residue (6 mg, 0.001 mmol, 75%). ^{1}H NMR (400 MHz, 25 °C, CD_3OD) δ: 7.25 (d, 24H, Ar-*H*, ^3J = 8 Hz), 7.17 (d, 24H, Ar-*H*, ^3J = 8 Hz), 5.37 (s, 24H, –C*H*$_2$–), 3.64–3.56 (m, 312H, *m*PEG$_{350}$), 3.48 (m, 36H, *m*PEG$_{350}$), 3.06 (t, 24H, *m*PEG$_{350}$, ^3J = 7 Hz) ppm. ^{11}B{^{1}H} NMR (128 MHz, 25 °C, CD_3OD) δ: -14.4 ppm. ESI-MS(–): 2833.8776 (calc'd, 2833.8900) *m/z*.

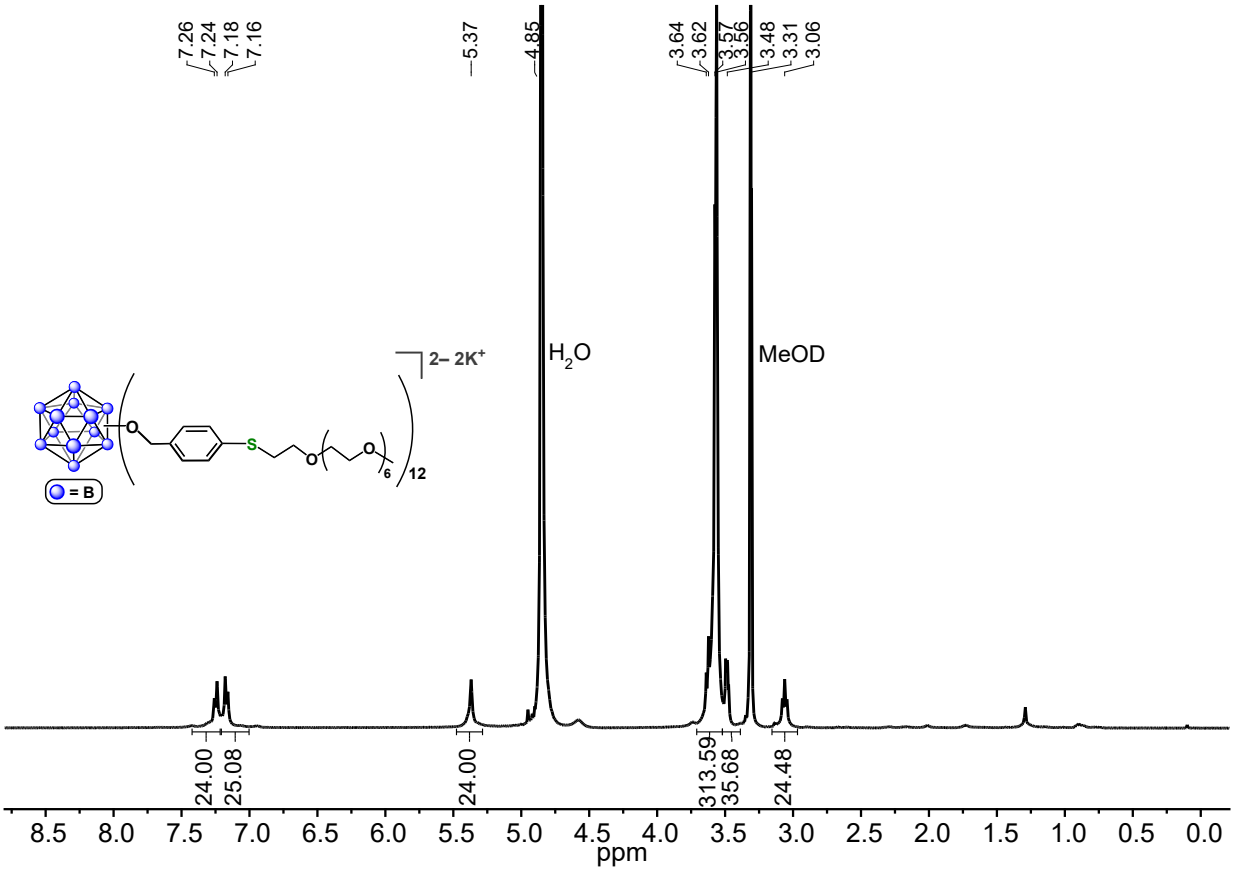

Figure S35. ^{1}H NMR spectrum of $[K_2][B_{12}(OCH_2C_6H_4(mPEG_{350}\ thiol))_{12}]$ (CD_3OD, 400 MHz, 25 °C).

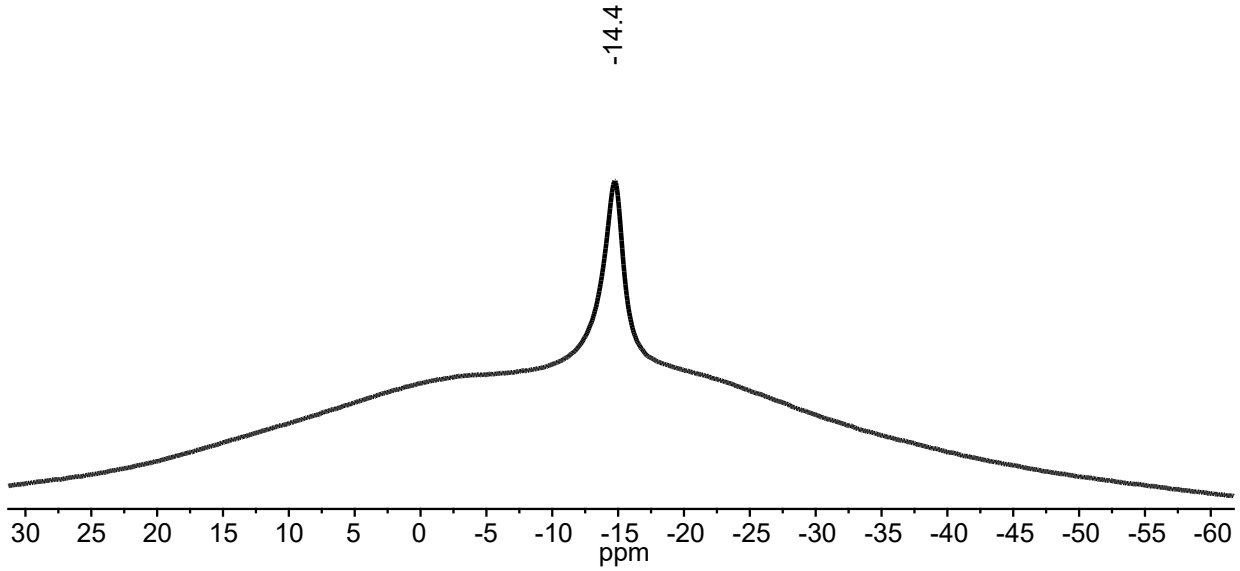

Figure S36. $^{11}B\{^{1}H\}$ NMR spectrum of $[K_2][B_{12}(OCH_2C_6H_4(m\text{PEG}_{350}\text{ thiol}))_{12}]$ (128 MHz, CD_3OD, 25 °C).

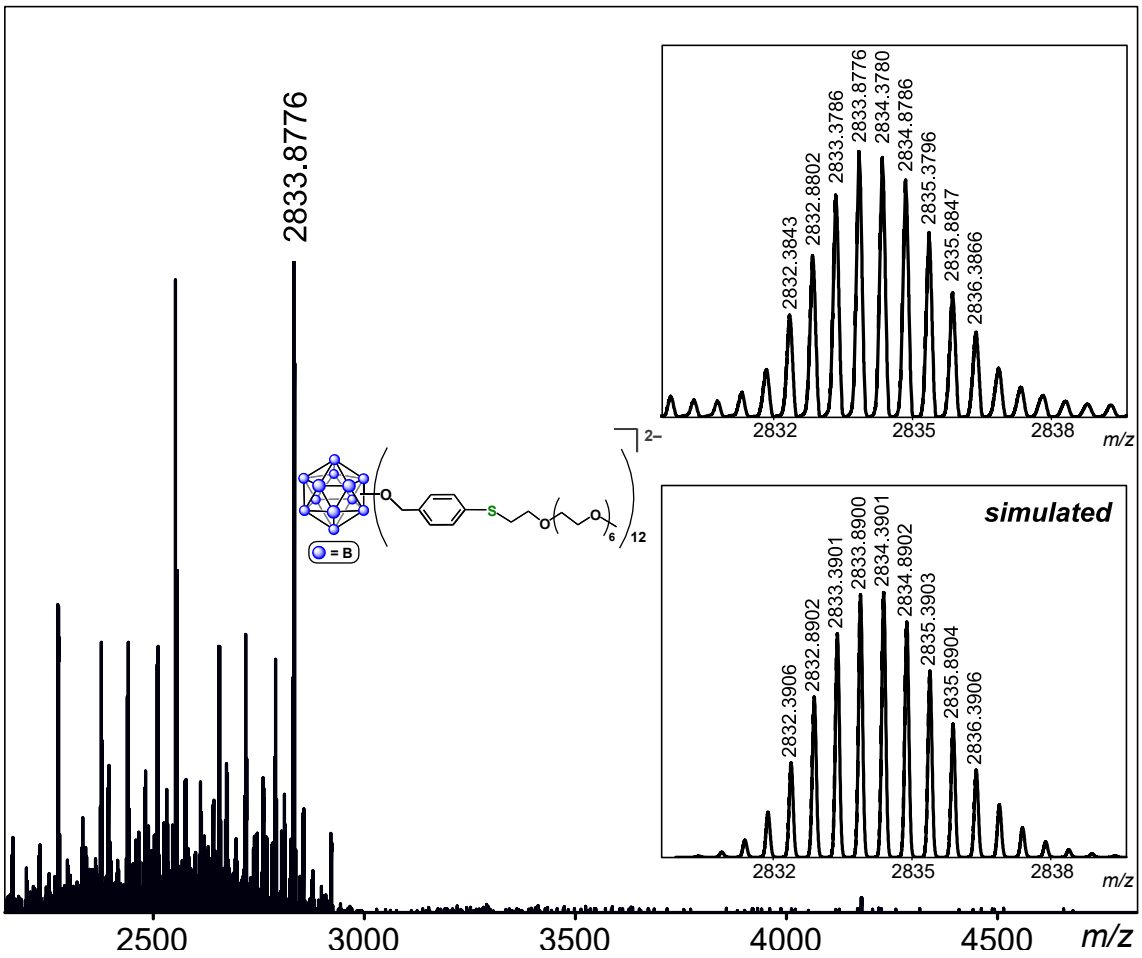

Figure S37. ESI-MS(–) of $[B_{12}(OCH_2C_6H_4(m\text{PEG}_{350}\text{ thiol}))_{12}]^{2-}$ (MeOH, 1.5 kV). A significant amount of fragmentation of the PEG polymer ($-OCH_2CH_2-$ units) is observed under ESI-MS conditions.

S2.13. $[Na_{14}][B_{12}(OCH_2C_6H_4(2\text{-thioethanesulfonate}))_{12}]$ ($[Na_{14}][9]$)

The general reaction procedure to generate $[\mathbf{1}][SbF_6]_{11}$ (**Section S2.5**) was followed. To a stirring solution of $[\mathbf{1}][SbF_6]_{11}$ (0.0014 mmol) and Na_3PO_4 (7 mg, 0.04 mmol, 30 equiv) in DMF (1 mL) was added a solution of sodium 2-mercaptoethanesulfonate (7 mg, 0.04 mmol, 30 equiv) in H_2O (1 mL). The purple reaction mixture was allowed to stir at 25 °C for a total of 15 min, during which time the solution gradually became colorless. All volatiles were then removed from the reaction mixture under reduced pressure. The resulting pale pink residue was suspended in H_2O (4 mL), sonicated for 10 min, and then centrifuged (2,200 × g, 5 min). The supernatant was removed and filtered through a 0.45 µm PTFE syringe filter and into a Pall Microsep™ Advance 1K Omega Centrifugal Filter sample reservoir.* The device was capped and centrifuged for 75 min at 7,500 × g. The device was then removed from the centrifuge, the solution in the filtrate receiver tube removed, and H_2O (5 mL) was added to the sample reservoir containing the aqueous solution of the product. This process was repeated twice more for a total of three centrifuge cycles. After the third cycle, the solution in the sample reservoir (ca. 0.5 mL) was removed, transferred to a 15 mL conical tube, and the H_2O was lyophilized overnight to afford $[Na_{14}][B_{12}(OCH_2C_6H_4(2\text{-thioethanesulfonate}))_{12}]$ as a pale-pink powder (3 mg, 0.9 µmol, 60%). ^{1}H NMR (400 MHz, 25 °C, D_2O) δ: 7.24 (two sets of doublets overlapping, 48H, Ar-*H*), 5.31 (s, 24H, –C*H*$_2$–), 3.33–3.26 (m, 24H, –C*H*$_2$–), 3.19–3.13 (m, 24H, –C*H*$_2$–) ppm. ^{11}B{^{1}H} NMR (128 MHz, 25 °C, D_2O) δ: -15.4 ppm. ESI-MS(–): 537.5129 ($[B_{12}(OCH_2C_6H_4(2\text{-thioethanesulfonate}))_{12}]^{14-}$ + $6Na^+$ + $2H^+]^{6-}$; calc'd, 537.5170) *m/z*.

*It is noted that prior to sample purification, the Pall Microsep™ Advance 1K Omega Centrifugal Filter was pre rinsed by filtering HPLC-grade H_2O (5 mL) through the device at 7,500 × g for 15 min. The filtrate was discarded prior to use.

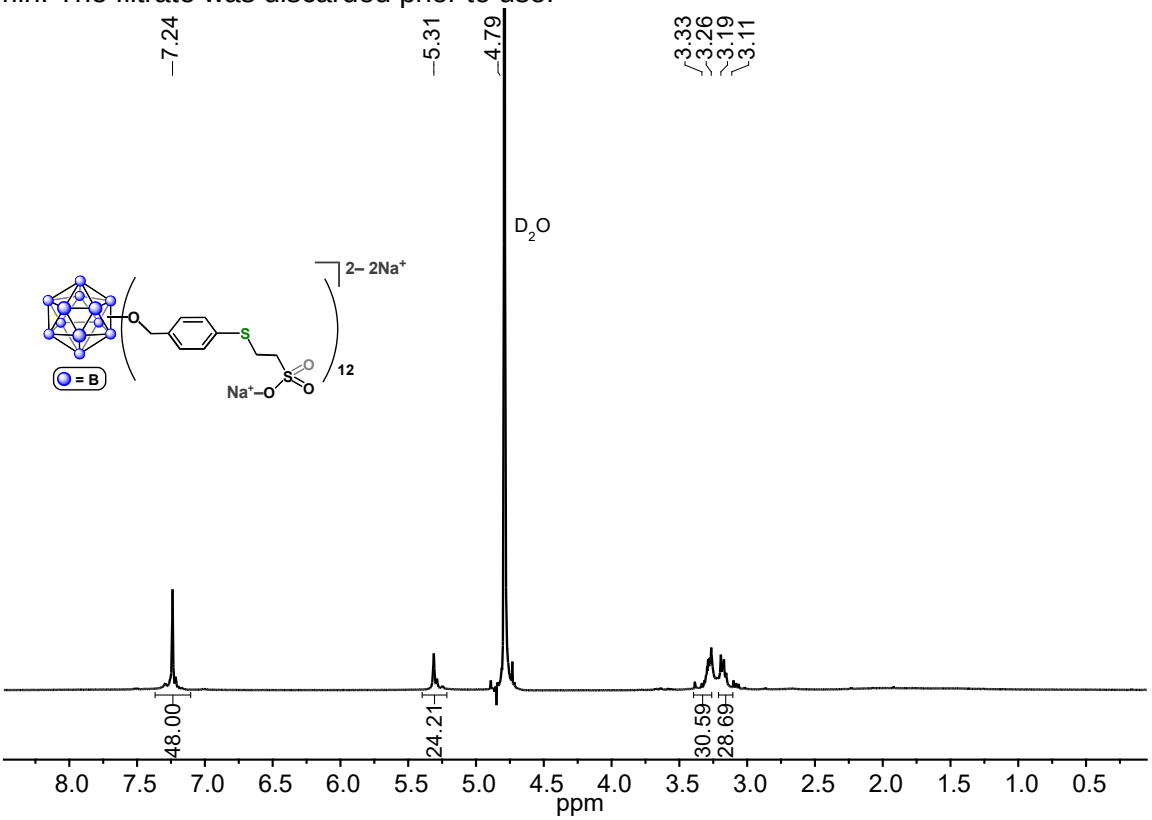

Figure S38. ^{1}H NMR spectrum of $[Na]_{14}[B_{12}(OCH_2C_6H_4(2\text{-thioethanesulfonate}))_{12}]$ (D_2O, 400 MHz, 25 °C).

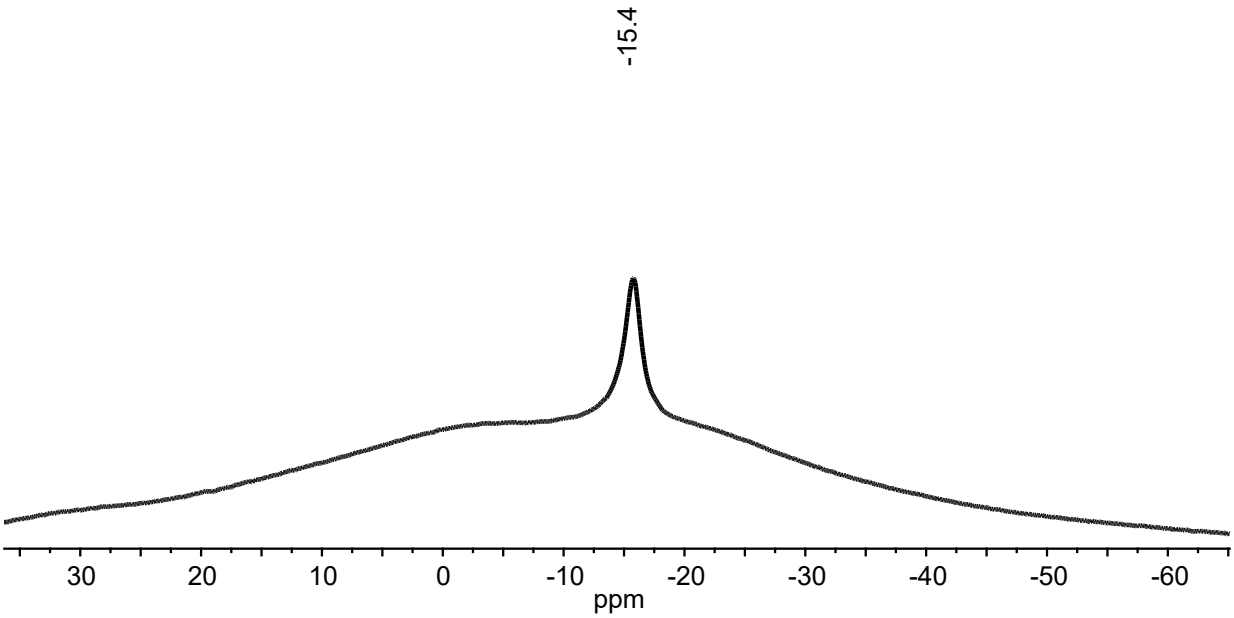

Figure S39. $^{11}B\{^{1}H\}$ NMR spectrum of $[Na]_{14}[B_{12}(OCH_2C_6H_4(2\text{-thioethanesulfonate}))_{12}]$ (D_2O, 128 MHz, 25 °C).

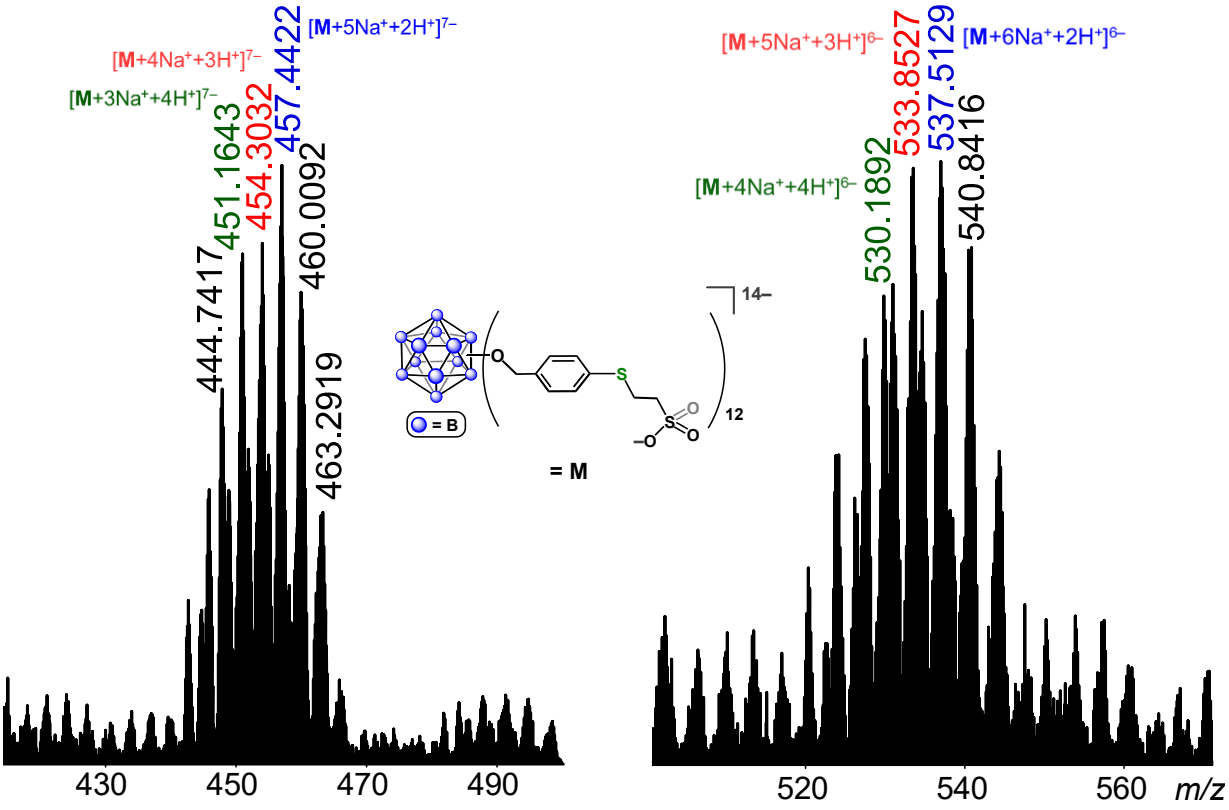

Figure S40. ESI-MS(–) of $[B_{12}(OCH_2C_6H_4(2\text{-thioethanesulfonate}))_{12}]^{14-}$ (MeOH, 1.5 kV) showing a distribution of species with charge-compensating cations (Na^+ and H^+) due to the highly anionic nature of the $[B_{12}(OCH_2C_6H_4(2\text{-thioethanesulfonate}))_{12}]^{14-}$ cluster.

S2.14. $[H_3NC(CH_2OH)_3/Na]_{14}[B_{12}(OCH_2C_6H_4(2\text{-thioethanesulfonate}))_{12}]$ ($[H_3NC(CH_2OH)_3/Na]_{14}$[9])

The general reaction procedure to generate [**1**][SbF_6]$_{11}$ (**Section S2.5**) was followed. To a stirring solution of [**1**][SbF_6]$_{11}$ (0.0014 mmol) in DMF (1 mL) was added sodium 2-mercaptoethanesulfonate (7 mg, 0.04 mmol, 30 equiv) in an aqueous solution of TRIS buffer (0.5 mL of a 200 mM solution, pH 8). The purple reaction mixture was allowed to stir at 25 °C for a total of 15 min, at which point all volatiles were removed under reduced pressure. The resulting purple residue was suspended in H_2O (4 mL), sonicated for 10 min, and then centrifuged (2,200 × g, 5 min). The purple supernatant was removed and filtered through a 0.45 µm PTFE filter into a Pall Microsep™ Advance 1K Omega Centrifugal Filter sample reservoir.* The device was capped and centrifuged for 75 min at 7,500 × g. The device was then removed from the centrifuge, the solution in the filtrate receiver tube removed, and H_2O (5 mL) was added to the sample reservoir containing the aqueous solution of the product. This process was repeated twice more for a total of three centrifuge cycles. After the third cycle, the solution in the sample reservoir (ca. 0.5 mL) was removed, transferred to a 15 mL conical tube, and the H_2O was lyophilized overnight to afford $[H_3NC(CH_2OH)_3/Na]_{14}[B_{12}(OCH_2C_6H_4(2\text{-thioethanesulfonate}))_{12}]$ as a light purple powder (4 mg). ^{1}H NMR (400 MHz, 25 °C, D_2O) δ: 7.24 (two sets of doublets overlapping, 48H, Ar-*H*), 5.32 (s, 24H, –C*H*$_2$–), 3.68 (s, 60H, [$H_3NC(CH_2OH)_3$]), 3.30–3.26 (m, 24H, –C*H*$_2$–), 3.19–3.16 (m, 24H, –C*H*$_2$–) ppm. ^{11}B{^{1}H} NMR (128 MHz, 25 °C, D_2O) δ: -15.4 ppm.

*It is noted that prior to sample purification, the Pall Microsep™ Advance 1K Omega Centrifugal Filter was pre rinsed by filtering HPLC-grade H_2O (5 mL) through the device at 7,500 × g for 15 min. The filtrate was discarded prior to use.

This reaction can be conducted using TRIS buffer as the base to generate the mixed cation species described above, or with Na_3PO_4 as the base to prepare the $[Na]_{14}[B_{12}(OCH_2C_6H_4(2\text{-thioethanesulfonate}))_{12}]$ salt as described in **Section S2.13.

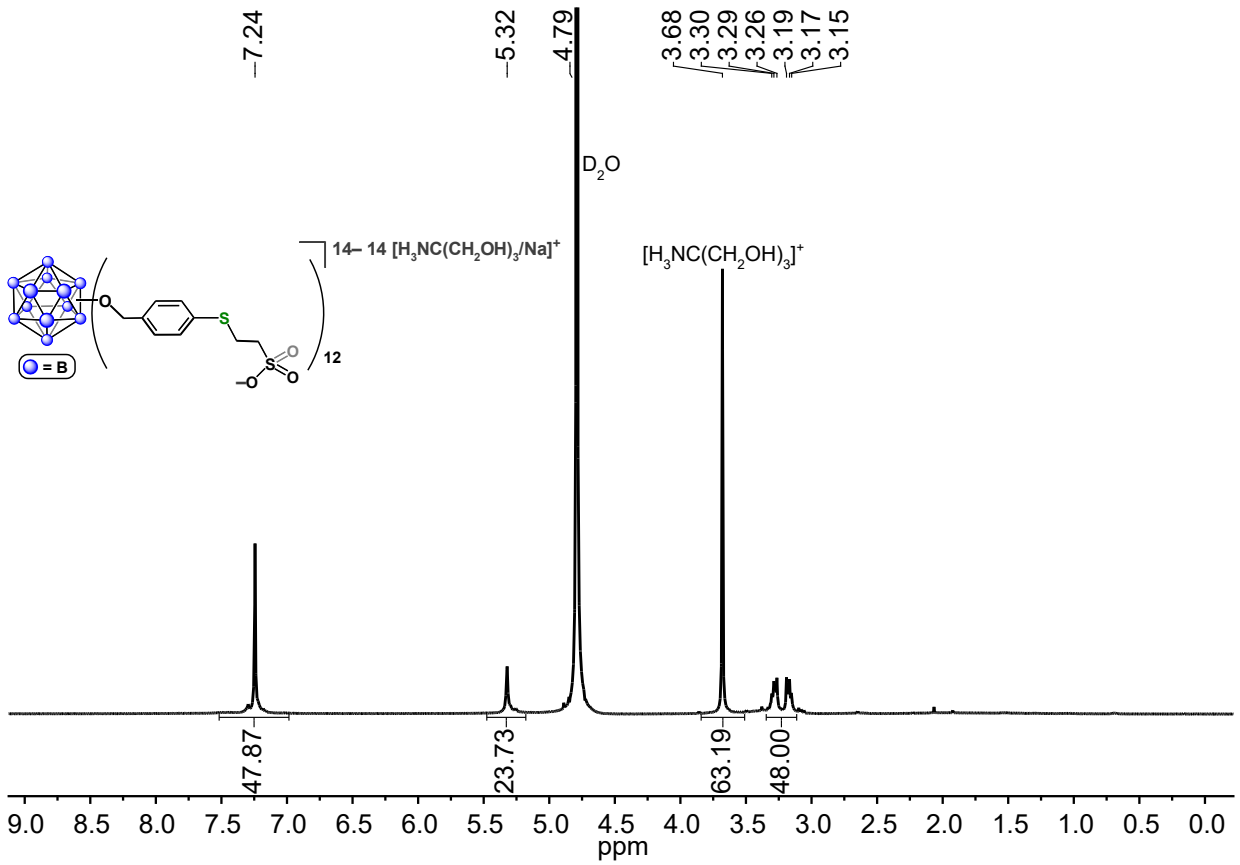

Figure S41. ^{1}H NMR spectrum of $[H_3NC(CH_2OH)_3/Na]_{14}[B_{12}(OCH_2C_6H_4(2\text{-thioethanesulfonate}))_{12}]$ (D_2O, 400 MHz, 25 °C).

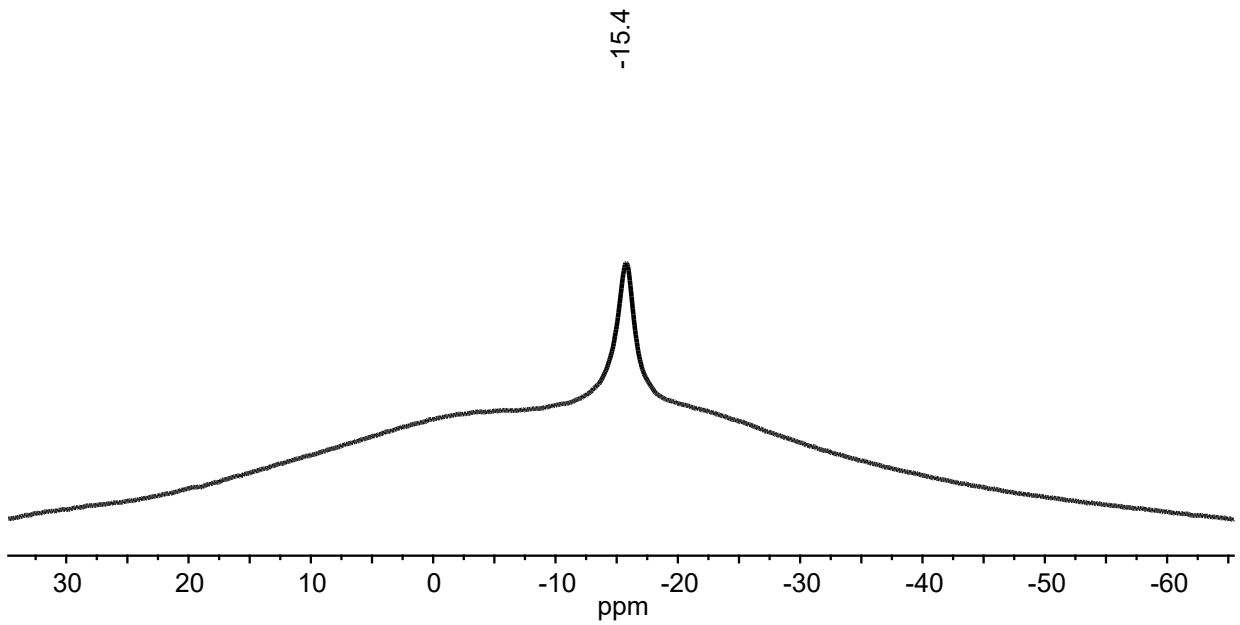

Figure S42. $^{11}B\{^{1}H\}$ NMR spectrum of $[H_3NC(CH_2OH)_3/Na]_{14}[B_{12}(OCH_2C_6H_4(2\text{-thioethanesulfonate}))_{12}]$ (D_2O, 128 MHz, 25 °C).

S2.15. $[K_2][B_{12}(OCH_2C_6H_4S(CH_2)_5CH_3)_{12}]$ ($[K_2][10]$)

The general reaction procedure to generate $[\mathbf{1}][SbF_6]_{11}$ (**Section S2.5**) was followed. The DMF solution containing $[\mathbf{1}][SbF_6]_{11}$ (0.0014 mmol, 1 mL) was transferred to a vial containing solid K_3PO_4 (9 mg, 0.04 mmol, 30 equiv), and a Teflon-coated stir bar. To this solution was added a solution of hexanethiol (60 µL of a 0.70 M solution in MeCN, 0.042 mmol, 30 equiv) with stirring. The color of the reaction mixture gradually changed from dark purple to colorless over the course of 20 min, at which point all volatiles were removed under reduced pressure with gentle heating (35 °C). The resulting colorless residue was suspended in an 80:20 hexanes:EtOAc mixture and loaded into a silica-packed pipette column. Using an 80:20 hexanes:EtOAc solvent combination, unreacted hexanethiol and the (Me-DalPhos)AuCl byproduct were eluted first, followed by elution of the $[K_2][B_{12}(OCH_2C_6H_4S(CH_2)_5CH_3)_{12}]$ product. The product fractions were combined, and all volatiles were removed under reduced pressure to afford $[K_2][B_{12}(OCH_2C_6H_4S(CH_2)_5CH_3)_{12}]$ as a pale-pink oily residue in 80% yield (3 mg, 0.001 mmol). ^{1}H NMR (400 MHz, 25 °C, acetone-d_6) δ: 7.29 (d, 24H, Ar-*H*, ^3J = 8 Hz), 7.13 (d, 24H, Ar-*H*, ^3J = 8 Hz), 5.44 (s, 24H, –C*H*$_2$–), 2.89 (t, 24H, S–C*H*$_2$–CH$_2$, ^3J = 7 Hz), 1.60 (quin, 24H, CH$_2$–C*H*$_2$–CH$_2$, ^3J = 7 Hz), 1.44 (quin, 24H, CH$_2$–C*H*$_2$–CH$_2$, ^3J = 7 Hz), 1.29 (m, 48H, CH$_2$–(C*H*$_2$)$_2$–CH$_3$), 0.88 (t, 24H, CH$_2$–C*H*$_3$, ^3J = 7 Hz) ppm. ^{11}B{^{1}H} NMR (128 MHz, 25 °C, acetone-d_6) δ: -15.3 ppm. ESI-MS(–): 1404.7557 (calc'd, 1404.7564) *m/z*.

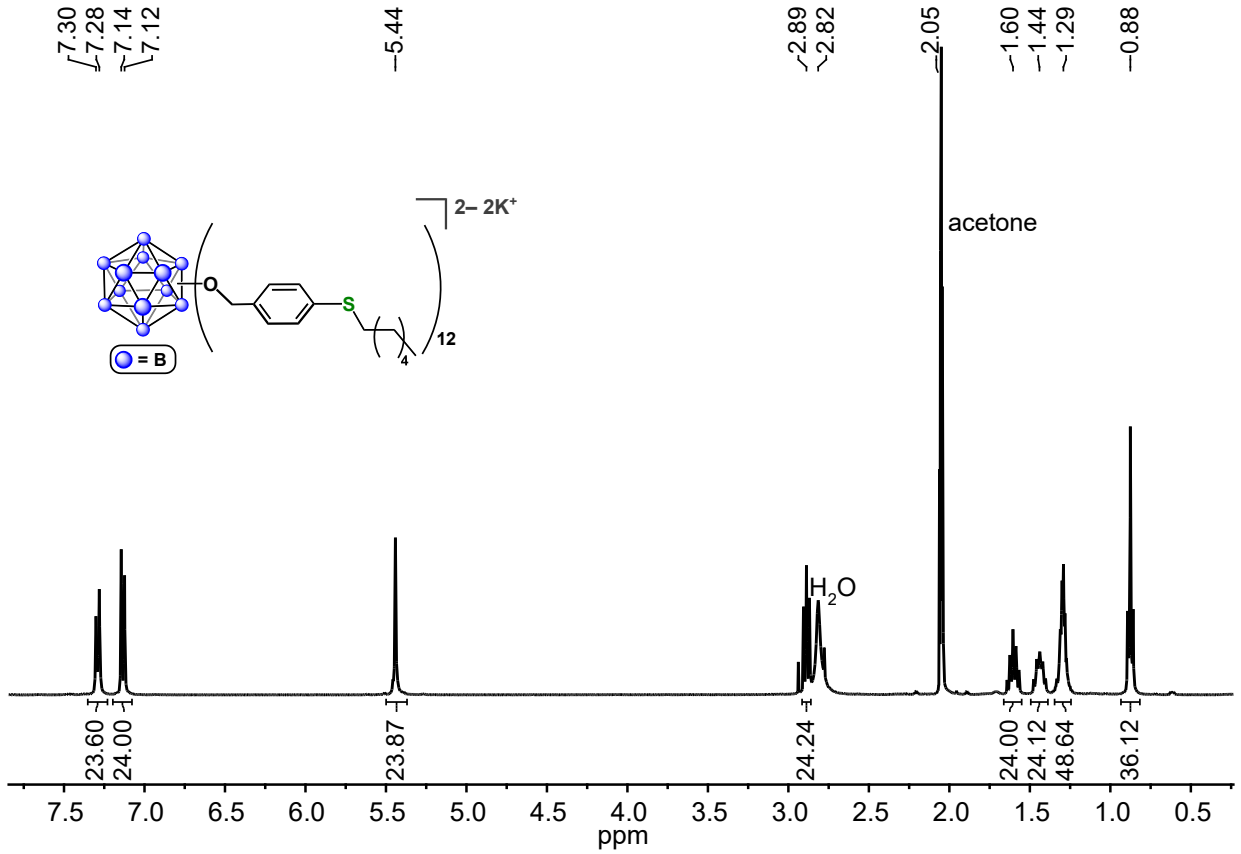

Figure S43. ^{1}H NMR spectrum of $[K_2][B_{12}(OCH_2C_6H_4S(CH_2)_5CH_3)_{12}]$ (400 MHz, acetone-d_6, 25 °C).

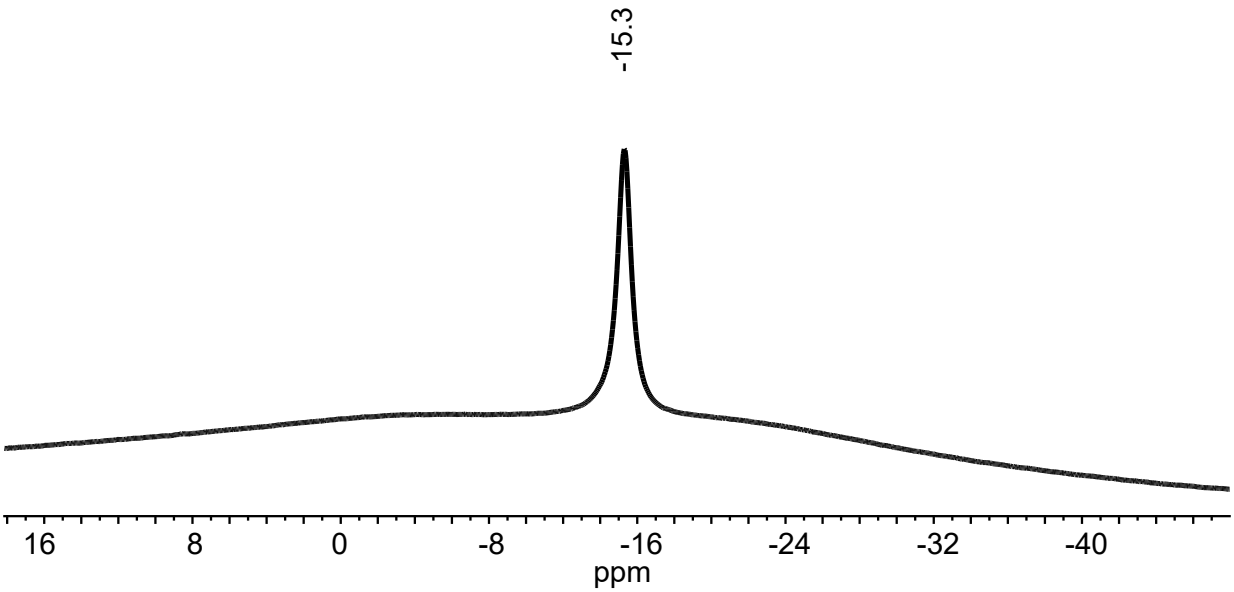

Figure S44. $^{11}B\{^{1}H\}$ NMR spectrum of $[K_2][B_{12}(OCH_2C_6H_4S(CH_2)_5CH_3)_{12}]$ (128 MHz, acetone-d_6, 25 °C).

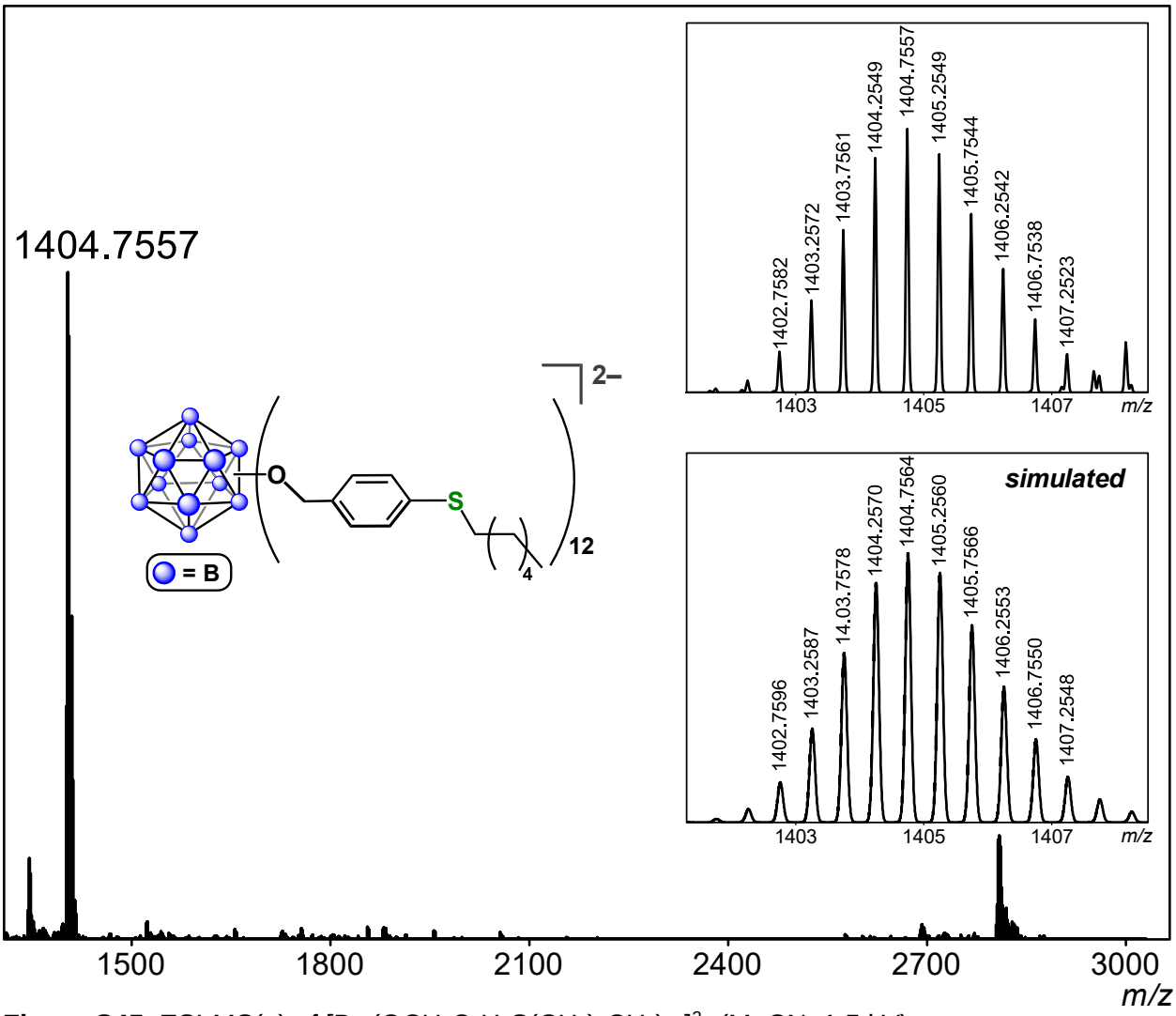

Figure S45. ESI-MS(–) of $[B_{12}(OCH_2C_6H_4S(CH_2)_5CH_3)_{12}]^{2-}$ (MeCN, 1.5 kV).

S2.16. $[K_2][B_{12}(OCH_2C_6H_4SC_6F_5)_{12}]$ ($[K_2][$**11**$]$)

The general reaction procedure to generate [**1**][SbF_6]$_{11}$ (**Section S2.5**) was followed. The DMF solution containing [**1**][SbF_6]$_{11}$ (0.0014 mmol, 1 mL) was transferred to a vial containing solid K_3PO_4 (9 mg, 0.04 mmol, 30 equiv), and a Teflon-coated stir bar. To this solution was added pentafluorothiophenol (6 µL, 0.04 mmol, 30 equiv) with stirring. The color of the reaction mixture gradually changed from dark purple to colorless over the course of 15 min, at which point all volatiles were removed under reduced pressure with gentle heating (35 °C). The resulting colorless residue was suspended in an 85:15 hexanes:EtOAc mixture and loaded into a silica-packed pipette column. Using an 85:15 hexanes:EtOAc solvent combination, unreacted pentafluorothiophenol and the (Me-DalPhos)AuCl byproduct were eluted first, followed by elution of the $[K_2][B_{12}(OCH_2C_6H_4SC_6F_5)_{12}]$ product with acetone. The product fractions were combined, and all volatiles were removed *in vacuo* to afford $[K_2][B_{12}(OCH_2C_6H_4SC_6F_5)_{12}]$ as a colorless residue in 80% yield (4 mg, 0.001 mmol). ^{1}H NMR (400 MHz, 25 °C, CD_2Cl_2) δ: 7.14–7.06 (two sets of doublets overlapping, 48H, Ar-*H*), 5.18 (s, 24H, –C*H*$_2$–) ppm. ^{19}F{^{1}H} NMR (376 MHz, 25 °C, CD_2Cl_2) δ: -132.86 (d, 24F, *ortho*-*F*), -152.21 (t, 12F, *para*-*F*), -161.30 (m, 24F, *meta*-*F*) ppm. ^{11}B{^{1}H} NMR (128 MHz, 25 °C, CD_2Cl_2) δ: -15.7 ppm. ESI-MS(–): 1896.0961 (calc'd, 1896.0981) *m/z*.

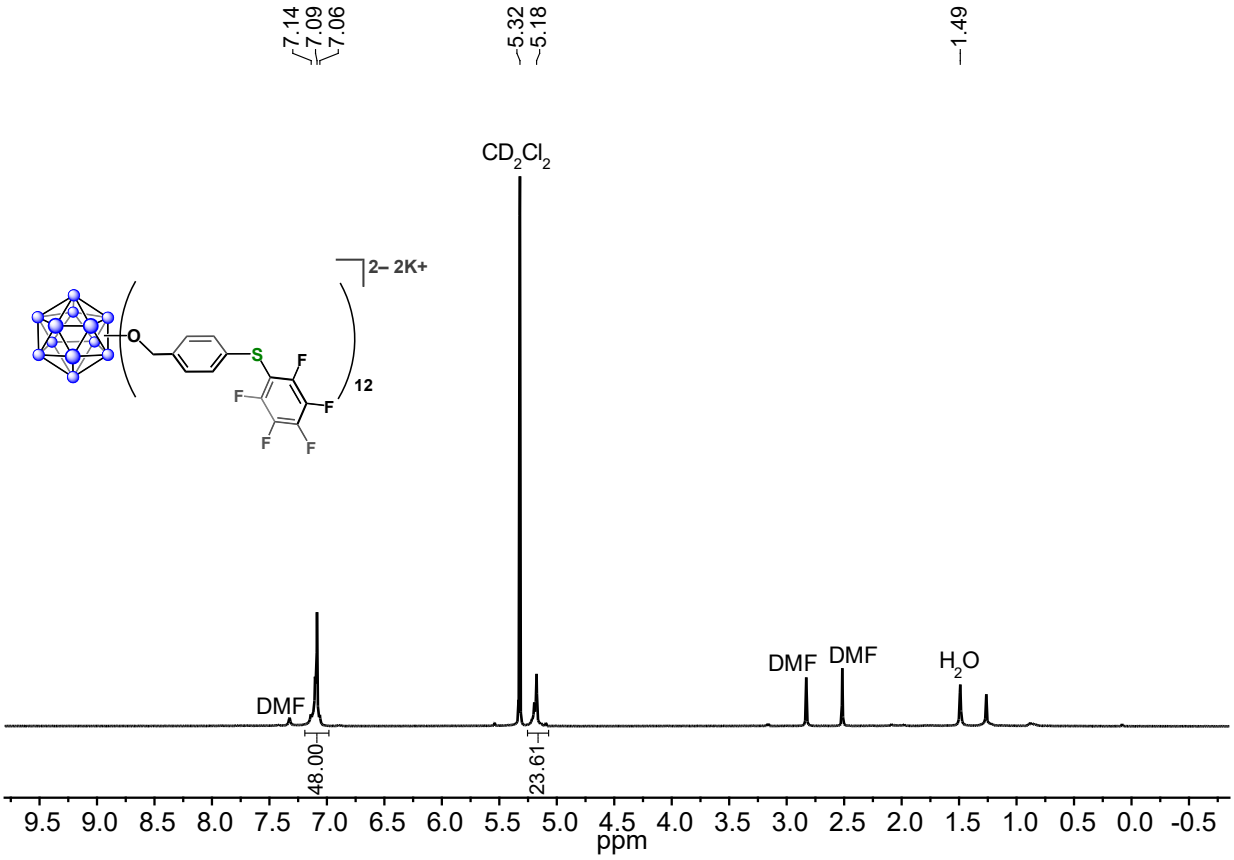

Figure S46. ^{1}H NMR spectrum of $[K_2][B_{12}(OCH_2C_6H_4SC_6F_5)_{12}]$ (400 MHz, CD_2Cl_2, 25 °C).

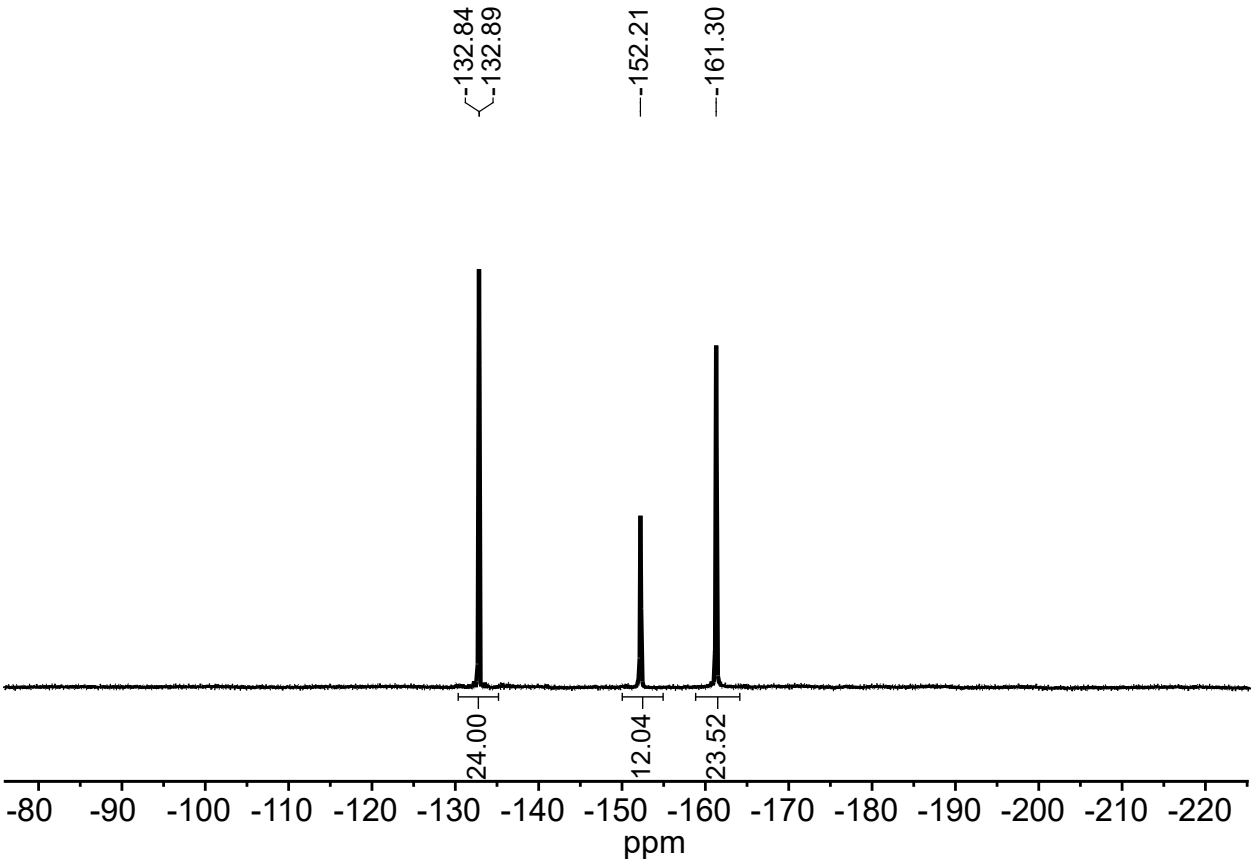

Figure S47. $^{19}F\{^{1}H\}$ NMR spectrum of $[K_2][B_{12}(OCH_2C_6H_4SC_6F_5)_{12}]$ (376 MHz, CD_2Cl_2, 25 °C).

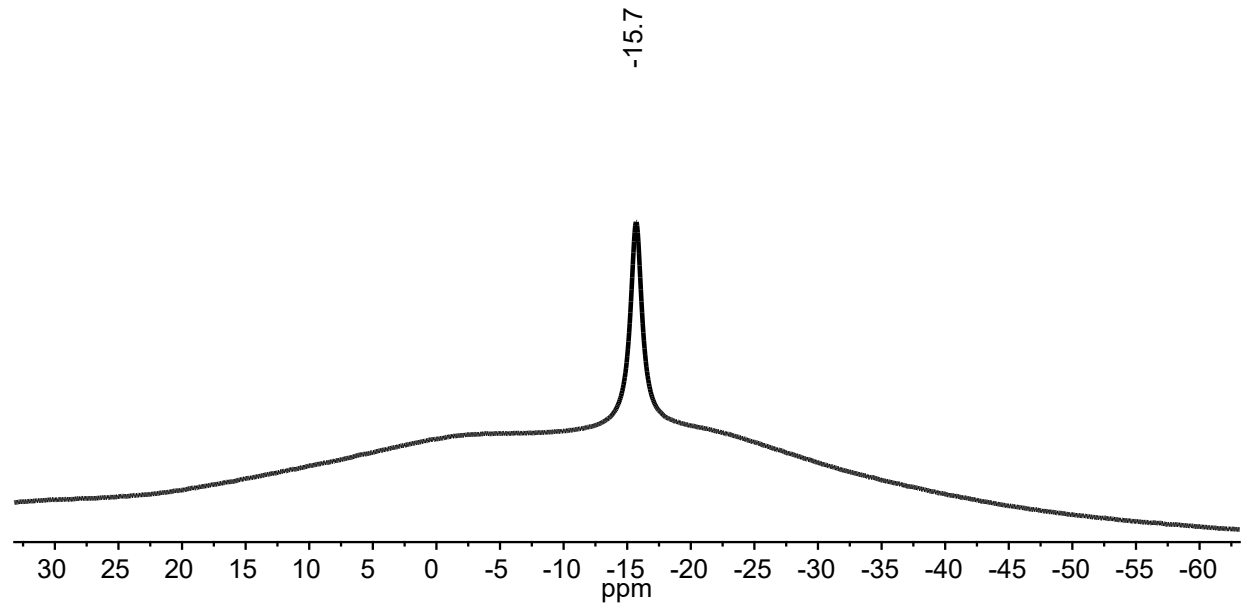

Figure S48. $^{11}B\{^{1}H\}$ NMR spectrum of $[K_2][B_{12}(OCH_2C_6H_4SC_6F_5)_{12}]$ (128 MHz, CD_2Cl_2, 25 °C).

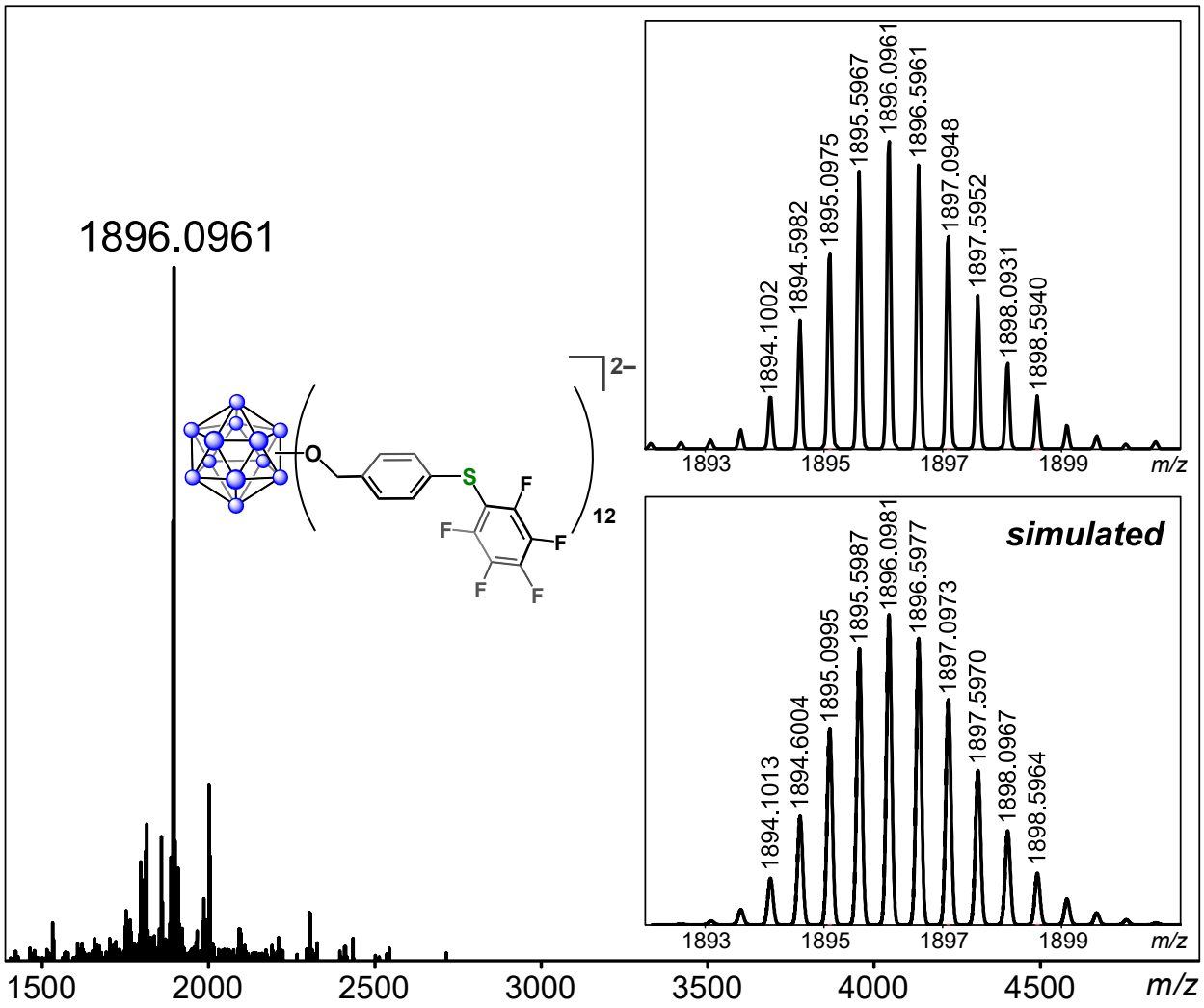

Figure S49. ESI-MS(–) of $[B_{12}(OCH_2C_6H_4SC_6F_5)_{12}]^{2-}$ (MeCN, 1.5 kV).

S2.17. $[H_3NC(CH_2OH)_3]_2[B_{12}(OCH_2C_6H_4(2\text{-thio-5-trifluoromethylpyridine}))_{12}]$ ($[H_3NC(CH_2OH)_3]_2$[12])

The general reaction procedure to generate [**1**][SbF_6]$_{11}$ (**Section S2.5**) was followed. The DMF solution (1 mL) containing [**1**][SbF_6]$_{11}$ (0.0014 mmol) was transferred to a vial containing solid 2-mercapto-5-trifluoromethylpyridine (5 mg, 0.03 mmol, 20 equiv), and a Teflon-coated stir bar. To this stirring solution was added a solution of TRIS buffer in DMF (50 mM, 0.5 mL). The reaction mixture was allowed to stir at 25 °C for a total of 15 min, during which time the color of the solution changed to colorless. All volatiles were removed from the reaction mixture under reduced pressure, and the resulting colorless residue was dissolved in MeOH (0.5 mL) and loaded into a column packed with Sephadex LH20 medium in MeOH. The pure product was eluted first, followed by elution of fractions containing (Me-DalPhos)AuCl and unreacted 2-mercapto-5-trifluoromethylpyridine. The fractions containing the pure product were combined, and all volatiles were removed under reduced pressure to afford $[H_3NC(CH_2OH)_3]_2[B_{12}(OCH_2C_6H_4(2\text{-thio-5-trifluoromethylpyridine}))_{12}]$ as a colorless solid in 60% yield (3 mg, 8 µmol). ^{1}H NMR (400 MHz, 25 °C, CD_3OD) δ: 8.49 (m, 12H, pyr H6), 7.61–7.59 (m, 36H, two resonances overlapping), 7.32 (d, 24H, Ar-*H*, ^3J = 8 Hz), 6.81 (d, 12H, pyr H3, ^3J = 9 Hz), 5.61 (br s, 24H, –CH_2–, this signal is broadened due to slow oxidation of the diamagnetic dianionic species to the paramagnetic monoanion in solution in the presence of air), 3.61 (s, 12H, $[H_3NC(CH_2OH)_3]^+$) ppm. ^{19}F{^{1}H} NMR (376 MHz, 25 °C, CD_3OD) δ: -63.70 ppm. ^{11}B{^{1}H} NMR (128 MHz, 25 °C, CD_3OD) δ: -14.5 ppm. ESI-MS(–): 1770.2774 (calc'd, 1770.2765) *m/z*.

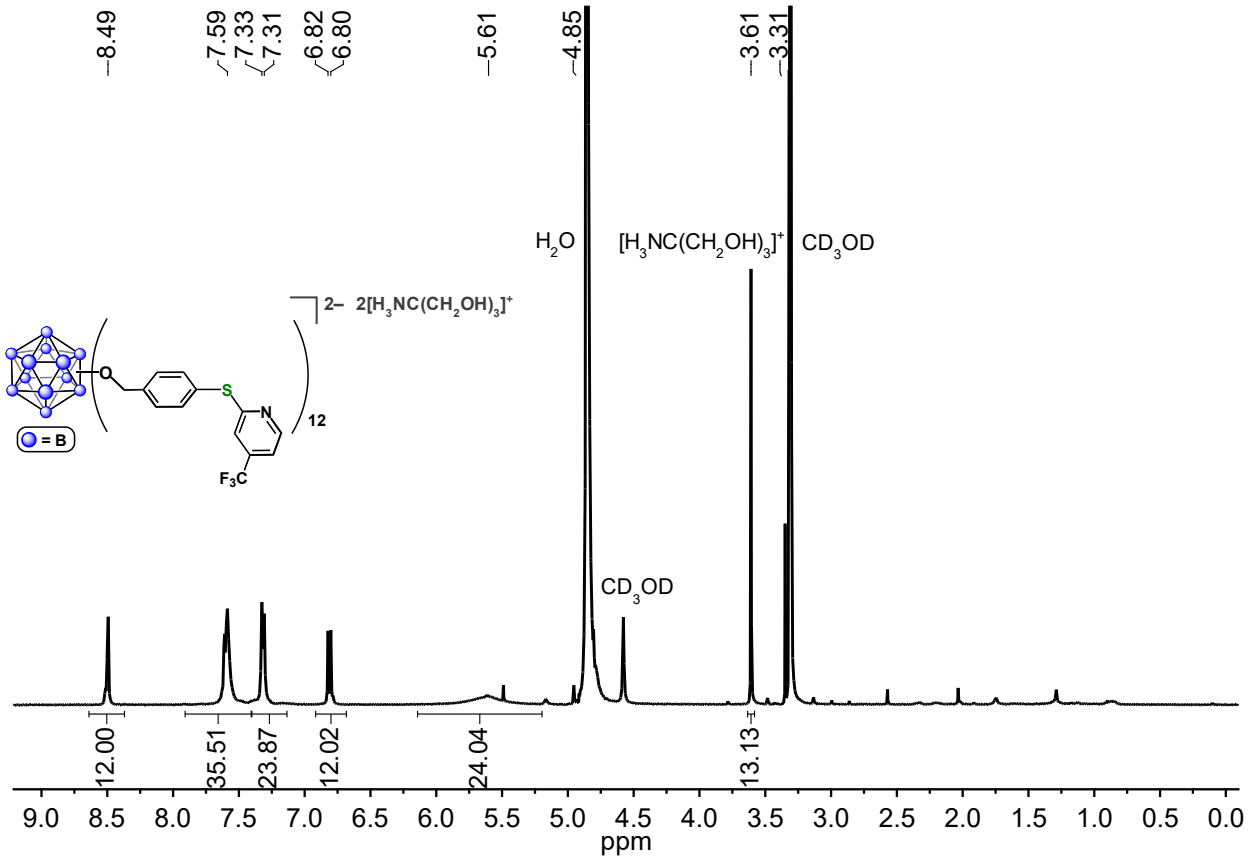

Figure S50. ^{1}H NMR spectrum of $[H_3NC(CH_2OH)_3]_2[B_{12}(OCH_2C_6H_4(2\text{-thio-5-trifluoromethylpyridine}))_{12}]$ (CD_3OD, 400 MHz, 25 °C).

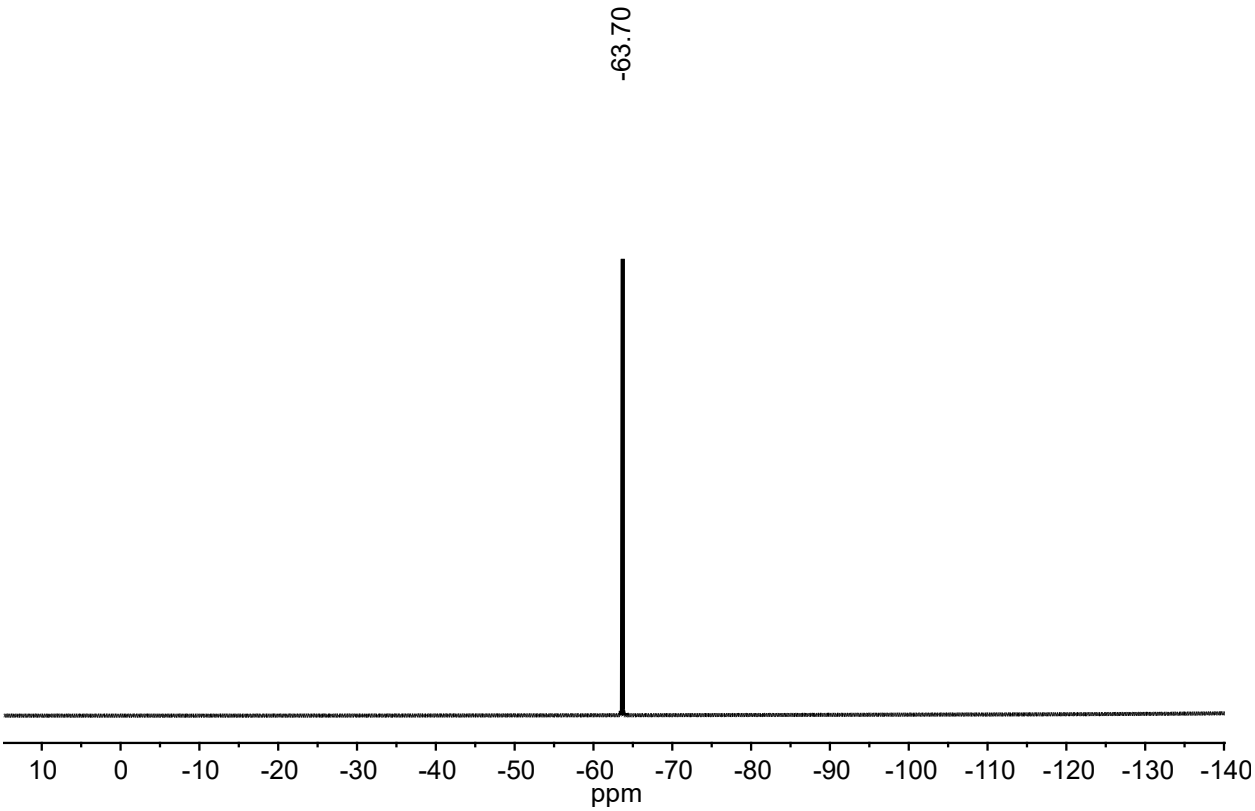

Figure S51. $^{19}F\{^{1}H\}$ NMR spectrum of $[H_3NC(CH_2OH)_3]_2[B_{12}(OCH_2C_6H_4(2\text{-thio-}5\text{-trifluoromethylpyridine}))_{12}]$ (CD_3OD, 376 MHz, 25 °C).

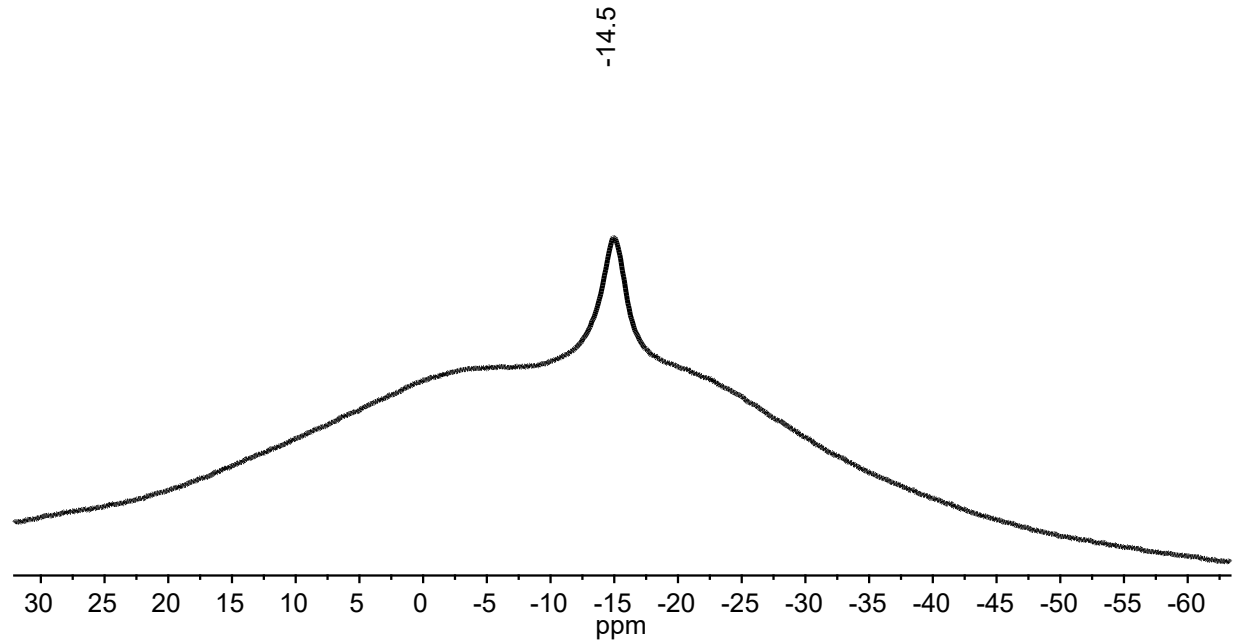

Figure S52. $^{11}B\{^{1}H\}$ NMR spectrum of $[H_3NC(CH_2OH)_3]_2[B_{12}(OCH_2C_6H_4(2\text{-thio-}5\text{-trifluoromethylpyridine}))_{12}]$ (CD_3OD, 128 MHz, 25 °C).

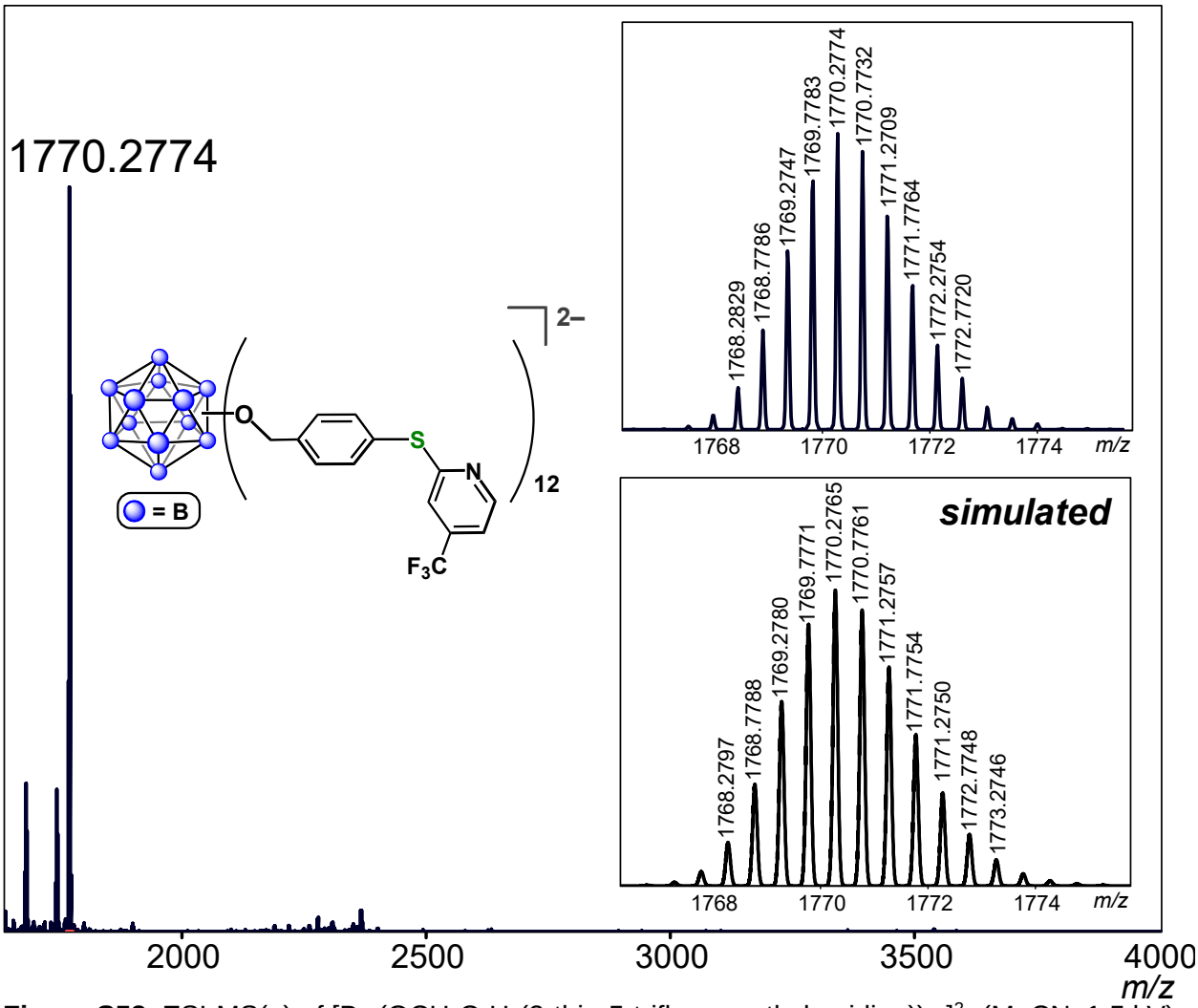

Figure S53. ESI-MS(–) of $[B_{12}(OCH_2C_6H_4(2\text{-thio-5-trifluoromethylpyridine}))_{12}]^{2-}$ (MeCN, 1.5 kV).

S2.18. $[K_2][B_{12}(OCH_2C_6H_4(2\text{-mercaptobenzothiazole}))_{12}]$ ($[K_2][\mathbf{13}]$)

The general reaction procedure to generate $[\mathbf{1}][SbF_6]_{11}$ (**Section S2.5**) was followed. The DMF solution (1 mL) containing $[\mathbf{1}][SbF_6]_{11}$ (0.0014 mmol) was transferred to a vial containing solid K_3PO_4 (9 mg, 0.04 mmol, 30 equiv), and 2-mercaptobenzothiazole (7 mg, 0.04 mmol, 30 equiv). The purple solution was allowed to stir at 25 °C for a total of 15 min, during which time the color of the reaction mixture changed to colorless. All volatiles were removed from the reaction mixture under reduced pressure, and the resulting colorless residue was suspended in EtOAc (0.5 mL) and loaded into a silica-packed pipette column. The unreacted 2-mercaptobenzothiazole and the (Me-DalPhos)AuCl byproduct were eluted first using EtOAc, followed by elution of the $[K_2][B_{12}(OCH_2C_6H_4(2\text{-mercaptobenzothiazole}))_{12}]$ product with acetone. The product fractions were combined, and all volatiles were removed *in vacuo* to afford $[K_2][B_{12}(OCH_2C_6H_4(2\text{-mercaptobenzothiazole}))_{12}]$ as a colorless solid in 80% yield (4 mg, 0.001 mmol). ^{1}H NMR (400 MHz, 25 °C, acetone-d_6) δ: 7.71 (d, 24H, Ar-*H*, ^3J = 8 Hz), 7.69 (d, 12H, Ar-*H*, ^3J = 8 Hz), 7.63 (d, 12H, Ar-*H*, ^3J = 8 Hz), 7.56 (d, 24H, Ar-*H*, ^3J = 8 Hz), 7.31 (t, 12H, Ar-*H*, ^3J = 8 Hz), 7.11 (t, 12H, Ar-*H*, ^3J = 8 Hz), 5.80 (s, 24H, –C*H*$_2$–) ppm. ^{11}B{^{1}H} NMR (128 MHz, 25 °C, acetone-d_6) δ: -15.0 ppm. ESI-MS(–): 1698.6726 (calc'd, 1698.6840) *m/z*.

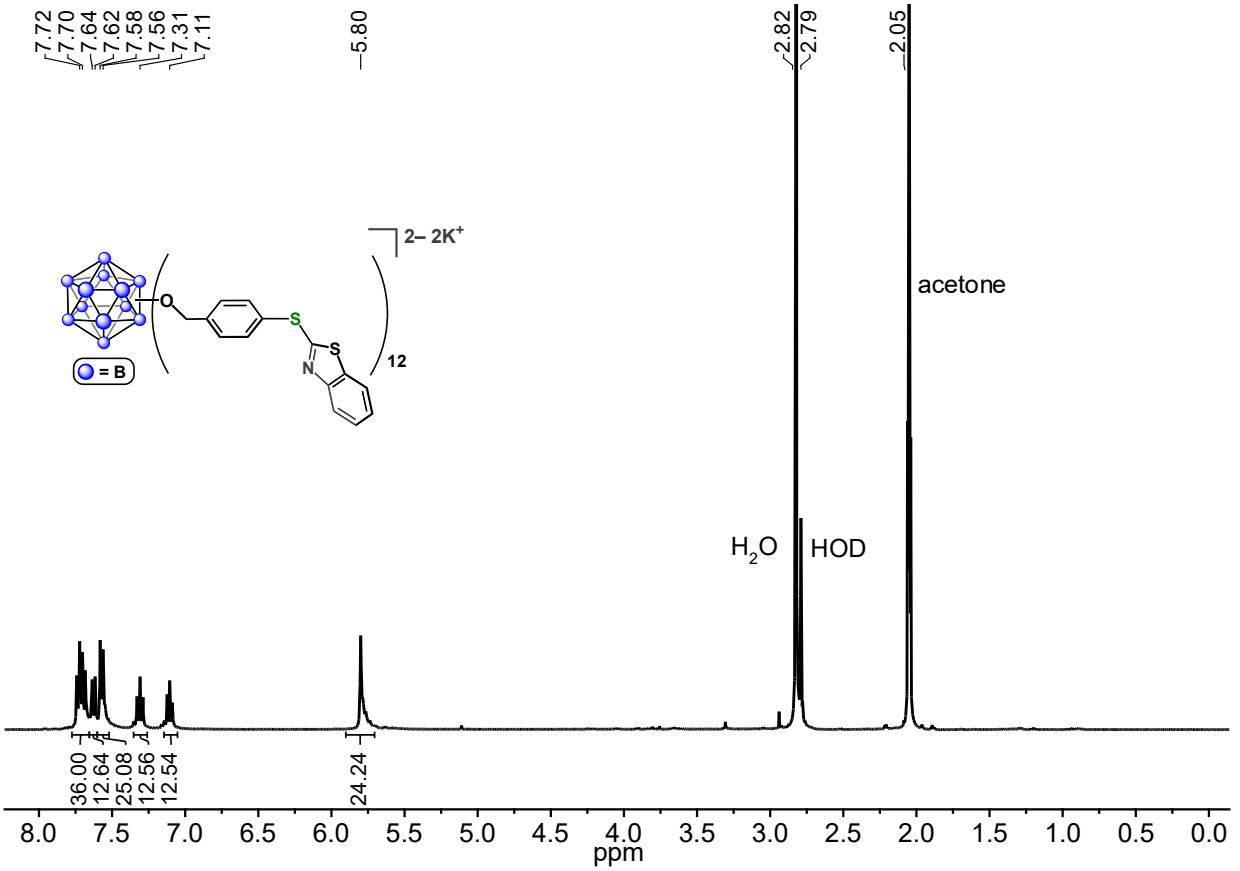

Figure S54. ^{1}H NMR spectrum of $[K_2][B_{12}(OCH_2C_6H_4(2\text{-mercaptobenzothiazole}))_{12}]$ (acectone-d_6, 400 MHz, 25 °C).

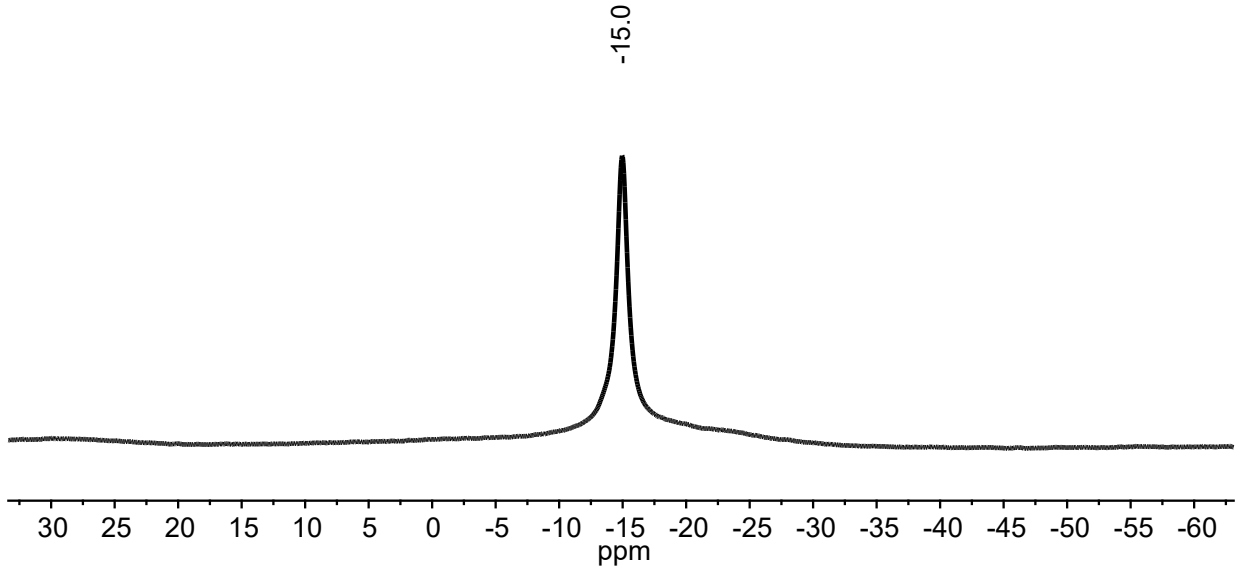

Figure S55. $^{11}B\{^{1}H\}$ NMR spectrum of $[K_2][B_{12}(OCH_2C_6H_4(2\text{-mercaptobenzothiazole}))_{12}]$ (acetone-d_6, 128 MHz, 25 °C).

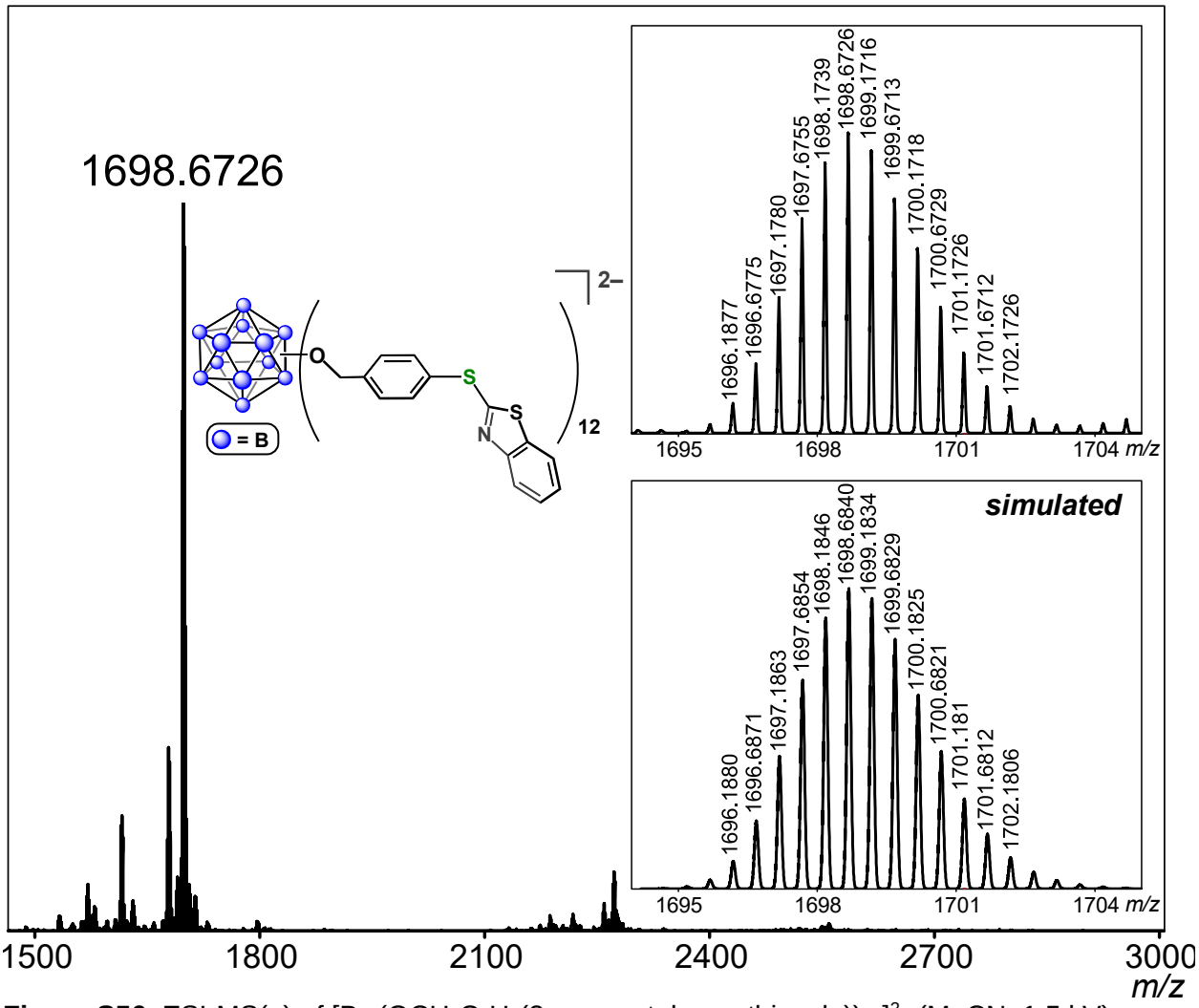

Figure S56. ESI-MS(–) of $[B_{12}(OCH_2C_6H_4(2\text{-mercaptobenzothiazole}))_{12}]^{2-}$ (MeCN, 1.5 kV).

S2.19. $[K_2][B_{12}(OCH_2C_6H_4(2\text{-thio-5-(4-pyridyl)-1,3,4-oxadiazole}))_{12}]$ ($[K_2][\mathbf{14}]$)

The general reaction procedure to generate $[\mathbf{1}][SbF_6]_{11}$ (**Section S2.5**) was followed. The DMF solution (1 mL) containing $[\mathbf{1}][SbF_6]_{11}$ (0.0014 mmol) was transferred to a vial containing solid K_3PO_4 (9 mg, 0.04 mmol, 30 equiv), and 2-thiol-5-(4-pyridyl)-1,3,4-oxadiazole (5 mg, 0.03 mmol, 20 equiv). The purple solution was allowed to stir at 25 °C for a total of 15 min, during which time the color of the reaction mixture changed to colorless. All volatiles were then removed from the reaction mixture under reduced pressure, and the resulting colorless residue was dissolved in MeOH (0.5 mL) and loaded into a column packed with Sephadex LH-20 medium in MeOH. The pure product was eluted first, followed by elution of fractions containing (Me-DalPhos)AuCl and unreacted 2-thiol-5-(4-pyridyl)-1,3,4-oxadiazole. The fractions containing the pure product were combined, and all volatiles were removed *in vacuo* to afford $[K_2][B_{12}(OCH_2C_6H_4(2\text{-thio-5-(4-pyridyl)-1,3,4-oxadiazole}))_{12}]$ as a colorless residue in 60% yield (3 mg, 0.8 µmol). ^{1}H NMR (400 MHz, 25 °C, CD_2Cl_2) δ: 8.67 (d, 24H, pyr-*H*, ^3J = 6 Hz), 7.69 (d, 24H, pyr-*H*, ^3J = 6 Hz), 7.59–7.53 (two sets of doublets overlapping, 48H, Ar-*H*), 5.63 (s, 24H, –C*H*$_2$–) ppm. ^{11}B{^{1}H} NMR (128 MHz, 25 °C, CD_2Cl_2) δ: -15.3 ppm. ESI-MS(–): 1770.3601 (calc'd, 1770.3588) *m/z*.

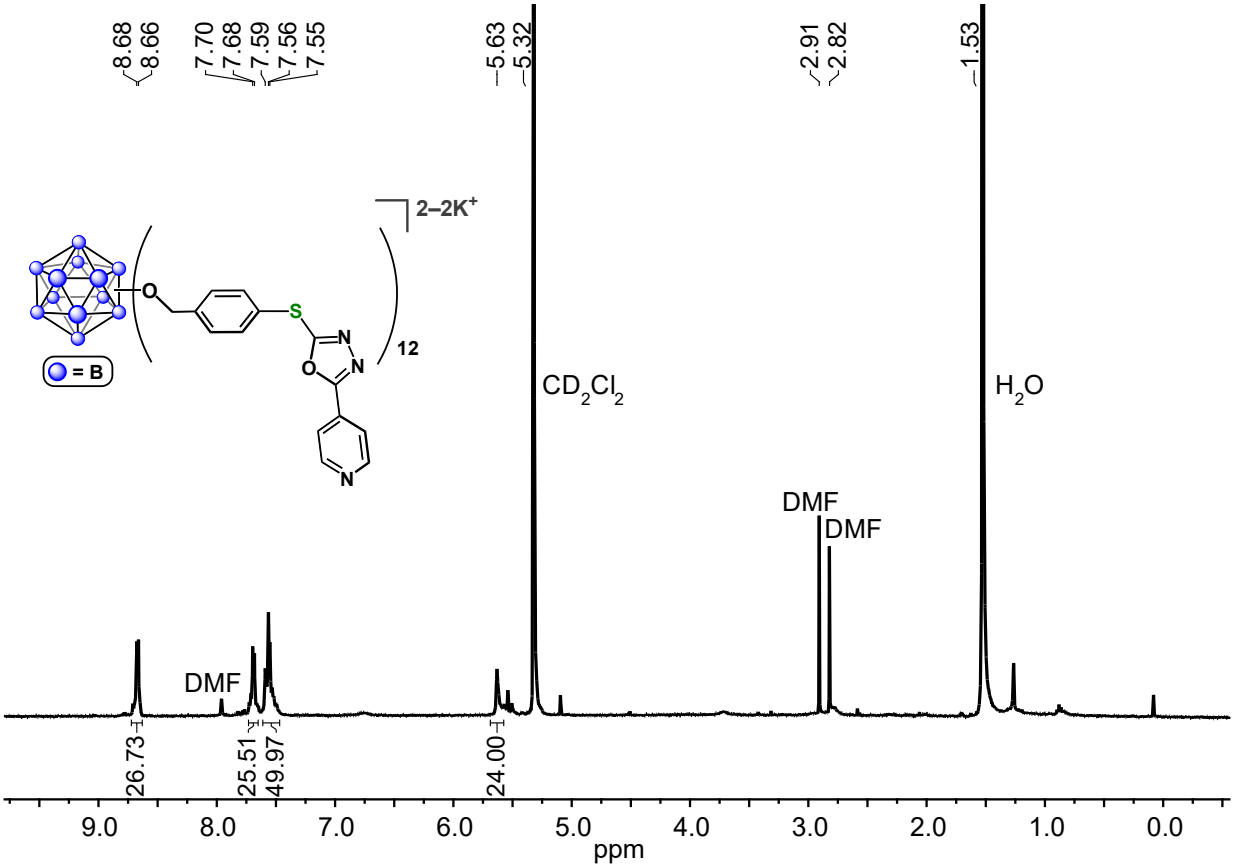

Figure S57. ^{1}H NMR spectrum of $[K_2][B_{12}(OCH_2C_6H_4(2\text{-thio-5-(4-pyridyl)-1,3,4-oxadiazole}))_{12}]$ (CD_2Cl_2, 400 MHz, 25 °C).

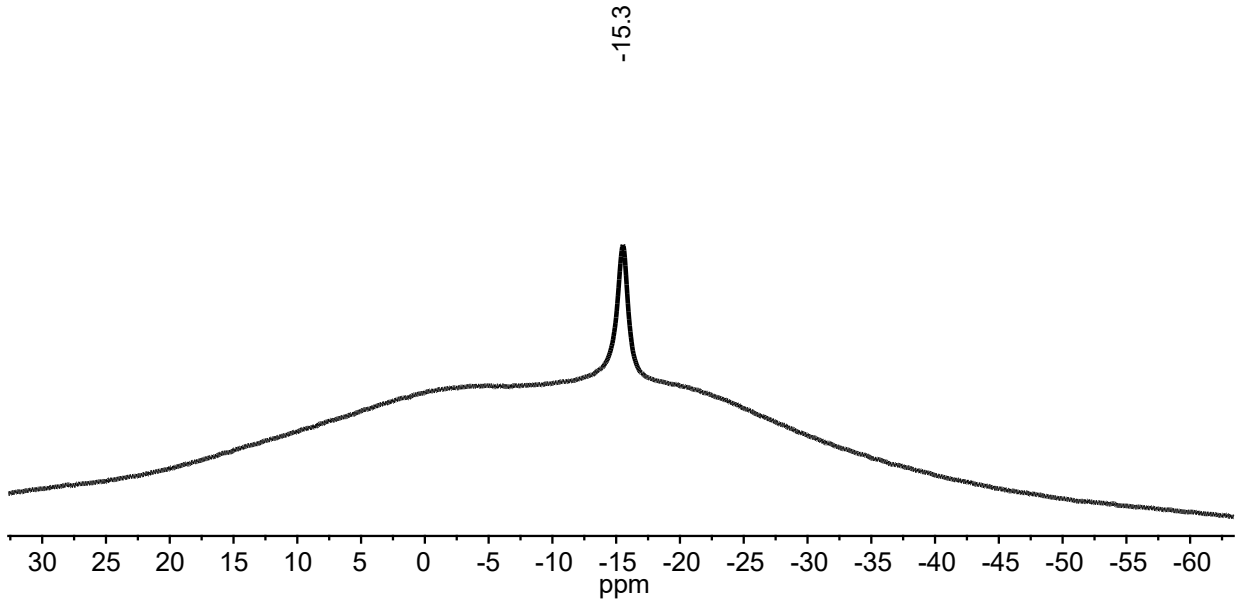

Figure S58. $^{11}B\{^{1}H\}$ NMR spectrum of $[K_2][B_{12}(OCH_2C_6H_4(2\text{-thio-5-(4-pyridyl)-1,3,4-oxadiazole}))_{12}]$ (CD_2Cl_2, 128 MHz, 25 °C).

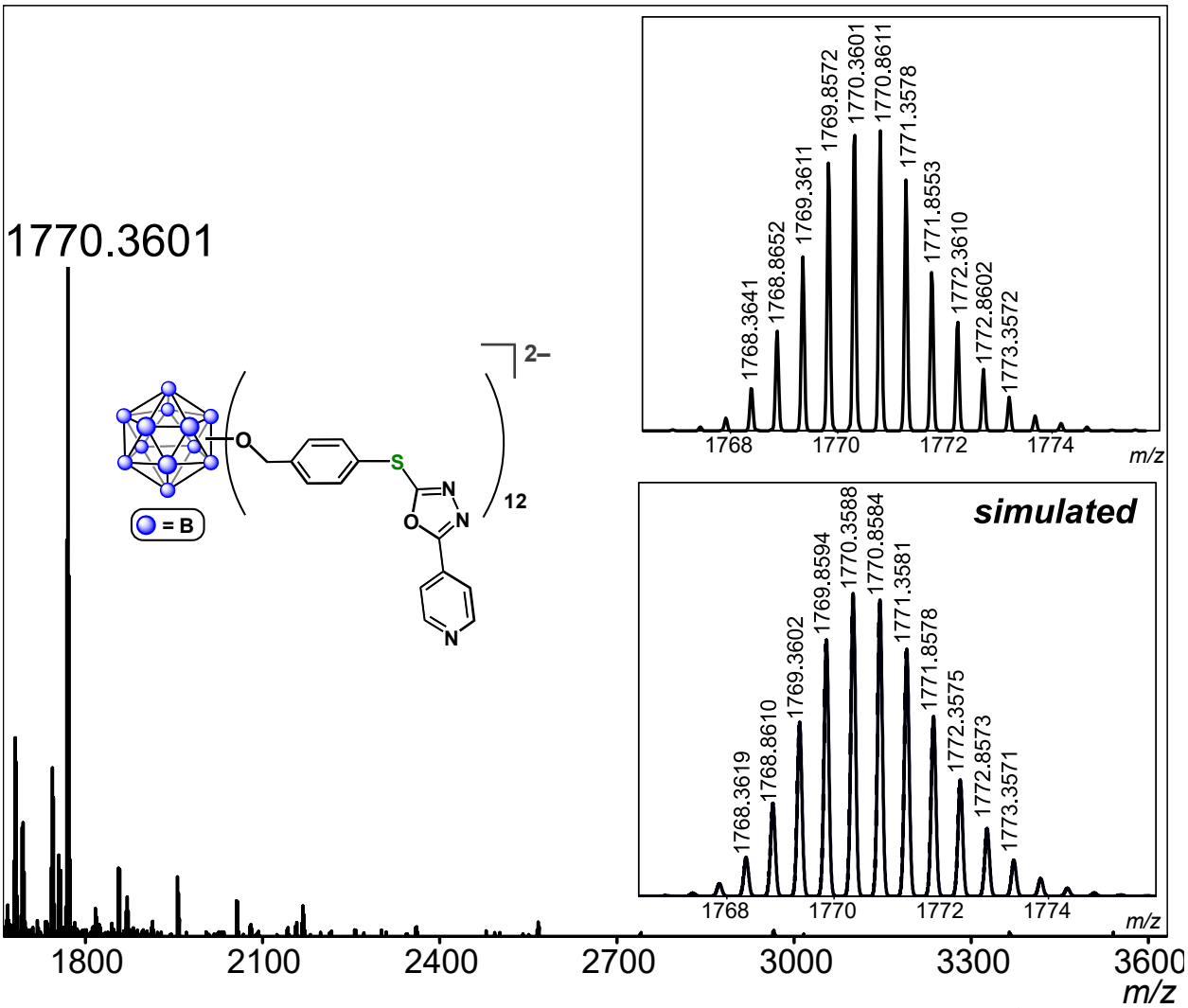

Figure S59. ESI-MS(–) of $[B_{12}(OCH_2C_6H_4(2\text{-thio-5-(4-pyridyl)-1,3,4-oxadiazole}))_{12}]^{2-}$ (MeCN, 1.5 kV).

S2.20. $[K_2][B_{12}(OCH_2C_6H_4(3\text{-thio-}1,2,4\text{-triazole}))_{12}]$ ($[K_2][15]$)

The general reaction procedure to generate $[\mathbf{1}][SbF_6]_{11}$ (**Section S2.5**) was followed. The DMF solution (1 mL) containing $[\mathbf{1}][SbF_6]_{11}$ (0.0014 mmol) was transferred to a vial containing solid K_3PO_4 (9 mg, 0.04 mmol, 30 equiv) and 3-thiol-1,2,4-triazole (4 mg, 0.04 mmol, 30 equiv). The purple solution was allowed to stir at 25 °C for a total of 15 min, during which time the color of the reaction mixture changed to colorless. All volatiles were then removed from the reaction mixture under reduced pressure, and the resulting colorless residue was suspended in EtOAc (0.5 mL) and loaded into a silica-packed pipette column. The unreacted 3-thiol-1,2,4-triazole and the (Me-DalPhos)AuCl byproduct were eluted first using EtOAc, followed by elution of the $[K_2][B_{12}(OCH_2C_6H_4(3\text{-thio-}1,2,4\text{-triazole}))_{12}]$ product with MeOH. The product fractions were combined and all volatiles were removed under reduced pressure to afford $[K_2][B_{12}(OCH_2C_6H_4(3\text{-thio-}1,2,4\text{-triazole}))_{12}]$ in 80% yield (3 mg, 0.001 mmol). ^{1}H NMR (400 MHz, 25 °C, CD_3OD) δ: 8.29 (s, 12H, C*H*, triazole), 7.22–7.17 (two sets of doublets overlapping, 24H, Ar-*H*), 5.31 (s, 24H, –C*H*$_2$–) ppm. ^{11}B{^{1}H} NMR (128 MHz, 25 °C, CD_3OD) δ: -15.3 ppm. ESI-MS(–): 1301.7943 (calc'd, 1301.7900) *m/z*.

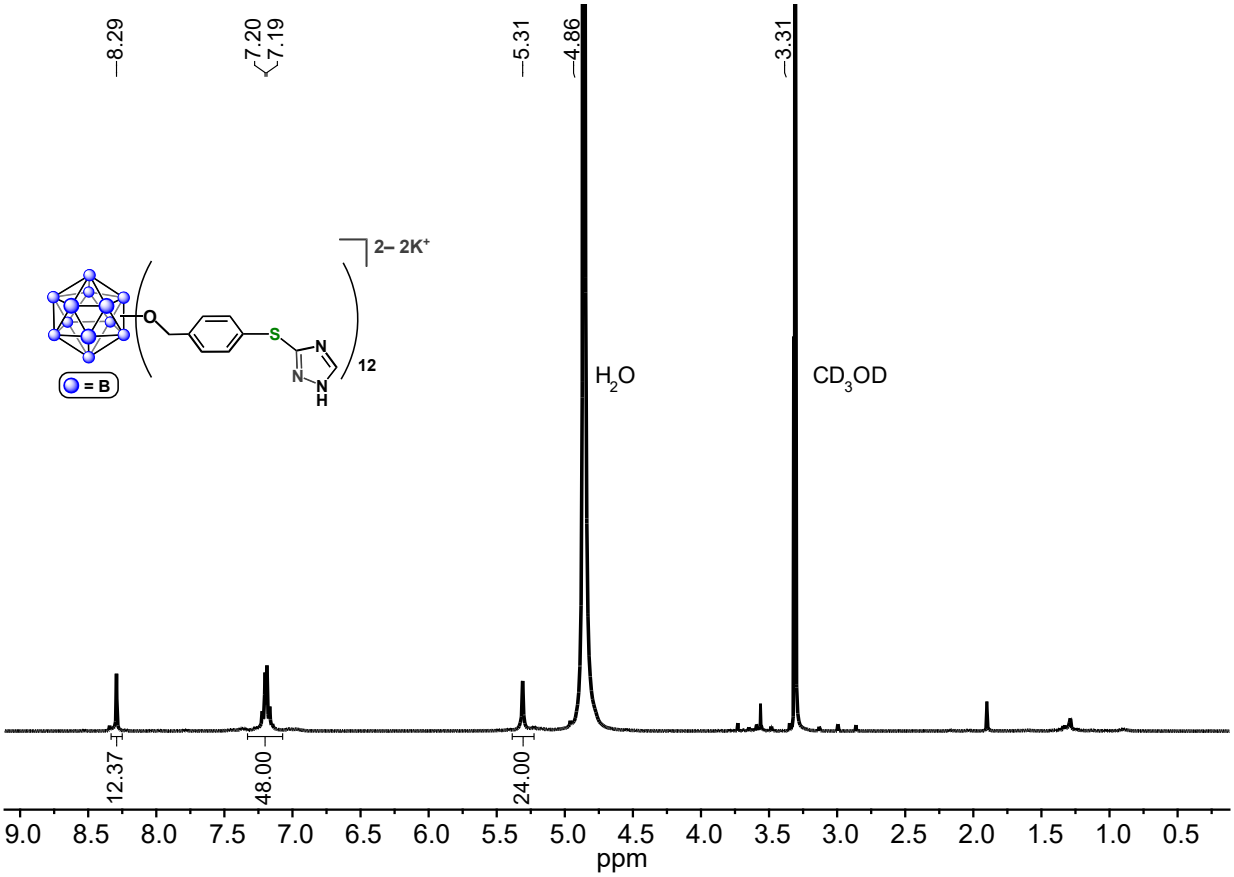

Figure S60. ^{1}H NMR spectrum of $[K_2][B_{12}(OCH_2C_6H_4(3\text{-thio-}1,2,4\text{-triazole}))_{12}]$ (CD_3OD, 400 MHz, 25 °C).

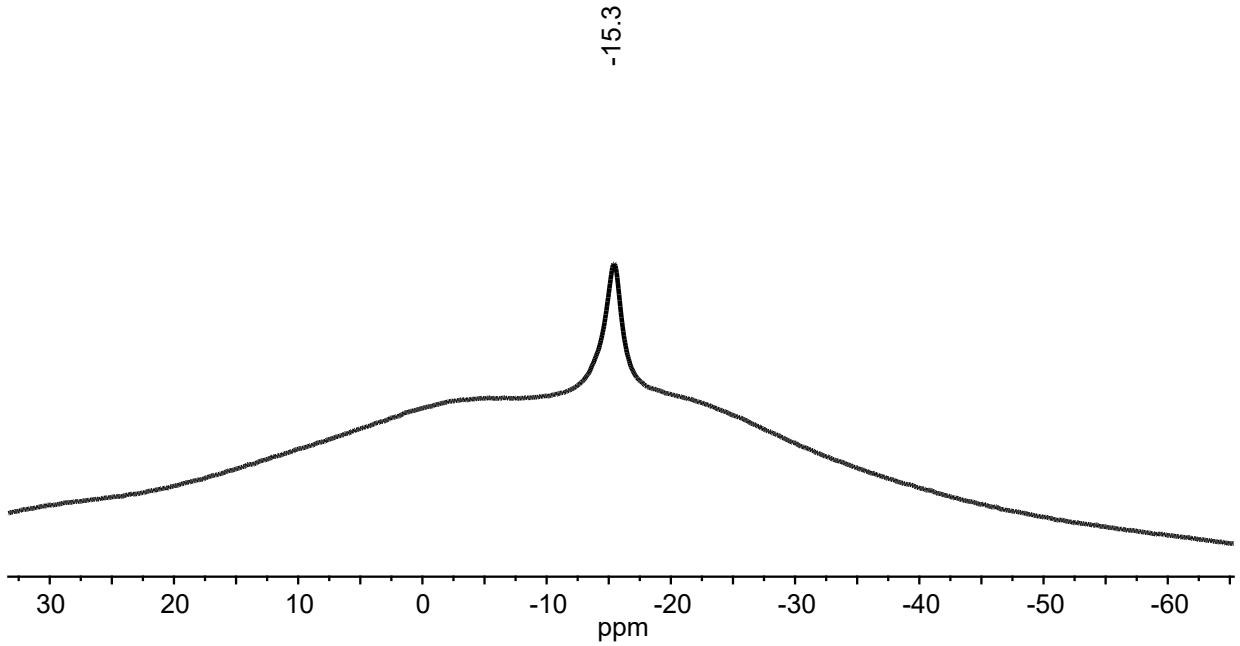

Figure S61. $^{11}B\{^{1}H\}$ NMR spectrum of $[K_2][B_{12}(OCH_2C_6H_4(3\text{-thio-}1,2,4\text{-triazole}))_{12}]$ (CD_3OD, 128 MHz, 25 °C).

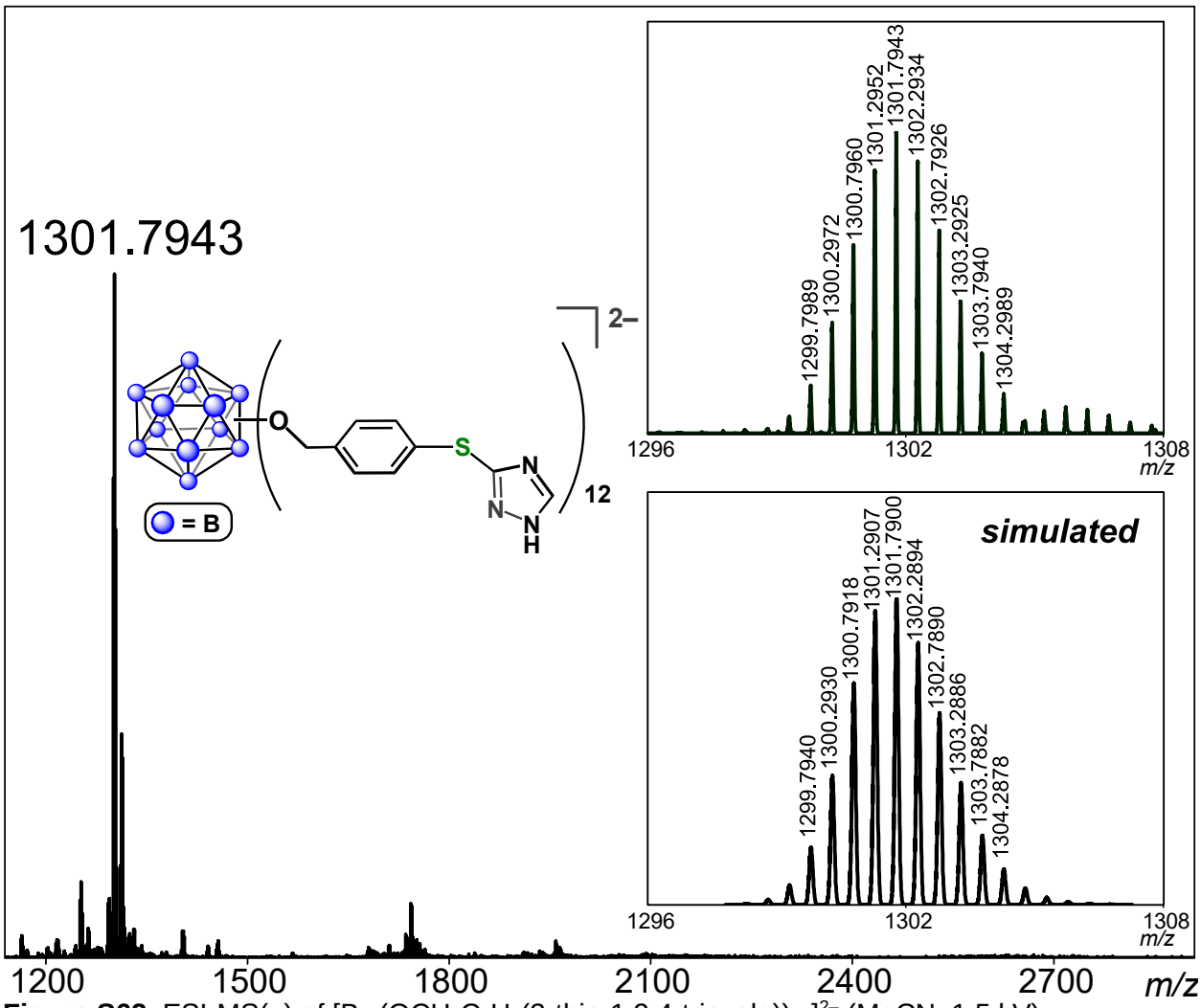

Figure S62. ESI-MS(–) of $[B_{12}(OCH_2C_6H_4(3\text{-thio-}1,2,4\text{-triazole}))_{12}]^{2-}$ (MeCN, 1.5 kV).

S2.21. $[K_2][B_{12}(OCH_2C_6H_4SePh)_{12}]$ ($[K_2]$[16])

The general reaction procedure to generate [**1**][SbF_6]$_{11}$ (**Section S2.5**) was followed. The DMF solution containing [**1**][SbF_6]$_{11}$ (0.0014 mmol, 1 mL) was transferred to a vial containing solid K_3PO_4 (9 mg, 0.04 mmol, 30 equiv) and a Teflon-coated stir bar. To this solution was added phenylselenol (3 µL, 0.03 mmol, 20 equiv) with stirring. The reaction mixture was allowed to stir at 25 °C for 15 min, during which time the color of the reaction mixture gradually changed from dark purple to colorless. All volatiles were then removed from the reaction mixture under reduced pressure with gentle heating (35 °C). The resulting colorless residue was suspended in an 85:15 hexanes:EtOAc mixture and loaded into a silica-packed pipette column. Using an 85:15 hexanes:EtOAc solvent combination, unreacted phenylselenol and the (Me-DalPhos)AuCl byproduct were eluted first, followed by elution of the $[K_2][B_{12}(OCH_2C_6H_4SePh)_{12}]$ product with DCM. The product fractions were combined, and all volatiles were removed *in vacuo* to afford $[K_2][B_{12}(OCH_2C_6H_4SePh)_{12}]$ as a pale-pink residue in 60% yield (3 mg, 0.9 µmol). ^{1}H NMR (400 MHz, 25 °C, acetone-d_6) δ: 7.35–7.18 (all aromatic resonances overlapping, m, 108H, Ar-*H*), 5.46 (s, 24H, –CH_2–) ppm. It is noted that there is ca. 13% of (Me-DalPhos)AuCl present as an impurity in the isolated material due to difficulty in its separation on silica gel. ^{11}B{^{1}H} NMR (128 MHz, 25 °C, acetone-d_6) δ: -15.3 ppm. ESI-MS(–): 1638.0519 (calc'd, 1638.0528) *m/z*.

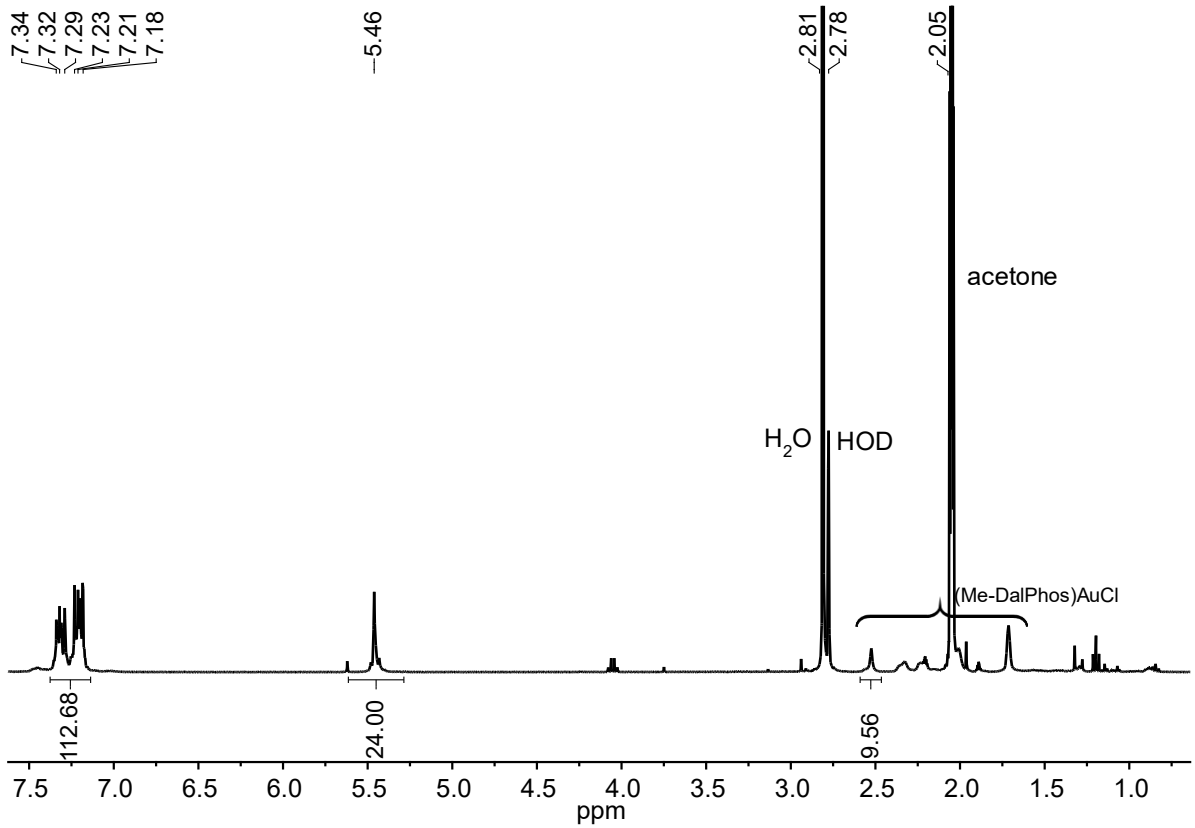

Figure S63. ^{1}H NMR spectrum of $[K_2][B_{12}(OCH_2C_6H_4SePh)_{12}]$ (400 MHz, acetone-d_6, 25 °C).

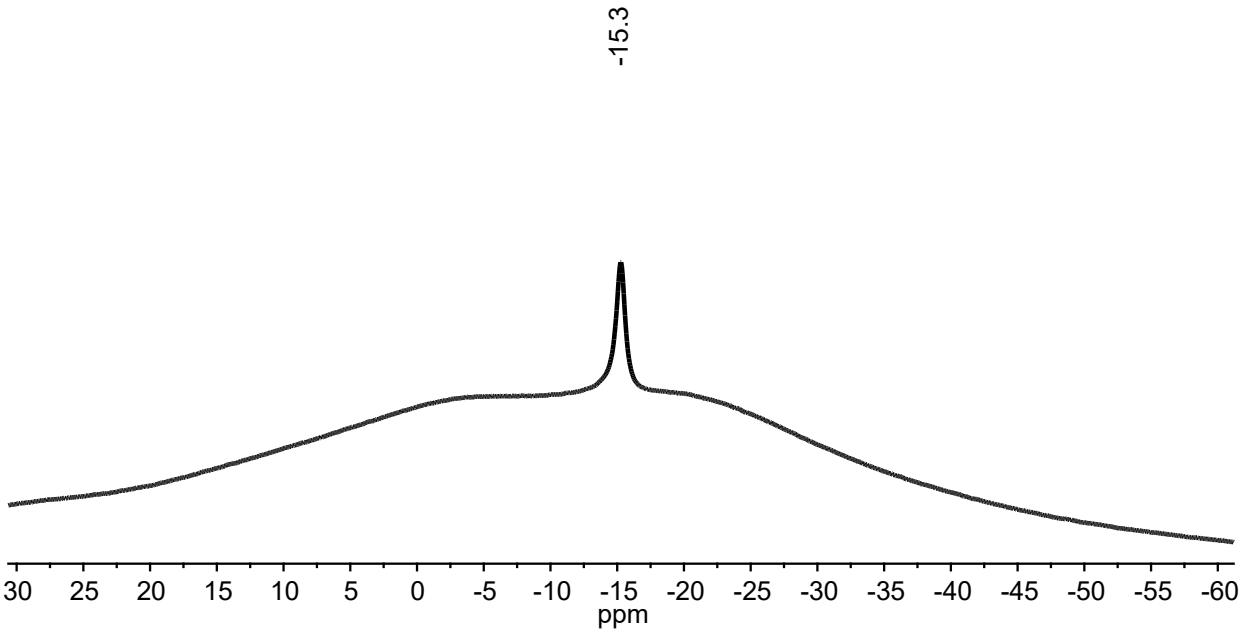

Figure S64. $^{11}B\{^{1}H\}$ NMR spectrum of $[K_2][B_{12}(OCH_2C_6H_4SePh)_{12}]$ (128 MHz, acetone-d_6, 25 °C).

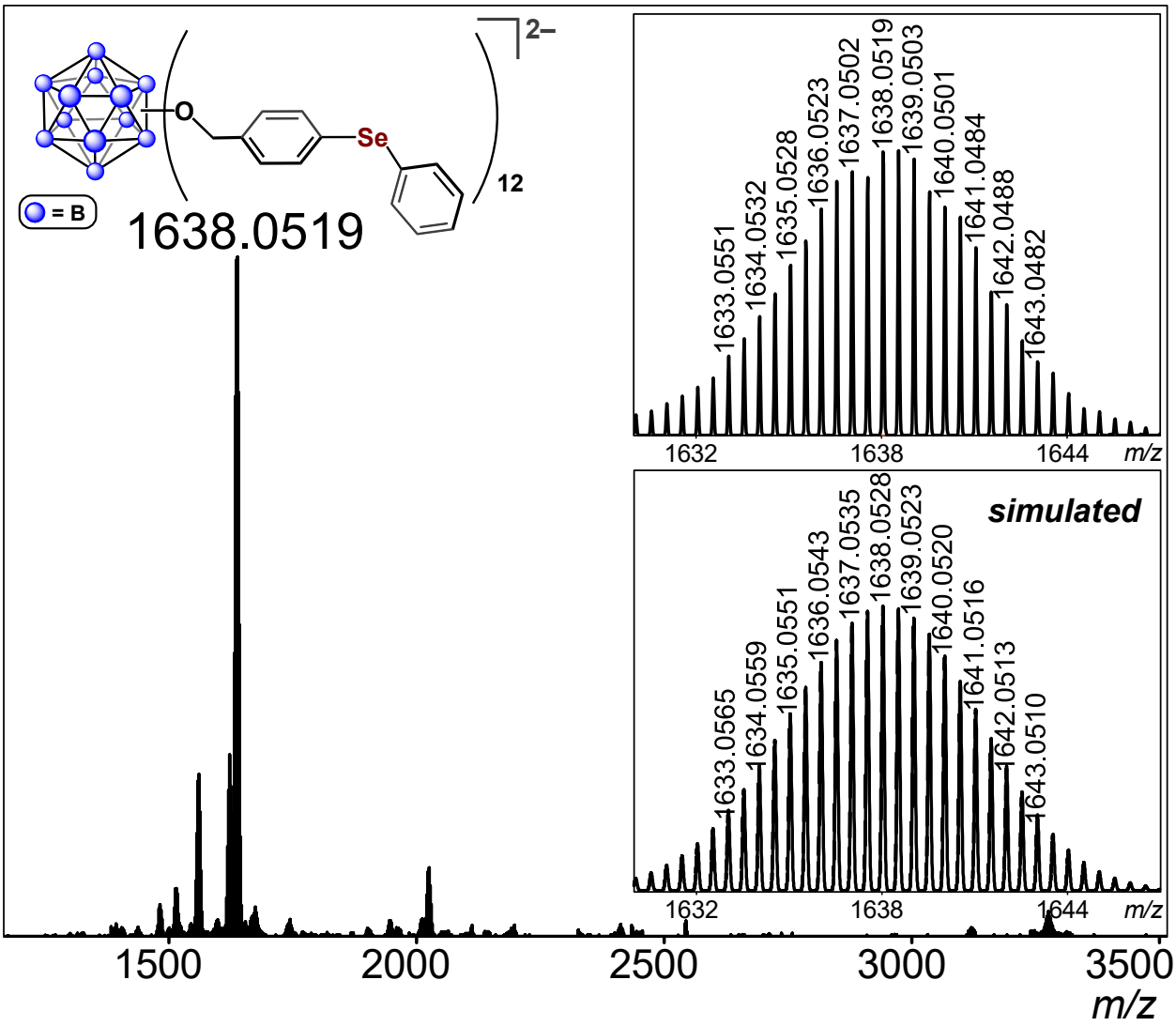

Figure S65. ESI-MS(–) of $[B_{12}(OCH_2C_6H_4SePh)_{12}]^{2-}$ (MeCN, 1.5 kV).

S2.22. $[H_3NC(CH_2OH)_3][B_{12}(OCH_2C_6H_4(glutathione))_{12}]$ ($[H_3NC(CH_2OH)_3][17]$)

The general reaction procedure to generate [**1**][SbF_6]$_{11}$ (**Section S2.5**) was followed. To a stirring solution of [**1**][SbF_6]$_{11}$ (0.0014 mmol) in DMF (1 mL) was added L-glutathione (6 mg, 0.02 mmol, 14 equiv) in an aqueous solution of TRIS buffer (1 mL of a 200 mM solution, pH 8). The purple reaction mixture was allowed to stir at 25 °C for a total of 15 min, at which point all volatiles were removed under reduced pressure. The resulting purple residue was suspended in H_2O spiked with 0.1% TFA (1.5 mL), sonicated for 10 min, and then centrifuged (2,200 × g, 5 min). The purple supernatant was removed and filtered through a 0.22 µm PTFE filter, resulting in a homogeneous purple solution containing the product. The product was purified by reversed-phase HPLC with an Agilent Technologies 1260 Infinity II HPLC instrument equipped with a Variable Wavelength Detector (VWD, 254, 214 nm) and using an Agilent ZORBAX SB-C18 reversed-phase column (9.4 × 250 mm, 5 µm) with the following method (solvent A: H_2O spiked with 0.1% TFA; solvent B: MeCN spiked with 0.1% TFA): 0–5 min, A (100%) : B (0%); 5–60 min, A (100–45%) : B (0–55%); 60–75 min, A (45–0%) : B (55–100%); 75–90 min, A (0%) : B (100%) and with a flow rate of 3 mL/min. The fractions containing the pure product were combined and the solvent was lyophilized to afford $[H_3NC(CH_2OH)_3][B_{12}(OCH_2C_6H_4(glutathione))_{12}]$ as a purple sold in 70% yield (5 mg, 0.001 mmol). ^{1}H NMR (400 MHz, 25 °C, D_2O spiked with CD_3CN) δ: 7.23 (br s, Ar-*H*), 4.59 (br s, glutathione), 3.82 (br s, glutathione), 3.37–3.23 (br m, glutathione), 2.45 (br s, glutathione) ppm. The signals observed in the ^{1}H NMR spectrum are paramagnetically broadened due to the monoanionic dodecaborate $[B_{12}]^-$ core. ^{11}B{^{1}H} NMR (128 MHz, 25 °C, D_2O spiked with CD_3CN) δ: A silent ^{11}B{^{1}H} NMR spectrum was observed due to the paramagnetic $[B_{12}]^-$ core. ESI-MS(–): 847.6064 (calc'd, 847.6001 for $[[B_{12}(OCH_2C_6H_4(glutathione))_{12}]^{2-} + 8H^+]^{6+}$) *m/z*. UV-vis ($H_2O$, 25 °C): λ_{max} 549 nm.

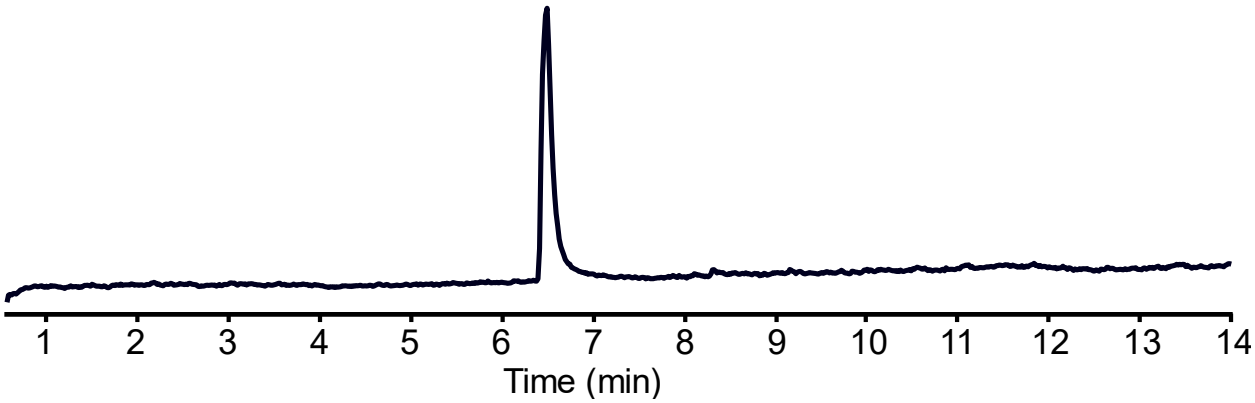

Figure S66. LC-trace of $[H_3NC(CH_2OH)_3][B_{12}(OCH_2C_6H_4(glutathione))_{12}]$. LC-MS method (solvent A: H_2O with 0.1% formic acid; solvent B: MeCN with 0.1% formic acid): 0–2 min, A (100%) : B (0%); 2–11 min, A (100–5%) : B (0–95%); 11–12 min, A (5–0%) : B (95–100%); 12–14 min, A (0%) : B (100%).

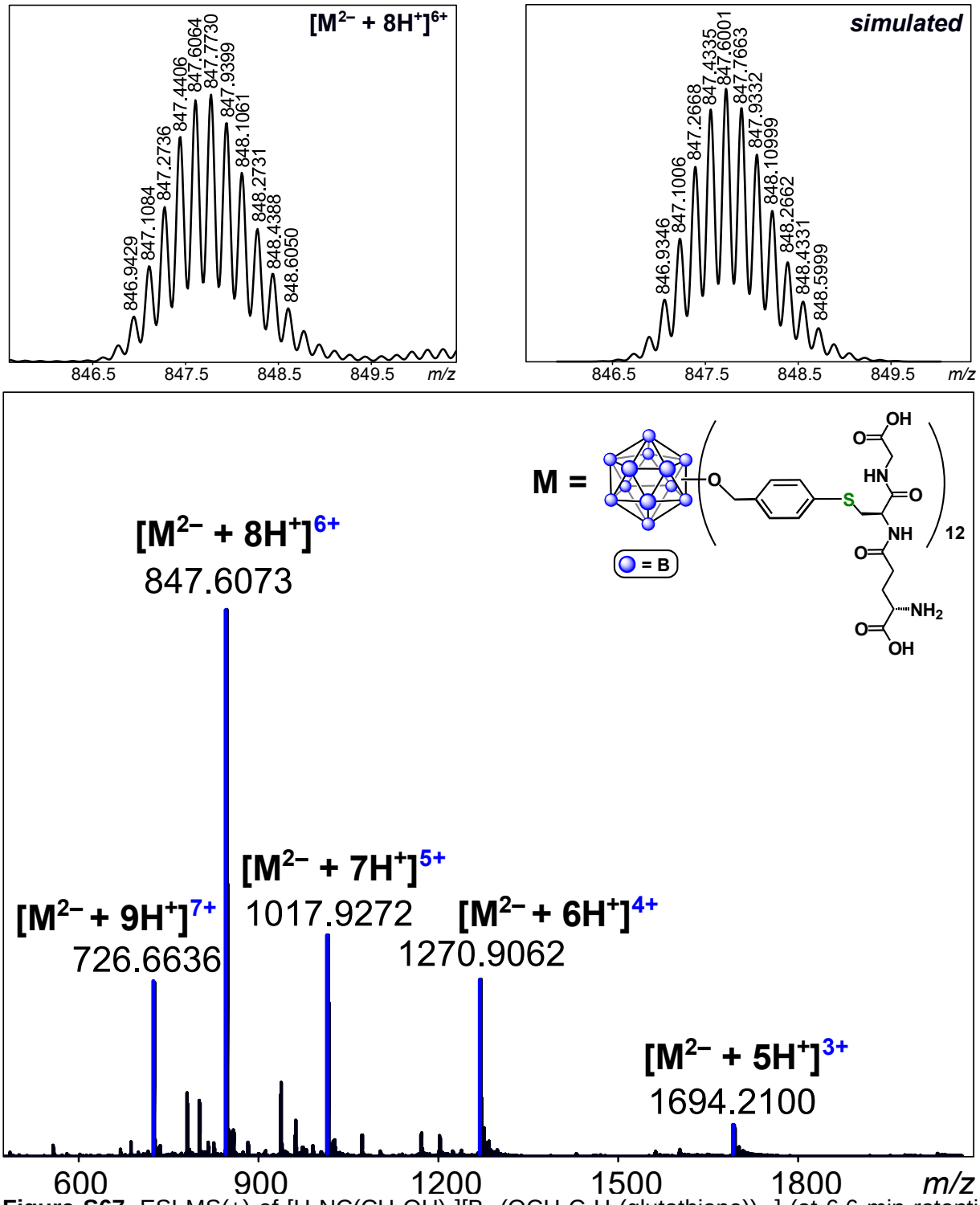

Figure S67. ESI-MS(+) of $[H_3NC(CH_2OH)_3][B_{12}(OCH_2C_6H_4(glutathione))_{12}]$ (at 6.6 min retention time from the LC-MS data; 50:50 H_2O/MeCN v/v with 0.1% formic acid).

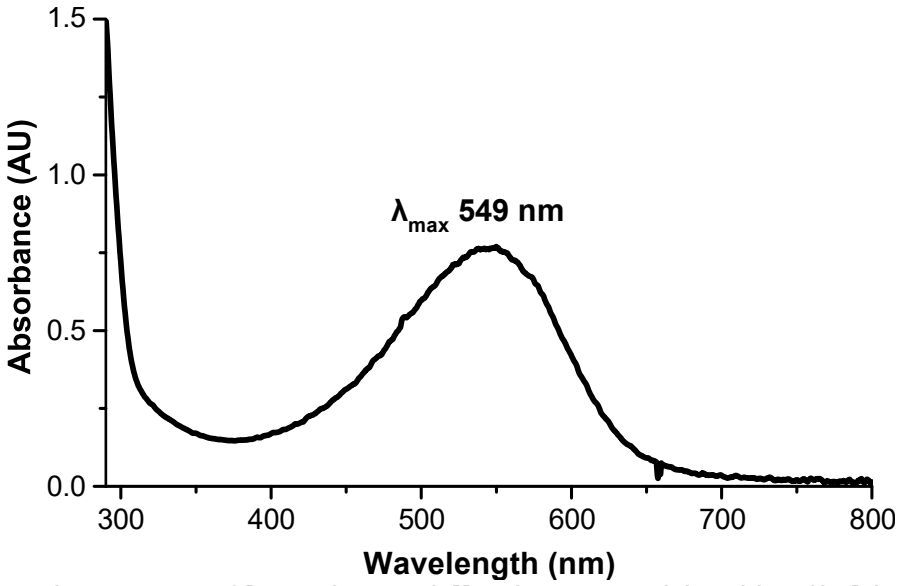

Figure S68. UV-vis spectrum of $[H_3NC(CH_2OH)_3][B_{12}(OCH_2C_6H_4(glutathione))_{12}]$ (H_2O, 25 °C).

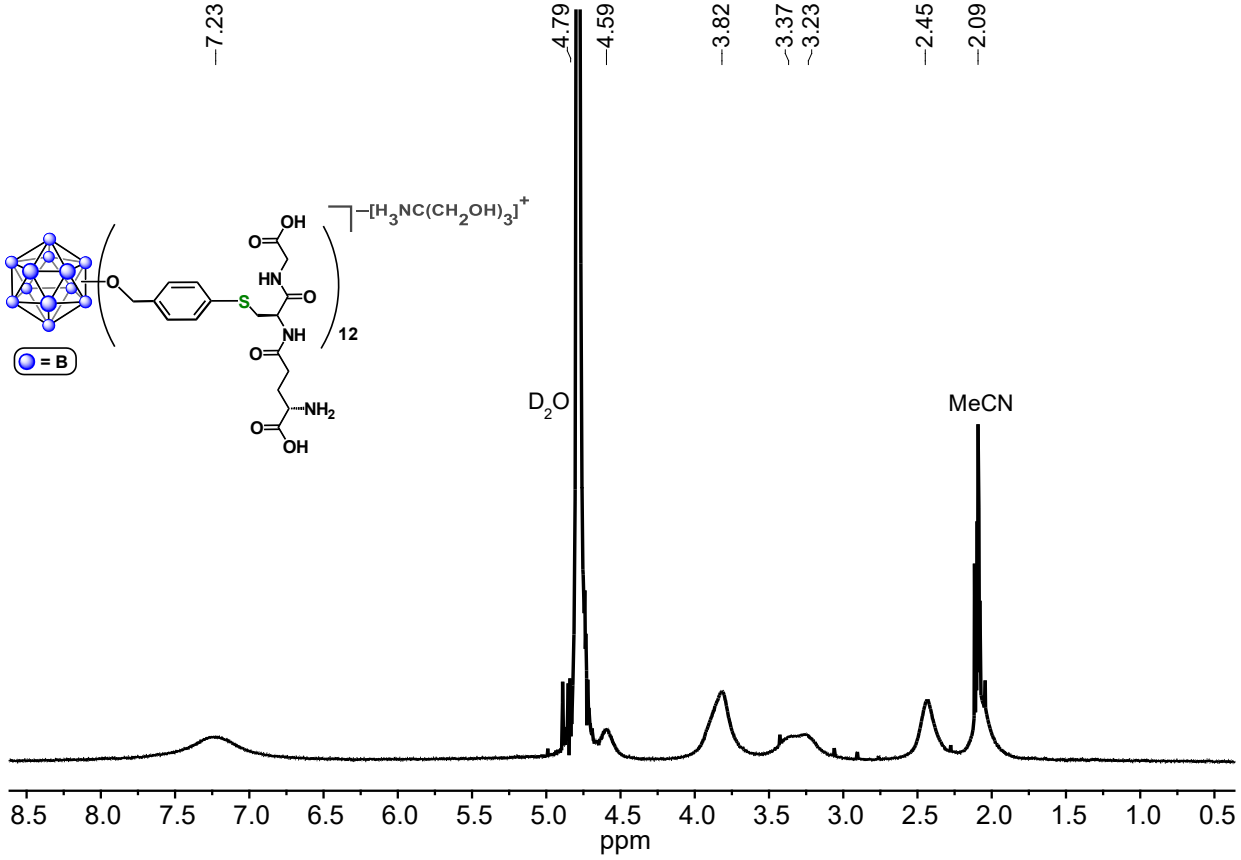

Figure S69. ^1H NMR spectrum of $[H_3NC(CH_2OH)_3][B_{12}(OCH_2C_6H_4(glutathione))_{12}]$ (D_2O spiked with CD_3CN, 400 MHz, 25 °C).

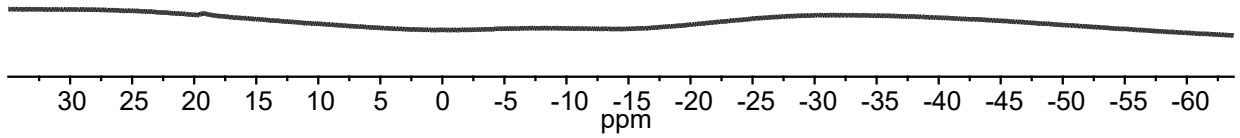

Figure S70. $^{11}B\{^{1}H\}$ NMR spectrum of $[H_3NC(CH_2OH)_3][B_{12}(OCH_2C_6H_4(glutathione))_{12}]$ (D_2O spiked with CD_3CN, 128 MHz, 25 °C).

S2.23. $[Na_2][B_{12}(OCH_2C_6H_4(1\text{-thio-}\beta\text{-D-glucose}))_{12}]$ ($[Na_2][18]$)

The general reaction procedure to generate $[\mathbf{1}][SbF_6]_{11}$ (**Section S2.5**) was followed. To a stirring solution of $[\mathbf{1}][SbF_6]_{11}$ (0.0014 mmol) in DMF (1 mL) was added a solution of Na[1-thio-β-D-glucose] (9 mg, 0.04 mmol, 30 equiv) in H_2O (0.5 mL). The resulting mixture was allowed to stir at 25 °C for 15 min, during which time the color of the solution changed from dark purple to colorless. All volatiles were then removed from the reaction mixture under reduced pressure, resulting in a colorless residue. To the solid residue was added H_2O (4.5 mL), resulting in a colorless suspension. The suspension was sonicated (5 min), and then centrifuged (2,200 × g, 5 min). The supernatant was then removed and filtered through a 0.45 µm PTFE filter into a Pall Microsep™ Advance 1K Omega Centrifugal Filter sample reservoir.* The device was capped and centrifuged for 75 min at 7,500 × g. The device was then removed from the centrifuge, the solution in the filtrate receiver tube was removed, and H_2O (5 mL) was added to the sample reservoir containing the aqueous solution of the product. This process was repeated twice more for a total of three centrifuge cycles. After the third cycle, the solution in the sample reservoir (ca. 0.5 mL) was removed, transferred to a 15 mL conical tube, and the H_2O was lyophilized overnight to afford $[Na_2][B_{12}(OCH_2C_6H_4(1\text{-thio-}\beta\text{-D-glucose}))_{12}]$ as a pale-pink powder (3 mg, 0.8 µmol, 60%). ^{1}H NMR (400 MHz, 25 °C, D_2O) δ: 7.38 (d, 24H, Ar-*H*, ^3J = 7 Hz), 7.24 (br d, 24H, Ar-*H*), 5.25 (br s, 24H, –C*H*$_2$–), 4.65 (d, 12H, *J* = 10 Hz, glc H1), 3.76 (d, 12H, *J* = 12 Hz, glc H6), 3.67–3.63 (dd, 12H, *J* = 5, 12 Hz, glc H6), 3.52 (t, 12H, *J* = 9 Hz, glc H3), 3.40 (t, 12H, *J* = 9 Hz, glc H5), 3.32 (t, 24H, *J* = 9 Hz, glc H4 and H2 signals overlapping) ppm (broadening of the aryl and methylene ^{1}H NMR signals is due to slow oxidation of the diamagnetic dianionic species to the paramagnetic monoanion in H_2O in the presence of air). $^{11}B\{^1H\}$ NMR (128 MHz, 25 °C, D_2O) δ: -16.0 ppm. ESI-MS(–): 1878.5102 (calc'd,1872.5103) *m/z*. ^{1}H NMR (400 MHz, 25 °C, CD_3OD) δ: 7.38 (d, 24H, Ar-*H*, ^3J = 8 Hz), 7.26 (d, 24H, Ar-*H*, ^3J = 8 Hz), 5.39 (s, 24H, –C*H*$_2$–), 4.55 (d, 12H, *J* = 10 Hz, glc H1), 3.84 (dd, 12H, *J* = 2, 12 Hz, glc H6), 3.67 (dd, 12H, *J* = 5, 12 Hz, glc H6), 3.42 (t, 12H, *J* = 9 Hz, glc H4), 3.29 (glc H3 and H5 resonances overlapping with CD_3OD solvent, 24H), 3.19 (dd, 12H, *J* = 9, 10 Hz, glc H2) ppm. $^{11}B\{^1H\}$ NMR (128 MHz, 25 °C, CD_3OD) δ: -14.9 ppm.

*It is noted that prior to sample purification, the Pall Microsep™ Advance 1K Omega Centrifugal Filter was pre rinsed by filtering HPLC-grade H_2O (5 mL) through the device at 7,500 × g for 15 min. The filtrate was discarded prior to use.

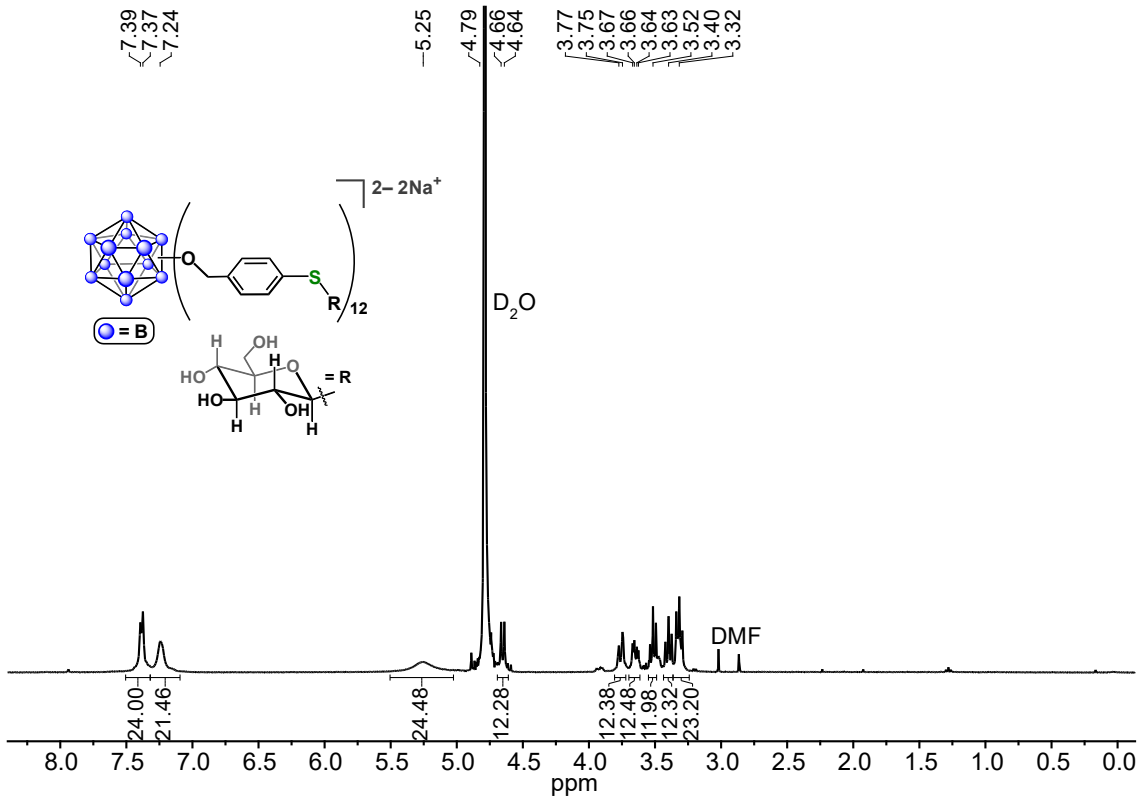

Figure S71. ^{1}H NMR spectrum of $[Na_2][B_{12}(OCH_2C_6H_4(1\text{-thio-}\beta\text{-D-glucose}))_{12}]$ (D_2O, 400 MHz, 25 °C).

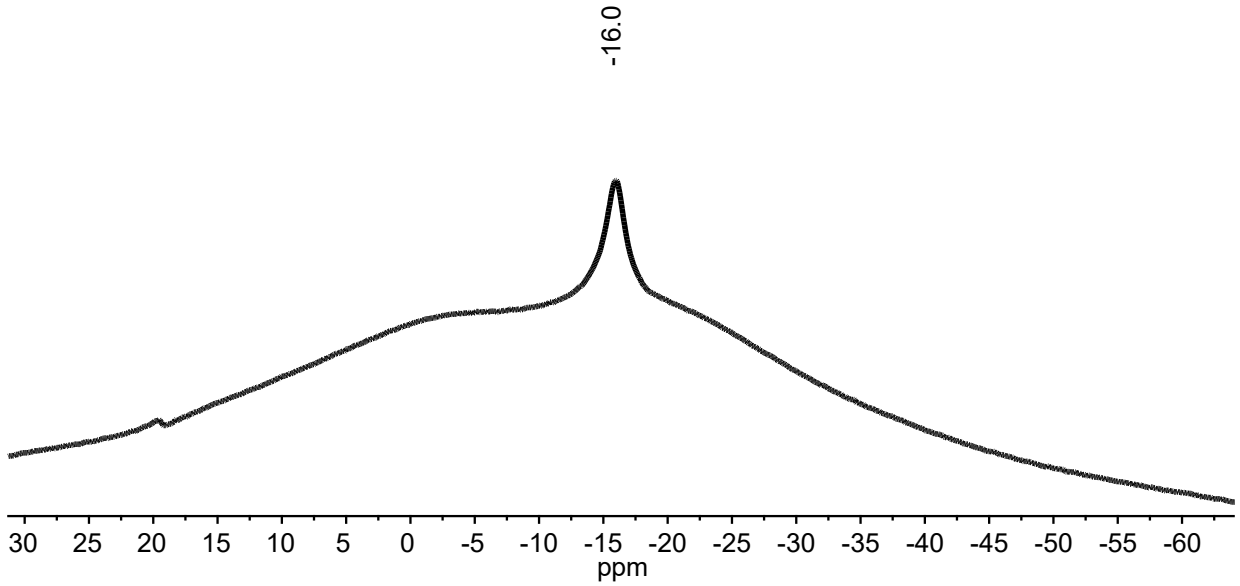

Figure S72. $^{11}B\{^{1}H\}$ NMR spectrum of $[Na_2][B_{12}(OCH_2C_6H_4(1\text{-thio-}\beta\text{-D-glucose}))_{12}]$ (D_2O, 128 MHz, 25 °C).

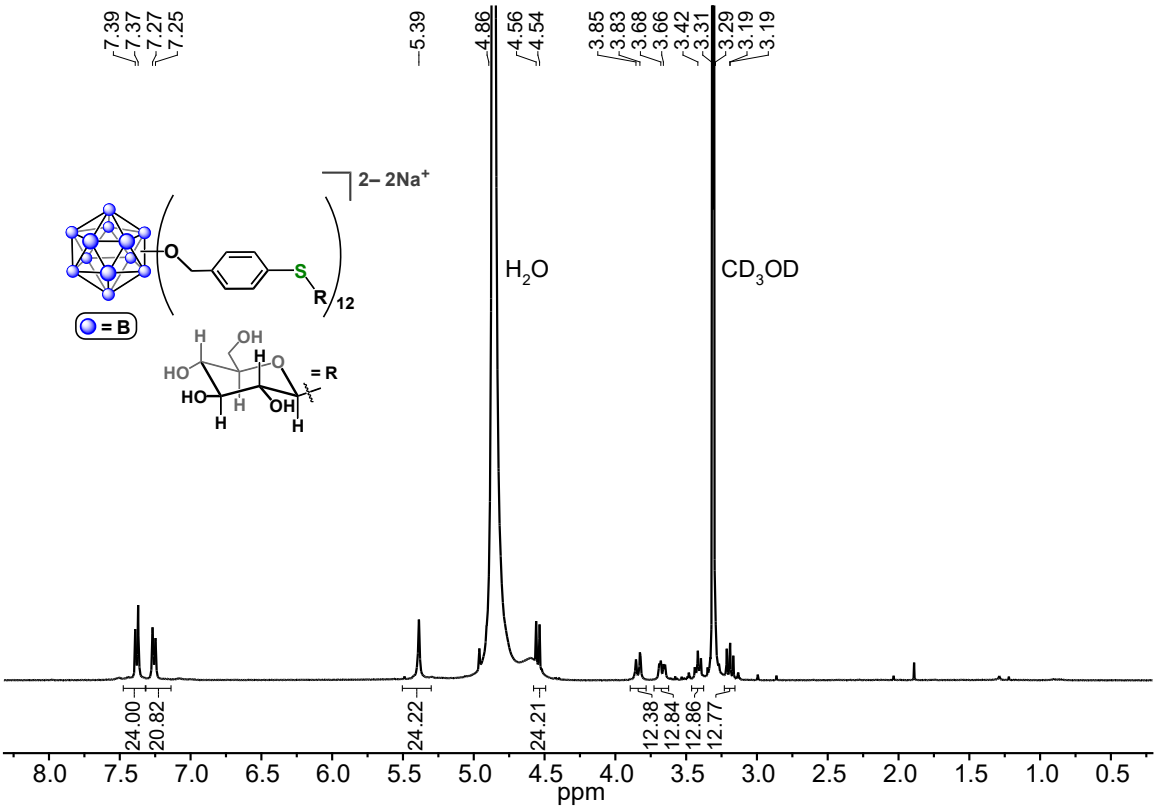

Figure S73. ^{1}H NMR spectrum of $[Na_2][B_{12}(OCH_2C_6H_4(1\text{-thio-}\beta\text{-D-glucose}))_{12}]$ (CD_3OD, 400 MHz, 25 °C).

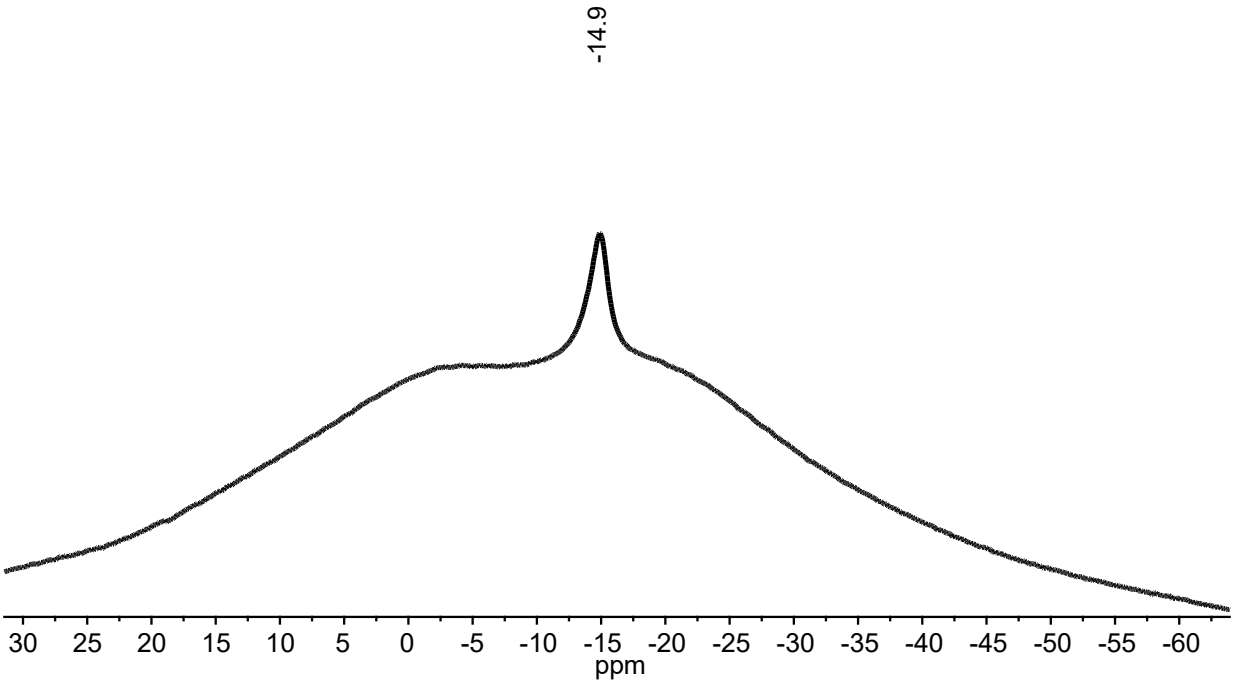

Figure S74. $^{11}B\{^{1}H\}$ NMR spectrum of $[Na_2][B_{12}(OCH_2C_6H_4(1\text{-thio-}\beta\text{-D-glucose}))_{12}]$ (CD_3OD, 128 MHz, 25 °C).

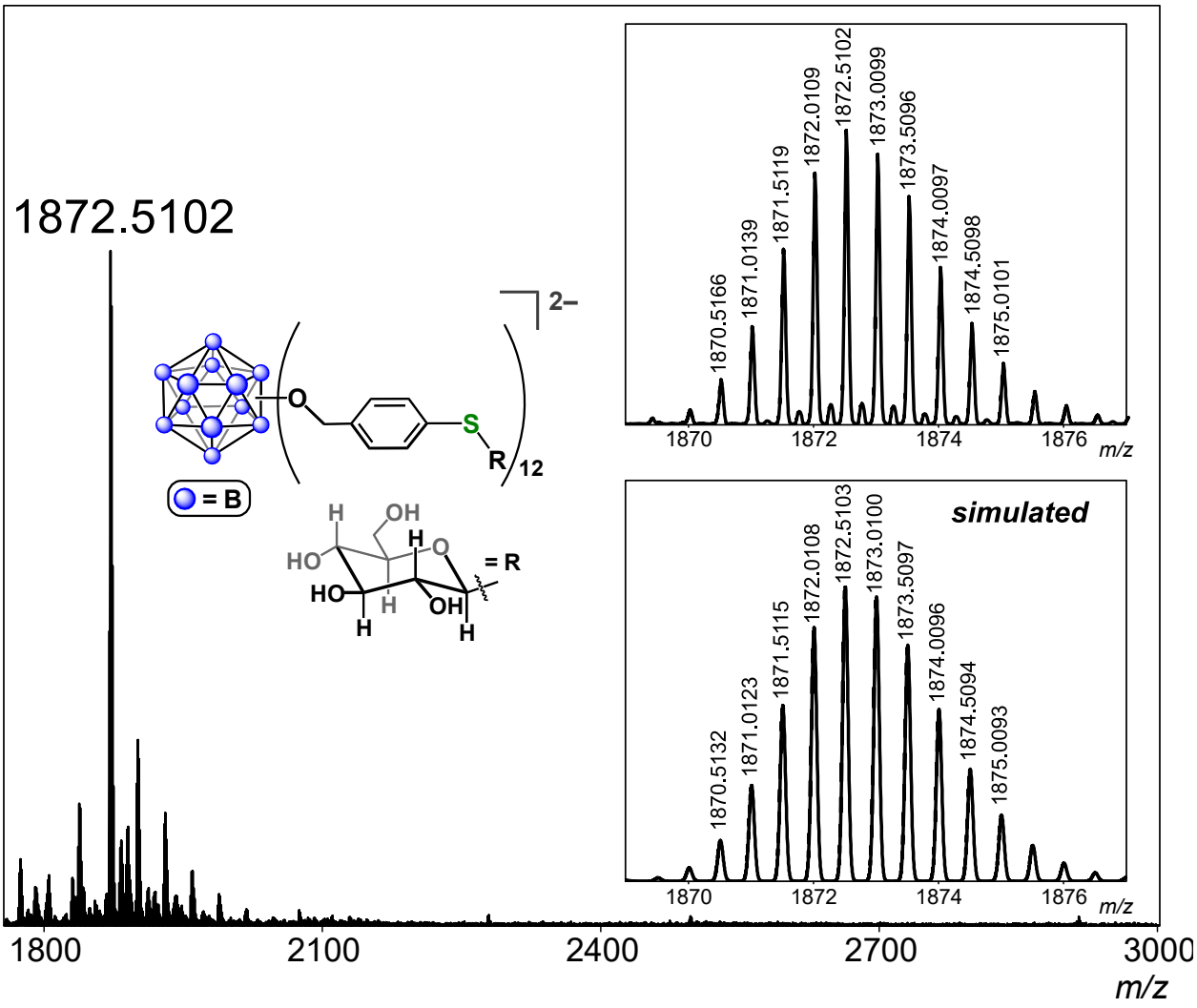

Figure S75. ESI-MS(–) of $[B_{12}(OCH_2C_6H_4(1\text{-thio-}\beta\text{-D-glucose}))_{12}]^{2-}$ (MeOH, 1.5 kV).

S2.24. $[Na_2][B_{12}(OCH_2C_6H_4(1\text{-thio-}\beta\text{-D-galactose}))_{12}]$ ($[Na_2][19]$)

The general reaction procedure to generate $[\mathbf{1}][SbF_6]_{11}$ (**Section S2.5**) was followed. To a stirring solution of $[\mathbf{1}][SbF_6]_{11}$ (0.0014 mmol) in DMF (1 mL) was added a solution of Na[1-thio-β-D-galactose] (9 mg, 0.04 mmol, 30 equiv) in H_2O (0.5 mL). The resulting mixture was allowed to stir at 25 °C for 15 min, during which time the color of the solution changed from dark purple to colorless. All volatiles were then removed from the reaction mixture under reduced pressure, resulting in a colorless residue. To the solid residue was added H_2O (4.5 mL), resulting in a colorless suspension. The suspension was sonicated (5 min), and then centrifuged (2,200 × g, 5 min). The supernatant was then removed and filtered through a 0.45 µm PTFE filter into a Pall Microsep™ Advance 1K Omega Centrifugal Filter sample reservoir.* The device was capped and centrifuged for 75 min at 7,500 × g. The device was then removed from the centrifuge, the solution in the filtrate receiver tube was removed, and H_2O (5 mL) was added to the sample reservoir containing the aqueous solution of the product. This process was repeated twice more for a total of three centrifuge cycles. After the third cycle, the solution in the sample reservoir (ca. 0.5 mL) was removed, transferred to a 15 mL conical tube, and the H_2O was lyophilized overnight to afford $[Na_2][B_{12}(OCH_2C_6H_4(1\text{-thio-}\beta\text{-D-galactose}))_{12}]$ as a pale-pink powder (3 mg, 0.8 µmol, 60%). ^{1}H NMR (400 MHz, 25 °C, D_2O) δ: 7.39 (d, 24H, Ar-*H*, ^3J = 8 Hz), 7.23 (d, 24H, Ar-*H*, ^3J = 8 Hz), 5.26 (br s, 24H, –C*H*$_2$–), 4.63 (d, 12H, *J* = 10 Hz, gal H1), 3.98 (d, 12H, *J* = 3 Hz, gal H4), 3.70–3.56 (m, 60H, gal H6, H5, H3, and H2 resonances overlapping) ppm (broadening of the aryl and methylene ^{1}H NMR signals is due to slow oxidation of the diamagnetic dianionic species to the paramagnetic monoanion in H_2O in the presence of air). ^{11}B{^{1}H} NMR (128 MHz, 25 °C, D_2O) δ: -15.8 ppm. ESI-MS(–): 1878.5051 (calc'd,1872.5103) *m/z*. ^{1}H NMR (400 MHz, 25 °C, CD_3OD spiked with D_2O) δ: 7.35 (d, 24H, Ar-*H*, ^3J = 8 Hz), 7.23 (d, 24H, Ar-*H*, ^3J = 8 Hz), 5.35 (s, 24H, –C*H*$_2$–), 4.57 (dd, 12H, *J* = 5, 10 Hz, gal H1), 3.94 (br m, 12H, gal H4), 3.77–3.67 (m, 24H, gal H6), 3.59 (m, 36H, gal H2 H3 and H5 resonances overlapping) ppm. ^{11}B{^{1}H} NMR (128 MHz, 25 °C, CD_3OD spiked with D_2O) δ: -15.6 ppm.

*It is noted that prior to sample purification, the Pall Microsep™ Advance 1K Omega Centrifugal Filter was pre rinsed by filtering HPLC-grade H_2O (5 mL) through the device at 7,500 × g for 15 min. The filtrate was discarded prior to use.

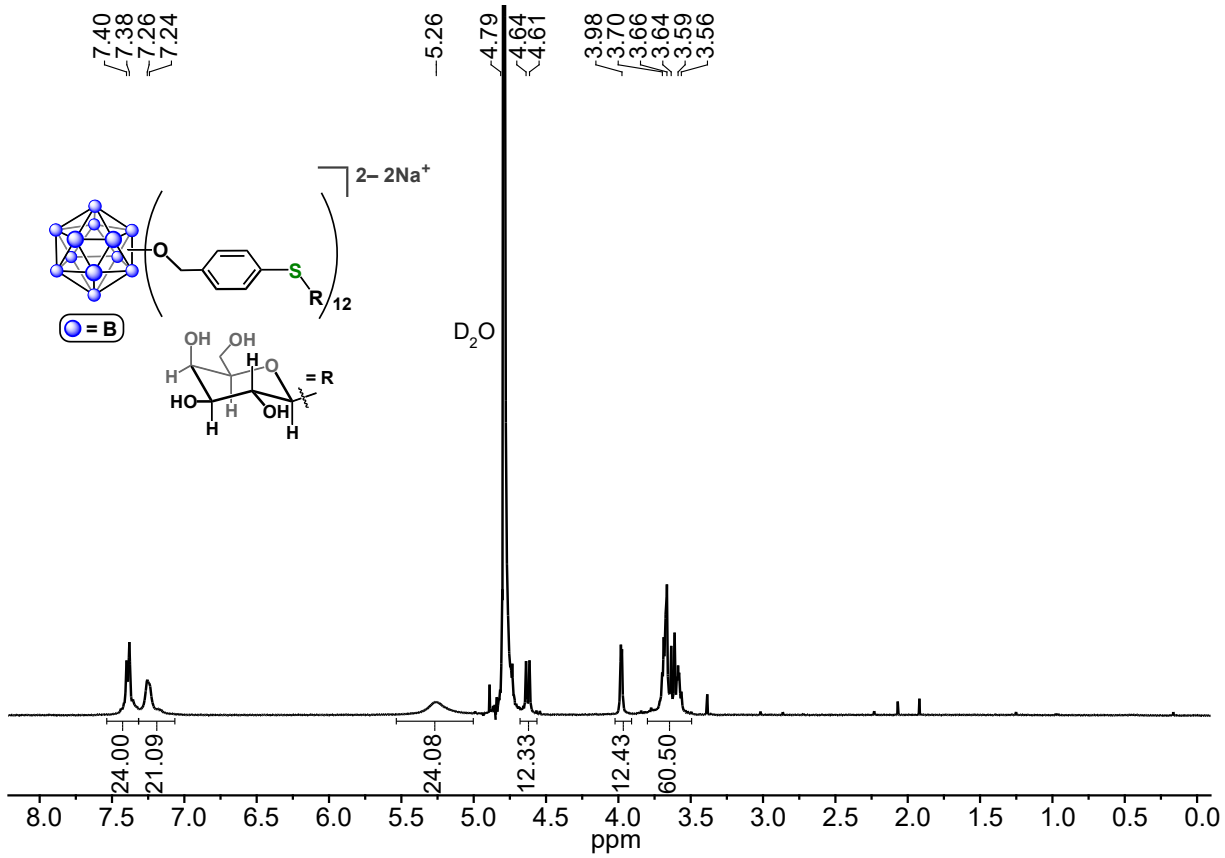

Figure S76. ^{1}H NMR spectrum of $[Na_2][B_{12}(OCH_2C_6H_4(1\text{-thio-}\beta\text{-D-galactose}))_{12}]$ (D_2O, 400 MHz, 25 °C).

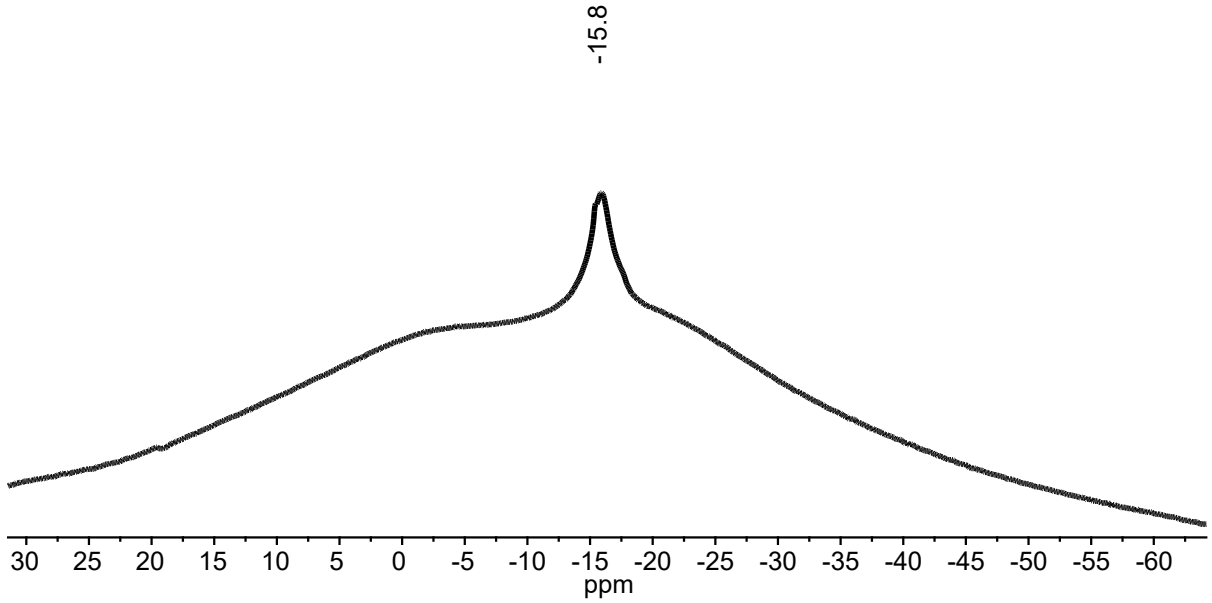

Figure S77. ^{11}B{^{1}H} NMR spectrum of $[Na_2][B_{12}(OCH_2C_6H_4(1\text{-thio-}\beta\text{-D-galactose}))_{12}]$ (D_2O, 128 MHz, 25 °C).

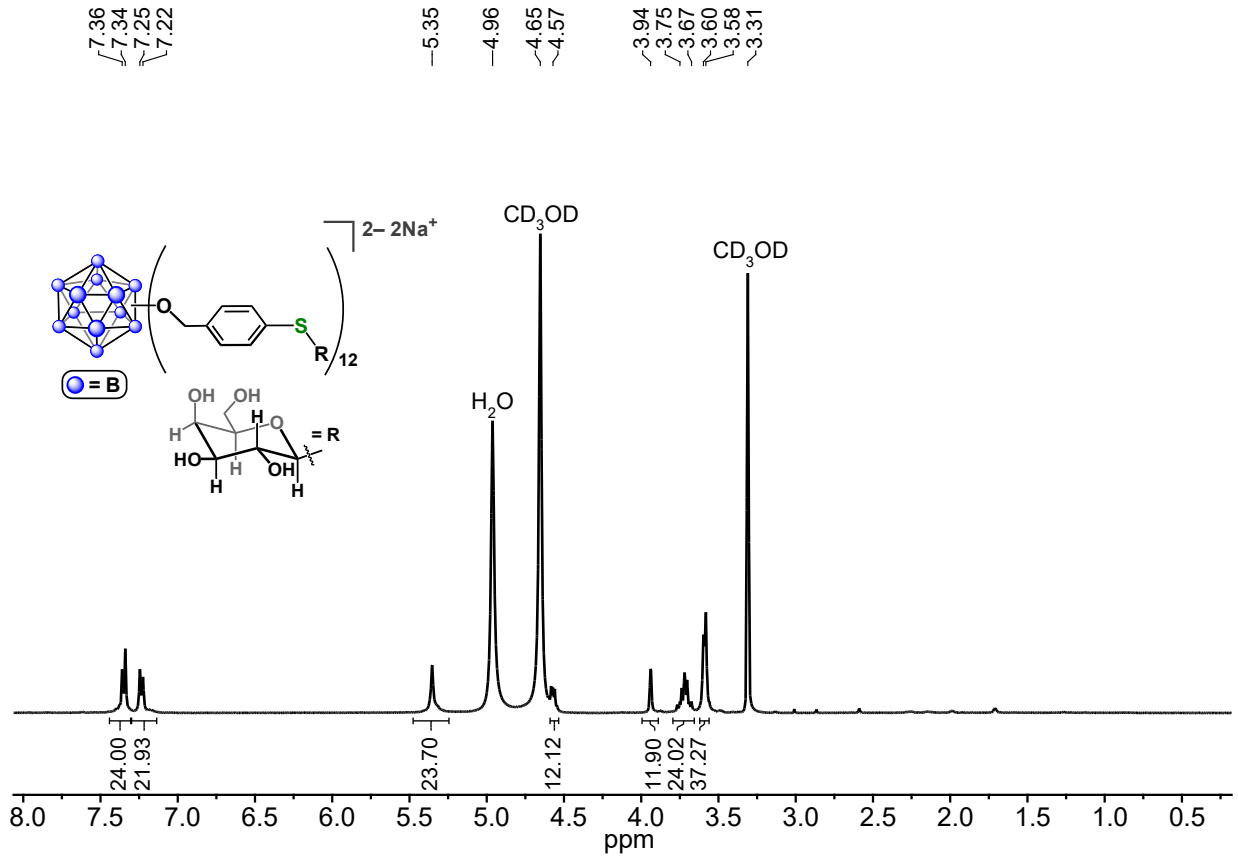

Figure S78. ^{1}H NMR spectrum of $[Na_2][B_{12}(OCH_2C_6H_4(1\text{-thio-}\beta\text{-D-galactose}))_{12}]$ (CD_3OD spiked with D_2O, 400 MHz, 25 °C).

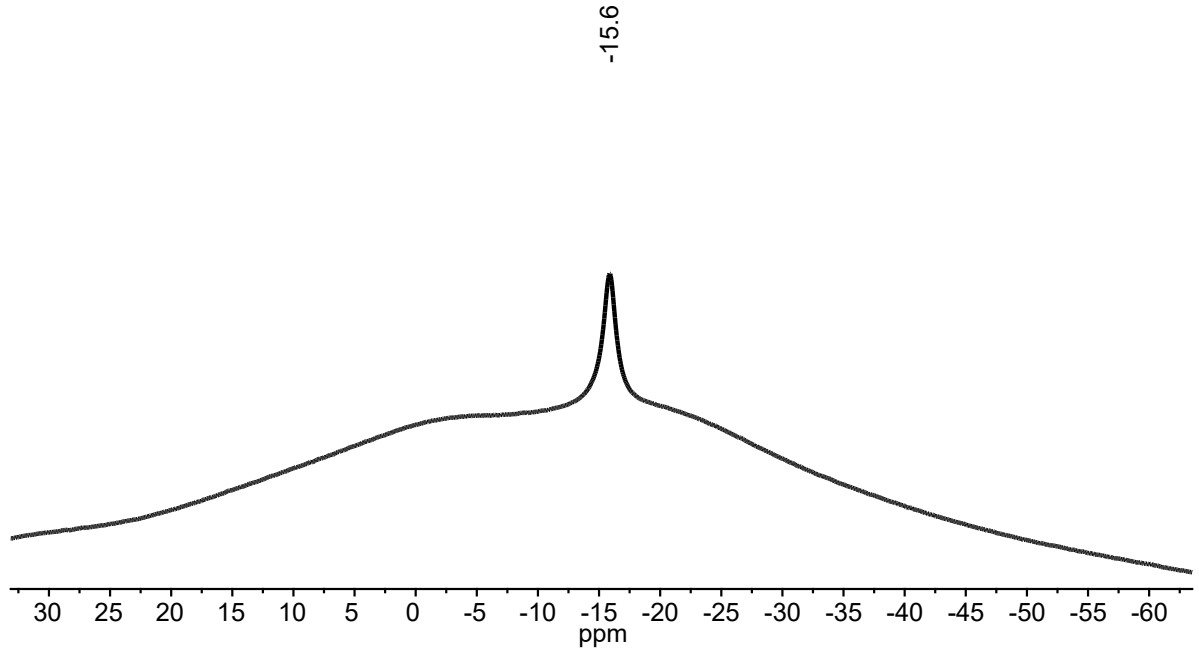

Figure S79. $^{11}B\{^{1}H\}$ NMR spectrum of $[Na_2][B_{12}(OCH_2C_6H_4(1\text{-thio-}\beta\text{-D-galactose}))_{12}]$ (CD_3OD spiked with D_2O, 128 MHz, 25 °C).

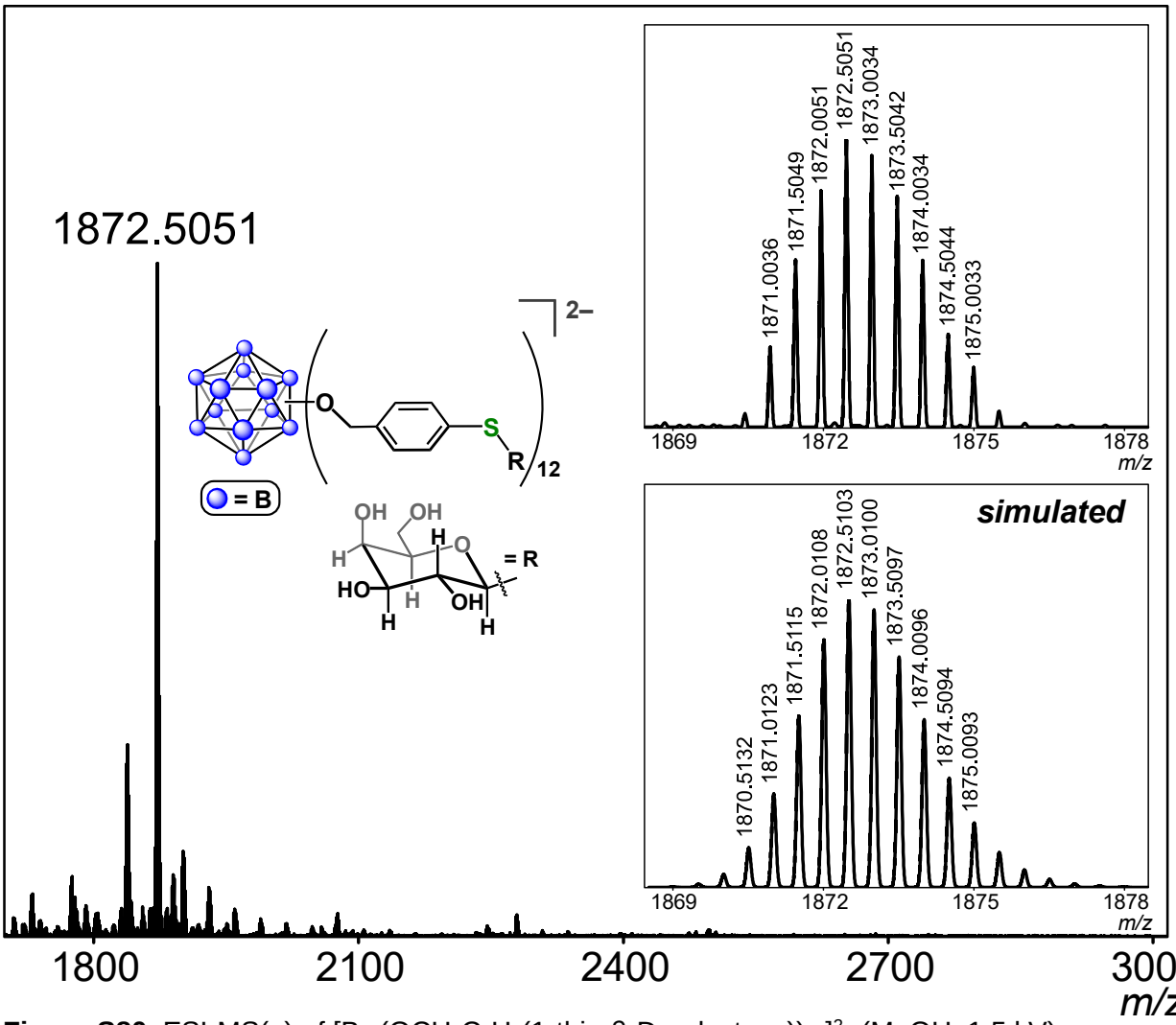

Figure S80. ESI-MS(–) of $[B_{12}(OCH_2C_6H_4(1\text{-thio-}\beta\text{-D-galactose}))_{12}]^{2-}$ (MeOH, 1.5 kV).

S2.25. $[Na_2][B_{12}(OCH_2C_6H_4(1\text{-thio-}\alpha\text{-D-mannose}))_{12}]$ ($[Na_2][20]$)

The general reaction procedure to generate $[\mathbf{1}][SbF_6]_{11}$ (**Section S2.5**) was followed. To a stirring solution of $[\mathbf{1}][SbF_6]_{11}$ (0.0014 mmol) in DMF (1 mL) was added a solution of Na[1-thio-α-D-mannose] (9 mg, 0.04 mmol, 30 equiv) in H_2O (0.5 mL). The resulting mixture was allowed to stir at 25 °C for 15 min, during which time the color of the solution changed from dark purple to colorless. All volatiles were then removed from the reaction mixture under reduced pressure, resulting in a colorless residue. To the solid residue was added H_2O (4.5 mL), resulting in a colorless suspension. The suspension was sonicated (5 min), and then centrifuged (2,200 × g, 5 min). The supernatant was then removed and filtered through a 0.45 µm PTFE filter into a Pall Microsep™ Advance 1K Omega Centrifugal Filter sample reservoir.* The device was capped and centrifuged for 75 min at 7,500 × g. The device was then removed from the centrifuge, the solution in the filtrate receiver tube was removed, and H_2O (5 mL) was added to the reservoir containing the aqueous solution of the product. This process was repeated twice more for a total of three centrifuge cycles. After the third cycle, the solution in the sample reservoir (ca. 0.5 mL) was removed, transferred to a 15 mL conical tube, and the H_2O was lyophilized overnight to afford $[Na_2][B_{12}(OCH_2C_6H_4(1\text{-thio-}\alpha\text{-D-mannose}))_{12}]$ as a pale-pink powder (2 mg, 5 µmol, 40%). ^{1}H NMR (400 MHz, 25 °C, D_2O spiked with CD_3OD) δ: 7.12–7.06 (two sets of doublets overlapping, 48H, Ar-*H*), 5.41 (s, 12H , man H1), 5.18 (br s, 24H, –C*H*$_2$–), 4.24–4.08 (m, 48H, gal resonances overlapping), 3.88–3.72 (m, 72H, gal resonances overlapping) ppm (broadening of the aryl and methylene ^{1}H NMR signals is due to slow oxidation of the diamagnetic dianionic species to the paramagnetic monoanion in H_2O in the presence of air). $^{11}B\{^1H\}$ NMR (128 MHz, 25 °C, D_2O spiked with CD_3OD) δ: -15.3 ppm. ESI-MS(–): 1248.0036 (calc'd, 1248.0046 for $([B_{12}(OCH_2C_6H_4(1\text{-thio-}\alpha\text{-D-mannose}))_{12} - H^+]^{3-}$) *m/z*.

*It is noted that prior to sample purification, the Pall Microsep™ Advance 1K Omega Centrifugal Filter was pre rinsed by filtering HPLC-grade H_2O (5 mL) through the device at 7,500 × g for 15 min. The filtrate was discarded prior to use.

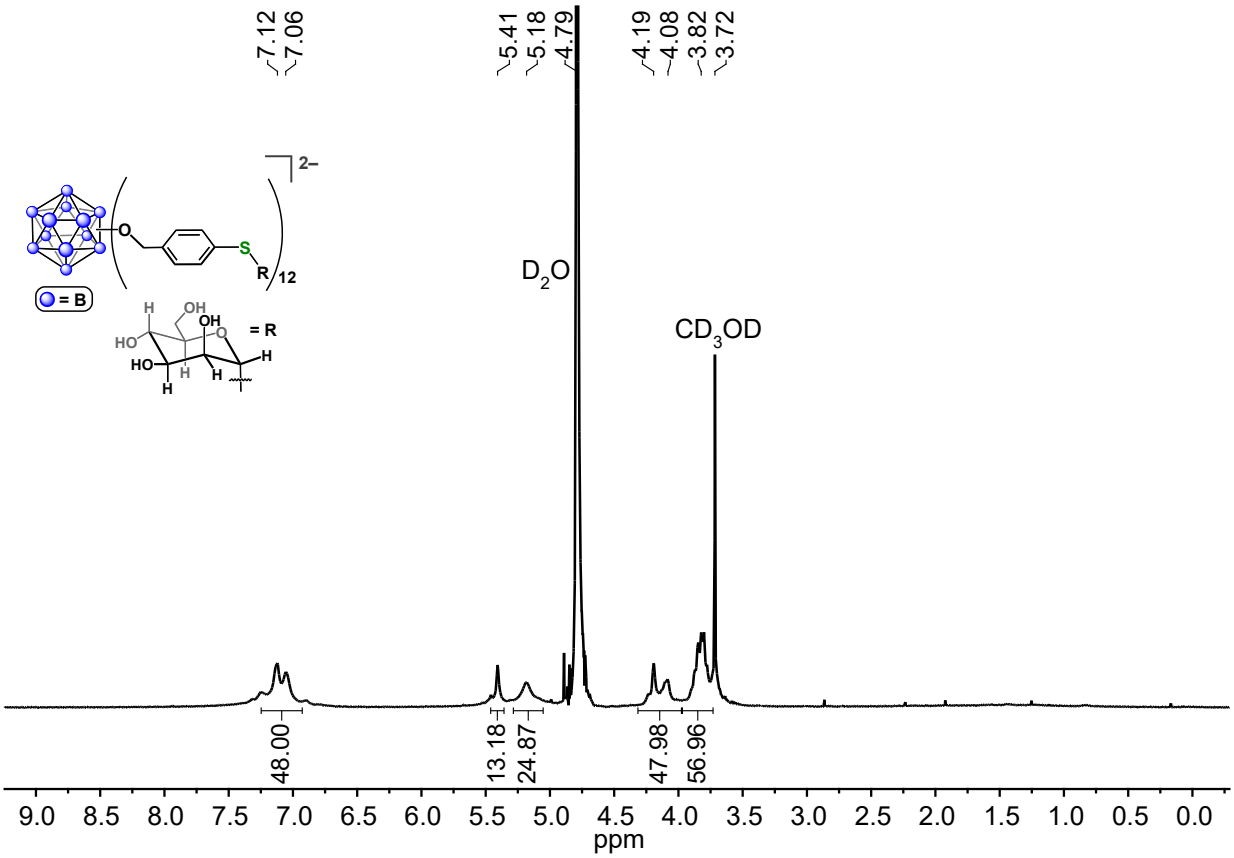

Figure S81. ^{1}H NMR spectrum of $[Na_2][B_{12}(OCH_2C_6H_4(1\text{-thio-}\beta\text{-D-mannose}))_{12}]$ (D_2O spiked with CD_3OD, 400 MHz, 25 °C).

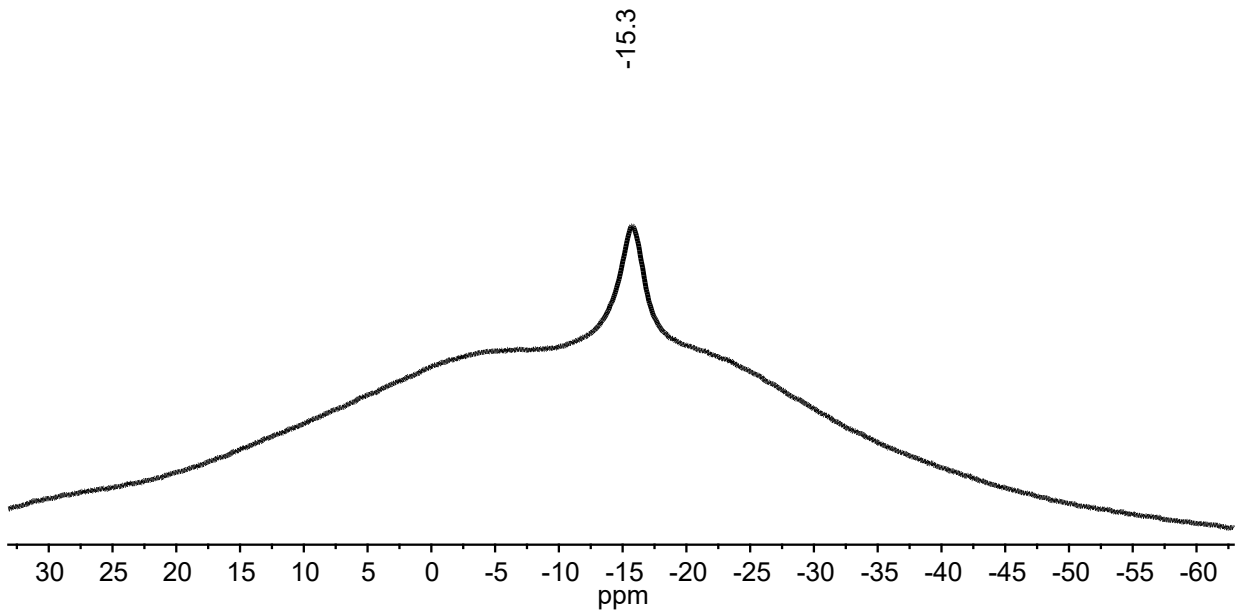

Figure S82. $^{11}B\{^{1}H\}$ NMR spectrum of $[Na_2][B_{12}(OCH_2C_6H_4(1\text{-thio-}\beta\text{-D-mannose}))_{12}]$ (D_2O spiked with CD_3OD, 128 MHz, 25 °C).

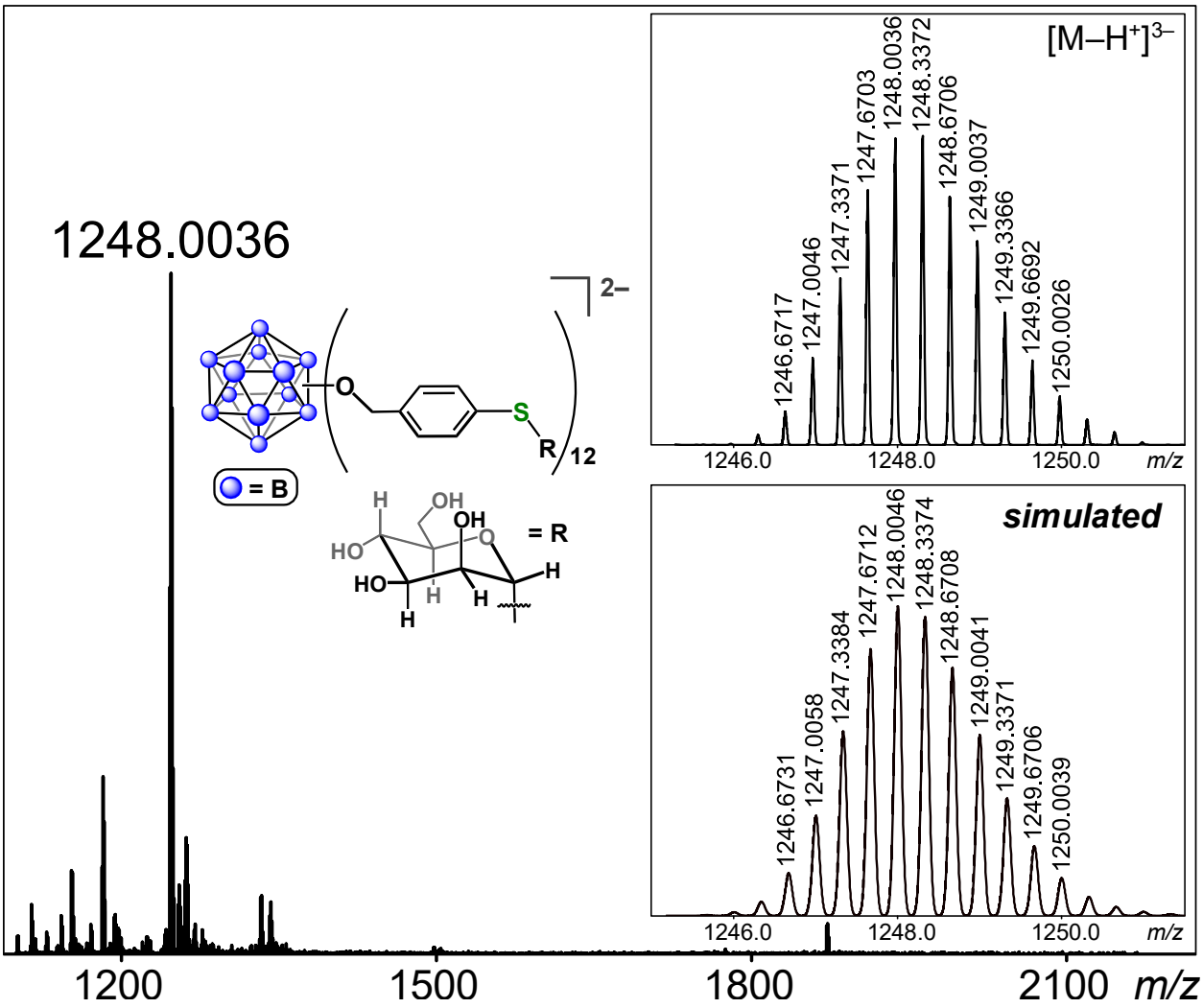

Figure S83. ESI-MS(–) of $[B_{12}(OCH_2C_6H_4(1\text{-thio-}\alpha\text{-D-mannose}))_{12}]^{2-}$ (MeOH, 1.5 kV). The monodeprotonated species, $[B_{12}(OCH_2C_6H_4(1\text{-thio-}\alpha\text{-D-mannose}))_{12} - H^+]^{3-}$, is observed under ESI-MS conditions.

S2.26. $[B_{12}(OCH_2C_6H_4SC_6H_4(Me\text{-}DalPhos)AuCl)_{12}][SbF_6]_{10}$ ([21][SbF_6]$_{10}$)

To a cooled (-4 °C) solution of $AgSbF_6$ (9 mg, 0.026 mmol, 16 equiv) in DCM (1 mL) was added a cooled solution (-4 °C) of [K_2][**3**] (7 mg, 0.002 mmol, 1 equiv, prepared as previously described in **Section S2.7**) and (Me-DalPhos)AuCl (17 mg, 0.026 mmol, 16 equiv) in DCM (1 mL) under protection from light. The reaction mixture was allowed to warm to 25 °C and then transferred to a pre-heated oil bath set to 45 °C and allowed to stir for a total of 20 h under protection from light. Throughout the course of the reaction, a color change from colorless to brick red was observed concomitant with the formation of gray precipitate. The red reaction mixture was then filtered through a pad of Celite, and the filtrate was dried under reduced pressure. The red residue was then dissolved in MeCN (1.5 mL), and this solution was filtered again through a pad of Celite. To the red filtrate was added Et_2O (20 mL) with vigorous stirring, resulting in the precipitation of pink solids from solution. The solids were isolated by filtration and dried under reduced pressure to afford $[B_{12}(OCH_2C_6H_4SC_6H_4(Me\text{-}DalPhos)AuCl)_{12}][SbF_6]_{10}$ as a bright pink solid (11 mg, 0.84 µmol, 42%). UV-vis (MeCN, 25 °C, 0.06 mM) [Ɛ]: 389 [8,300 $M^{-1}cm^{-1}$], 541 [8,170 $M^{-1}cm^{-1}$] nm. ^{1}H NMR (400 MHz, 25 °C, CD_3CN) δ: 8.02 (m, 12H, Ar-*H* Me-DalPhos), 7.95 (m, 24H, Ar-*H* Me-DalPhos), 7.69 (m, 12H, Ar-*H* Me-DalPhos), 7.45 (br m, 48H, Ar-*H*), 7.11 (br m, 48H, Ar-*H*), 3.44 (s, 72H, N(CH_3)$_2$), 2.22 (m, 72H, 1-Ad), 1.99 (m, 144H, 1-Ad, signals overlapping with CD_3CN residual solvent signal), 1.61 (m, 144H, 1-Ad) ppm. The aromatic and methylene protons resonances of the benzyl linker are broadened due to partial oxidation of the dianionic $[B_{12}]^{2-}$ cluster core to the paramagnetic, monoanionic $[B_{12}]^-$ core in air. ^{31}P{^{1}H} (162 MHz, 25 °C, CD_3CN) δ: 76.6 ppm. ^{11}B{^{1}H} NMR (128 MHz, 25 °C, CD_3CN) δ: -14.9 ppm.

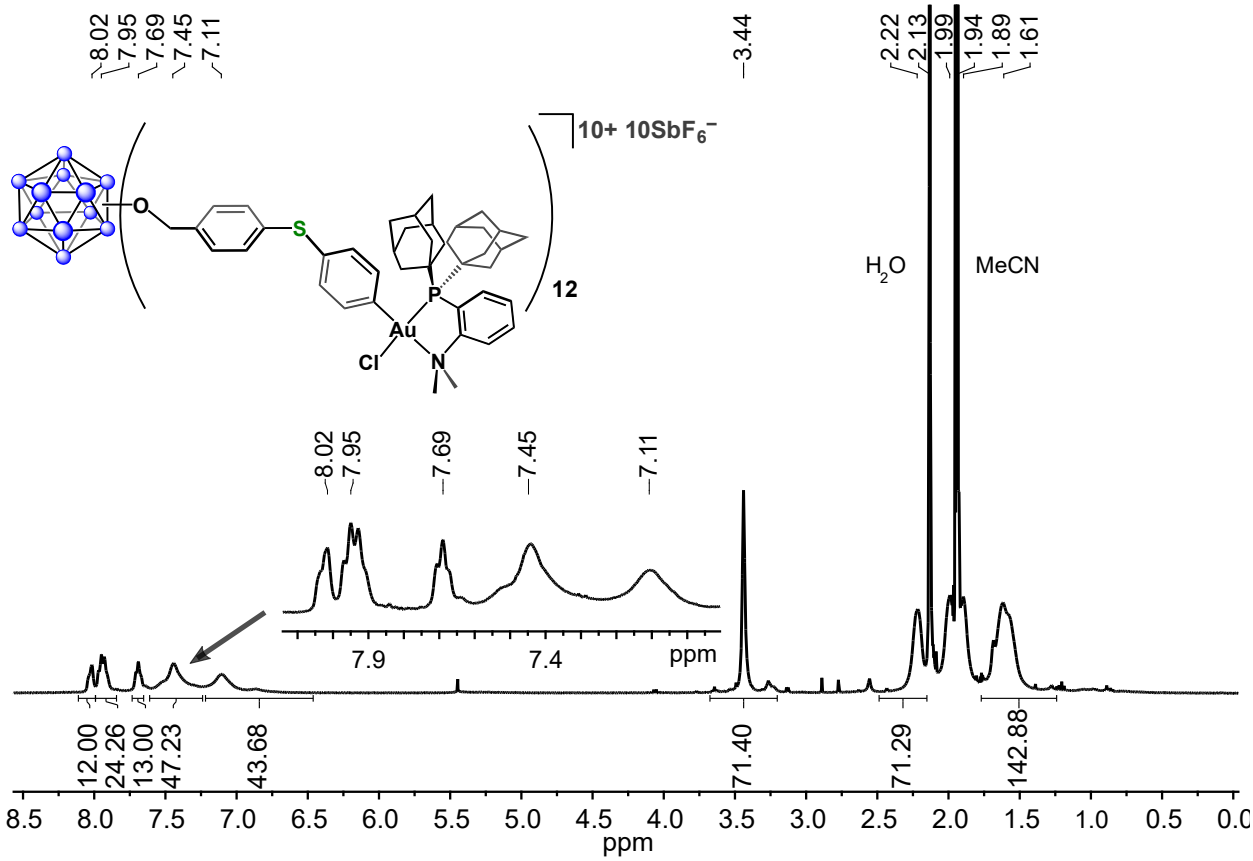

Figure S84. ^{1}H NMR spectrum of $[B_{12}(OCH_2C_6H_4SC_6H_4(Me\text{-}DalPhos)AuCl)_{12}][SbF_6]_{10}$ (CD_3CN, 400 MHz, 25 °C).

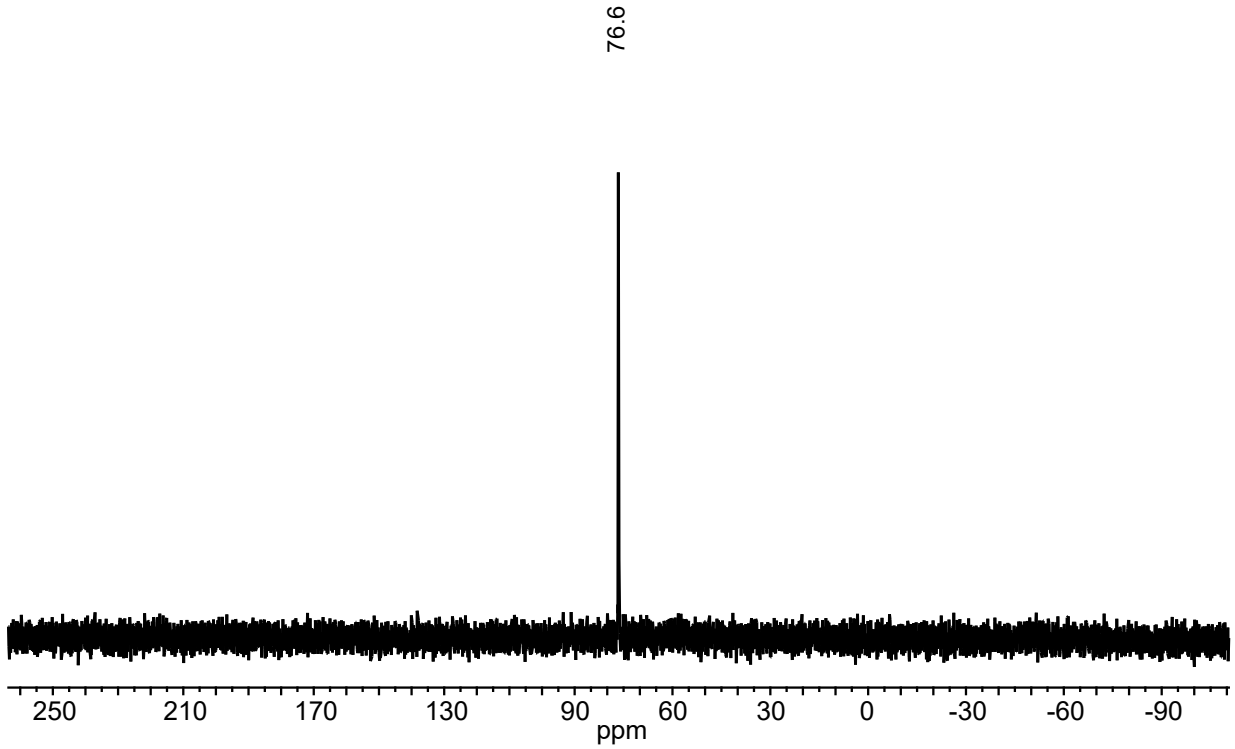

Figure S85. $^{31}P\{^{1}H\}$ NMR spectrum of $[B_{12}(OCH_2C_6H_4SC_6H_4(Me\text{-}DalPhos)AuCl)_{12}][SbF_6]_{10}$ (CD_3CN, 162 MHz, 25 °C).

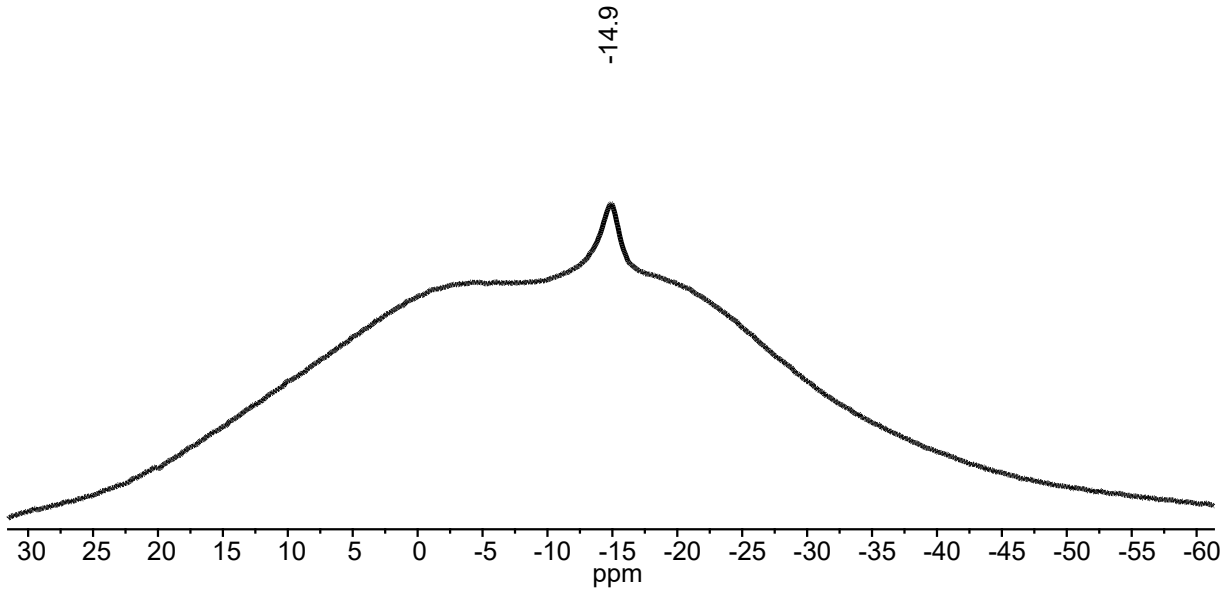

Figure S86. $^{11}B\{^{1}H\}$ NMR spectrum of $[B_{12}(OCH_2C_6H_4SC_6H_4(Me\text{-}DalPhos)AuCl)_{12}][SbF_6]_{10}$ (CD_3CN, 128 MHz, 25 °C).

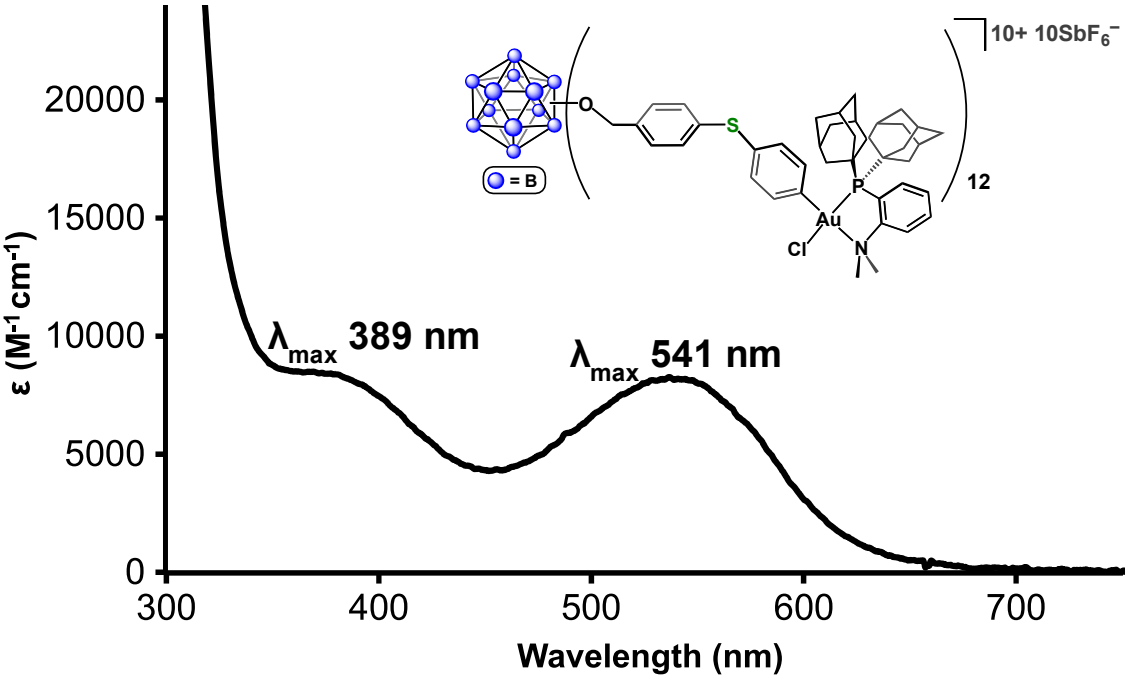

Figure S87. UV-vis spectrum of $[B_{12}(OCH_2C_6H_4SC_6H_4(Me\text{-}DalPhos)AuCl)_{12}][SbF_6]_{10}$ (MeCN, 0.06 mM, 25 °C).

S2.27. General procedure for conjugation reactions with [21][SbF_6]$_{10}$

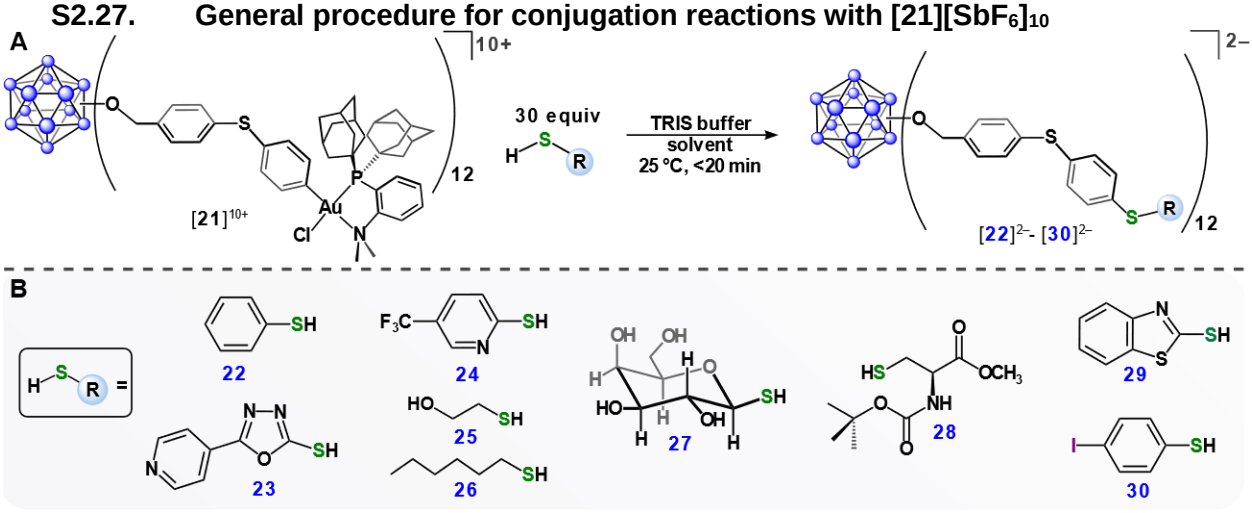

Figure S88. (A) General scheme for conjugation reactions of [**21**][SbF_6]$_{10}$ with thiol-containing substrates. (B) Scope of nanocluster thioether conjugates. All species were observed *in situ* by ESI-MS(–).

To a cooled (-4 °C) solution of $AgSbF_6$ (7 mg, 0.02 mmol, 16 equiv) in DCM (1 mL) was added a cooled solution (-4 °C) of [K_2][**3**] (5 mg, 0.001 mmol, 1 equiv, prepared as previously described in **Section S2.7**) and (Me-DalPhos)AuCl (13 mg, 0.019 mmol, 16 equiv) in DCM (1 mL) under protection from light. The reaction mixture was allowed to warm to 25 °C and then transferred to a pre-heated oil bath set to 45 °C and allowed to stir for a total of 20 h under protection from light. Throughout the course of the reaction, a color change from colorless to brick red was observed concomitant with the formation of gray precipitate. The red reaction mixture was then filtered through a pad of Celite, and the filtrate was dried under reduced pressure. The red residue was then dissolved in MeCN (1 mL), and this solution was filtered again through a pad of Celite. This MeCN solution (1 mM) was used in subsequent conjugation reactions described in this section.

S2.28. $[H_3NC(CH_2OH)_3]_2[B_{12}(OCH_2C_6H_4SC_6H_4SPh)_{12}]$ ($[H_3NC(CH_2OH)_3]_2$[22])

The general procedure to generate a solution of [**21**][SbF_6]$_{10}$ in MeCN (1 mM) described in **Section S2.27** was followed. A 50 µL (0.07 µmol, 1 equiv) aliquot of this solution was removed and treated with a solution of thiophenol in MeCN (18 µL of a 0.1 M solution, 1.8 µmol, 30 equiv) followed by a solution of TRIS buffer in DMF (50 µL of a 50 mM solution) while stirring. The reaction mixture changed from purple to colorless after ca. 5 min of stirring, at which point an aliquot was removed, diluted with MeCN, and analyzed by ESI-MS(–), which confirmed the formation and identity of the $[B_{12}(OCH_2C_6H_4SC_6H_4SPh)_{12}]^{2-}$ species. ESI-MS(–): 2005.3916 (calc'd, 2005.4015) *m/z*.

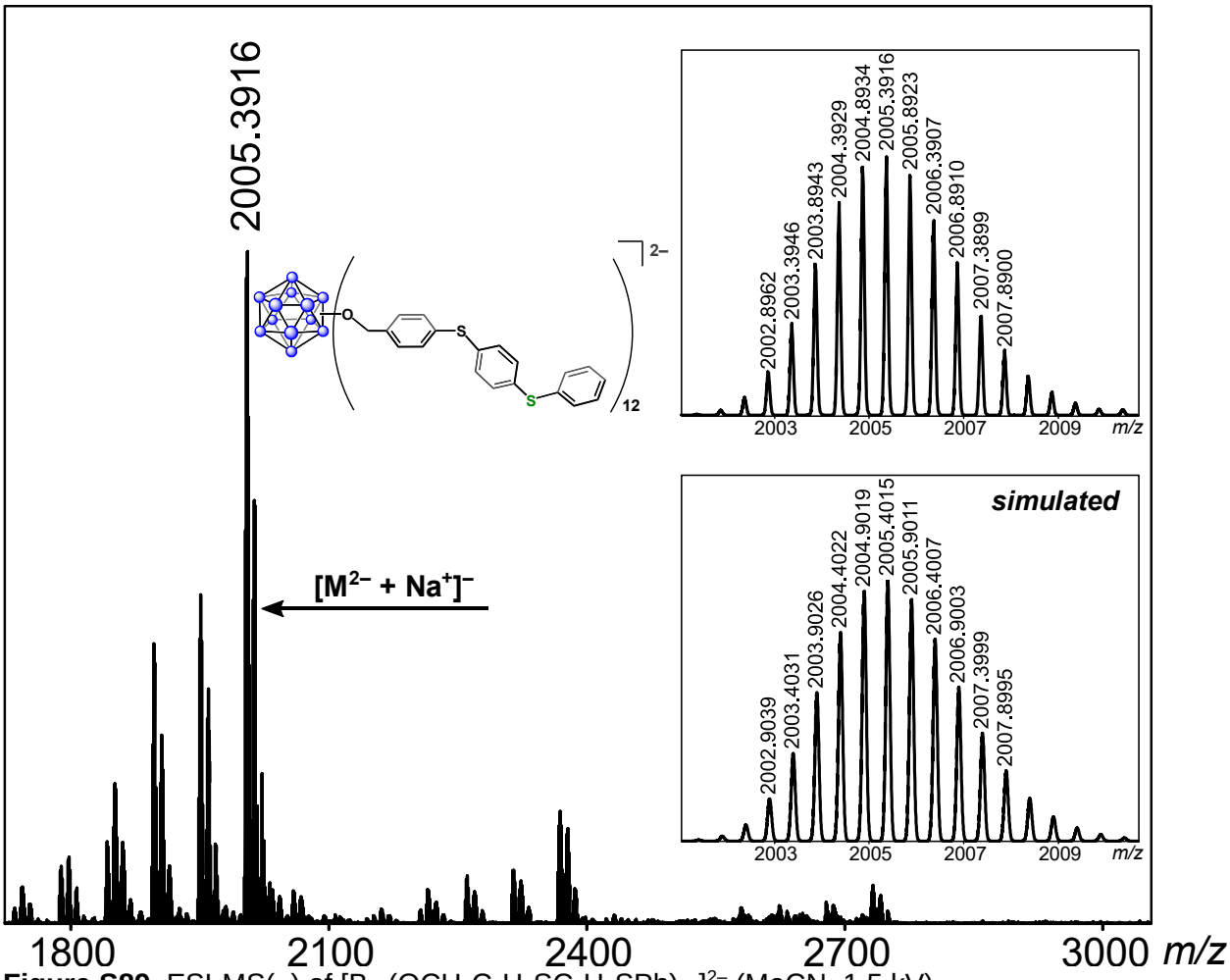

Figure S89. ESI-MS(–) of $[B_{12}(OCH_2C_6H_4SC_6H_4SPh)_{12}]^{2-}$ (MeCN, 1.5 kV).

S2.29. $[H_3NC(CH_2OH)_3]_2[B_{12}(OCH_2C_6H_4SC_6H_4(5\text{-}(4\text{-pyridyl})\text{-oxadiazole-2-thiol}))_{12}]$ ($[H_3NC(CH_2OH)_3]_2$[23])

The general procedure to generate a solution of [**21**][SbF_6]$_{10}$ in MeCN (1 mM) described in **Section S2.27** was followed. A 50 µL (0.07 µmol, 1 equiv) aliquot of this solution was removed and treated with a solution of 5-(4-pyridyl)-oxadiazole-2-thiol in DMF (106 µL of a 17 mM solution, 1.8 µmol, 30 equiv) followed by a solution of TRIS buffer in DMF (100 µL of a 50 mM solution) while stirring. The reaction mixture changed from purple to colorless after ca. 5 min of stirring, at which point an aliquot was removed, diluted with MeCN, and analyzed by ESI-MS(–), which confirmed the formation and identity of the $[B_{12}(OCH_2C_6H_4SC_6H_4(5\text{-}(4\text{-pyridyl})\text{-oxadiazole-2-thiol}))_{12}]^{2-}$ species. ESI-MS(–): 2419.2896 (calc'd, 2419.3796) *m/z*.

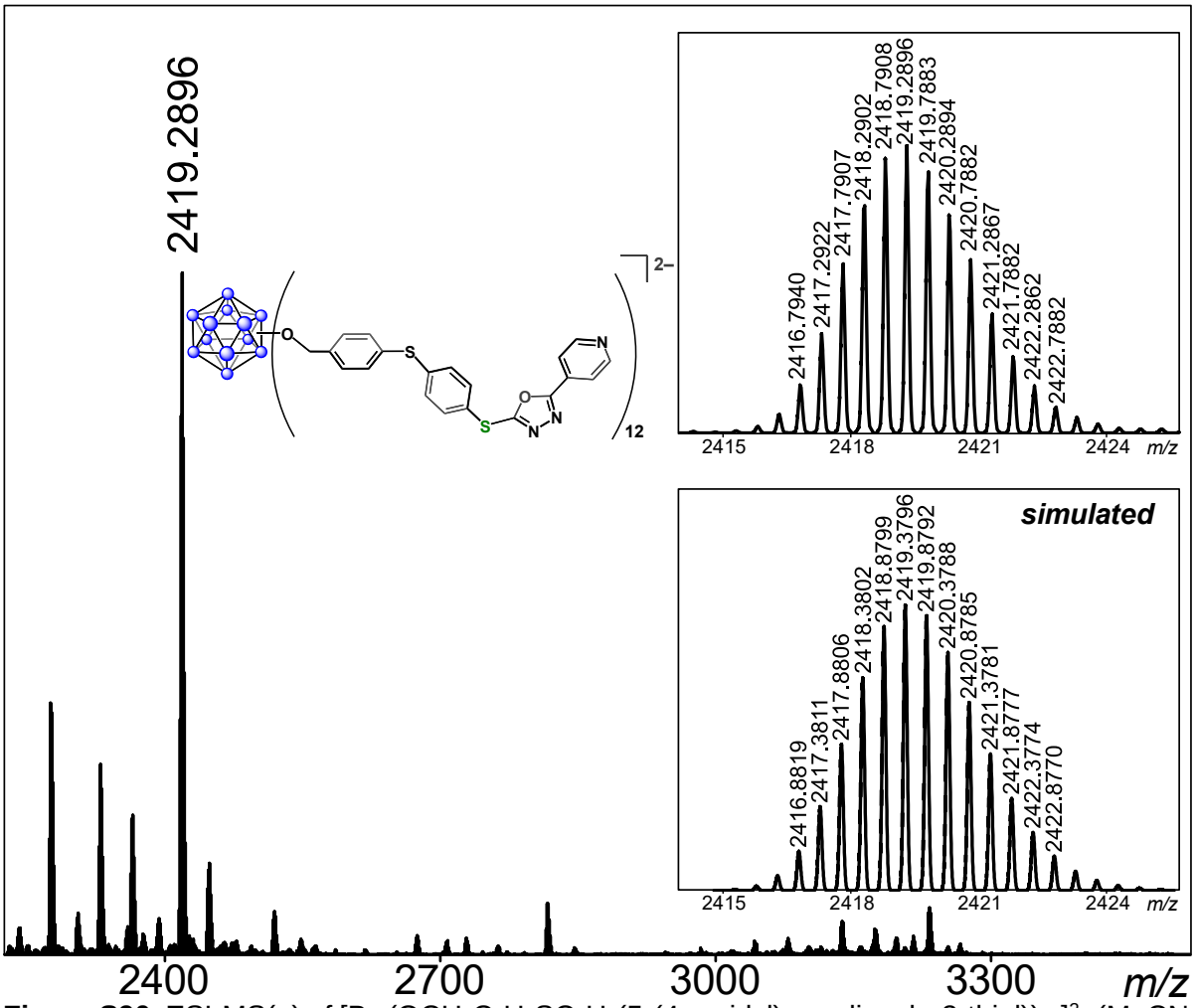

Figure S90. ESI-MS(–) of $[B_{12}(OCH_2C_6H_4SC_6H_4(5\text{-}(4\text{-pyridyl})\text{-oxadiazole-2-thiol}))_{12}]^{2-}$ (MeCN, 1.5 kV).

S2.30. $[H_3NC(CH_2OH)_3]_2[B_{12}(OCH_2C_6H_4SC_6H_4(2\text{-thio-5-trifluoromethylpyridine}))_{12}]$ ($[H_3NC(CH_2OH)_3]_2$[24])

The general procedure to generate a solution of [**21**][SbF_6]$_{10}$ in MeCN (1 mM) described in **Section S2.27** was followed. A 50 µL (0.07 µmol, 1 equiv) aliquot of this solution was removed and treated with a solution of 2-thio-5-trifluoromethylpyridine in DMF (108 µL of a 17 mM solution, 1.8 µmol, 30 equiv) followed by a solution of TRIS buffer in DMF (50 µL of a 50 mM solution) while stirring. The reaction mixture changed from purple to colorless after ca. 5 min of stirring, at which point an aliquot was removed, diluted with MeCN, and analyzed by ESI-MS(–), which confirmed the formation and identity of the $[B_{12}(OCH_2C_6H_4SC_6H_4(2\text{-thio-5-trifluoromethylpyridine}))_{12}]^{2-}$ species. ESI-MS(–): 2419.2898 (calc'd, 2419.2794) *m/z*.

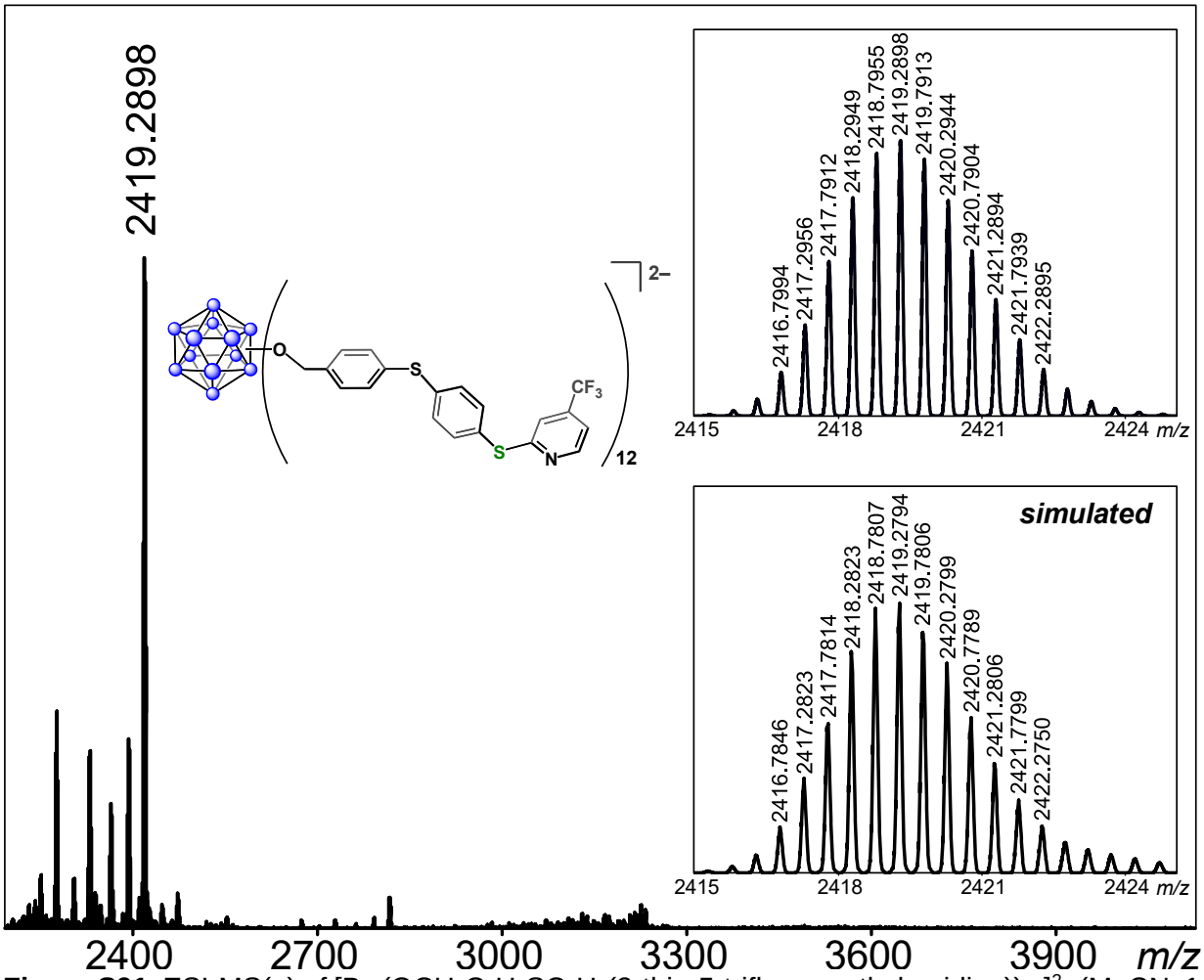

Figure S91. ESI-MS(–) of $[B_{12}(OCH_2C_6H_4SC_6H_4(2\text{-thio-5-trifluoromethylpyridine}))_{12}]^{2-}$ (MeCN, 1.5 kV).

S2.31. $[H_3NC(CH_2OH)_3]_2[B_{12}(OCH_2C_6H_4SC_6H_4(2\text{-mercaptoethanol}))_{12}]$ ($[H_3NC(CH_2OH)_3]_2$[25])

The general procedure to generate a solution of [**21**][SbF_6]$_{10}$ in MeCN (1 mM) described in **Section S2.27** was followed. A 50 µL (0.07 µmol, 1 equiv) aliquot of this solution was removed and treated with a solution of 2-mercaptoethanol in MeCN (18 µL of a 0.10 M solution, 1.8 µmol, 30 equiv) followed by a solution of TRIS buffer in DMF (50 µL of a 50 mM solution) while stirring. The reaction mixture changed from purple to colorless after ca. 5 min of stirring, at which point an aliquot was removed, diluted with MeCN, and analyzed by ESI-MS(–), which confirmed the formation and identity of the $[B_{12}(OCH_2C_6H_4SC_6H_4(2\text{-mercaptoethanol}))_{12}]^{2-}$ species. ESI-MS(–): 1812.8703 (calc'd, 1812.8702) *m/z*.

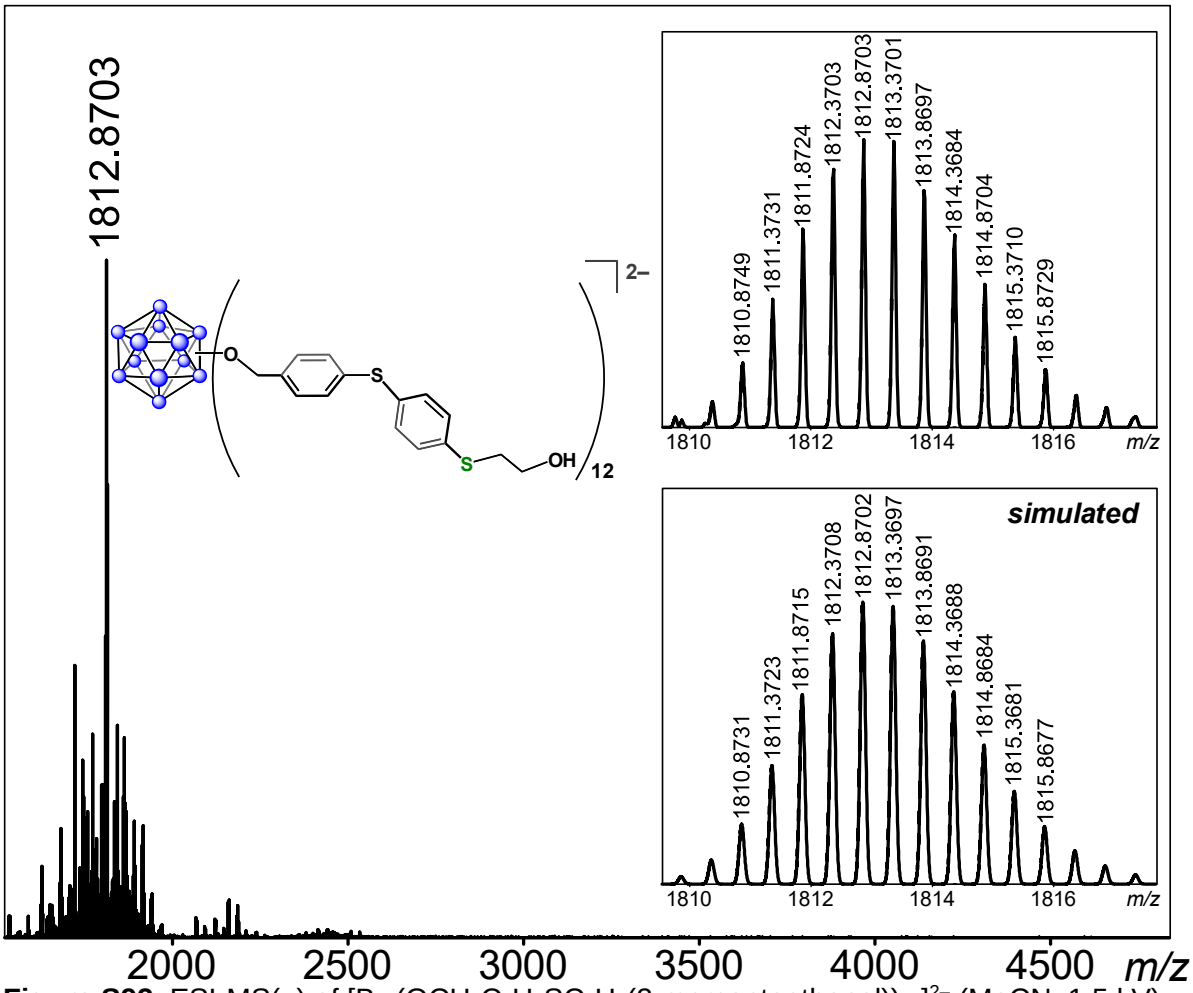

Figure S92. ESI-MS(–) of $[B_{12}(OCH_2C_6H_4SC_6H_4(2\text{-mercaptoethanol}))_{12}]^{2-}$ (MeCN, 1.5 kV).

S2.32. $[H_3NC(CH_2OH)_3]_2[B_{12}(OCH_2C_6H_4SC_6H_4S(CH_2)_5CH_3)_{12}]$ ($[H_3NC(CH_2OH)_3]_2$[26])

The general procedure to generate a solution of [**21**][SbF_6]$_{10}$ in MeCN (1 mM) described in **Section S2.27** was followed. A 50 µL (0.07 µmol, 1 equiv) aliquot of this solution was removed and treated with a solution of hexanethiol in MeCN (18 µL of a 0.10 M solution, 1.8 µmol, 30 equiv) followed by a solution of TRIS buffer in DMF (50 µL of a 50 mM solution) while stirring. The reaction mixture changed from purple to colorless after ca. 5 min of stirring, at which point an aliquot was removed, diluted with MeCN, and analyzed by ESI-MS(–), which confirmed the formation and identity of the $[B_{12}(OCH_2C_6H_4SC_6H_4S(CH_2)_5CH_3)_{12}]^{2-}$ species. ESI-MS(–): 2053.7671 (calc'd, 2053.7772) *m/z*.

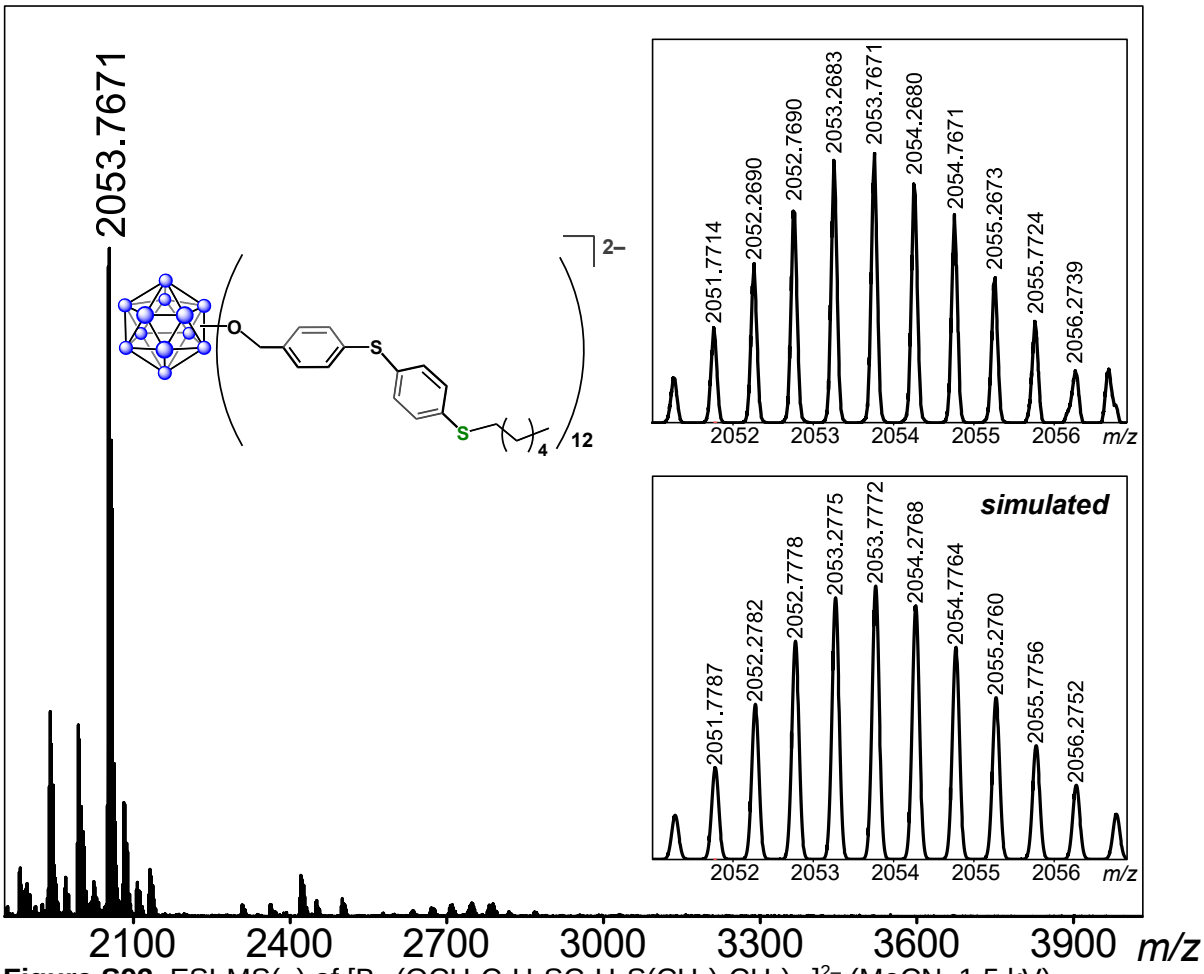

Figure S93. ESI-MS(–) of $[B_{12}(OCH_2C_6H_4SC_6H_4S(CH_2)_5CH_3)_{12}]^{2-}$ (MeCN, 1.5 kV).

S2.33. $[Na_2][B_{12}(OCH_2C_6H_4SC_6H_4(1\text{-thio-}\beta\text{-D-galactose}))_{12}]$ ($[Na_2][27]$)

The general procedure to generate a solution of [**21**][SbF_6]$_{10}$ in MeCN (1 mM) described in **Section S2.27** was followed. A 50 µL (0.07 µmol, 1 equiv) aliquot of this solution was removed and treated with a solution of Na[1-thio-β-D-galactose] in H_2O (36 µL of a 30 mM solution, 1.8 µmol, 30 equiv) followed by dilution with DMF (30 µL) while stirring. The reaction mixture changed from purple to colorless after ca. 5 min of stirring, at which point an aliquot was removed, diluted with MeOH, and analyzed by ESI-MS(–), which confirmed the formation and identity of the $[B_{12}(OCH_2C_6H_4SC_6H_4(1\text{-thio-}\beta\text{-D-galactose}))_{12}]^{2-}$ species. ESI-MS(–): 1680.6948 (calc'd, 1680.6848 for $[M^{2-}\text{-}H^+]^{3-}$) *m/z*.

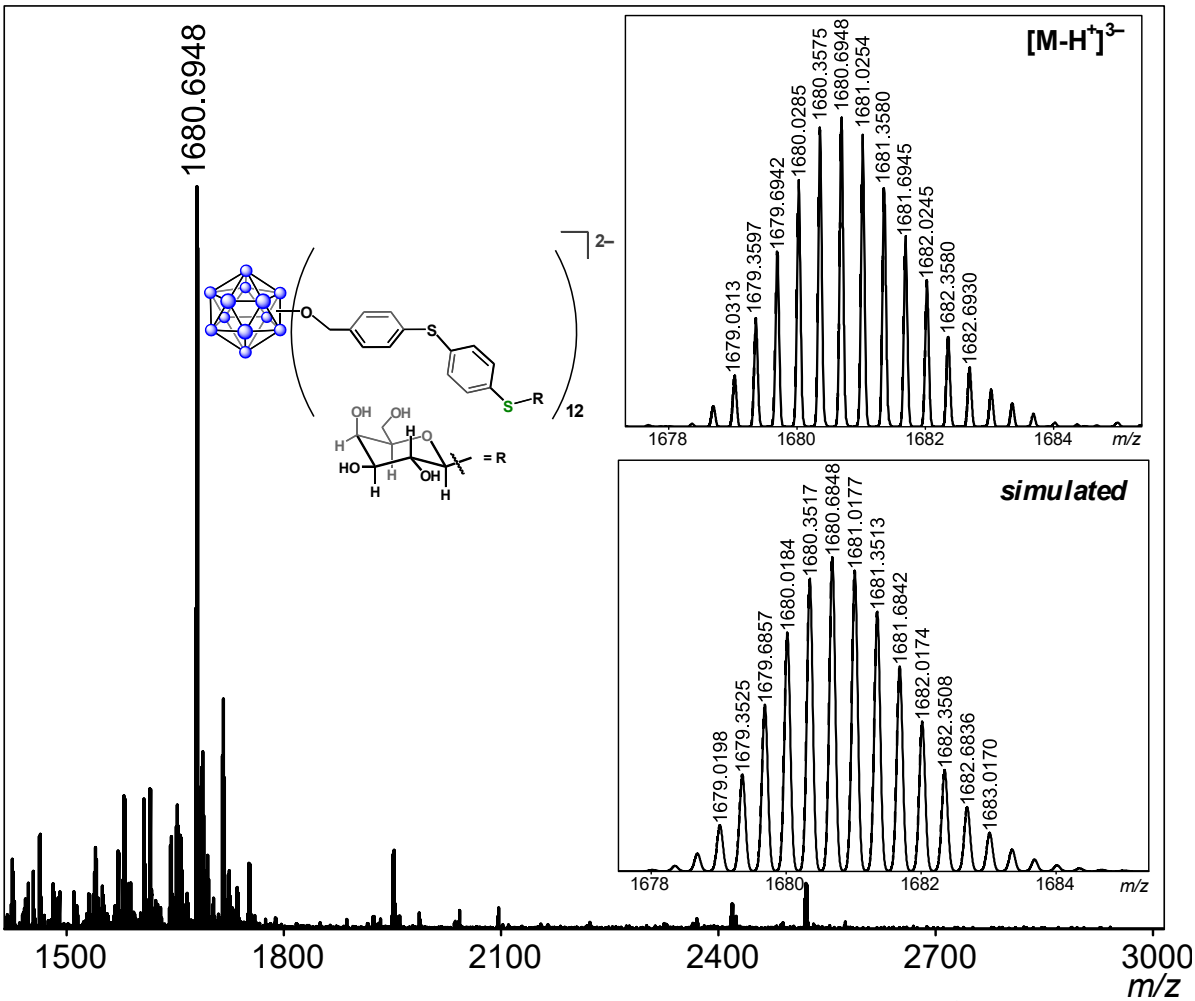

Figure S94. ESI-MS(–) of $[B_{12}(OCH_2C_6H_4SC_6H_4(1\text{-thio-}\beta\text{-D-galactose}))_{12}]^{2-}$ (MeOH, 1.5 kV). The monodeprotonated, trianionic species, $[M^{2-}\text{-}H^+]^{3-}$, is observed under ESI-MS conditions.

S2.34. $[H_3NC(CH_2OH)_3]_2[B_{12}(OCH_2C_6H_4SC_6H_4(N\text{-}(tert\text{-butoxycarbonyl})\text{-L-cysteine methyl ester}))_{12}$ ($[H_3NC(CH_2OH)_3]_2$[28])

The general procedure to generate a solution of [**21**][SbF_6]$_{10}$ in MeCN (1 mM) described in **Section S2.27** was followed. A 50 µL (0.07 µmol, 1 equiv) aliquot of this solution was removed and treated with a solution of *N*-(*tert*-butoxycarbonyl)-L-cysteine methyl ester in MeCN (18 µL of a 0.10 M solution, 1.8 µmol, 30 equiv) followed by a solution of TRIS buffer in DMF (50 µL of a 50 mM solution) while stirring. The reaction mixture changed from purple to colorless after ca. 5 min of stirring, at which point an aliquot was removed, diluted with MeCN, and analyzed by ESI-MS(–), which confirmed the formation and identity of the $[B_{12}(OCH_2C_6H_4SC_6H_4(N\text{-}(tert\text{-butoxycarbonyl})\text{-L-cysteine methyl ester}))_{12}]^{2-}$ species. ESI-MS(–): 2755.7974 (calc'd, 2755.8152) *m/z*.

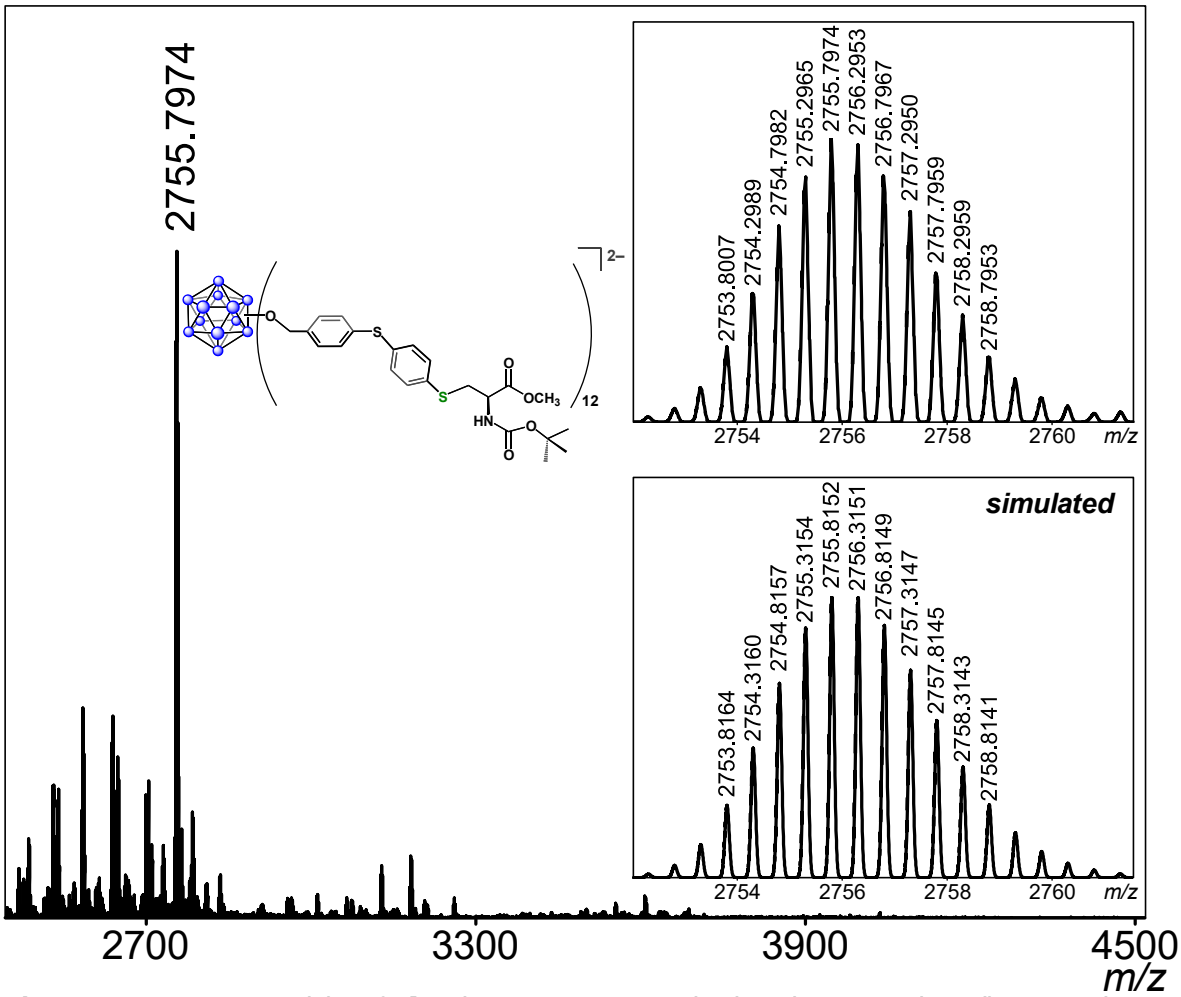

Figure S95. ESI-MS(–) of $[B_{12}(OCH_2C_6H_4SC_6H_4(N$-(tert-butoxycarbonyl)-L-cysteine methyl ester$))_{12}]^{2-}$ (MeCN, 1.5 kV).

S2.35. $[H_3NC(CH_2OH)_3]_2[B_{12}(OCH_2C_6H_4SC_6H_4(2\text{-mercaptobenzothiazole}))_{12}]$ ($[H_3NC(CH_2OH)_3]_2$[29])

The general procedure to generate a solution of [**21**][SbF_6]$_{10}$ in MeCN (1 mM) described in **Section S2.27** was followed. A 50 µL (0.07 µmol, 1 equiv) aliquot of this solution was removed and treated with a solution of 2-mercaptobenzothiazole in DMF (60 µL of a 30 mM solution, 1.8 µmol, 30 equiv) followed by a solution of TRIS buffer in DMF (50 µL of a 50 mM solution) while stirring. The reaction mixture changed from purple to colorless after ca. 5 min of stirring, at which point an aliquot was removed, diluted with MeCN, and analyzed by ESI-MS(–), which confirmed the formation and identity of the $[B_{12}(OCH_2C_6H_4SC_6H_4(2\text{-mercaptobenzothiazole}))_{12}]^{2-}$ species. ESI-MS(–): 2347.6916 (calc'd, 2347.7046) *m/z*.

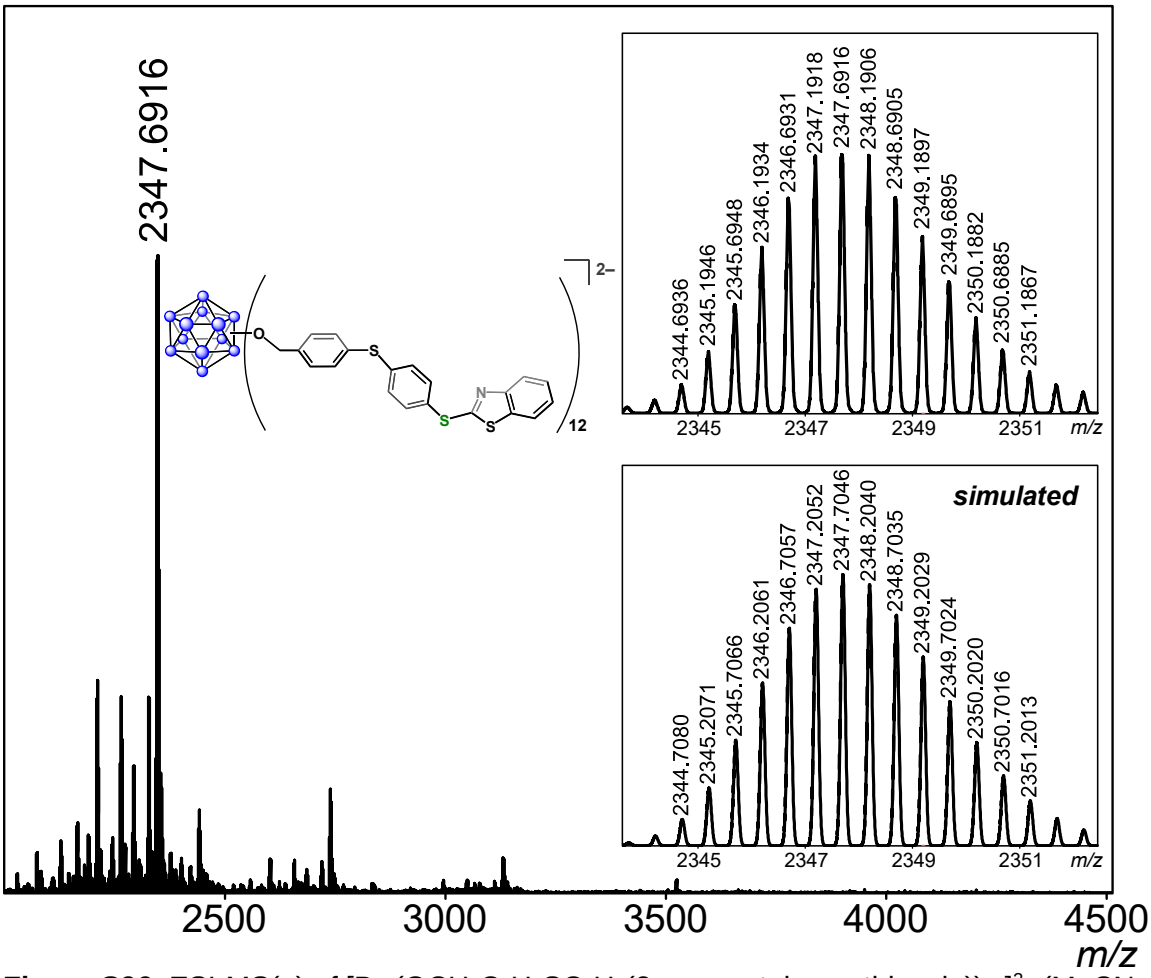

Figure S96. ESI-MS(–) of $[B_{12}(OCH_2C_6H_4SC_6H_4(2\text{-mercaptobenzothiazole}))_{12}]^{2-}$ (MeCN, 1.5 kV).

S2.36. $[H_3NC(CH_2OH)_3]_2[B_{12}(OCH_2C_6H_4SC_6H_4SC_6H_4I)_{12}]$ ($[H_3NC(CH_2OH)_3]_2$[30])

The general procedure to generate a solution of [**21**][SbF_6]$_{10}$ in MeCN (1 mM) described in **Section S2.27** was followed. A 50 µL (0.07 µmol, 1 equiv) aliquot of this solution was removed and treated with a solution of *para*-iodothiophenol in DMF (138 µL of a 13 mM solution, 1.8 µmol, 30 equiv) followed by a solution of TRIS buffer in DMF (50 µL of a 50 mM solution) while stirring. The reaction mixture changed from purple to colorless after ca. 5 min of stirring, at which point an aliquot was removed, diluted with MeCN, and analyzed by ESI-MS(–), which confirmed the formation and identity of the $[B_{12}(OCH_2C_6H_4SC_6H_4SC_6H_4I)_{12}]^{2-}$ species. ESI-MS(–): 2760.7586 (calc'd, 2760.7814) *m/z*.

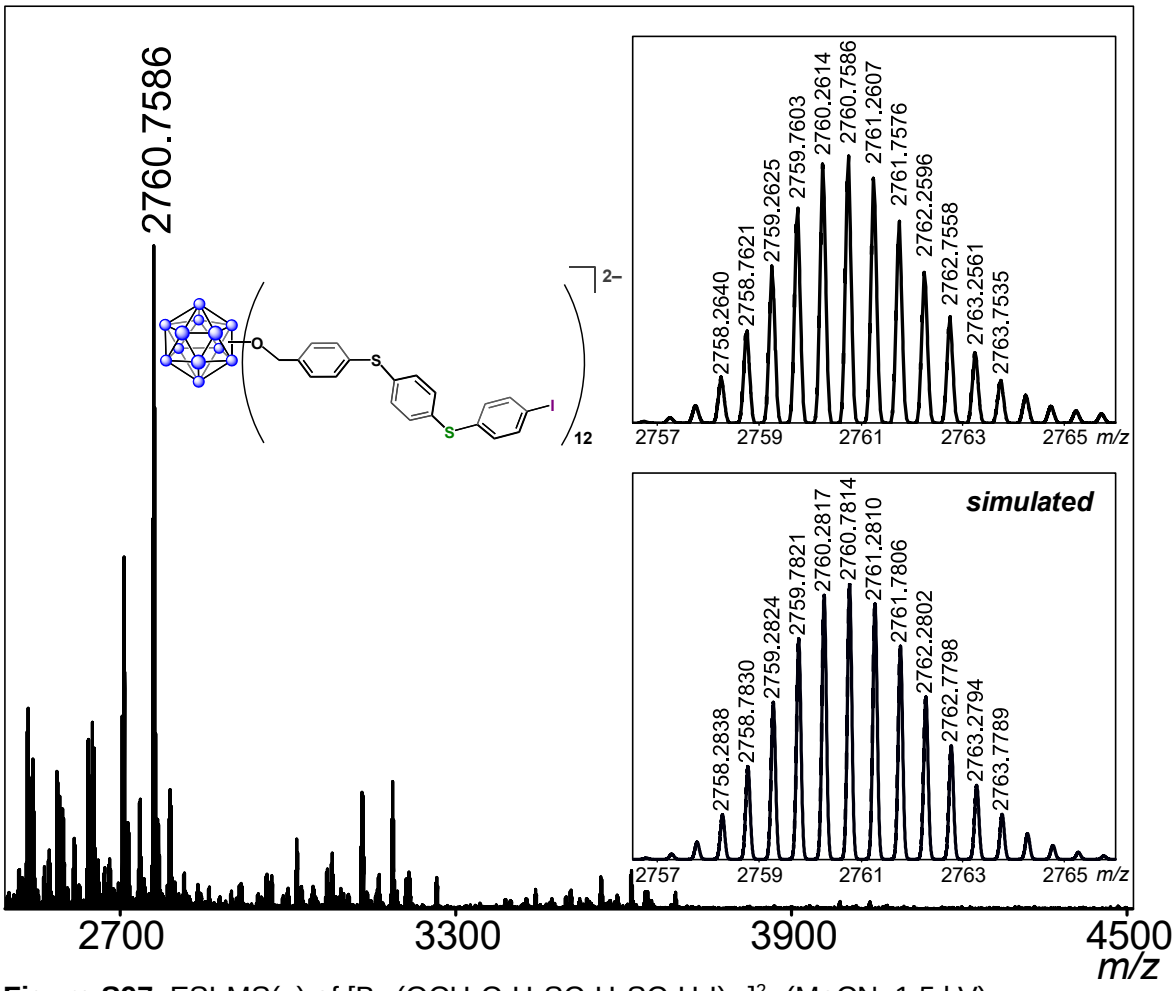

Figure S97. ESI-MS(–) of $[B_{12}(OCH_2C_6H_4SC_6H_4SC_6H_4I)_{12}]^{2-}$ (MeCN, 1.5 kV).

S2.37. (1-thio-β-D-galactose)$_2$C$_6$H$_4$

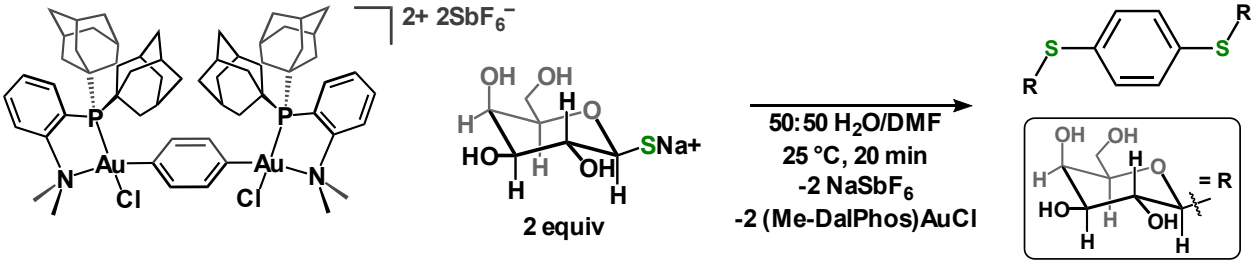

Scheme S1. Reaction protocol for the preparation of (1-thio-β-D-galactose)$_2$C$_6$H$_4$.

The [((Me-DalPhos)AuCl)$_2$C$_6$H$_4$][SbF$_6$]$_2$ complex was prepared following a previously reported procedure.[3]

To a stirring solution of Na[1-thio-β-D-galactose] (6 mg, 0.03 mmol, 2 equiv) in H_2O (1 mL) was added a solution of [((Me-DalPhos)AuCl)$_2$C$_6$H$_4$][SbF$_6$]$_2$ (24 mg, 0.013 mmol, 1.0 equiv) in DMF (1.5 mL). The color of the reaction mixture gradually changed from yellow to colorless over the course of 15 min, at which point all volatiles were removed under reduced pressure. The resulting colorless residue was suspended in H_2O (2 mL). The resulting suspension was sonicated (5 min), and then centrifuged (2,200 × g, 5 min). The supernatant was removed and filtered through a 0.22 µm PTFE membrane syringe filter to remove any insoluble (Me-DalPhos)AuCl remaining in the solution. The filtrate was then lyophilized to afford (1-thio-β-D-galactose)$_2$C$_6$H$_4$ as a colorless solid (5 mg, 0.01 mmol, 80%). ^{1}H NMR (400 MHz, 25 °C, D_2O) δ: 7.55 (s, 4H, Ar-*H*), 4.01 (d, 2H, gal), 4.01–3.64 (m, 12H, gal) ppm.

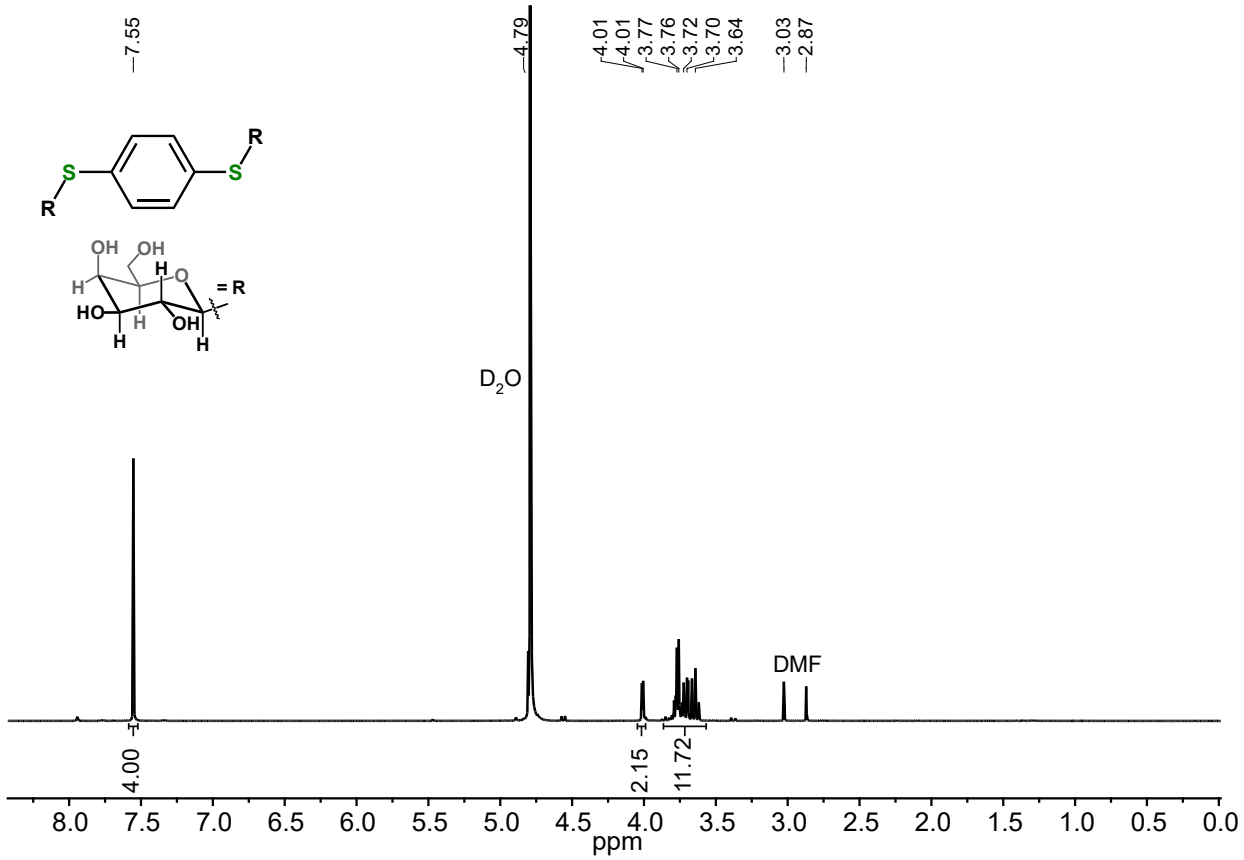

Figure S98. ^{1}H NMR spectrum of (1-thio-β-D-galactose)$_2$C$_6$H$_4$ (D_2O, 400 MHz, 25 °C).

S3. Stability studies of $[Na_2][B_{12}(OCH_2C_6H_4(1\text{-thio-}\beta\text{-D-glucose}))_{12}]$ under biologically relevant conditions

The $[Na_2][B_{12}(OCH_2C_6H_4(1\text{-thio-}\beta\text{-D-glucose}))_{12}]$ cluster was prepared according to the procedure described in **Section S2.23** and used in the stability studies described in the following subsections.

S3.1. Fetal bovine serum cell culture medium

A sample of $[Na_2][B_{12}(OCH_2C_6H_4(1\text{-thio-}\beta\text{-D-glucose}))_{12}]$ (2 mg) was dissolved in fetal bovine serum RPMI 1640 cell medium (0.5 mL, Sigma Aldrich). The solution was transferred to an NMR tube, and an initial $^{11}B\{^1H\}$ NMR spectrum of the sample was immediately collected. A second $^{11}B\{^1H\}$ NMR spectrum was collected after allowing the sample to stand for 24 h at 25 °C. $^{11}B\{^1H\}$ NMR spectra of the sample were collected every 24 h for a total of seven days without any observable cluster degradation as displayed in **Figure S99**. After monitoring the solution for one week at 25 °C, the same sample was heated at 37 °C and monitored by $^{11}B\{^1H\}$ NMR spectroscopy every 24 h for an additional seven days. The $^{11}B\{^1H\}$ NMR spectra collected during the course of this study are displayed in **Figure S100**, which indicate that the cluster maintains its structural integrity under these conditions. The sample was also analyzed by ESI-MS(–) after the two week stability study (**Figure S101**), confirming the presence of the intact cluster.

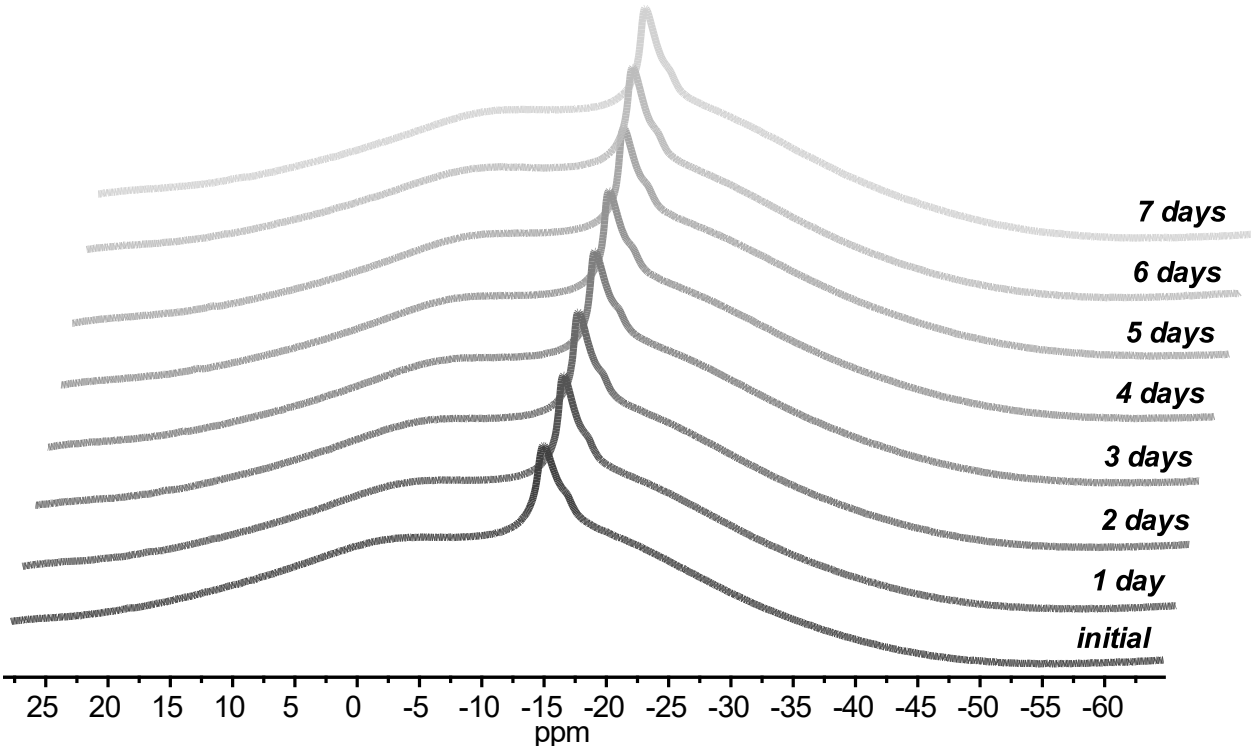

Figure S99. $^{11}B\{^1H\}$ NMR spectra of $[Na_2][B_{12}(OCH_2C_6H_4(1\text{-thio-}\beta\text{-D-glucose}))_{12}]$ collected throughout the course of 7 days at 25 °C in fetal bovine serum cell culture medium (128 MHz, 25 °C).

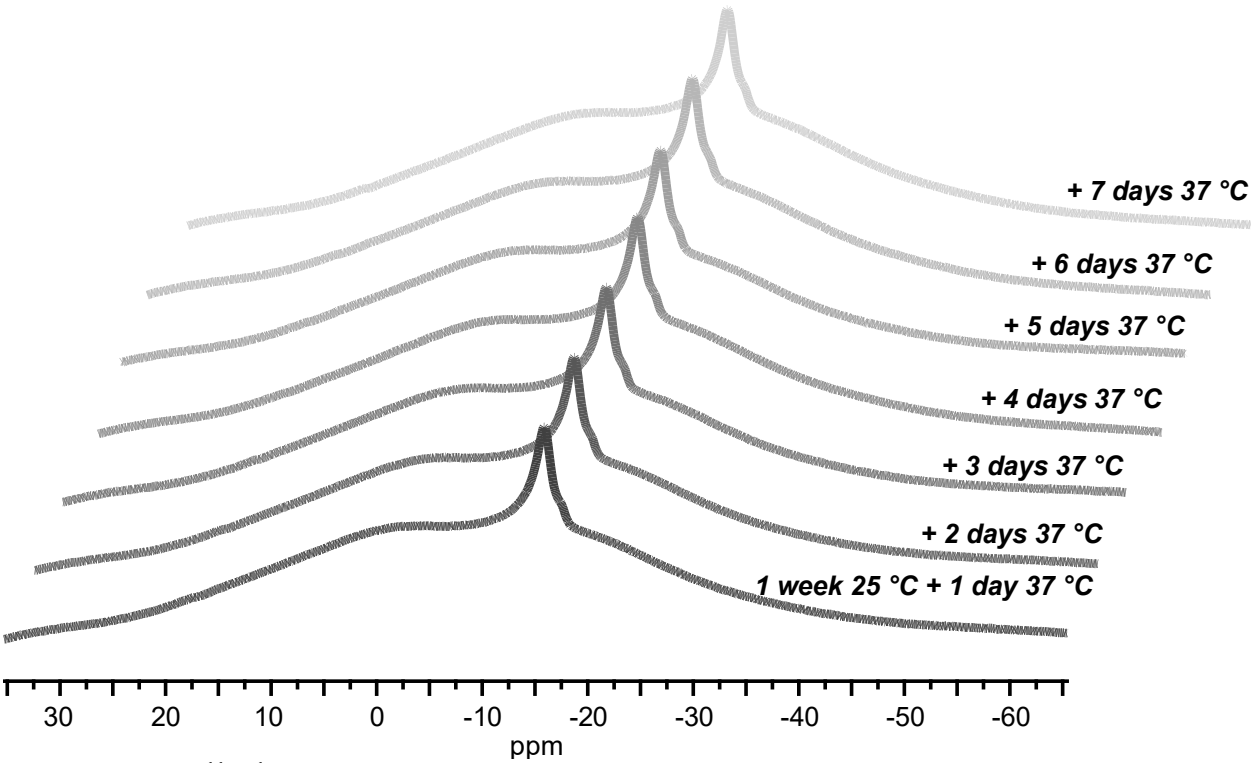

Figure S100. $^{11}B\{^{1}H\}$ NMR spectra of $[Na_2][B_{12}(OCH_2C_6H_4(1\text{-thio-}\beta\text{-D-glucose}))_{12}]$ collected throughout the course of an additional 7 days at 37 °C in fetal bovine serum cell culture medium (128 MHz, 25 °C).

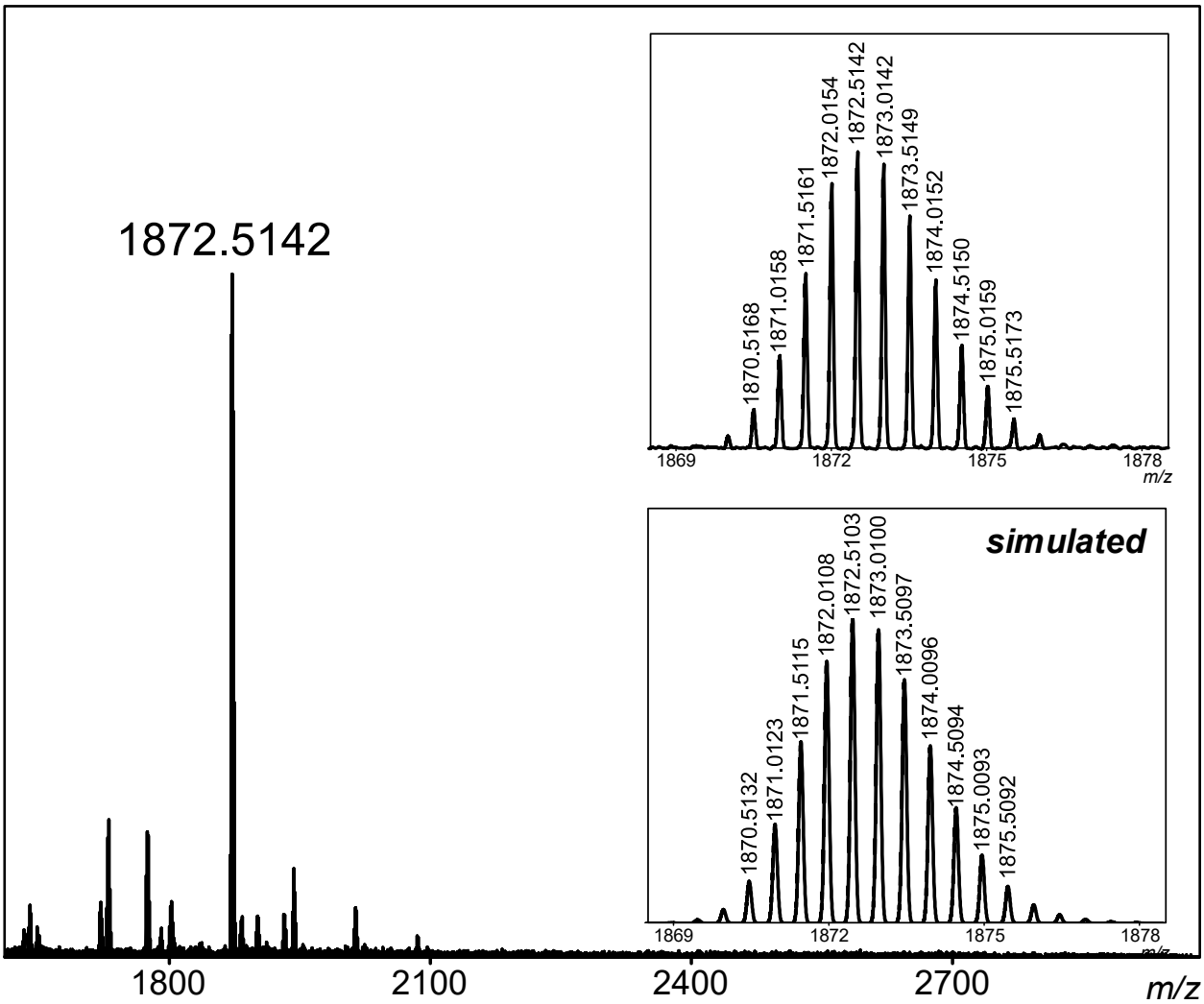

Figure S101. ESI-MS(–) of $[Na_2][B_{12}(OCH_2C_6H_4(1\text{-thio-}\beta\text{-D-glucose}))_{12}]$ collected after 14 days in fetal bovine serum cell culture medium (sample diluted with MeOH, 1.5 kV).

S3.2. pH 10

A sample of $[Na_2][B_{12}(OCH_2C_6H_4(1\text{-thio-}\beta\text{-D-glucose}))_{12}]$ (2 mg) was dissolved in an aqueous solution of TRIS buffer (adjusted to pH 10). The solution was transferred to an NMR tube, and an initial $^{11}B\{^1H\}$ NMR spectrum of the sample was immediately collected. A second $^{11}B\{^1H\}$ NMR spectrum was collected after allowing the sample to stand for 24 h at 25 °C. $^{11}B\{^1H\}$ NMR spectra of the sample were collected every 24 h for a total of seven days without any observable cluster degradation as displayed in **Figure S102**. The sample was also analyzed by ESI-MS(–) after the one week stability study (**Figure S103**), confirming the presence of the intact cluster.

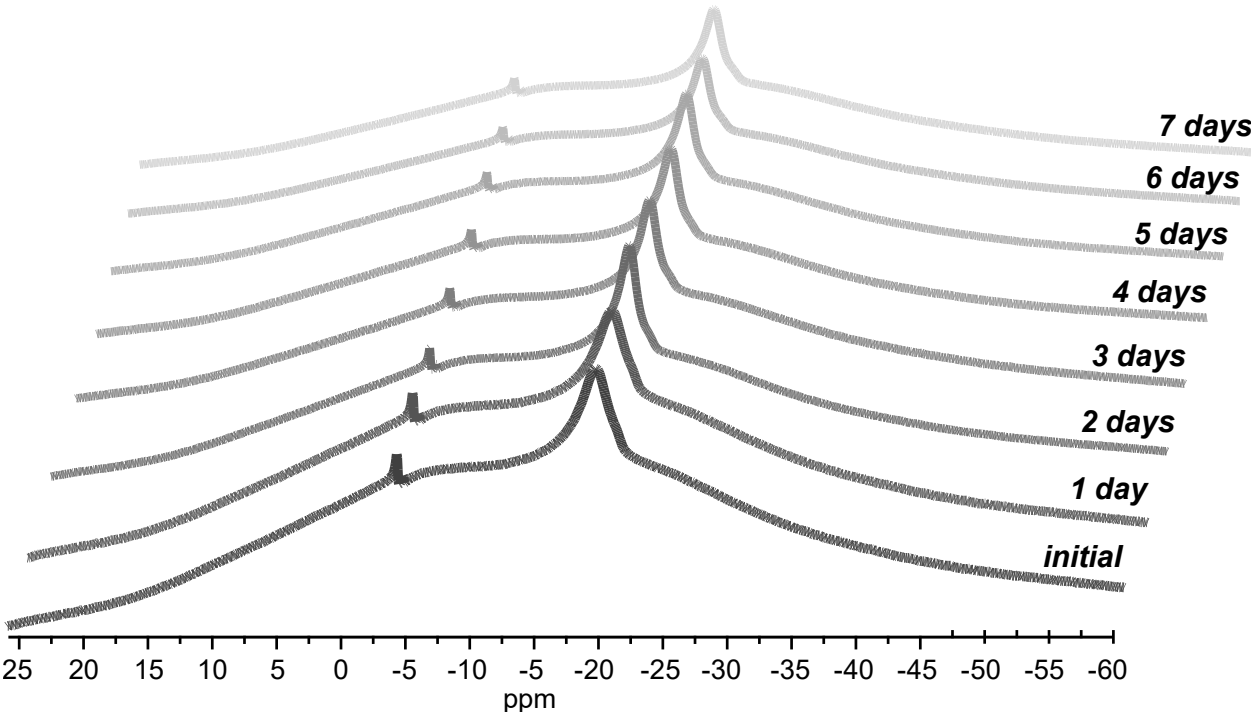

Figure S102. $^{11}B\{^1H\}$ NMR spectra of $[Na_2][B_{12}(OCH_2C_6H_4(1\text{-thio-}\beta\text{-D-glucose}))_{12}]$ collected throughout the course of 7 days at 25 °C in an aqueous solution of TRIS buffer (pH 10) (128 MHz, 25 °C).

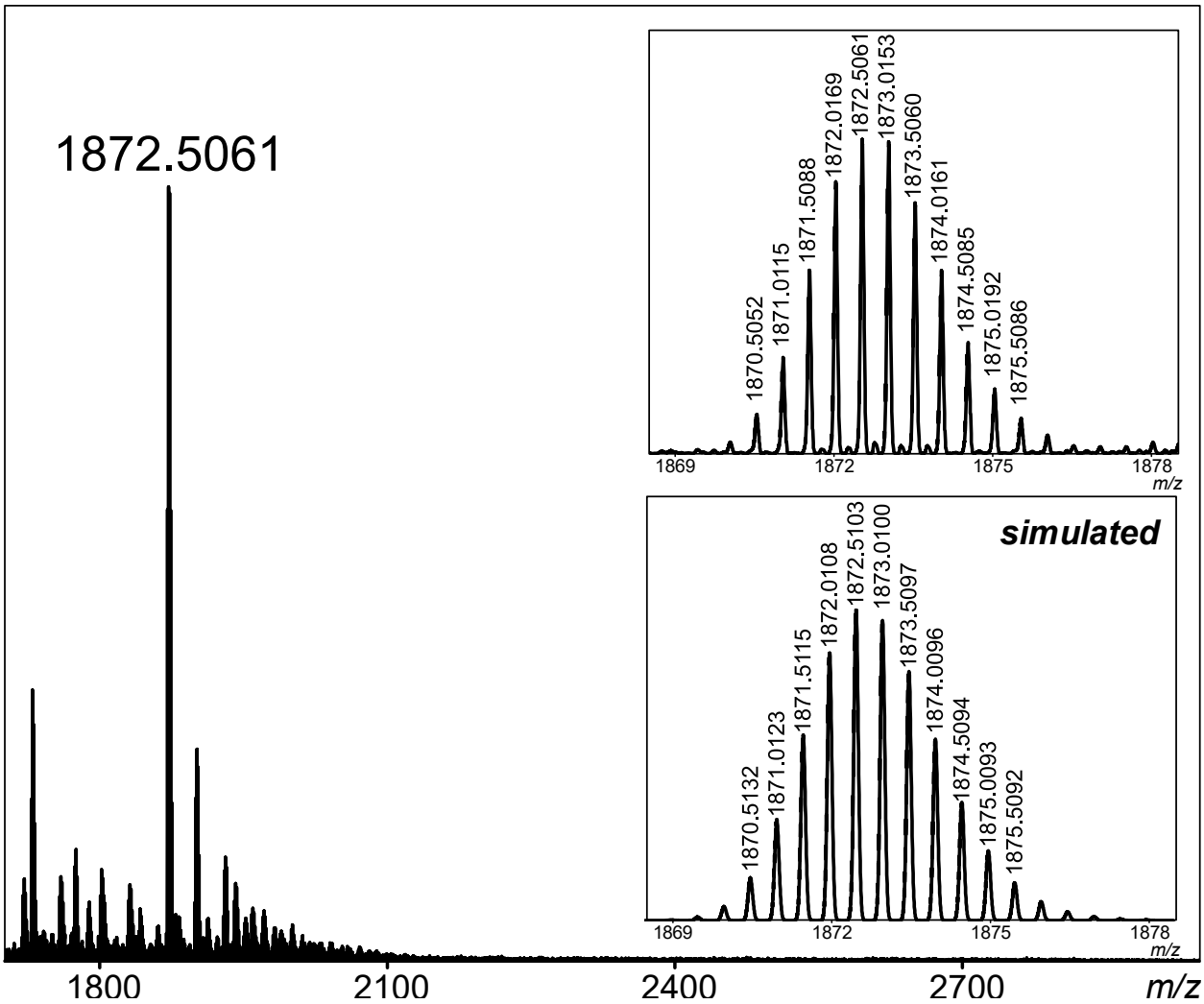

Figure S103. ESI-MS(–) of $[Na_2][B_{12}(OCH_2C_6H_4(1\text{-thio-}\beta\text{-D-glucose}))_{12}]$ collected after 7 days at 25 °C in an aqueous solution of TRIS buffer (pH 10) (sample diluted with MeOH, 1.5 kV).

S3.3. pH 5

A sample of $[Na_2][B_{12}(OCH_2C_6H_4(1\text{-thio-}\beta\text{-D-glucose}))_{12}]$ (2 mg) was dissolved in an aqueous solution of acetate buffer (pH 5 solution prepared by dissolution of NaOAc (7 mL of a 0.2 M solution) and HOAc (3 mL of a 0.2M solution) in 10 mL Milli-Q H_2O). The solution was transferred to an NMR tube, and an initial $^{11}B\{^1H\}$ NMR spectrum of the sample was immediately collected. A second $^{11}B\{^1H\}$ NMR spectrum was collected after allowing the sample to stand for 24 h at 25 °C. $^{11}B\{^1H\}$ NMR spectra of the sample were collected every 24 h for a total of seven days without any observable cluster degradation as displayed in **Figure S104**. The sample was also analyzed by ESI-MS(–) after the one week stability study (**Figure S105**), confirming the presence of the intact cluster.

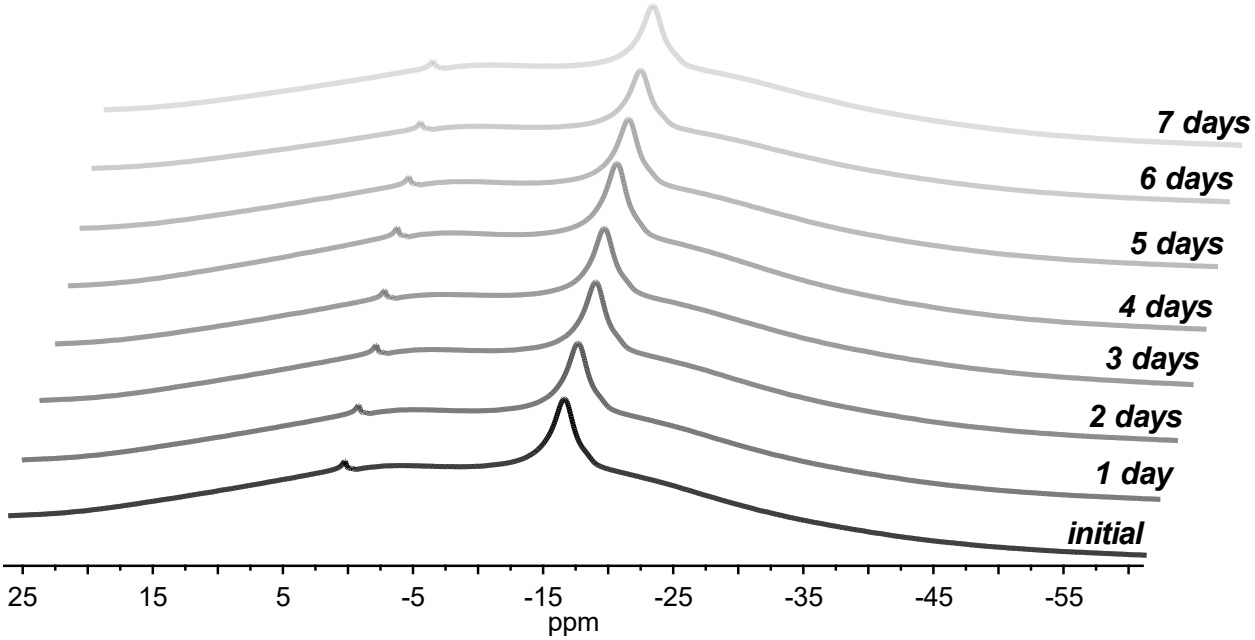

Figure S104. $^{11}B\{^1H\}$ NMR spectra of $[Na_2][B_{12}(OCH_2C_6H_4(1\text{-thio-}\beta\text{-D-glucose}))_{12}]$ collected throughout the course of 7 days at 25 °C in an aqueous solution of acetate buffer (pH 5) (128 MHz, 25 °C).

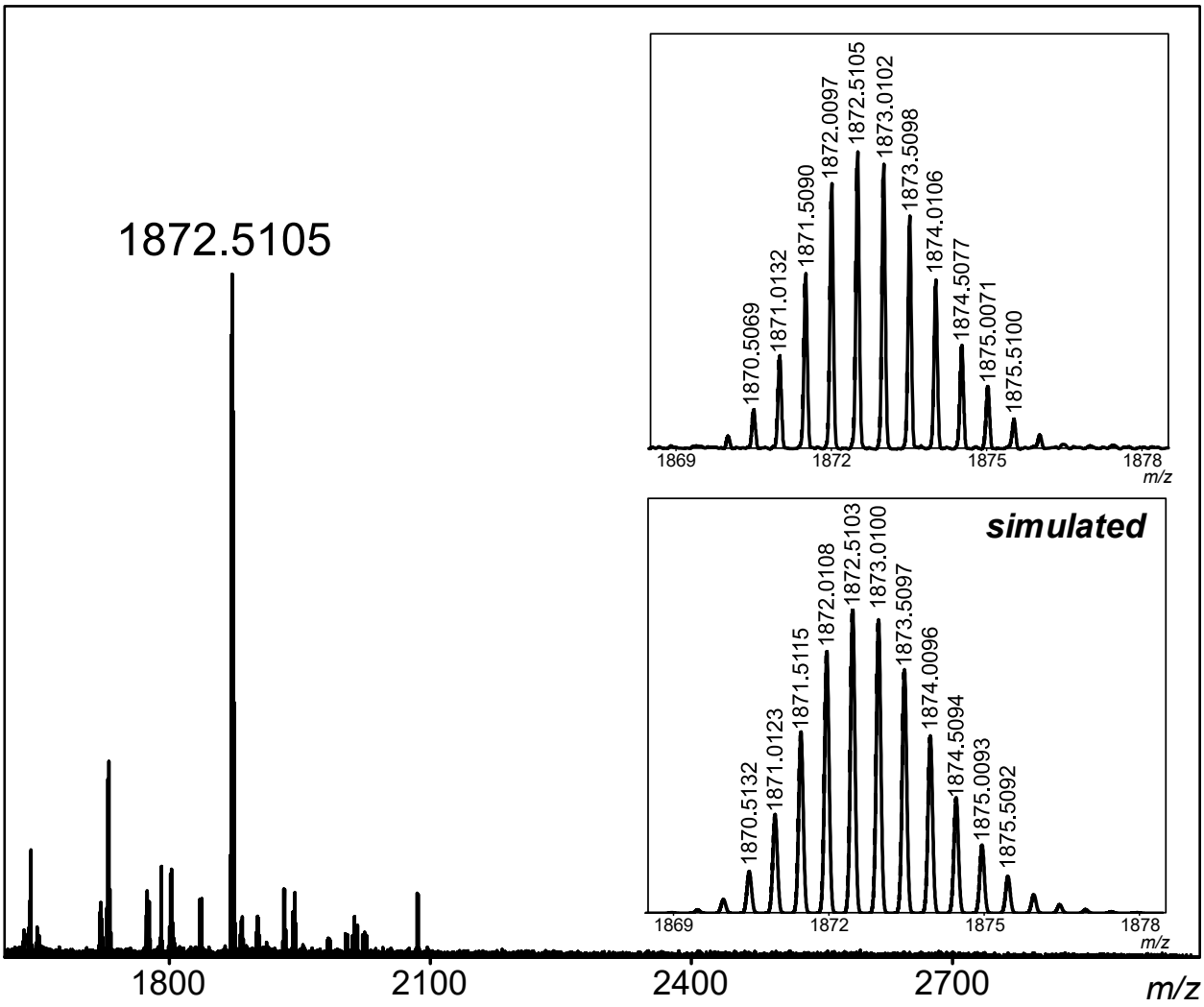

Figure S105. ESI-MS(–) of $[Na_2][B_{12}(OCH_2C_6H_4(1\text{-thio-}\beta\text{-D-glucose}))_{12}]$ collected after 7 days at 25 °C in an aqueous solution of acetate buffer (pH 5) (sample diluted with MeOH, 1.5 kV).

S4. Monitoring the conjugation reaction between [1][SbF_6]$_{11}$ and Na[1-thio-β-D-galactose] by ^{31}P NMR spectroscopy

The general reaction procedure to generate [**1**][SbF_6]$_{11}$ (**Section S2.5**) was followed. The DMF solution containing [**1**][SbF_6]$_{11}$ (0.0014 mmol, 1 mL) was transferred to an NMR tube containing a solution of $OPPh_3$ (5 mg, 0.02 mmol) dissolved in DMF (75 µL) in a sealed capillary tube. A $^{31}P\{^1H\}$ NMR spectrum of the sample was collected (**Figure S106**, top), and then the solution was transferred to a vial equipped with a Teflon-coated stir bar. To this solution was added a solution of Na[1-thio-β-D-galactose] (9 mg, 0.04 mmol, 30 equiv) in water (0.5 ml) with stirring. The reaction mixture was allowed to stir at 25 °C for 15 min, during which time the color of the solution changed from dark purple to colorless. The reaction mixture was then transferred an NMR tube containing the same $OPPh_3$ internal standard, and a $^{31}P\{^1H\}$ NMR spectrum of the sample was collected (**Figure S106**, bottom), indicating complete conversion of [**1**][SbF_6]$_{11}$ to (Me-DalPhos)AuCl. We note that the slight difference in the integration values of [**1**][SbF_6]$_{11}$ (0.88 compared to $OPPh_3$) when compared with the integration value of the (Me-DalPhos)AuCl byproduct (0.78 compared to $OPPh_3$) is likely due to loss of sample while transferring the reaction solution.

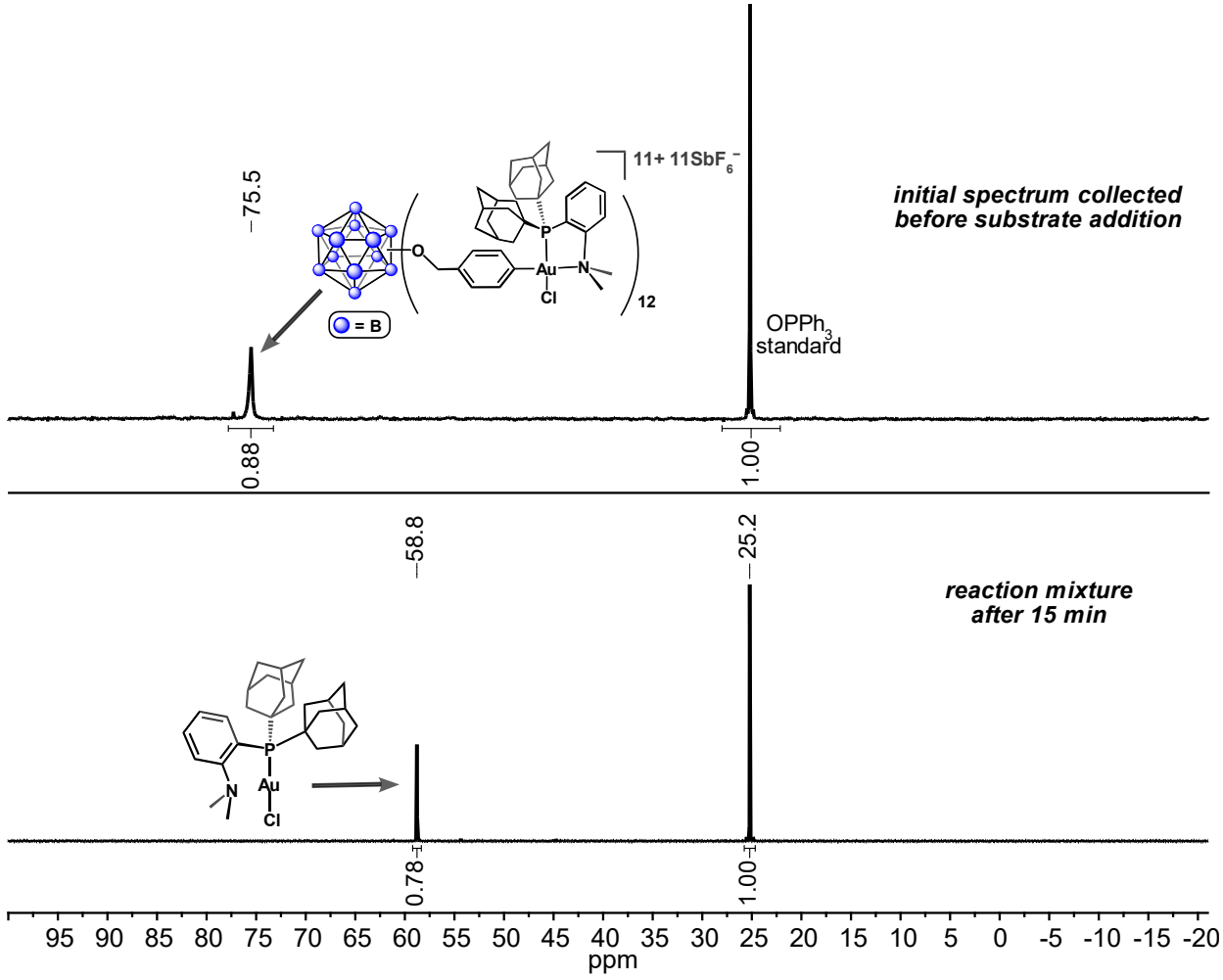

Figure S106. $^{31}P\{^1H\}$ NMR spectra taken of an initial DMF solution of [**1**][SbF_6]$_{11}$ before addition of Na[1-thio-β-D-galactose] (*top*), and of the crude reaction mixture 15 min after substrate addition (*bottom*) (DMF, 162 MHz, 25 °C).

S5. Procedure for (Me-DalPhos)AuCl recovery after conjugation reactions

The DCM washes from the preparation of [**1**][SbF_6]$_{11}$ (described in **Section S2.5**) were combined in addition to all fractions that did not contain the desired [K_2/Na_2][B_{12}($OCH_2C_6H_4SR$)] products from the previously described conjugation reactions (Sections **S2.6**–**S2.25**). The recovered solutions from 12 independent reactions were used for this procedure. Many of these fractions contained the unreacted thiol substrate, small amounts of the [K_2/Na_2][B_{12}(OCH_2Ar)] clusters, and the (Me-DalPhos)AuCl complex. All volatiles were removed from the combined fractions under reduced pressure, and a ^{1}H NMR spectrum (**Figure S107**, top) of the resulting solids was collected. The (Me-DalPhos)AuCl species was purified away from all other byproducts in this complex mixture by column chromatography on silica gel by elution with an 85:15 hexanes:EtOAc mixture. The fractions containing pure (Me-DalPhos)AuCl were combined and dried under reduced pressure to afford the recovered (Me-DalPhos)AuCl material as a colorless solid (62 mg, 0.095 mmol, 30% recovery*).

*Calculation based on the amount of (Me-DalPhos)AuCl used for twelve conjugation reactions (0.027 mmol for each reaction = 0.32 mmol for 12 total reactions as described in **Section S2.5**).

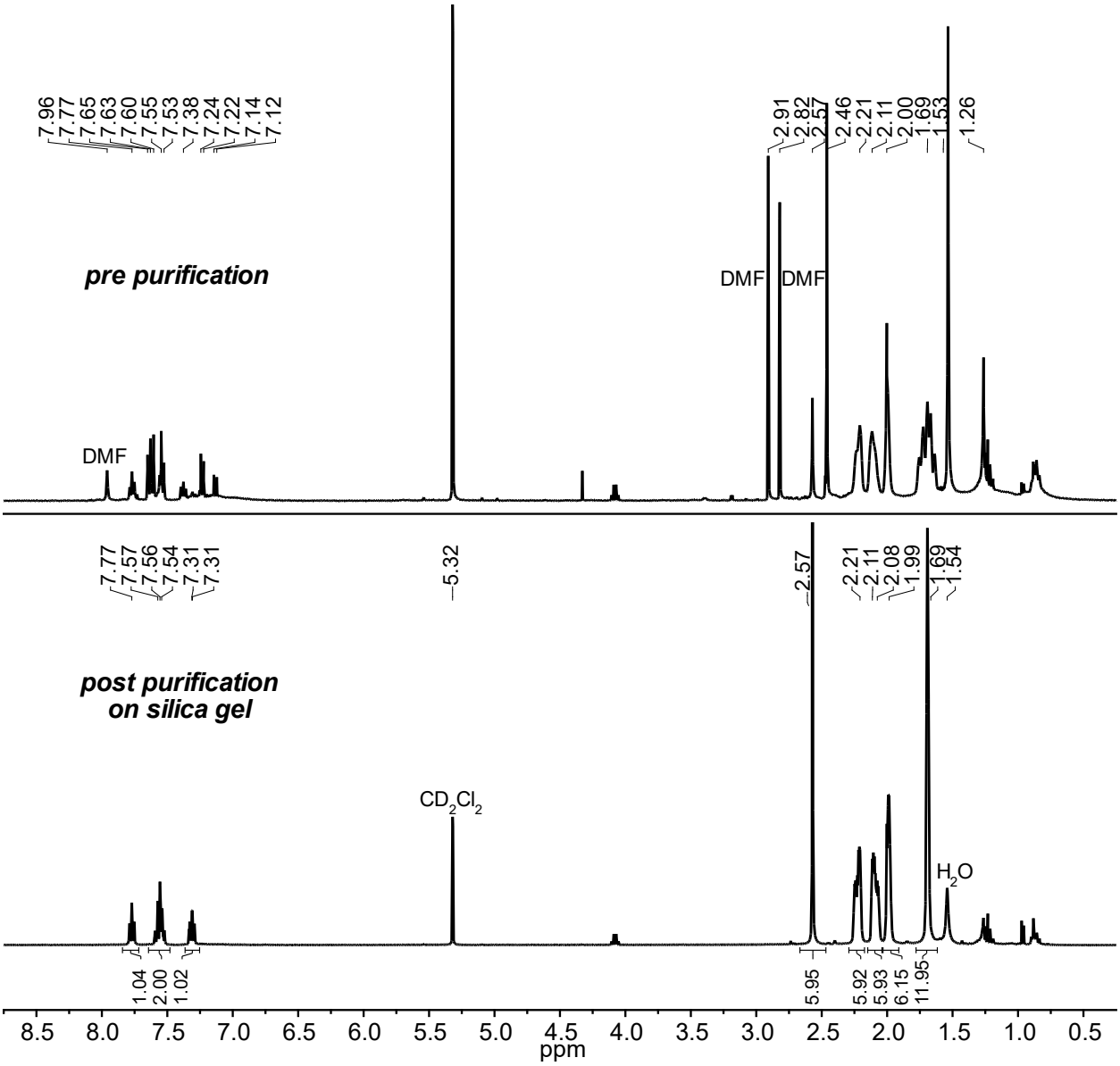

Figure S107. ^{1}H NMR spectra of mixture collected from conjugation reactions before purification (*top*) and recovered (Me-DalPhos)AuCl post purification (*bottom*) (CD_2Cl_2, 400 MHz, 25 °C).

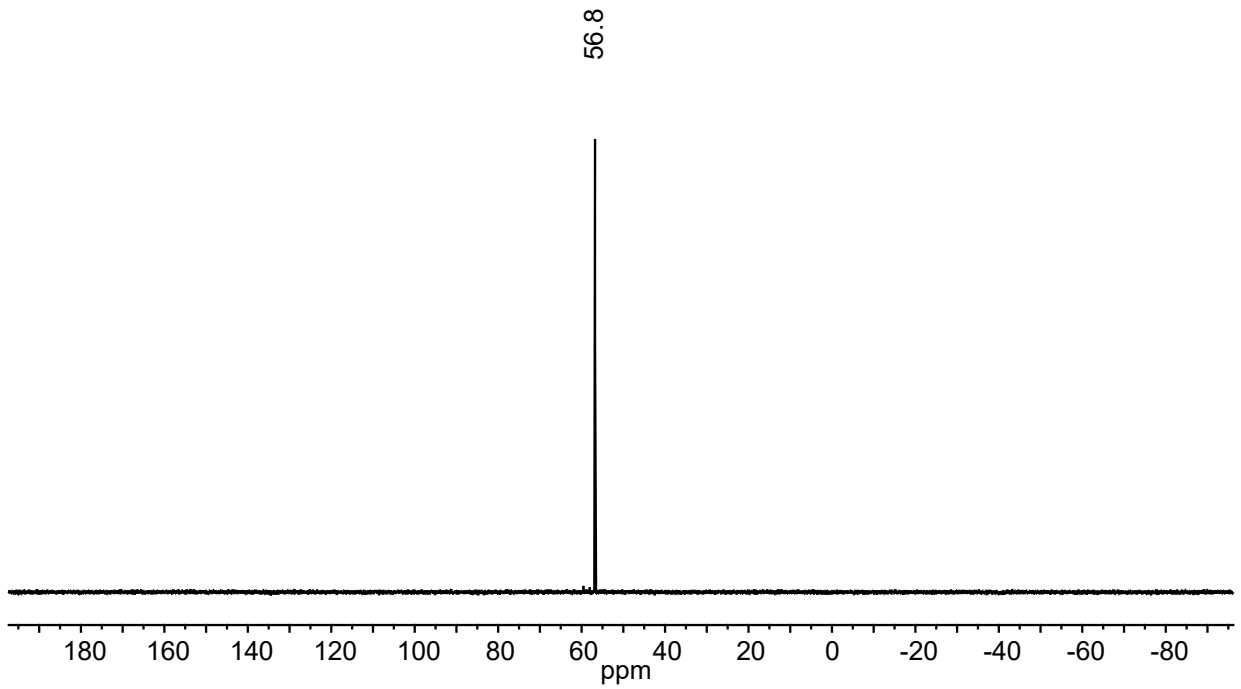

Figure S108. $^{31}P\{^{1}H\}$ NMR spectrum of recovered (Me-DalPhos)AuCl after purification (CD_2Cl_2, 162 MHz, 25 °C).

S6. Surface Plasmon Resonance (SPR) measurements

All experiments were performed on a Biacore T200 instrument with Series S CM5 chips (GE Healthcare Life Sciences). The binding curves were fitted to the Langmuir 1:1 binding model on the Biacore T200 analysis software for determination of the binding affinity (K_D).

S6.1. Concanavalin A (ConA)

The running buffer was composed of an aqueous solution of HEPES buffer (10 mM, pH 7.4), $CaCl_2$ (1 mM), $MgCl_2$ (1 mM), $MnCl_2$ (1 mM), and TWEEN® 20 (0.005% by volume). First, the surface of flow cell #2 was activated with a mixture of EDC (0.4 M) and NHS (0.1 M) (1:1 v/v in H_2O) over 30 min, followed by injection of ConA (0.1 mg/mL) in the running buffer over 40 min and then ethanolamine HCl (1 M in H_2O, pH 8.5) over 30 min. Then, flow cell #1 was prepared as a reference channel by activation of its surface with a mixture of EDC (0.4 M) and NHS (0.1 M) (1:1 v/v in H_2O) over 30 min, followed by injection of ethanolamine HCl (1 M in H_2O, pH 8.5) over 30 min. Analyte samples ($[Na_2][B_{12}(OCH_2C_6H_4(1\text{-thio-}\beta\text{-D-glucose}))_{12}]$ ($[Na_2]$[**18**]), 0.5, 1, 2, 4 mg/L; $[K_2][B_{12}(OCH_2C_6H_4(m PEG_{350}\text{thiol}))_{12}]$ ($[K_2]$[**8**]), 4 mg/L; D-glucose, 30 mg/L (**Figure S109**)) were injected in tandem over both cells for 6 min, followed by a 6 min dissociation period with buffer flow. The surfaces were regenerated by injection of HCl (10 mM) over 2 min, followed by injection of glycine HCl (10 mM in H_2O, pH 2.5) over 2 min. A flow rate of 5 µL/min was used throughout the experiment.

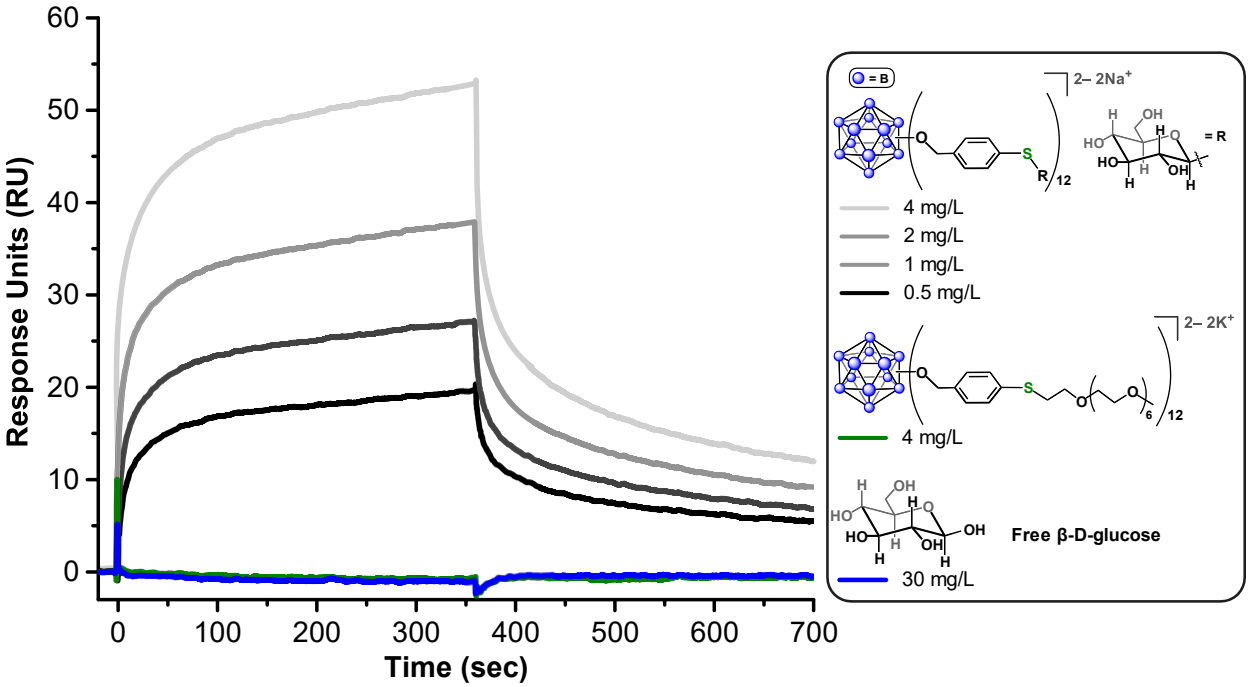

Figure S109. SPR sensorgram for the binding of $[Na_2][B_{12}(OCH_2C_6H_4(1\text{-thio-}\beta\text{-D-glucose}))_{12}]$ (0.5, 1, 2, 4 mg/L concentrations) to ConA with $[K_2][B_{12}(OCH_2C_6H_4(m PEG_{350}$ thiol$))_{12}]$ (4 mg/L) and free D-glucose (30 mg/L) controls.
k_a: 2.09 x 10^4 $M^{-1}s^{-1}$, k_d: 2.35 x 10^{-3} s^{-1}, $\boldsymbol{K_D}$**: 116 nM**

S6.2. Shiga Toxin 1, B Subunit (Stx1B)

The running buffer was composed of an aqueous solution of HEPES buffer (10 mM, pH 7.4), NaCl (150 mM), and TWEEN® 20 (0.005% by volume). First, the surface of flow cell #2 was activated with a mixture of EDC (0.4 M) and NHS (0.1 M) (1:1 v/v in H_2O) over 30 min at a flow rate of 10 µL/min, followed by injection of Stx1B (0.05 mg/mL) in a sodium acetate buffer solution (10 mM, pH 5.2) over 8 minutes at a flow rate of 40 µL/min followed by a solution of ethanolamine HCl (1 M, pH 8.5) over 10 min at a flow rate of 10 µL/min. Then, flow cell #1 was prepared as a reference channel by activation of its surface with a mixture of EDC (0.4 M) and NHS (0.1 M) (1:1 v/v in H_2O) over 30 min at a flow rate of 10 µL/min, followed by injection of ethanolamine HCl (1 M in H_2O, pH 8.5) over 10 min at a flow rate of 10 µL/min. Analyte samples ($[Na_2][B_{12}(OCH_2C_6H_4$(1-thio-β-D-galactose))$_{12}]$ ($[Na_2]$[**19**]), 15, 30, 45, 60 mg/L; (1-thio-β-D-galactose)$_2C_6H_4$, 100 mg/L; D-galactose, 100 mg/L (**Figure S110**); $[K_2][B_{12}(OCH_2C_6H_4(m\text{PEG}_{350}\text{thiol}))_{12}]$ ($[K_2]$[**8**]), 40, 60, 80, 100 mg/L (**Figure S111**)) were injected in tandem over both cells for 6 min, followed by a 6 min dissociation period with buffer flow. Surfaces were regenerated by injection of HCl (10 mM, pH 4.3) over 2 min at a flow rate of 5 µL/min.

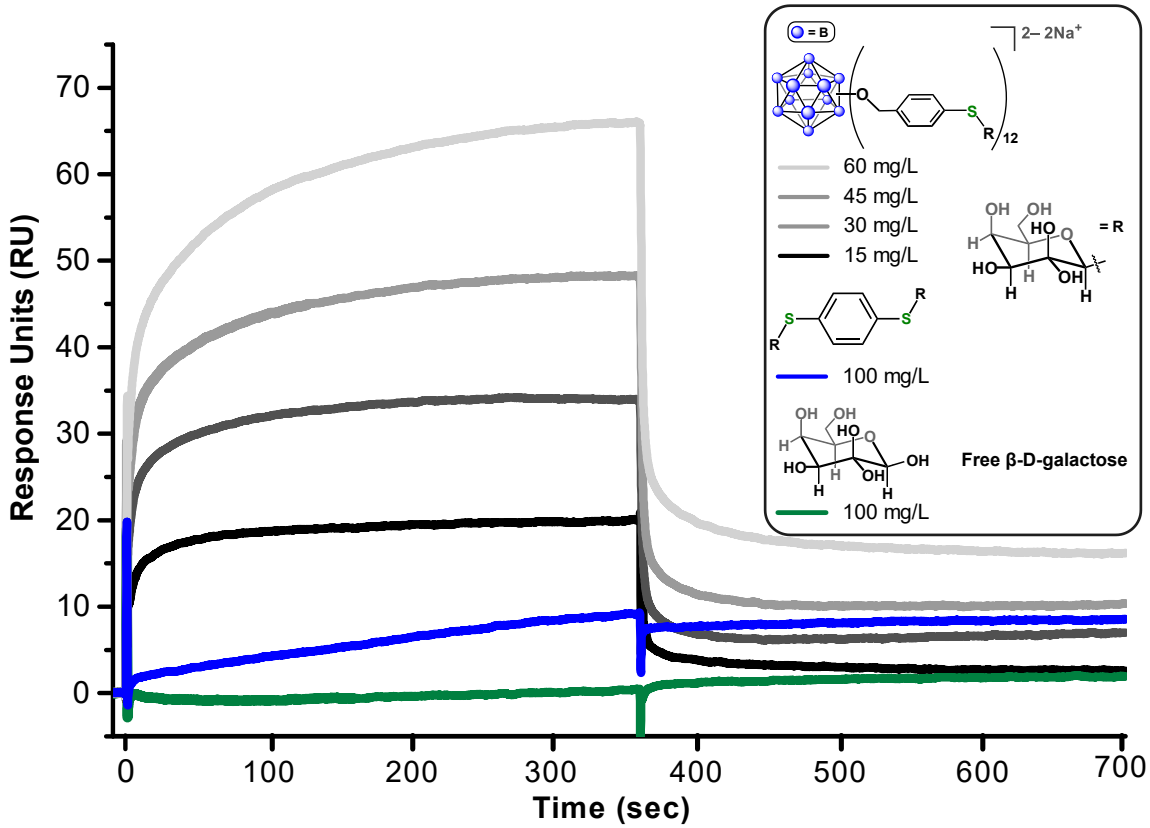

Figure S110. SPR sensorgram for the binding of $[Na_2][B_{12}(OCH_2C_6H_4$(1-thio-β-D-galactose))$_{12}]$ (15, 30, 45, 60 mg/L concentrations) to Stx1B with (1-thio-galactose)$_2C_6H_4$ (100 mg/L) and free D-galactose (100 mg/L) controls.
k_a: 7.42 x 10^2 $M^{-1}s^{-1}$, k_d: 1.10 x 10^{-3} s^{-1}, $\boldsymbol{K_D}$**: 1.51 µM**

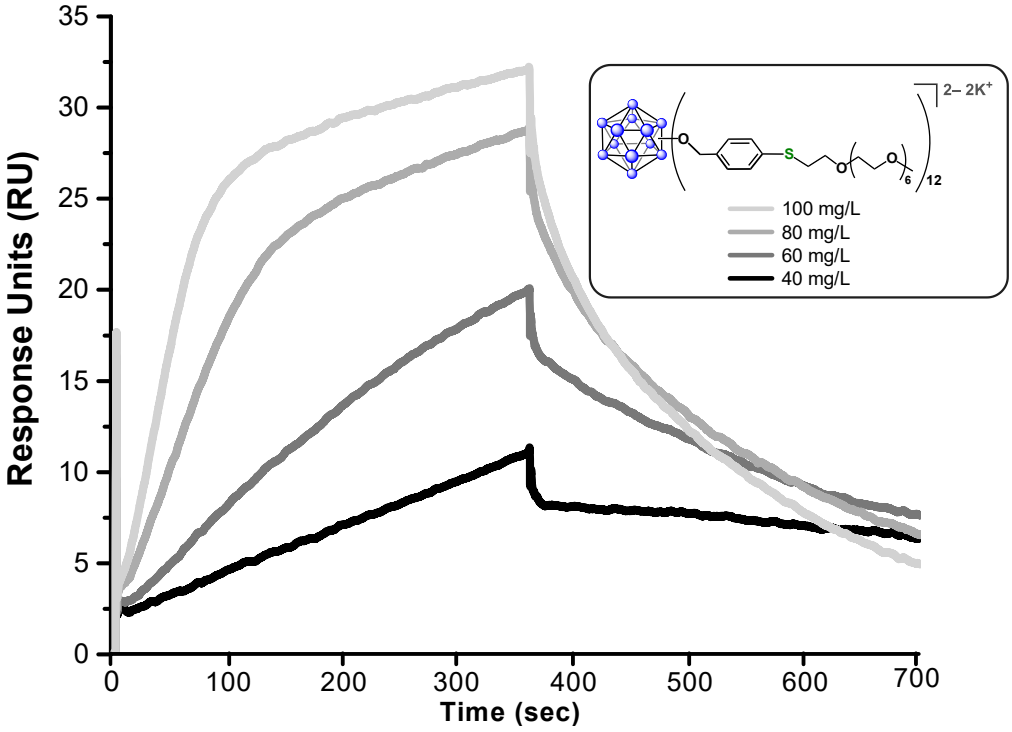

Figure S111. SPR sensorgram for the binding of $[K_2][B_{12}(OCH_2C_6H_4(m\text{PEG}_{350}\text{thiol}))_{12}]$ (40, 60, 80, 100 mg/L concentrations) to Stx1B.
k_a: 3.59 x 10^2 $M^{-1}s^{-1}$, k_d: 3.77 x 10^{-3} s^{-1}, $\boldsymbol{K_D}$**: 10.1 µM**

S6.3. DC-SIGN ECD

The running buffer was composed of an aqueous solution of HEPES buffer (10 mM, pH 7.4), NaCl (150 mM), $CaCl_2$ (5 mM), and TWEEN® 20 (0.005% by volume). First, the surface of flow cell #2 was activated with a mixture of EDC (0.4 M) and NHS (0.1 M) (1:1 v/v in H_2O) over 5 min, followed by injection of DC-SIGN ECD (0.01 mg/mL) in the running buffer over 45 min and then ethanolamine HCl (1 M in H_2O, pH 8.5) over 10 min. Then, flow cell #1 was prepared as a reference channel by activation of its surface with a mixture of EDC (0.4 M) and NHS (0.1 M) (1:1 v/v in H_2O) over 5 min, followed by injection of ethanolamine HCl (1 M in H_2O, pH 8.5) over 10 min. Analyte samples ($[Na_2][B_{12}(OCH_2C_6H_4(1\text{-thio-}\alpha\text{-D-mannose}))_{12}]$, 1, 2, 3, 4 mg/L; $[K_2][B_{12}(OCH_2C_6H_4(m PEG_{350}\text{thiol}))_{12}]$, 8 mg/L; D-mannose, 20 mg/L (**Figure S112**)) were injected in tandem over both cells for 6 min, followed by a 6 min dissociation period with buffer flow. Surfaces were regenerated by injection of an aqueous solution of HEPES buffer (10 mM, pH 7.4), NaCl (150 mM), TWEEN® 20 (0.005% by volume), and EDTA (10 mM) over 2 min. A flow rate of 5 µL/min was used throughout the experiment.

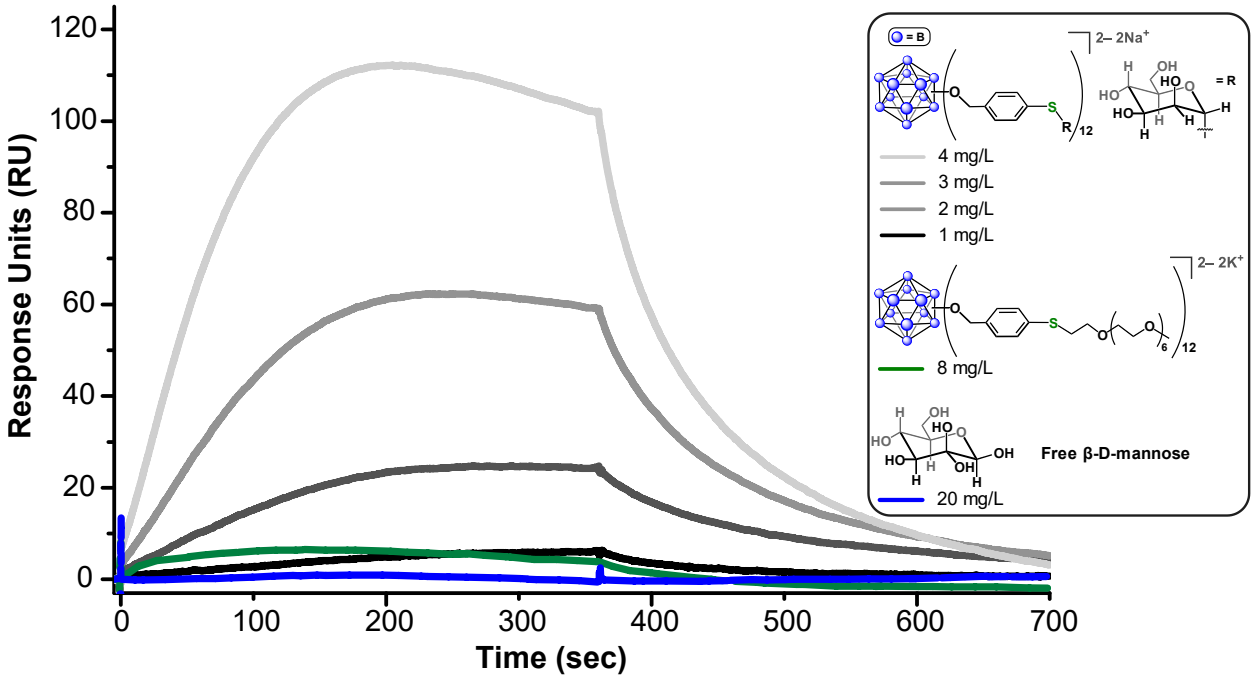

Figure S112. SPR sensorgram for the binding of $[Na_2][B_{12}(OCH_2C_6H_4(1\text{-thio-}\alpha\text{-D-mannose}))_{12}]$ (1, 2, 3, 4 mg/L concentrations) to DC-SIGN with $[K_2][B_{12}(OCH_2C_6H_4(m PEG_{350}$ thiol$))_{12}]$ (8 mg/L) and free D-mannose (20 mg/L) controls.
k_a: 2.99 x 10^3 $M^{-1}s^{-1}$, k_d: 1.11 x 10^{-2} s^{-1}, $\boldsymbol{K_D}$**: 3.70 µM**

S7. Confocal microscopy studies with DC-SIGN

Raji DC-SIGN+ cells were harvested and resuspended in D-PBS buffer (Fisher Scientific) supplemented with 1% bovine serum albumin (Fisher Scientific) and $CaCl_2$ (2 mM, Fisher Scientific) for a density of 2×10^6 cells/mL, and then aliquoted into populations of 2×10^5 cells. After 30 min of incubation at 25 °C, Human BD Fc Block (1.5 µL, BD Biosciences) was added to each cell population and incubated for 10 min at 25 °C. Solutions of each analyte ($[K_2]$[**8**], $[Na_2]$[**20**], and D-mannose) in DMSO (1 µL of a 10 mM stock solution) were independently mixed with a solution of HIV-1 gp120-FITC (ImmunoDX, 1 µL of a 1 mg/mL solution), and then the resulting mixture (2 µL total) was subsequently added to the cell population (100 µL) and mixed. The mixtures were then incubated for 30 min at 37 °C, after which the cells were washed with D-PBS (3 × 1 mL). Fluoroshield mounting medium (Abcam) was added to each sample and mixed, and then the cells were transferred to microscope slides. After 5 min, a coverslip was applied to each slide. After an additional 20 min, the edges were sealed with clear nail polish. The slides were then taken to a Leica TCS SPE confocal microscope, where images were acquired in z-stacks (25 sections, 20 µm) in both fluorescence and brightfield modes with a 40× lens and 30% excitation laser intensity. This procedure was repeated using a DMSO solution in the absence of any added analyte as a control. **Figure S113A** displays side-by-side image comparisons of the described experiments, and the following subsections include additional images.

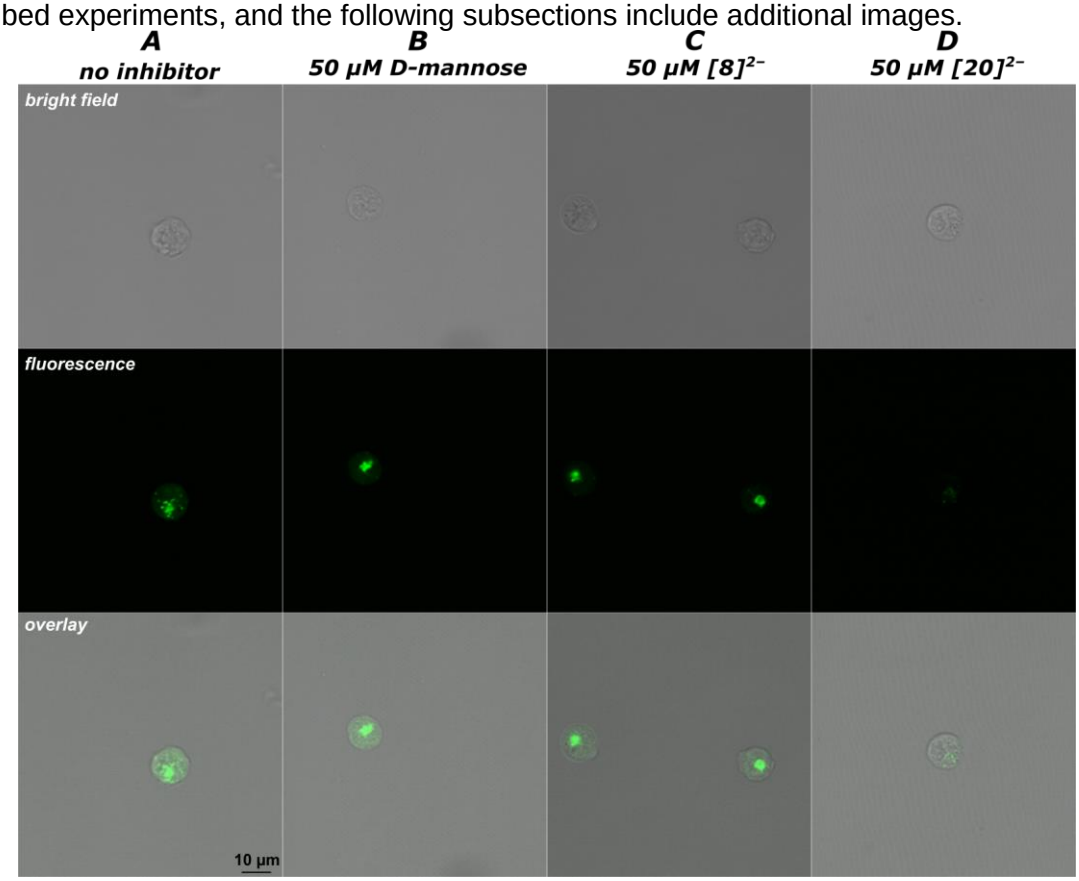

Figure S113. Confocal laser scanning microscopy images (bright field, fluorescence, and overlay) of Raji DC-SIGN+ cells incubated with gp120-FITC (83 nM) and (A) DMSO as a control; (B) free D-mannose (50 µM solution in DMSO); (C) $[K_2]$[**8**] (50 µM solution in DMSO); (D) $[Na_2]$[**20**] (50 µM solution in DMSO), demonstrating significant reduction in cellular uptake of gp120-FITC in the presence of the $[Na_2]$[**20**] inhibitor, and no observable reduction in gp120-FITC cellular uptake for the control experiments (B, C).

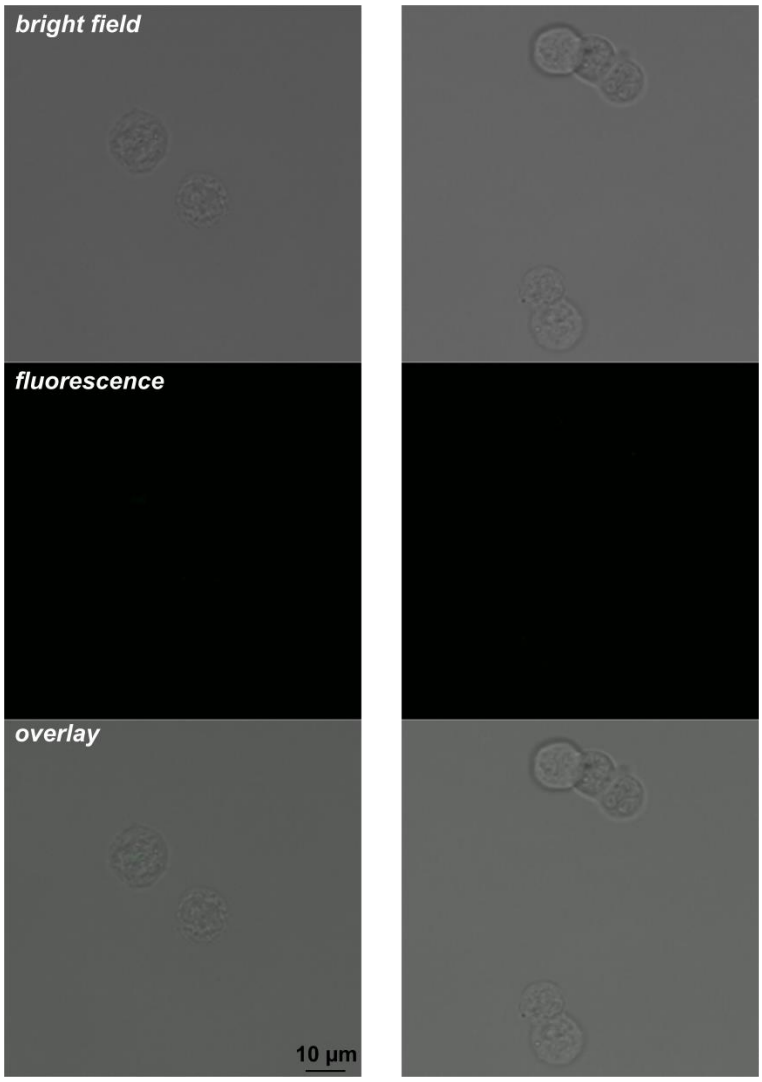

Figure S114. Two sets of confocal microscopy images of Raji cells (no DC-SIGN) exposed to gp120-FITC and DMSO (bright field, fluorescence, and overlay).

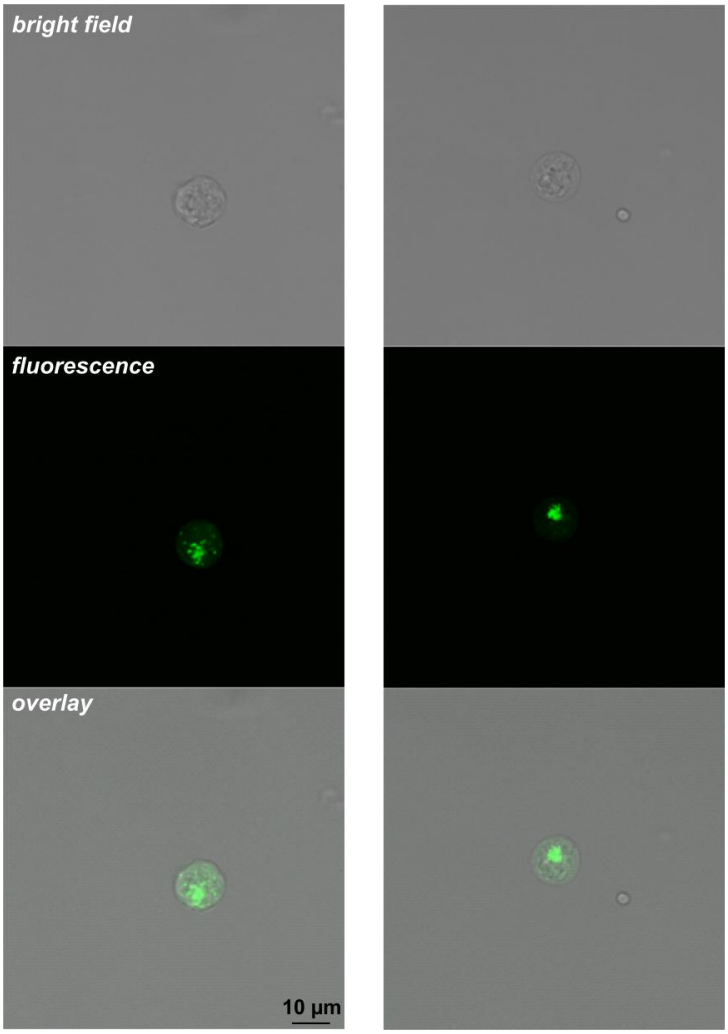

Figure S115. Two sets of confocal microscopy images of Raji DC-SIGN+ cells exposed to gp120-FITC and DMSO (bright field, fluorescence, and overlay).

S7.1. Free D-mannose control

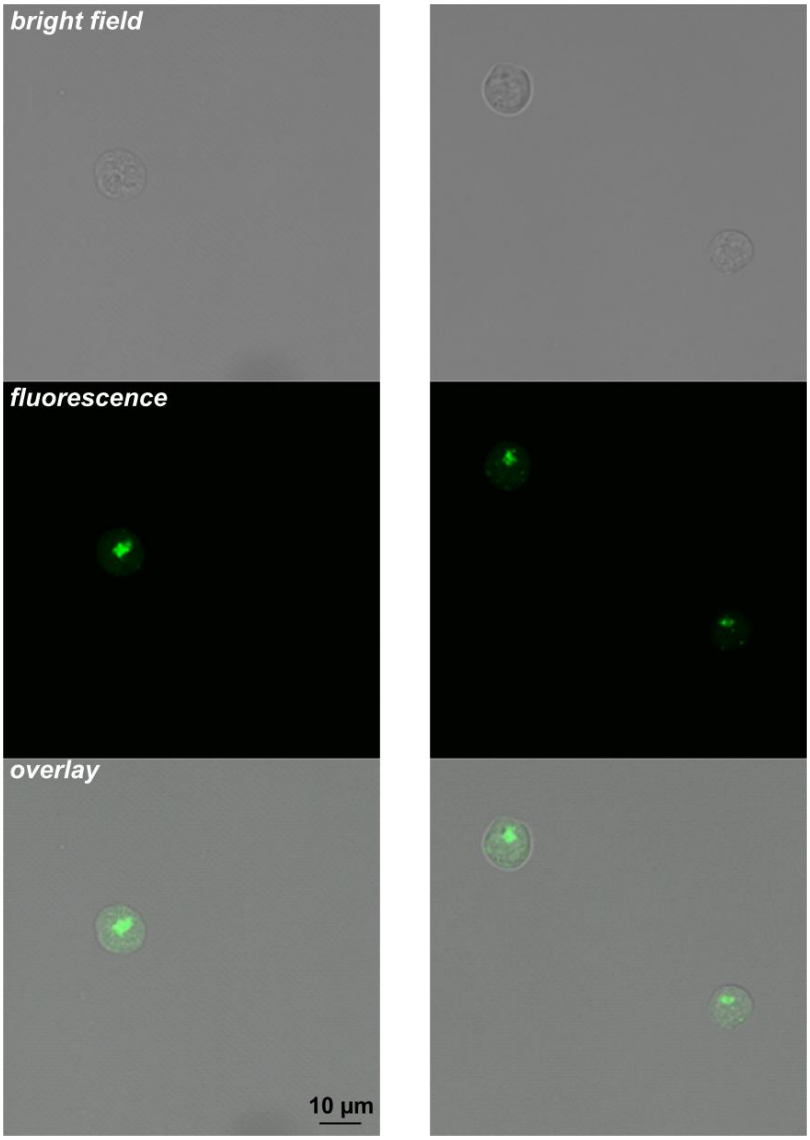

Figure S116. Two sets of confocal microscopy images of Raji DC-SIGN+ cells exposed to gp120-FITC and free D-mannose (50 µM) (bright field, fluorescence, and overlay).

S7.2. [K_2][8] control

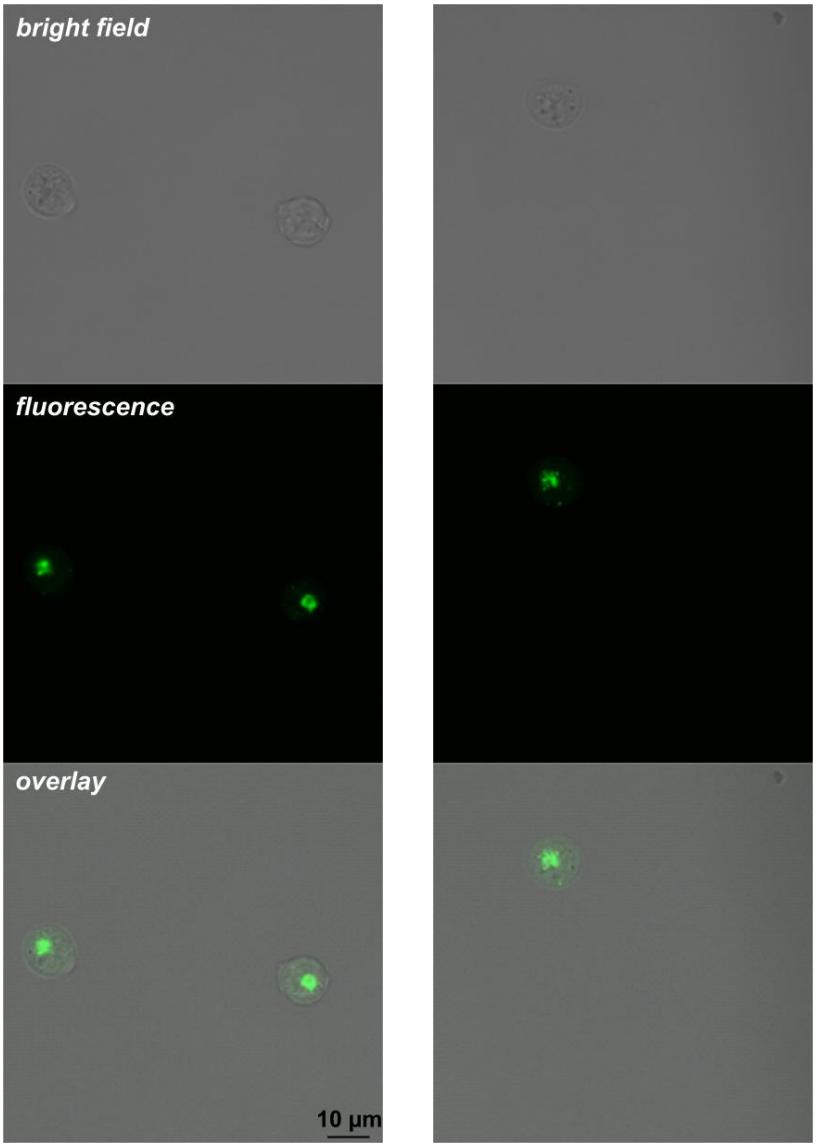

Figure S117. Two sets of confocal microscopy images of Raji DC-SIGN+ cells exposed to gp120-FITC and [K_2][**8**] (50 µM) (bright field, fluorescence, and overlay).

S7.3. [Na_2][20] inhibitor

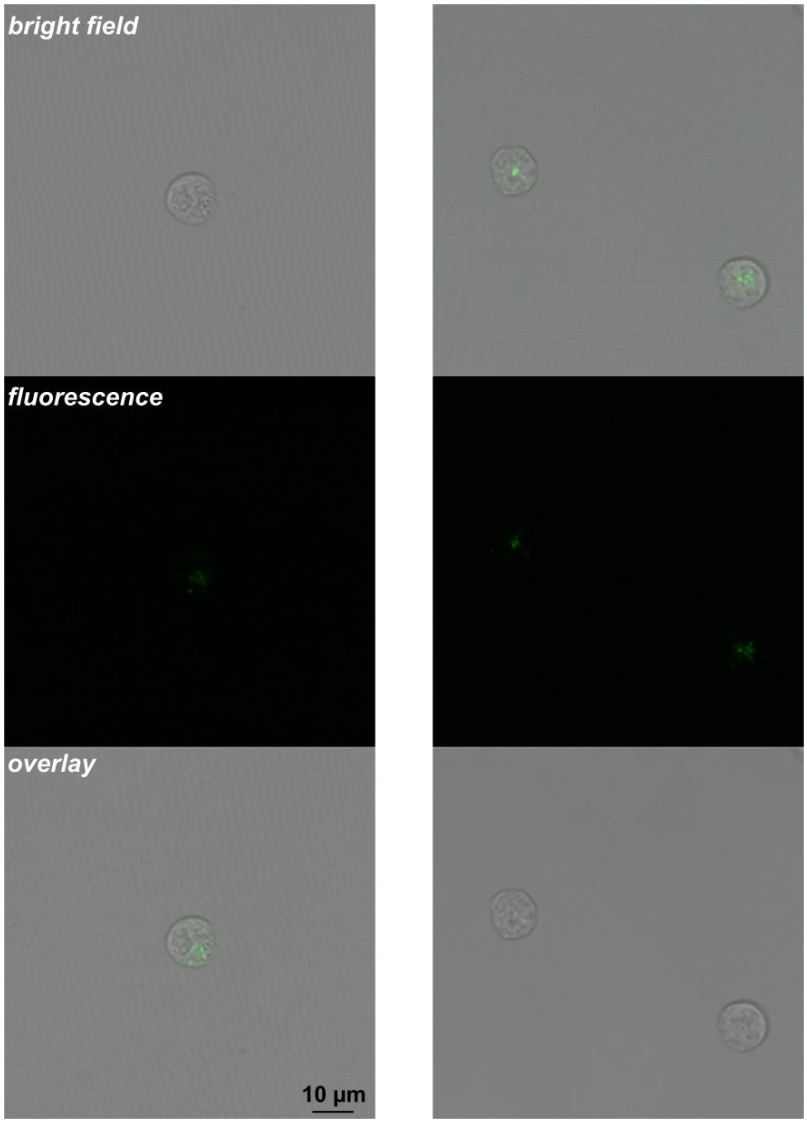

Figure S118. Two sets of confocal microscopy images of Raji DC-SIGN+ cells exposed to gp120-FITC and [K_2][**20**] (50 µM) (bright field, fluorescence, and overlay).

S8. Computational studies

S8.1. Systems and methods

In order to assess the binding between the saccharide-grafted nanoclusters and their respective protein targets, atomistic molecular dynamics simulations were performed. Concanavalin A (ConA PDB code 1ONA)[11] was used as target protein for the 1-thio-D-glucose-functionalized boron cluster ([**18**]$^{2-}$), Stx1B (PDB code 1CQF)[12] was the target for the boron clusters grafted with either 1-thio-D-galactose ([**19**]$^{2-}$) or PEG_{350} ([**8**]$^{2-}$), and DC-SIGN (PDB code 1k9I)[13] was used as the target for the 1-thio-D-mannose-functionalized boron cluster ([**20**]$^{2-}$).

The target proteins were described by a CHARMM36[14] force field, while the clusters were described by a CHARMM general force field.[15] The atomic charges of the boron clusters and their methylbenzene substituents were recalculated by DFT-BLYP[16] with the RESP[17] method. The simulations were performed with NAMD.[18] The Particle Mesh Ewald (PME)[19] method was used for the evaluation of long-range Coulombic interactions. The time step was set to 2.0 fs. The simulations were performed in the NPT ensemble (p = 1 bar and T = 300 K), using the Langevin dynamics (γ_{Lang} = 1 ps^{-1}). After 2,000 steps of minimization, ions and water molecules were equilibrated for 2 ns around the protein and cluster, which were restrained using harmonic forces with a spring constant of 1 kcal/(mol $Å^2$). The last frames of the restrained equilibration were used to start simulations of the free cluster and partial constrained protein.

S8.1.1. Binding of nanoclusters to protein targets

Figure S123, **Figure S125**, **Figure S127**, and **Figure S129** display snapshots from the four nanocluster/protein binding simulations. The proteins are shown in cartoon representation (light blue), and the appended saccharides of the cluster are in gray, with boron, carbon, oxygen, calcium and manganese atoms represented in pink, gray, red, purple, and cyan, respectively. The amino acids color scheme is Asn: orange, Trp: purple, Asp: red, Arg: blue, Tyr: green, Leu: light blue, Val: ochre, Ser: yellow, Gly: white, and Glu: pink. The term “ligand” is used in this section to refer to one appended group on the cluster periphery (*i.e.* [**18**]$^{2-}$ contains 12 glucose ligands). **Figure S124**, **Figure S126**, **Figure S128**, and **Figure S130** display plots that represent the number of ligands of each nanocluster that are within 4 Å of the amino acid residues on the protein binding sites.

S8.2. Calculated structures

S8.2.1. $[18]^{2-}$

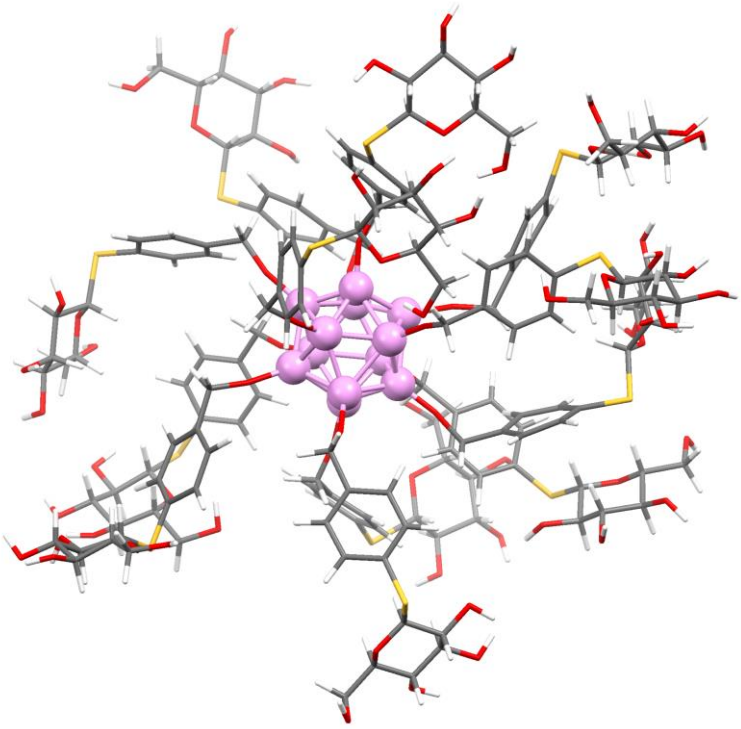

Figure S119. Calculated structure of [**18**]$^{2-}$. Gray: C; white: H; red: O; yellow: S; pink: B.

S8.2.2. $[19]^{2-}$

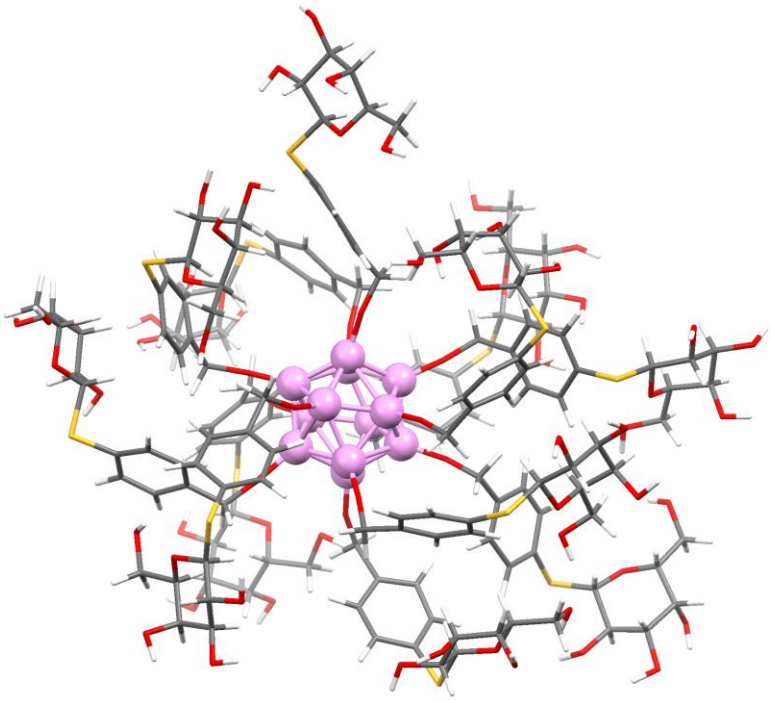

Figure S120. Calculated structure of [**19**]$^{2-}$. Gray: C; white: H; red: O; yellow: S; pink: B.

S8.2.3. $[20]^{2-}$

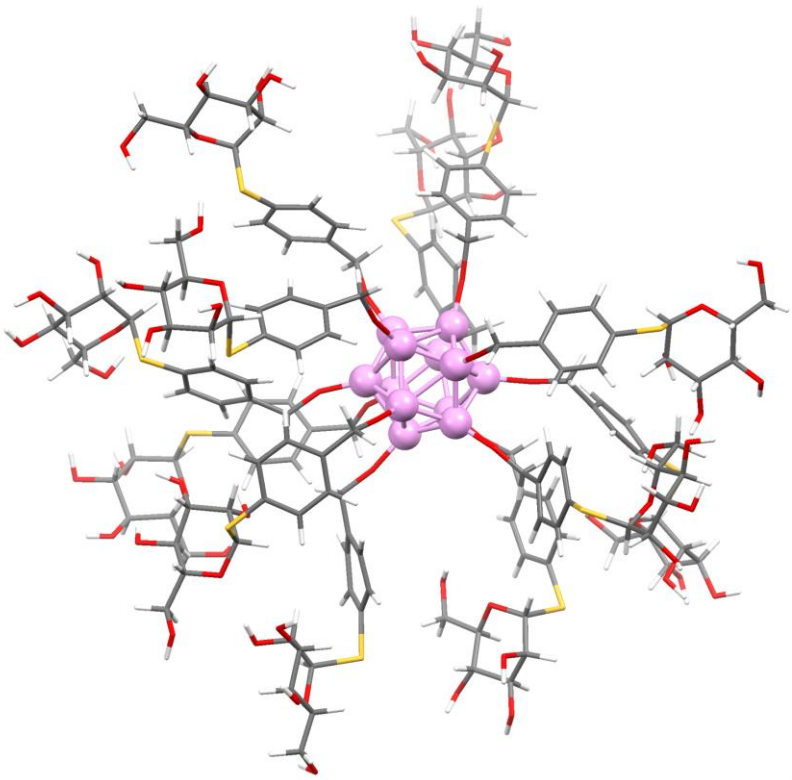

Figure S121. Calculated structure of [**20**]$^{2-}$. Gray: C; white: H; red: O; yellow: S; pink: B.

S8.2.4. $[8]^{2-}$

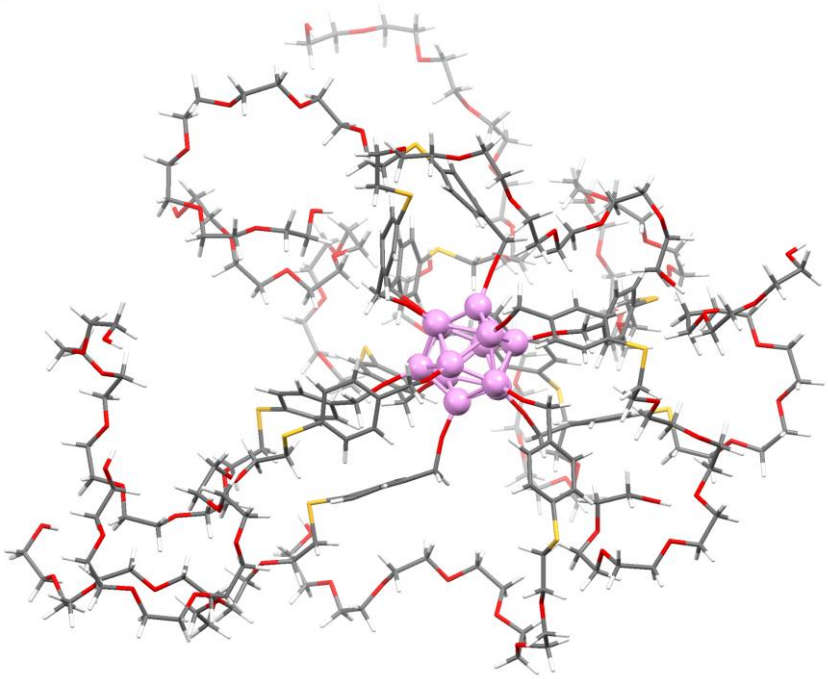

Figure S122. Calculated structure of [**8**]$^{2-}$. Gray: C; white: H; red: O; yellow: S; pink: B.

S8.3. Binding of $[18]^{2-}$ with ConA

Four $[\mathbf{18}]^{2-}$ nanoclusters were initially positioned near the typical sugar binding sites of Con A (Tyr 12, Tyr 100, Pro 13, Asn 14, Thr 15, Asp 16, Asp 208, Arg 228, and Leu 229), which are highlighted in **Figure S123a**. After the 20 ns simulation (**Figure S123b**), the $[\mathbf{18}]^{2-}$-*1* nanocluster remains bound to the same binding pocket at which it was originally positioned, as shown in **Figure S123c**. After the 20 ns simulation, the $[\mathbf{18}]^{2-}$-*2* cluster is bound to the surrounding amino acid residues of the binding pocket (**Figure S123d**), while the $[\mathbf{18}]^{2-}$-*3* cluster spans the binding pocket (**Figure S123e**), and the $[\mathbf{18}]^{2-}$-*4* cluster is dissociated from the protein binding site. As shown in **Figure S124**, there are on average two glucose ligands from $[\mathbf{18}]^{2-}$-*1* and two from $[\mathbf{18}]^{2-}$-*2* that interact with the amino acids of the binding pocket, while fewer ligands (<2) from the $[\mathbf{18}]^{2-}$-*3* and $[\mathbf{18}]^{2-}$-*4* clusters bind to the surrounding amino acids throughout the simulation. Since the four binding pockets are separated from each other, there are four distinct binding scenarios observed.

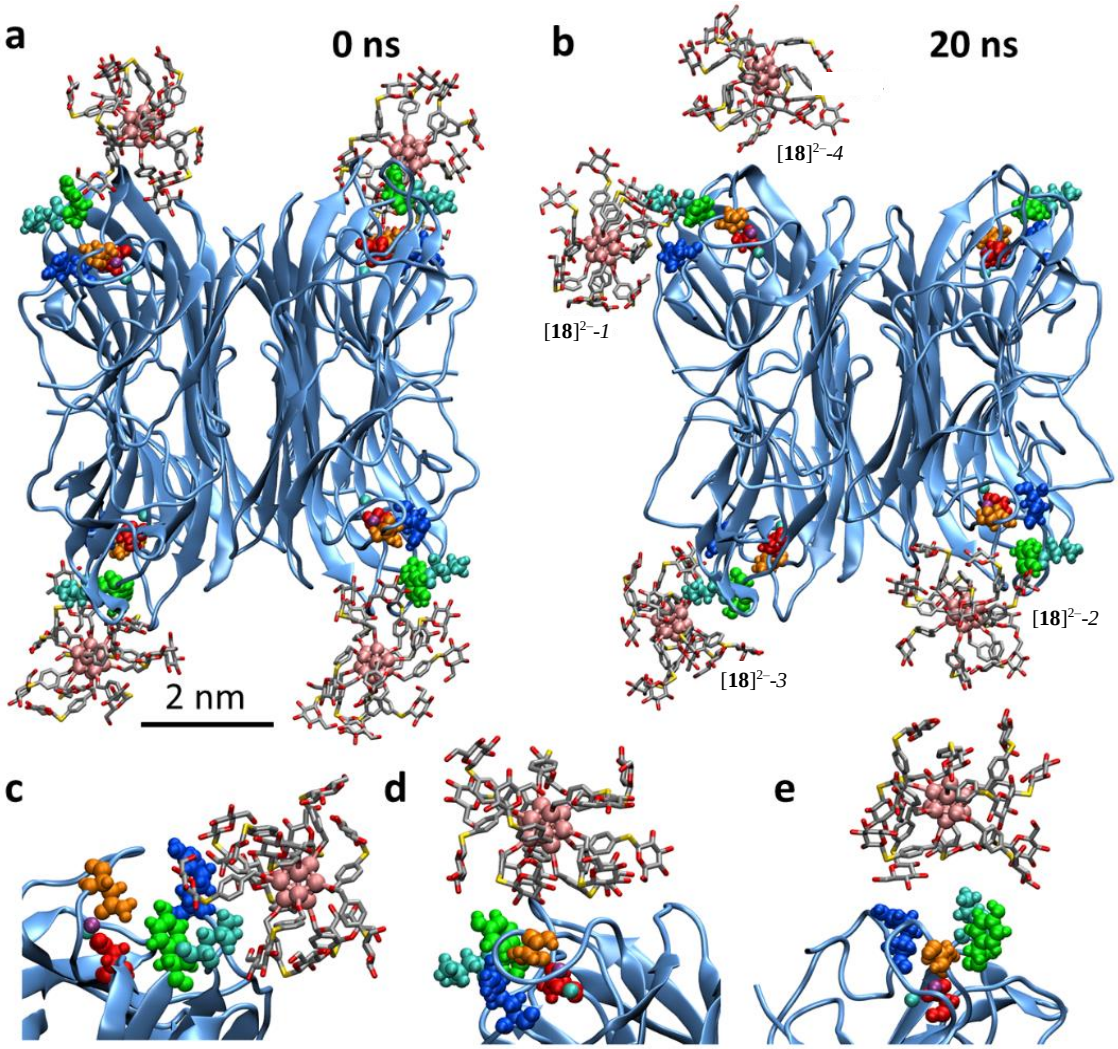

Figure S123. Binding of four independent $[\mathbf{18}]^{2-}$ molecules to the four distinct binding sites of ConA. (a) Initial configuration of the four $[\mathbf{18}]^{2-}$ clusters with ConA. (b) Final configuration after the 20 ns simulation. (c) Zoomed-in image of $[\mathbf{18}]^{2-}$-*1* interacting with one of the four sugar binding pockets. (d) Zoomed-in image of $[\mathbf{18}]^{2-}$-*2* binding to the surrounding residues of the pocket. (e) Zoomed-in image of $[\mathbf{18}]^{2-}$-*3* showing the glucose ligands spanning the binding pocket.

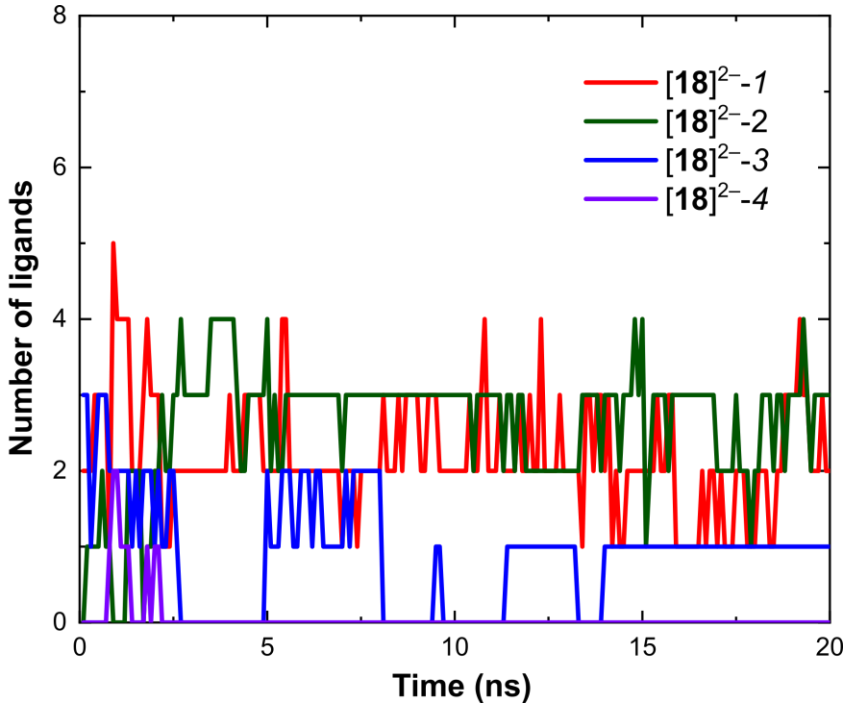

Figure S124. Plot displaying the number of ligands of the [**18**]$^{2-}$-*1* - [**18**]$^{2-}$-*4* clusters that interact with the specific binding pocket of ConA over the course of the 20 ns simulation.

S8.4. Binding of $[19]^{2-}$ and $[8]^{2-}$ with Stx1B

The $[\mathbf{19}]^{2-}$ and $[\mathbf{8}]^{2-}$ clusters were initially positioned on the side of Stx1B (sugar binding sites 1 and 2)[20] and above the binding surface of Stx1B (binding site 3) as shown in **Figure S125** and **Figure S127**. Both $[\mathbf{19}]^{2-}$ and $[\mathbf{8}]^{2-}$ bind to the edge of Stx1B (sites 1 and 2) with a maximum of 7 and 8 binding ligands, respectively. Similarly, both clusters interact with the polar residues on the surface of Stx1B (site 3), with $[\mathbf{19}]^{2-}$ having up to 10 interacting ligands (galactose), while $[\mathbf{8}]^{2-}$ has up to 7 interacting ligands (PEG) during the course of the 20 ns simulation (**Figure S126** and **Figure S128**). Although $[\mathbf{19}]^{2-}$ has shorter ligands than $[\mathbf{8}]^{2-}$, it shows stronger multivalent binding towards the broad binding surface of Stx1B. The $[\mathbf{8}]^{2-}$/Stx1B binding simulation suggests there is an interaction between the PEGylated cluster and the surface of Stx1B. This result is consistent with the binding response observed by SPR studies for this system; however, the K_D value calculated for the $[\mathbf{8}]^{2-}$ cluster (10.1 µM) is significantly lower than that of the $[\mathbf{19}]^{2-}$ cluster (1.51 µM) with Stx1B (see **Section S6.2** for details).

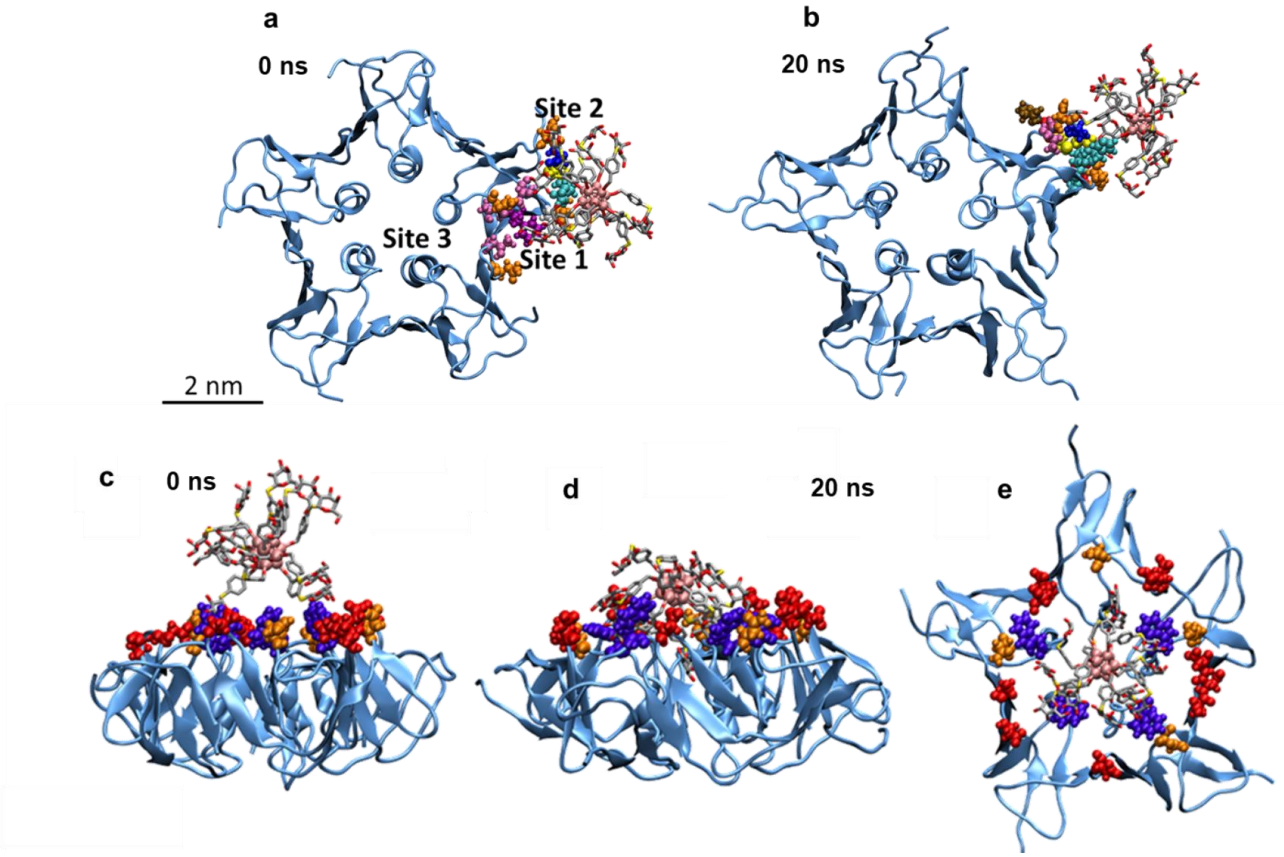

Figure S125. Binding of $[\mathbf{19}]^{2-}$ to Stx1B. (a) Initial configuration at sites 1 and 2. (b) Final binding configuration at sites 1 and 2 after 20 ns. (c) Initial configuration at site 3. (d, e) Two views of the final binding configuration at site 3 after 20 ns.

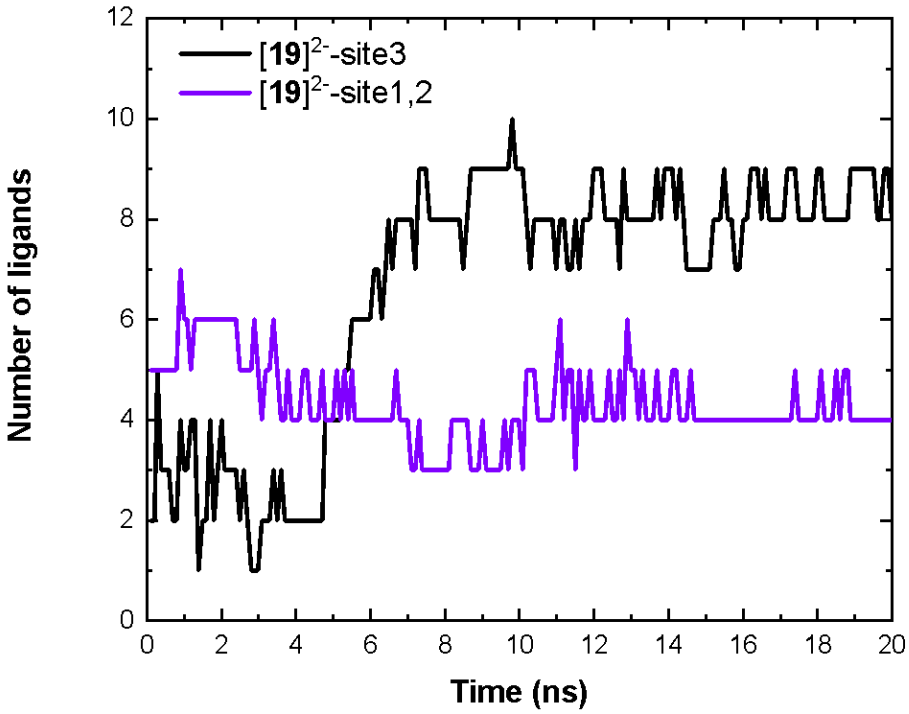

Figure S126. Plot displaying the number of ligands of the $[\mathbf{19}]^{2-}$ cluster that interact with the specific binding sites of Stx1B over the course of the 20 ns simulation.

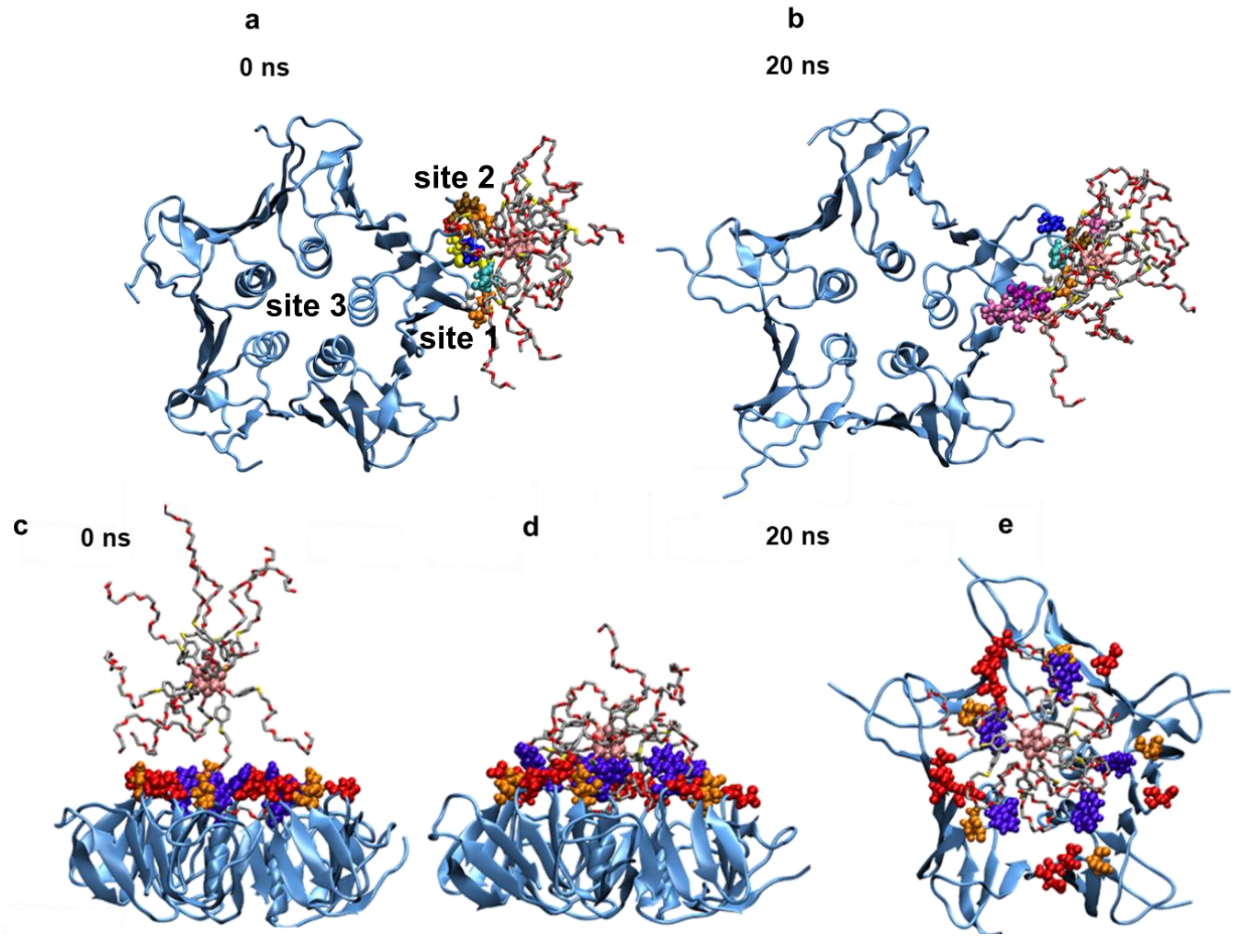

Figure S127. Binding of [**8**]$^{2-}$ to Stx1B. (a) Initial configuration at sites 1 and 2. (b) Final binding configuration at sites 1 and 2 after 20 ns. (c) Initial configuration at site 3. (d, e) Two views of the final binding configuration at site 3 after 20 ns.

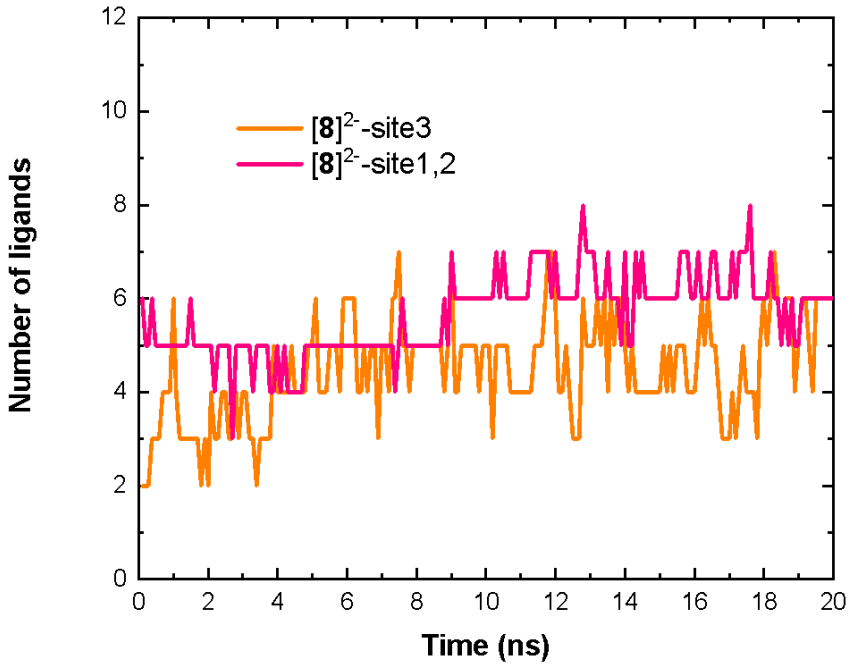

Figure S128. Plot displaying the number of ligands of the [**8**]$^{2-}$ cluster that interact with the specific binding sites of Stx1B over the course of the 20 ns simulation.

S8.5. Binding of $[20]^{2-}$ with DC-SIGN

The $[\mathbf{20}]^{2-}$ cluster was initially positioned near one binding pocket of DC-SIGN (Asp 336, Glu 347, Asn 349, Val 351, Glu 354, and Asn 365). During the first 10 ns of the simulation, the cluster binds to the specific sugar binding pockets with a maximum of three ligands interacting with the pocket. It then dissociates from the binding site with only one ligand interacting with the residues of the protein (**Figure S129** and **Figure S130**).

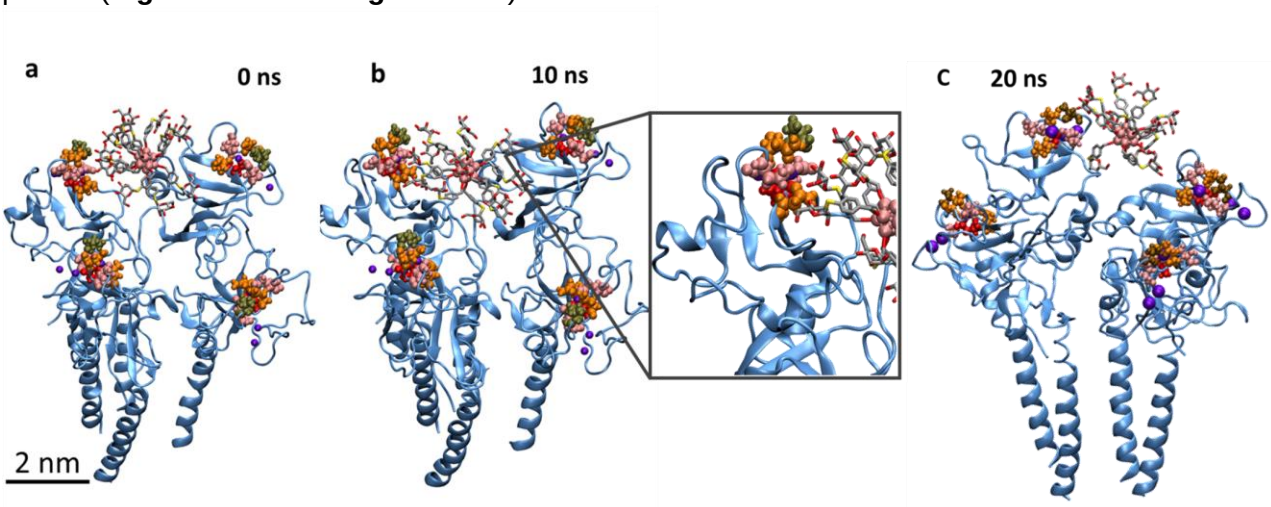

Figure S129. Binding of $[\mathbf{20}]^{2-}$ to DC-SIGN. (a) Initial configuration. (b) Configuration at 10 ns with zoomed-in image. (c) Final binding configuration after 20 ns.

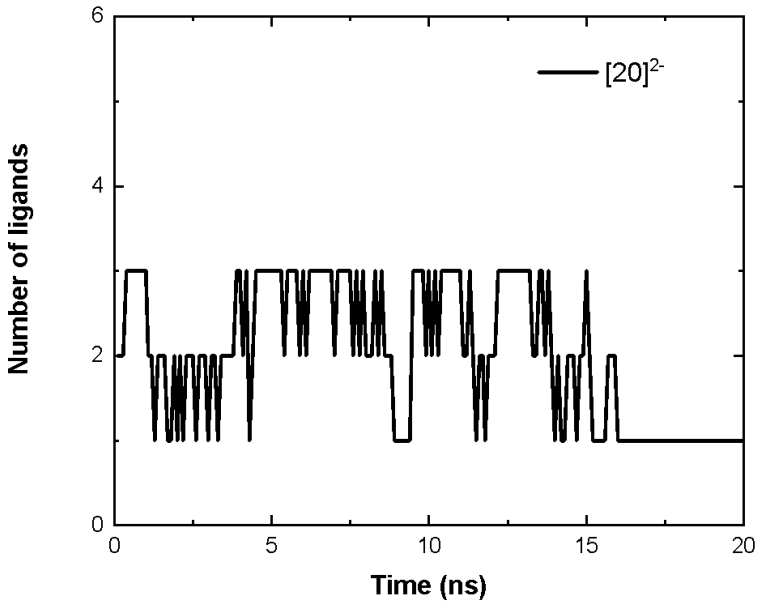

Figure S130. Plot displaying the number of ligands of the $[\mathbf{20}]^{2-}$ cluster that interact with the specific binding pocket of DC-SIGN over the course of the 20 ns simulation.

S9. X-ray crystallographic details

S9.1. $B_{12}(OCH_2C_6H_4I)_{12}$

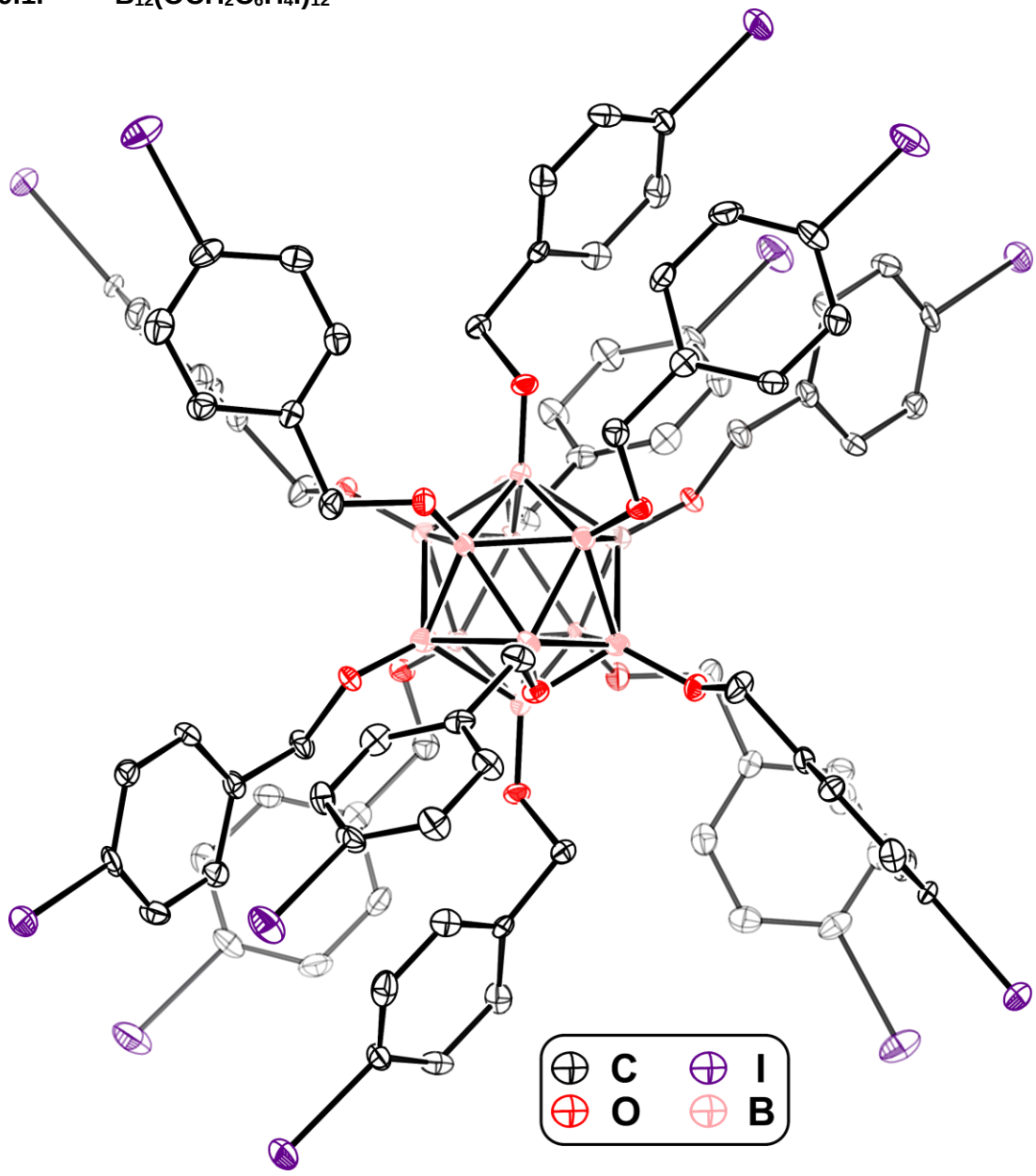

Figure S131. Solid-state structure of $B_{12}(OCH_2C_6H_4I)_{12}$ with thermal ellipsoids rendered at the 50% probability level with PLATON[21] and with hydrogen atoms omitted for clarity.

Table S1. Crystallographic and structure refinement information for $B_{12}(OCH_2C_6H_4I)_{12}$

CCDC code	1942748	
Empirical formula	C_{84} H_{72} B_{12} I_{12} O_{12}	
Formula weight	2925.93	
Temperature	100.0 K	
Wavelength	0.71073 Å	
Crystal system	Triclinic	
Space group	$P\bar{1}$	
Unit cell dimensions	a = 10.6995(10) Å	α = 113.864(3)°
	b = 15.7093(14) Å	β = 90.520(3)°
	c = 16.1872(14) Å	γ = 109.249(3)°
Volume	2316.9(4) Å^3	
Z, Z'	1, 0.5	
Density (calculated)	2.097 Mg/m^3	
Absorption coefficient	4.068 mm^{-1}	
F(000)	1368	
Crystal size	0.33 x 0.29 x 0.08 mm^3	
Theta range for data collection	2.056 to 25.405°	
Index ranges	-12<=h<=12, -18<=k<=18, -19<=l<=18	
Reflections collected	25884	
Independent reflections	8477 [R(int) = 0.0395]	
Completeness to theta = 25.242°	99.8 %	
Absorption correction	Semi-empirical from equivalents	
Max. and min. transmission	0.1480 and 0.0945	
Refinement method	Full-matrix least-squares on F^2	
Data / restraints / parameters	8477 / 0 / 541	
Goodness-of-fit on F^2	1.022	
Final R indices [I>2σ(I)]	R1 = 0.0308, wR2 = 0.0593	
R indices (all data)	R1 = 0.0462, wR2 = 0.0640	
Largest diff. peak and hole	1.045 and -0.976 e.Å^{-3}	

S9.2. $[B_{12}(OCH_2C_6H_4((Me\text{-}DalPhos)AuCl))_{12}][SbF_6]_{11}$ ([1][SbF_6]$_{11}$)

Single crystal X-ray diffraction data were collected at the BL02B1 beamline at the SPring-8 synchrotron radiation facility (Hyogo, Japan) for a rhombohedral plate-shaped pink crystal of [**1**][SbF_6]$_{11}$. The diffractometer was equipped with Dectris PILATUS3 X CaTe 1M (DECTRIS Ltd., Switzerland). The diffraction data were collected at 298.2 K with a crystal enclosed in a glass capillary (borosilicate glass). The structure was solved by direct method using SHELXT[22] programs and refined by full-matrix least-squares on *F* including all reflections by SHELXL-2016.[23] All calculations were performed using the CrysAlisPro crystallographic software package.[24] Three out of twelve Au organometallic fragments are modeled with reduced occupancy (87%, 68% and 60% for each). We reasoned that there were some 11-substituted clusters co-crystallized with the dodeca-functionalized major product. In addition to the internal molecular motion due to its large molecular size (>10,000 amu) and the ambient temperature (298.2 K) data collection, there were many heavily disordered SbF_6^- counter anions and solvent molecules within the voids. Such disordered parts and molecules were restrained to the same thermal displacement parameter and bond length by using the SIMU, RIGU, SAME and SADI commands. Particularly, a few of the highly disordered SbF_6^- counter anions were restrained by the EADP command. All hydrogen atoms were refined by using the AFIX command. Finally, the diffused electron densities resulting from disordered solvent molecules in the void spaces were removed by the SQUEEZE command in PLATON[21] and the results were appended in the CIF file.

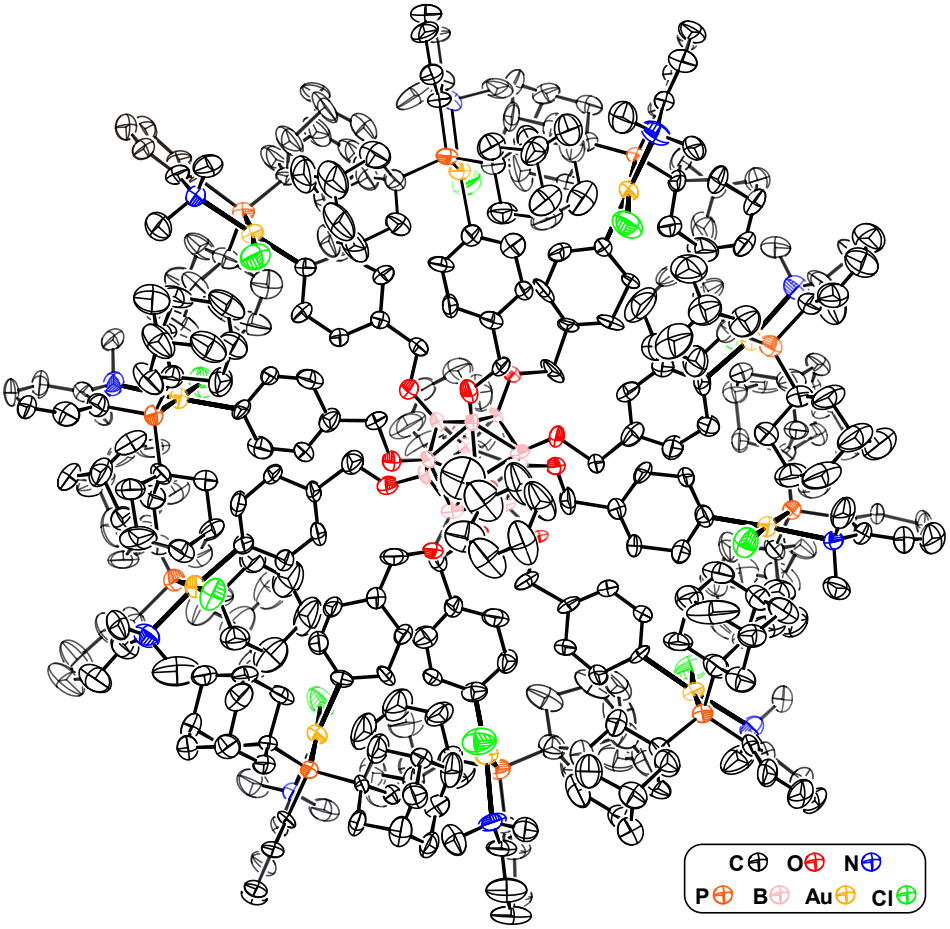

Figure S132. Solid-state structure of [**1**]$^{11+}$ with thermal ellipsoids rendered at the 50% probability level with PLATON[21] and with hydrogen atoms and SbF_6^- anions omitted for clarity.

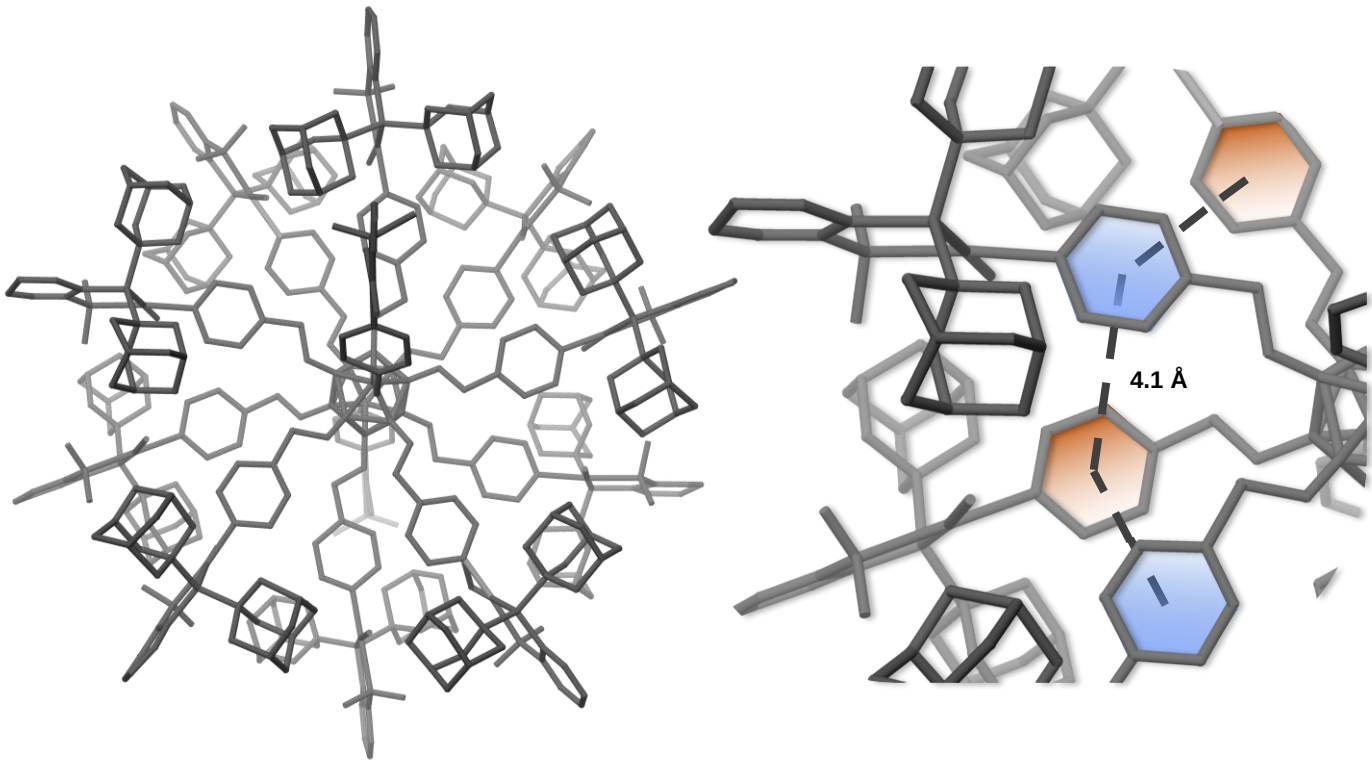

Figure S133. Solid-state structure of [**1**]$^{11+}$ (left) with zoomed-in image (right) displaying the benzyl group π-stacking interactions.

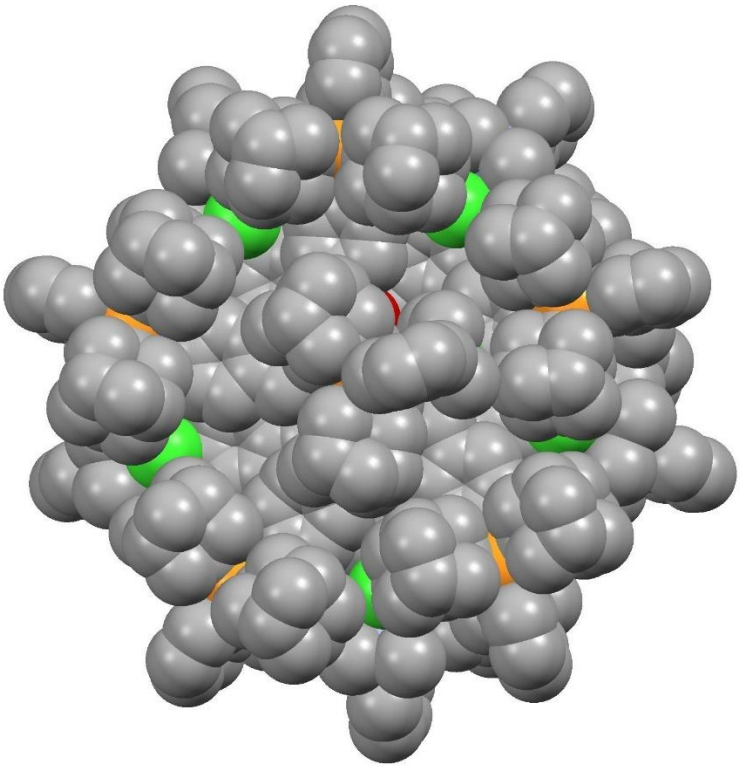

Figure S134. Space-filling model of [**1**]$^{11+}$ with hydrogen atoms and SbF_6^- counter anions omitted.

Table S2. Crystallographic and structure refinement information for [**1**][SbF_6]$_{11}$

CCDC code	1949777	
Empirical formula	$C_{396.2}H_{514}Au_{11.2}B_{12}Cl_{11.2}F_{58.3}N_{11.2}O_{12}P_{11.2}Sb_{9.7}$	
Formula weight	10984.21	
Temperature	298.2 K	
Wavelength	0.4934 Å	
Crystal system	Monoclinic	
Space group	*Cc*	
Unit cell dimensions	*a* = 45.6445(4) Å	*α* = 90°
	b = 29.7686(3) Å	*β* = 93.524(1)°
	c = 41.2098(6) Å	*γ* = 90°
Volume	55888.7(11) Å^3	
Z, *Z*'	4, 1	
Density (calculated)	1.305 g/mm^3	
Absorption coefficient	3.474 mm^{-1}	
F(000)	21536	
Crystal size	0.1 x 0.07 x 0.02 mm^3	
Theta range for data collection	1.458 to 17.291°	
Index ranges	-54<=*h*<=54, -35<=*k*<=35, -49<=*l*<=49	
Reflections collected	338876	
Independent reflections	101864 [*R*(int) = 0.0622]	
Completeness to theta = 17.29°	99.80 %	
Absorption correction	multi-scan	
Max. and min. transmission	1.00000 and 0.05141	
Refinement method	Full-matrix least-squares on F^2	
Data / restraints / parameters	101864 / 7952 / 5257	
Goodness-of-fit on F^2	1.053 *[1.027]	
Final *R* indices [F_o>4σ(F_o)]	*R*1 = 0.0561, w*R*2 = 0.1717	
	*[*R*1 = 0.0697, w*R*2 = 0.2355]	
R indices (all data)	*R*1 = 0.0730 *[*R*1 = 0.0876]	
Largest diff. peak and hole	1.37 and -0.86 e.Å^{-3} *[1.92 and -0.91 e.Å^{-3}]	

*indicates values before applying SQUEEZE[21]

S10. References

(1) Jennum, K.; Vestergaard, M.; Pedersen, A.; Fock, J.; Jensen, J.; Santella, M.; Led, J.; Kilså, K.; Bjørnholm, T.; Nielsen, M. Synthesis of Oligo(Phenyleneethynylene)s with Vertically Disposed Tetrathiafulvalene Units. *Synthesis (Stuttg).* **2011**, 539–548.

(2) Lundgren, R. J.; Sappong-Kumankumah, A.; Stradiotto, M. A Highly Versatile Catalyst System for the Cross-Coupling of Aryl Chlorides and Amines. *Chem. - A Eur. J.* **2010**, *16* (6), 1983–1991.

(3) Messina, M. S.; Stauber, J. M.; Waddington, M. A.; Rheingold, A. L.; Maynard, H. D.; Spokoyny, A. M. Organometallic Gold(III) Reagents for Cysteine Arylation. *J. Am. Chem. Soc.* **2018**, *140*, 7065–7069.

(4) Wixtrom, A. I.; Shao, Y.; Jung, D.; Machan, C. W.; Kevork, S. N.; Qian, E. A.; Axtell, J. C.; Khan, S. I.; Kubiak, C. P.; Spokoyny, A. M. Rapid Synthesis of Redox-Active Dodecaborane B12(OR)12 Clusters Under Ambient Conditions. *Inorg. Chem. Front.* **2016**, *3*, 711–717.

(5) Hesp, K. D.; Stradiotto, M. Stereo- and Regioselective Gold-Catalyzed Hydroamination of Internal Alkynes with Dialkylamines. *J. Am. Chem. Soc.* **2010**, *132*, 18026–18029.

(6) Su, S. V.; Hong, P.; Baik, S.; Negrete, O. A.; Gurney, K. B.; Lee, B. DC-SIGN Binds to HIV-1 Glycoprotein 120 in a Distinct but Overlapping Fashion Compared with ICAM-2 and ICAM-3. *J. Biol. Chem.* **2004**, *279* (18), 19122–19132.

(7) Axtell, J. C.; Saleh, L. M. A.; Qian, E. A.; Wixtrom, A. I.; Spokoyny, A. M. Synthesis and Applications of Perfunctionalized Boron Clusters. *Inorg. Chem.* **2018**, *57* (5), 2333–2350.

(8) Lee, M. W.; Farha, O. K.; Hawthorne, M. F.; Hansch, C. H. Alkoxy Derivatives of Dodecaborate: Discrete Nanomolecular Ions with Tunable Pseudometallic Properties. *Angew. Chemie - Int. Ed.* **2007**, *46* (17), 3018–3022.

(9) Barton, J. L.; Wixtrom, A. I.; Kowalski, J. A.; Qian, E. A.; Jung, D.; Brushett, F. R.; Spokoyny, A. M. Perfunctionalized Dodecaborate Clusters as Stable Metal-Free Active Materials for Charge Storage. *ACS Appl. Energy Mater.* **2019**, *2* (7) 4907–4913.

(10) Heravi, M. M.; Ghavidel, M.; Mohammadkhani, L. Beyond a Solvent: Triple Roles of Dimethylformamide in Organic Chemistry. *RSC Adv.* **2018**, *8* (49), 27832–27862.

(11) Poortmans, F.; Wyns, L.; Bouckaert, J. A Structure of the Complex Between Concanavalin A and Methyl-3,6-Di-O-(Alpha-D-Mannopyranosyl)-Alpha-D-Mannopyranoside Reveals Two Binding Modes. *J. Biol. Chem.* **1996**, *271* (48), 30614–30618.

(12) Jacobson, J. M.; Yin, J.; Kitov, P. I.; Mulvey, G.; Griener, T. P.; James, M. N. G.; Armstrong, G.; Bundle, D. R. The Crystal Structure of Shiga Toxin Type 2 with Bound Disaccharide Guides the Design of a Heterobifunctional Toxin Inhibitor. *J. Biol. Chem.* **2014**, *289* (2), 885–894.

(13) Feinberg, H.; Castelli, R.; Drickamer, K.; Seeberger, P. H.; Weis, W. I. Multiple Modes of

Binding Enhance the Affinity of DC-SIGN for High Mannose N-Linked Glycans Found on Viral Glycoproteins. *J. Biol. Chem.* **2007**, *282* (6), 4202–4209.

(14) MacKerell, A. D.; Bashford, D.; Bellott, M.; Dunbrack, R. L.; Evanseck, J. D.; Field, M. J.; Fischer, S.; Gao, J.; Guo, H.; Ha, S.; Joseph-McCarthy, D; Kuchnir, L.; Kuczera, K.; Lau, F. T. K.; Mattos, C.; Michnick, S.; Ngo, T.; Nguyen, D. T.; Prodhom, B.; Reiher, W. E.; Roux, B.; Schlenkrich, M.; Smith, J. C.; Stote, R.; Straub, J.; Watanabe, M.; Wiórkiewicz-Kuczera, J.; Yin, D.; Karplus, M. All-Atom Empirical Potential for Molecular Modeling and Dynamics Studies of Proteins. *J. Phys. Chem. B* **1998**, *102* (18), 3586–3616.

(15) Vanommeslaeghe, K.; MacKerell, A. D. Automation of the CHARMM General Force Field (CGenFF) I: Bond Perception and Atom Typing. *J. Chem. Inf. Model.* **2012**, *52* (12), 3144–3154.

(16) Becke, A. D. Density-Functional Exchange Approximation with Correct Asymptotic Behaviour. *Phys. Rev. A* **1988**, *38* (6), 3098–3100.

(17) Bayly, C. I.; Cieplak, P.; Cornell, W. D.; Kollman, P. A. A Well-Behaved Electrostatic Potential Based Method Using Charge Restraints for Deriving Atomic Charges: The RESP Model. *J. Phys. Chem.* **1993**, *97* (40), 10269–10280.

(18) Phillips, J. C.; Braun, R.; Wang, W.; Gumbart, J.; Tajkhorshid, E.; Villa, E.; Chipot, C.; Skeel, R. D.; Kalé, L.; Schulten, K. Scalable Molecular Dynamics with NAMD. *J. Comput. Chem.* **2005**, *26* (16), 1781–1802.

(19) Darden, T.; York, D.; Pedersen, L. Particle Mesh Ewald: An N·log(N) Method for Ewald Sums in Large Systems. *J. Chem. Phys.* **1993**, *98* (12), 10089–10092.

(20) Ling, H.; Boodhoo, A.; Hazes, B.; Cummings, M. D.; Armstrong, G. D.; Brunton, J. L.; Read, R. J. Structure of the Shiga-Like Toxin I B-Pentamer Complexed with an Analogue of Its Receptor Gb3. *Biochemistry* **1998**, *37* (7), 1777–1788.

(21) Spek, A. L. Structure Validation in Chemical Crystallography. *Acta Crystallogr. Sect. D* **2009**, *65*, 148–155.

(22) Sheldrick, G. M. SHELXT - Integrated Space-Group and Crystal-Structure Determination. *Acta Crystallogr. Sect. A Found. Crystallogr.* **2015**, *71* (1), 3–8.

(23) Sheldrick, G. M. Crystal Structure Refinement with SHELXL. *Acta Crystallogr. Sect. C Struct. Chem.* **2015**, *71* (Md), 3–8.

(24) Dolomanov, O. V.; Bourhis, L. J.; Gildea, R. J.; Howard, J. A. K.; Puschmann, H. OLEX2: A Complete Structure Solution, Refinement and Analysis Program. *J. Appl. Crystallogr.* **2009**, *42* (2), 339–341.